IMPACT OF BIOTURBATION ON SEDIMENT REDISTRIBUTION IN COASTAL CHILE

-

As estimated by combining remote sensing, machine learning and semi-empirical modelling

Kumulative Dissertation

zur

Erlangung des Doktorgrades der Naturwissenschaften

(Dr. rer. nat.)

dem Fachbereich Geographie

der Philipps-Universität Marburg

vorgelegt von

Paulína Grigušová

aus Kežmarok / Slowakei

Erschienen: Marburg an der Lahn 2023
Supervised by: Prof. Dr. Jörg Bendix
Abgabe: 10.3.2023
Disputation: 17.5.2023
Kennziffer: 1180

Für meinen Opa Štefan Kuric (*24.5.1920 †14.2.2008),

der sich sein Leben lang für gleiche Bildungschancen

für alle eingesetzt hat.

Contents

1. Introduction 1

1.1 Research gap and motivation 1

1.1 Previously applied methods 2

2. Conceptual design of the thesis 4

2.1 Hypothesis 4

2.2 Study area 4

2.3 Bioturbators in Chile 5

2.4 Workflow 6

2.5 Data used in this study 7

References 9

3. Area-Wide Prediction of Vertebrate and Invertebrate Hole Density and Depth Across a Climate Gradient in Chile Based on UAV and Machine Learning 21

Abstract 22

3.1. Introduction 23

3.2. Materials and Methods 24

3.3. Results 32

3.4. Discussion 37

3.5. Conclusions 39

References 40

Supplementary material 49

4. Higher sediment redistribution rates related to burrowing animals than previously assumed as revealed by Time-Of-Flight based monitoring 63

Abstract 64

4.1. Introduction 65

4.2. Study area 66

4.3. Methodology 69

4.4. Results 75

4.5. Discussion 81

References 86

Supplementary Material 93

5. Mammalian bioturbation amplifies rates of both, hillslope sediment erosion and accumulation, in coastal Chile 111

Abstract 112

5.1. Introduction 113

5.2. Study area 115

5.3. Methodology **116**
5.4 Results **122**
5.5. Discussion **130**
5.6. Conclusion **133**
References **133**
Supplementary material **142**
6. Conclusion **157**
6.1 Hypothesis **157**
6.2 Suitability of the applied methods **158**
6.3 New contributions **158**
6.4 Perspectives and future investigations **159**
References **159**
Zusammenfassung **162**
Erklärung **165**
Curriculum Vitae **167**

Acknowledgments

“Wir steigen nicht auf Berge, um Gipfel zu erreichen, sondern heimzukehren in eine Welt, die uns als neue Chance erscheint.“ Reinhold Messner

In diesem Sinne möchte ich mich bei denen bedanken, die mir über die Jahre an meiner universitären Hochtour nah standen, sich über meine Erfolge gefreut und in stressigen Zeiten mitgefiebert haben, mich mit Ratschlägen unterstützt haben und dazu beigetragen haben, dass ich auf meine Uni Zeit als eine vom sorglosen bis zum lernreichen Lebensabschnitt zurückblicken werde.

Mein größter Dank für die Dissertation geht an meinen Doktorvater Jörg Bendix. Danke für die Aufmunterung, wenn ich am Zweifeln war; für die Mails, die sehr oft mitten in der Nacht kamen; für die Korrekturen, die sich nicht nur auf Fehlern konzentrierten, sondern auch ausreichend Smileys erhielten; und für die konstante Unterstützung, offenes Ohr, Motivation und Zeit, die Du dir genommen hast. Ein sehr großer Dank für Deine Geduld, dass du mir die Möglichkeit gegeben hast, mich weiterzuentwickeln, eigene Ideen zu verfolgen und mich als Menschen angenommen hast.

Danke Annegret, dass ich dank dir an meinen sozialen Fähigkeiten arbeiten konnte, meine Stärken und Schwächen identifizieren konnte und herausgefunden habe, wer und wie ich sein will. Danke für die zahlreichen Telegram-Nachrichten, dass du meine Artikel immer ausgedruckt hast und sie nicht nur mit Kommentaren, sondern auch mit zahlreichen motivierenden Zeichnungen korrigiert hast, und letztlich für die Zeit in Wageningen. Danke Nina und Roland für die Diskussionen in unseren Meetings. Ich verspreche, dass ich irgendwann mal die richtige Position des Semikolons lerne und sollte ich irgendwann einmal Hunde in Marburg vorhersagen, werde ich euch auf jeden Fall Bescheid geben.

Vielen Dank an das gesamte EarthShape – Projekt, alle Doktorand*Innen und PIs, und die Möglichkeit, Teil eines Großprojektes zu sein, die mich selbstbewusster und standhafter gemacht hat. Vor allem aber an die, die mir von Anfang an mit Rat, Zeit und Unterstützung beistanden. Großer Dank geht an Kirstin, Liesbeth und zahlreiche Mitarbeiter von CONAF, die bei der Datengewinnung und Feldarbeit eine große Unterstützung waren. Sehr großer Dank an Sebastian A., für deine Geduld und Zeit, vor allem in meinem ersten Jahr. Ebenfalls möchte ich mich bei meinen Hiwis Alex, Robin und Jadzia bedanken, da ohne eure Zuarbeit mein Workload noch viel enormer wäre. Danke für unsere zahlreichen „Arbeitstreffen“ im Café Wertvoll, das zu unserem Stammlokal geworden ist. Danke, Olga, für deine Mühen, Zeit, freundliches Empfangen und Motivation während meiner Zeit im Labor. Für das Girl' Day, das doch anders als geplant gelaufen ist. Aber vor allem dafür, dass ich dank dir an die Zeit im Labor rückblickend als die schönsten Monate meiner Promotionszeit zurückblicke.

Ich möchte mich sehr bei meiner AG LCRS bedanken, für die Zeit bei euch, die leider durch Corona und home office sehr verkürzt wurde. Ich freue mich sehr, dass die Treffen im letzten Jahr wieder erlebt wurden und für unsere gemeinsamen Mittagessen. Danke an Nazli, Michaela, Christina, Linda, Chrissi, Oliver, Marius, Sheetabh und Isabel für die gemeinsame Bestreitung des PhD-Weges. Danke an Maik für die Beantwortung der zahlreichen Technikfragen. Großen Dank geht auch an Birgit, für ihre Geduld und Hilfsbereitschaft, wenn ich mal mit den Anträgen und Formularen wieder einmal durcheinanderkam.

Da mit meiner Verteidigung auch ein besonderer Abschnitt in meinem Leben endet, nach dem ich die Studentenwelt verlasse, möchte ich mich auch bei denen bedanken, die meine persönliche Entwicklung in dieser Zeit geprägt haben.

Danke an die Uni Bonn, für die schönste und sorgloste Zeit in meinem Leben. Ebenfalls an Bernd Diekkrüger, Constanze Leemhuis und Geoffrey Gabiri, dass ich mit euch innerhalb von GlobE-Projekts mitarbeiten durfte und mich zum ersten Mal als richtige Wissenschaftlerin fühlte.

Ich möchte mich ebenfalls bei Christoph Reudenbach bedanken, der mir in unseren sporadischen, desto intensiven und lehrreichen Gesprächen sehr viel mitgegeben hat. Danke für deine Direktheit und für deine Denkanstöße, auch wenn ich für sie leider manchmal Tage bis Monate gebraucht habe, bis ich deren Sinn verstanden habe, aber von denen ich sehr viel ins weitere Leben mitnehmen werde.

Die Uni-Zeit wäre nichts wert, wenn man keine richtigen Freunde beiseite hätte. Danke Lenka, Alena, Anja, Morgan, Benedikt, Kalini, Ash, Enas und Janina, für die Spiel- und Kochabende, für die Photo-Challenges, für Picknicks und Pasta Parties, dass ihr meine Launen ertragen habt und mir immer beistanden. Es sind sehr viele kleine Momente, die sich damals als banal und unwichtig anfühlten, an die ich aber jetzt mit Melancholie und Dankbarkeit zurückblicke.

Einen besonders großen Dank schön möchte ich meinen Freunden, Kletterpartnern und Kursleitern aus dem Alpenverein aussprechen. Danke, Tony, Leon, Julian, Betty, Micha, Chris, Matze, Julia, Sönke, Franzi, Sina, Chrissi, Sophie, Nico und Alex für die unvergesslichen Momente von Cube, über Arco bis nach Finale, und für eure Geduld und Motivation, wenn mich meine Ängste an der Wand doch wieder eingeholt haben. Auch wenn es euch nicht bewusst ist, mit eurer Lebenseinstellung und Selbstverständlichkeit, mit der ihr das Klettern und Fliegen angeht, habt ihr die Grenzen des auch für mich je Vorstellbaren und Möglichen Schritt für Schritt erweitert und mein bisheriges Selbstbild in sehr positivem Sinne herausfordert. Ihr prägt mein Leben nachhaltig weit jenseits des Bergsports und ich bin sehr dankbar, letztes Jahr so viele Vorbilder gewonnen zu haben.

Ausgiebig möchte ich mich bei meiner Familie in der Slowakei bedanken. Danke, dass ihr die letzten 10 Jahre aus der Ferne an mich gedacht habt, mitgefiebert habt und in Gedanken immer bei mir wart. Ein großer Dank geht allerdings dabei vor allem an meine Eltern und meinen Bruder. Ich weiß, dass ihr manchmal wahrscheinlich nur zitternd gewartet habt, was den demnächst kommt, von lila Haaren und Skateboard, über meinen Umzug ins Ausland und Südafrika, über das Hofgarten-Fest in Bonn, bei dem ich diejenige mit dem besten Foto war, weil nur ihr wusstet, wo man sich bei Hüte werfen hinstellen soll, bis zur Chile, Klettern und Paragliding. Danke für die enorme Unterstützung seit meiner Kindheit, den Glauben an meine Träume und die gegebene Freiheit mich zu erkunden.

Mein letzter Dank geht an Philipp, dessen Leben sich die letzten vier Jahre um Bodenwühler gedreht hat und der wohl schon der Experte in dem Thema ist. Vielen Dank, dass du dir seit Jahren meine endlosen Monologe über meine Begeisterungsthemen anhörst, meine Beschwerden aushältst ohne selber ins Beschwerdemodus zu kommen, dass du für mich das Klettern und meine anderen Leidenschaften ausprobierst und mitmachst. Aber vor allem dafür, dass ich bei dir ich selbst sein kann, dass wir uns verstehen, auch ohne etwas sagen zu müssen, und dass wir uns doch in genau den richtigen Gegensätzen vervollständigen.

1. Introduction

Erosion leads to on-site sediment loss and increased sediment accumulation downstream, hinders runoff ways, which increases potentials for flooding, decreases reservoir capacity, degrades water quality, and on long-term influences soil productivity and weathering (Xiong et al., 2019; Anache et al., 2017; García-Ruiz et al., 2017). Erosion rates were observed to be increasing across landscapes and climate zones. (Borrelli et al., 2021; Li and Zhang, 2001) and due to its heavy impacts, it is thus of importance to understand the drivers of erosions.

One of the major local biotic factors influencing erosion is the burrowing activity of terrestrial bioturbators (Gabet et al., 2003). Previous studies showed that bioturbation affects microtopography (Reichman and Seabloom, 2002; Kinlaw and Grasmueck, 2012), roughness of the surface (Yair, 1995; Jones et al., 2010; Hancock and Lowry, 2021), and physical properties of the soil (Ridd, 1996; Yair, 1995; Hall et al., 1999; Reichman and Seabloom, 2002; Hancock and Lowry, 2021; Coombes, 2016; Larsen et al., 2021; Corenblit et al., 2021). Through the reworking of sediment, bioturbators increase soil permeability and porosity, leading to impacts on infiltration and erosion rates (Shipitalo and Le Bayon, 2004; Bowker et al., 2013; Wilkinson et al., 2009; Gabet et al., 2003; Nkem et al., 2000). The construction of underground burrows redistributes and concentrates nutrients (Platt et al., 2016; Zhang et al., 2020; Yu et al., 2017) and especially positively influences soil carbon storage (Frouz et al., 2009; Qin et al., 2021). These effects ultimately decrease the ratio of stable and unstable soil carbonate aggregates (Don et al., 2019).

Previous studies showed both, positive (Hazelhoff et al., 1981; Black and Montgomery, 1991; Chen et al., 2021) and negative impact of burrowing animals on sediment redistribution (Imeson and Kwaad, 1976; Hakonson, 1999). Increased bioturbation activity was observed with higher (Milstead et al., 2007; Meserve, 1981; Tews et al., 2004; Wu et al., 2021; Ferro and Barquez, 2009), as well as with lower vegetation cover (Simonetti, 1989; Zhang et al., 2020; Zhang et al., 2019; Qin et al., 2021). What is more, vertical soil mixing rates are not uniform throughout the year but depend on the animal phenological cycles (Eccard and Herde, 2013; Jimenez et al., 1992; Katzman et al., 2018; Malizia, 1998; Morgan and Duzant, 2008; Monteverde and Piudo, 2011; Gray et al., 2020; Yu et al., 2017). The habitat preferences of bioturbators were shown to be species dependent (Qin et al., 2021; Turnock et al., 2017; Tang et al., 2019; Tajik et al., 2020; Jacob, 2008) and were associated with cacti (Milstead et al., 2007) , herbs (Meserve, 1981) , grass or shrubs (Ferro and Barquez, 2009; Tews et al., 2004) , rocks (Simonetti, 1989) or increased diversity (Louw et al., 2019).

1.1 Research gap and motivation

Previous studies failed to address several significant issues. The studies concentrated only on the habitat preferences of the single bioturbator species. However, they did not consider varying amount of excavated sediment and burrow density between single species. It thus remains unclear which environmental parameters are mostly associated with high density and distribution of all present vertebrate bioturbators' burrows. Furthermore, previous studies did not address the daily excavation dynamics of the sediment by the animal, if and how it is connected to catchment-wide rainfall – driven sediment redistribution, and how much sediment the bioturbators excavate throughout the year to the surface.

What is more, previous studies estimating the impact of bioturbation on sediment redistribution were all case studies, concentrating on one animal species and several particular burrows. All of these studies failed to estimate the impacts of bioturbation on sediment redistribution in spatio-temporal context for the whole

catchment. For this, an area–wide estimation of sediment redistribution caused by the bioturbation at a very high resolution is needed but was never addressed.

Furthermore, it is unknown how these impacts differ along a climate gradient. Previous case studies came to contrasting results, showing both positive and negative influence of bioturbation on sediment redistribution. None of them addressed the question, how the impacts of bioturbation on sediment redistribution changes in the space throughout the catchment. Finally, it is also unknown, which environmental parameters drive these impacts.

It is of utmost importance to close the stated research gaps for several reasons. Only when the spatial distribution of burrows is known, we can estimate the magnitude of the sediment reworked and excavated to the surface by the animal. The ongoing excavation processes need to be monitored for the same reason on a very high spatial and temporal scale - as can assume that the burrow structures do not stay the same but change over time due to rainfall, expansion of the burrow by the animal or burrow abandonment. As this animal – driven sediment redistribution was shown to redistribute nutrients (Platt et al., 2016; Zhang et al., 2020; Yu et al., 2017) and especially positively influences soil carbon storage (Frouz et al., 2009; Qin et al., 2021), it is if urgent importance to accurately estimate the burrow distribution and excavation processes.

Secondly, bioturbation has significant impacts on soil properties and previous field-based case studies came to contrasting results regarding influence of bioturbation on sediment redistribution (Ridd, 1996; Yair, 1995; Hall et al., 1999; Reichman and Seabloom, 2002; Hancock and Lowry, 2021; Coombes, 2016; Larsen et al., 2021; Corenblit et al., 2021). It can be thus assumed that bioturbation will have a significant impact on catchment-wide surface processes. This might affect habitats, influence weathering processes and shape the landforms on long-term. It is thus out of importance to estimate the role of bioturbation on daily sediment redistribution to provide better understanding of its contributions to these processes. Due to varying precipitation patterns, soil properties and vegetation coverage, the impacts must be estimated separately for each climate zone. Finally, it is important to know what drives the positive or negative impact of bioturbation on sediment redistribution to be able to upscale the results toward large spatial and temporal scales.

1.1 Previously applied methods

Previous studies failed to address the stated research gap in the interplays between bioturbation, sediment redistribution and environment. This reason for this was the insufficiency of applied methods to comprehend spatial and temporal variations in sediment redistribution caused by the animals.

First, methods to estimate density of burrows were mostly labour-intensive in-situ measurements (Übernickel et al. 2019). Remote sensing offers here a more practical approach, as it provides opportunities for effective area-wide spatial estimates. Previous studies used UAVs to directly map the burrows and mounds created by burrowing animals by using image segmentation (Sandino et al., 2017) or classification approaches (Bycroft et al., 2019; Old et al., 2019; Albores-Barajas et al., 2018; Tang et al., 2019). All of these studies were conducted in areas where the burrows were directly recognizable on images. However, the approaches heavily underestimated the amount of burrows and the detection success predominantly depended on the vegetation density and height (Old et al., 2019).

In cases where the burrows were partly or completely overlaid by vegetation, solely the habitats populated by bioturbators were delineated. Remotely sensed estimated vegetation height and volume have previously been

used as predictors to delineate vertebrate habitats (Olsoy et al., 2018). Similarly, land cover classification derived from satellite images was used to predict animal distribution (Fritz et al., 2018; Szantoi et al., 2017) or population sizes (Guo et al., 2012). Furthermore, texture metrics and diversity indices were shown to be suitable for predictions of species richness or habitat structures in diverse ecosystems (St-Louis et al., 2006; Culbert et al., 2012; Wallis et al., 2017; Gholizadeh et al., 2018). In these cases, MaxEnt models (Koshkina et al., 2020) based on vegetation (Young et al., 2017) or topographic predictors (Borgatti et al., 2017) were used. Thus, none of the previous studies estimated density and distribution of burrows in areas with dense with vegetation canopy.
Effects of bioturbators on sediment redistribution were mostly measured using rainfall simulators. Previous authors estimated the volume of sediment excavated by the animal or set up instruments such as erosion pins, splash boards, or simple rulers in the field (Imeson and Kwaad, 1976; Reichman and Seabloom, 2002; Wei et al., 2007; Le Hir et al., 2007; Li et al., 2018; Li et al., 2019b; Li et al., 2019c; Voiculescu et al., 2019; Chen et al., 2021; Übernickel et al., 2021a; Li et al., 2019a). However, rainfall simulators were not capable to study redistribution processes under real life conditions. When using erosion pins or splash boards, the data were obtained only sporadically (Imeson and Kwaad, 1976; Hazelhoff et al., 1981; Richards and Humphreys, 2010).
To explain the soil mixing processes, box measurements were conducted and linked them with mathematical equations, such as random walks (Boudreau, 1986; Wheatcroft et al., 1990), stochastic differential equations (Boudreau, 1989; Milstead et al., 2007), finite difference mass balancing (Soetaert et al., 1996; François et al., 1997) or Markov chain theory (Jumars et al., 1981; Foster, 1985; Trauth, 1998; Shull, 2001).
High-resolution, ground-based monitoring techniques have the potential to address temporal and spatial variations of sediment redistribution caused by bioturbation. Terrestrial laser scanner systems are already broadly used for the estimation of sediment redistribution and erosion processes (Nasermoaddeli and Pasche, 2008; Afana et al., 2010; Eltner et al., 2016a; Eltner et al., 2016b; Longoni et al., 2016). Another high resolution surface monitoring technique is based on Time-of-Flight (ToF) technology. ToF-based cameras illuminate the targeted object with a light source for a known amount of time and then estimate the distance between the camera and the object by measuring the time needed for the reflected light to reach the camera sensor (Sarbolandi et al., 2018). This approach would thus enable to cost-effectively monitor surface change at a high resolution (Eitel et al., 2011; Hänsel et al., 2016), however, it was never tested before.
An approach to estimate catchment-wide impacts of bioturbation on sediment redistribution offer raster-based models. Most process models do not yet implement impacts of bioturbators on sediment redistribution in their algorithms (Brosens et al., 2020; 121 Anderson et al., 2019; Braun et al., 2016; Cohen et al., 2015; Cohen et al., 2010; Carretier et al., 2014; 122 Welivitiya et al., 2019). Few models do consider bioturbation (Black and Montgomery, 1991; 104 Meysman et al., 2003; Yoo et al., 2005; Schiffers et al., 2011, (Temme and Vanwalleghem, 2016; Vanwalleghem et al., 2013; Yoo and Mudd, 2008; Pelletier et al., 2013).
However, all of these models are landscape evolution models, which intend to predict into thousands of years. Furthermore, the inclusion of bioturbation into modelling has severe limitations: (i) models include vertical soil mixing caused by invertebrates but not burrow structures caused by vertebrate bioturbators; (ii) bioturbation is always precoded to be positively associated with vegetation cover, although field-base studies show positive and negative association of bioturbation with vegetation; (iii) bioturbation is precoded to increase erosion which makes all of the models incapable to study impact of bioturbation on soil erosion. Thus, none of these models consider that the interaction of bioturbation with environmental parameters and the effect on sediment

redistribution may not be uniform but context dependent. To really comprehend the dynamics between bioturbation, sediment redistribution and environment, a model including bioturbation as an independent variable, which is capable to predict the processes at a very high spatial and temporal resolution is needed, but missing.

2. Conceptual design of the thesis

2.1 Hypothesis

To close the stated research gaps and estimate the interplay between bioturbation, sediment redistribution and environment, the aims of my thesis were thus to:

A1: Predict the density of burrows from vegetation patterns.

A2: Monitor animal-triggered sediment redistribution at a very high temporal and spatial scale and estimate their spatial-wide impact on sediment redistribution.

A3: Identify environmental parameters which determine the magnitude of the burrow' impact on redistribution.

To fulfil the aims, I applied following approaches:

M1: Machine-learning to test the predictability of burrow density from remotely sensed vegetation patterns.

M2: High resolution Time-of-Flight cameras for surface monitoring.

M3: Including burrow structures created by bioturbating animals into a soil erosion model.

I tested following hypothesis:

H1: Distribution of burrows created by bioturbating animals depends on vegetation patterns.

H2: Bioturbators-driven sediment redistribution depends on rainfall-driven redistribution.

H3: Surrounding environment determines the magnitude of the burrow' impact on redistribution.

H4: Presence of burrows created by bioturbators increases sediment redistribution.

2.2 Study area

My thesis was part of EarthShape consortium (DFG SPP 1803) with the overarching research question how the microorganisms, animals, and plants influence the shape and development of the Earth's surface.

The study was performed within four study sites along Chilean Coastal Cordillera preselected by the consortium: Pan de Azúcar (PdA) National Park (NP), Santa Gracia (SG), La Campana (LC) NP, and Nahuelbuta (NA) NP (Figure 2.1). The reason for the selection of these site were similarities regarding topography, rock types and distance to the coast (Übernickel et al., 2021c). Each study site consisted of one north-facing and one south-facing catchment.

PdA is located in the arid climate zone in the southern part of the Atacama Desert, with almost no rainfall. The vegetation cover is less than 5 % and dominated by desert shrubs, cacti and biocrusts (Lehnert et al., 2018). SG is a natural reserve located in the semi-arid climate zone near La Serena. Vegetation consists of shrubs and cacti, which cover up to 40 % of the surface. LC is in the Mediterranean climate zone in the Valparaiso Region and is affected by cattle. The study site is dominated by an evergreen sclerophyllous forest with endemic palms and understory consisting of deciduous shrubs and herbs. NA is in the humid-temperate climate zone

and is characterized by a dense evergreen *Araucaria* Forest. The ground is covered by bamboo, shrubs, and herbs (Bernhard et al., 2018; Oeser et al., 2018).

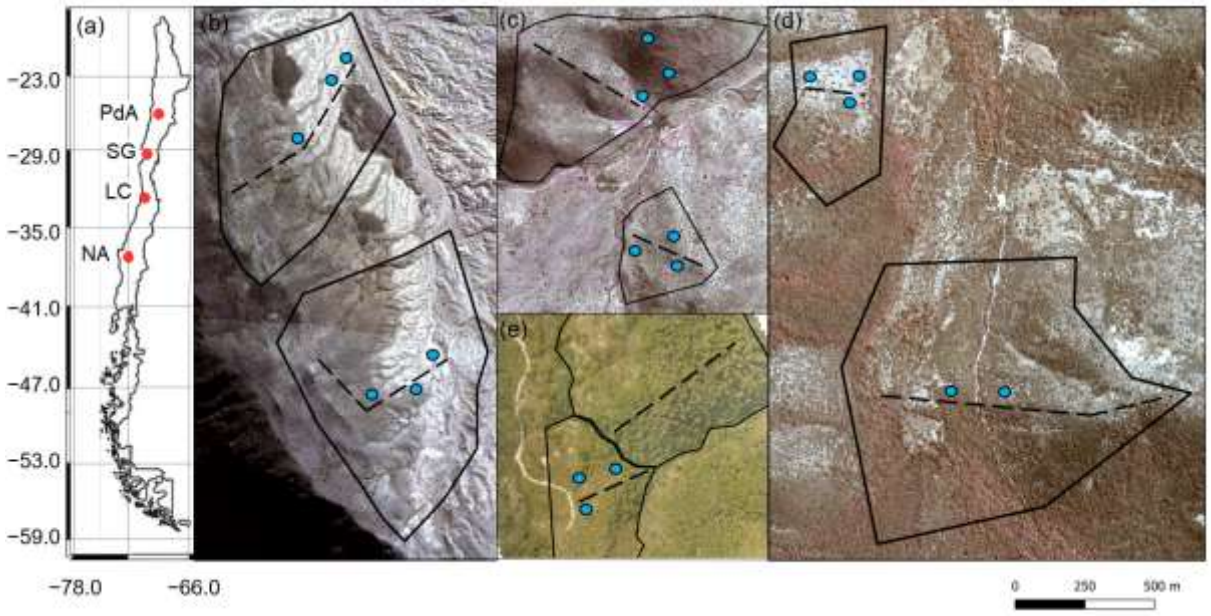

Figure 2.1. Study area and study sites. Black solid lines outline the catchments. Black dashed lines symbolize the catena, along which the in-situ data (burrow locations, soil samples, vegetation) were collected. The blue circles are the positions of sediment fences. 3 fences were located on each hillside: on the upper, middle and lower part of the hillside. Time-of-Flight cameras were located ultimately uphill on the fences on the upper and middle part of the catchment. 80 plots were located randomly around the catena. (a) Position of the study sites along the climate gradient. PdA = Pan de Azúcar, SG = Santa Gracia, LC = La Campana, NA = Nahuelbuta. (b) PdA; (c) SG; (d) LC; and (e) NA. The background image is an RGB-composite calculated from WorldView-2 satellite imagery. Images were obtained with a single license from GAF AG.

2.3 Bioturbators in Chile

There are at least 45 vertebrate and over 300 invertebrate burrowing species in Chile (Übernickel et al., 2021b). The most common vertebrate burrowing animals are in PdA carnivores (*Lycalopex culpaeus*, *Lycalopex griseus*); marsupials (*Didelphis marsupialis*, *Didelphis albiventris*) and rodents (*Phyllotis xanthopygus*, *Phyllotis limatus*, *Abrothrix andinus*) (Jimenez et al., 1992; Cerqueira, 1985); in SG marsupials (*Thylamys elegans*) and rodents (*Phyllotis darwini*, *Abrothrix olivaceus*, *Octodon degus*, *Abrocoma bennetti*, *Rattus rattus*) (Milstead et al., 2007); in LC and NA rodents (*Octodon degus*, *Rattus norvegicus and Phyllotis darwini*) and carnivores (*Lycalopex griseus*) (Muñoz-Pedreros et al., 2018) (Figure 2.2)

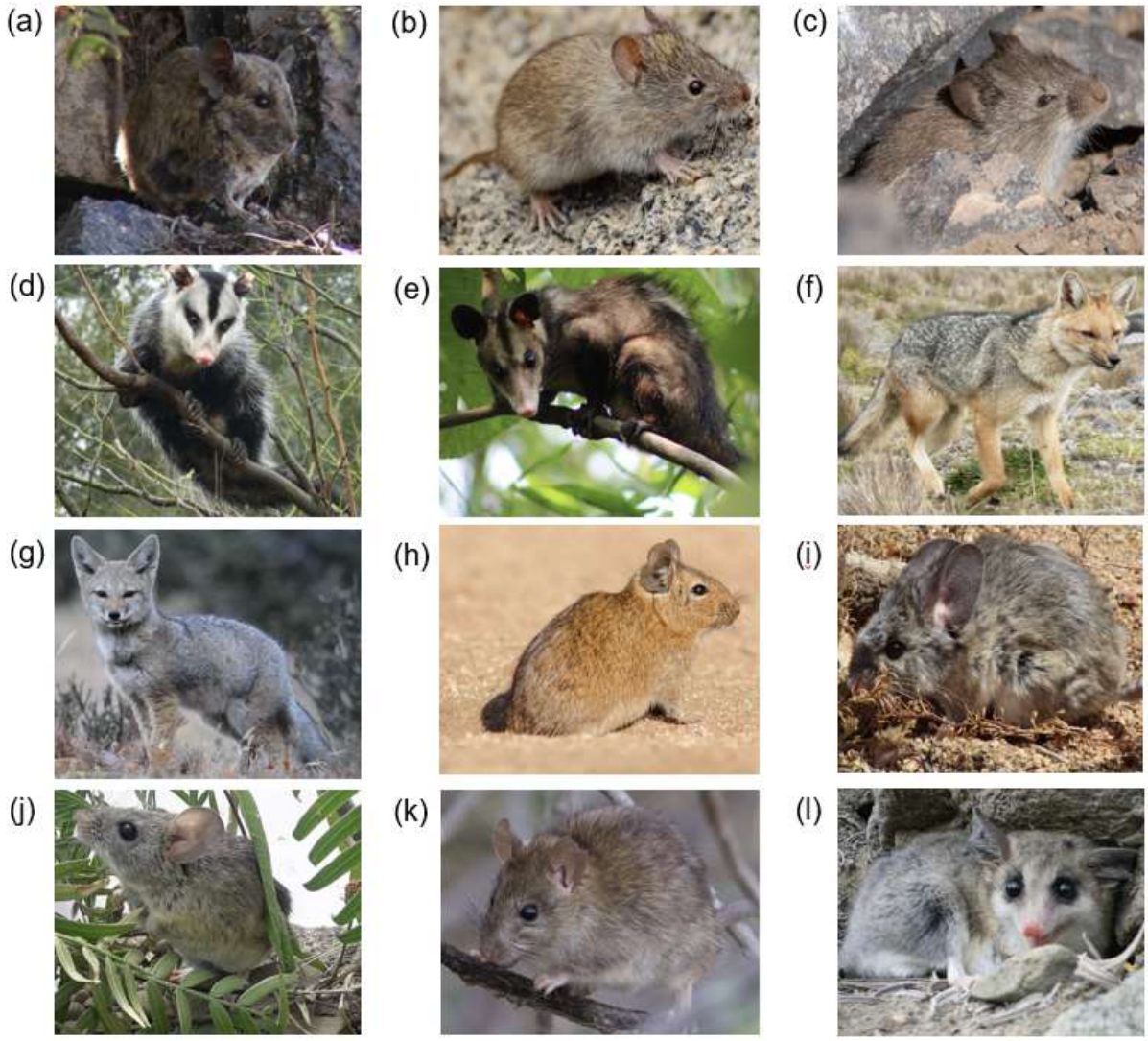

Figure 2.2. Burrowing vertebrate animals found in Chile. (a) *Abrocoma bennetti*, (b) *Abrothrix olivaceus*, (c) *Abrothrix andinus*, (d) *Didelphis albiventris*, (e) *Didelphis marsupialis*, (f) *Lycalopex culpaeus*, (g) *Lycalopex griseus*, (h) *Octodon degu*, (i) *Phyllotis darwinii*, (j) *Phyllotis xanthopygus*, (k) *Rattus rattus*, (l) *Thylamys elegans*. Source: https://inaturalist.mma.gob.cl/

2.4 Workflow

The workflow consisted of 3 working packages with the final goal to estimate catchment-wide impacts of bioturbation (Figure 2.3).

WP1: Within the first working package, I tested the H1, concretely, if the distribution of burrows created by bioturbating animals depends on vegetation structures. I tested if the density of the burrows and burrow distribution and be predicted by vegetation patterns estimated from UAV and WorldView-2 data. I then used the best model for a catchment-wide prediction. The processing is described in sections 3 and 5.

WP2: Within the second working package, I tested the hypothesis H2, saying that bioturbator-driven sediment redistribution depends on rainfall-driven sediment redistribution. For this, I set up several Time-of-Flight based cameras monitoring the sediment redistribution on the burrow surface and around the burrow. I estimated (i) sediment excavation rates by the animal during monitoring period (bioturbator-driven redistribution); (ii)

Sediment redistribution during rainfall events (rainfall-driven redistribution); (iii) if the bioturbator-driven redistribution depends on rainfall driven redistribution. The processing is described in section 4.

WP3: Within the third working package, I tested the H3, saying that surrounding environment determines the magnitude of the burrow' impact on redistribution; as well as H4, presence of burrows created by bioturbating animals increases sediment redistribution. I first included bioturbation into a soil erosion model. For the inclusion, I used the catchment-wide prediction of burrow distribution from WP1 and the findings about the dependency between bioturbators-driven and rainfall-driven redistribution from WP2. The processing is described in section 5.

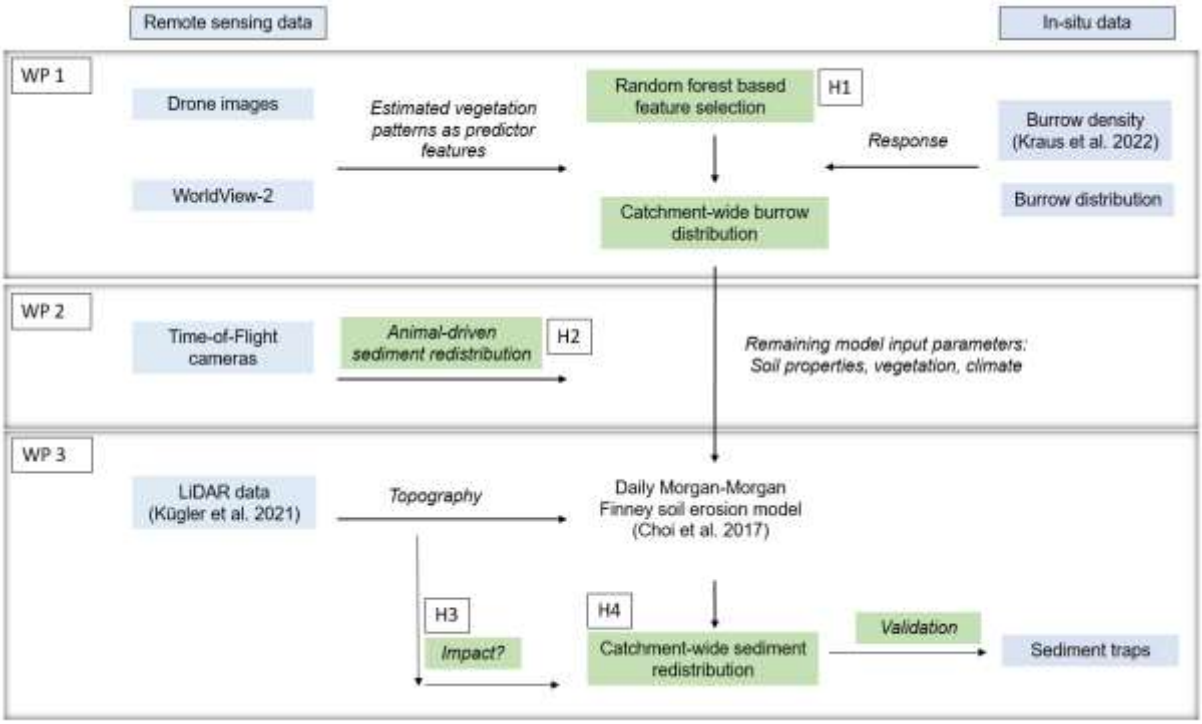

Figure 1.3. Workflow of this thesis. Blue indicates remote sensing and in-situ datasets. Green indicates results. WP are working packages. H indicates results which confirm or reject a hypothesis.

2.5 Data used in this study

For the WP1, I needed in-situ measured density and distribution of burrows, as well as UAV and WorldView-2 data to estimate vegetation patterns and for the WP2, I needed several Time-Flight cameras. To parametrize the soil erosion model within WP3, I used the results from WP1 and WP2. Additionally, I needed to estimate soil properties, vegetation cover and topography of the catchment. To run the model, I needed to know daily precipitation and temperature. To validate the model, I needed to collect sediment redistributed in-situ.

I collected needed in-situ data during a field campaign from September until November 2019 within plots and along a catena (Table 2.1). For catena measurements, I defined a line with a width of one meter from the top to the base of each hillside catchment. I subdivided the track into tiles of 1 m^2 and saved the GPS information of each tile. Additionally, I used 10 plots per catchment with a size of 10 m × 10 m. The plots were dispersed randomly and the distance between the plots was at least 20 m.

Along the catena, I mapped the locations of burrows, estimated the land cover and extracted soil samples. I noted the size of the burrow, vegetation cover and land cover types (bare soil, herbs, shrubs, trees) and I extracted 162 soil samples. From the plots, I used the information on the density of burrows (Kraus et al. 2022) soil samples from mounds created by bioturbators (Kraus et al. 2023); and I mapped the vegetation coverage and type.

Furthermore, I set up sediment traps, with six traps per site, two of which were located at the catchment base and four were located on two random positions within the catchment. The sediment traps consisted of geotextile vertically attached to wooden poles to enable the collection of sediment. The traps had a length of 2 m – 5 m, a width of ~1.5 m and a height of ~1 m. I retrieved the climate information from our project-internal climate stations, located within a short distance to our catchments (Lehnert et al., 2018; Übernickel et al., 2020).

Table 2.1. In-situ data used in this study. Response means, I used this data as a response variable within a machine-learning model to predict the variable into the area. Parameter means, I used this data as one of the model input parameters. Validation means, I used this data for the validation of my model.

Measure	Sampling strategy	Data	Number	Purpose for study	Working package
Burrows	Catena	Presence or absence	845	Response	1
	Plots	Density (Kraus et al. 2022)	80	Response	1
Vegetation	Catena	Type	845	Response	3
	Plots	Density, cover, type, size	80	Response	1
Soil samples	Catena	Soil properties Photo of the surface	162	Response	3
	Plots	Soil properties (Kraus et al. 2023)	151	Parameter	3
Sediment fences	Catena	Eroded sediment	21	Validation	3
Climate station	One per site	Climate information (Übernickel et al. 2021)	4	Parameter	3

I conducted UAV flights during the same field campaign from September to November 2019. I used a 3D Robotics SOLO quadrocopter equipped with a GoPRO Hero 4 Black RGB camera. The digital elevation models (DEM) were calculated from the LiDAR data (Kügler et al., 2022; Horn, 1981) at a resolution of 0.5 m. Single license stereo WorldView-2 images with a resolution of 0.5 m were retrieved from GAF Munich GmbH. Lastly, 21 Time-of-Flight based cameras were installed in March 2019 to monitor the burrows. The monitoring took place for seven months, and I collected the data in October 2019 (Table 2.2).

Table 2.2. Remote sensing data used in this study. Predictor means, I used this data as a response variable within a machine-learning model to predict the variable into the area. Parameter means, I used this data as one of the model input parameters. Monitoring means, I used this data for direct monitoring of redistribution.

Remote sensing data	Platform	Resolution	Coverage	Purpose for study	Working package
Orthophotos	UAV	2.3 cm	catchments	Predictor	1
WorldView-2	Airborne	0.5 m	catchments	Predictor	1
Time-Of-Flight	Cameras	0.3 cm	burrows	Monitoring	2
LiDAR	Airborne	0.5 m	catchments	Parameter	3

References

Afana, A., Solé-Benet, A., and Pérez, J. L.: Determination of Soil Erosion Using Laser Scanners, last access: 22 December 2021, 2010.

Albores-Barajas, Y. V., Soldatini, C., Ramos-Rodríguez, A., Alcala-Santoyo, J. E., Carmona, R., and Dell'Omo, G.: A new use of technology to solve an old problem: Estimating the population size of a burrow nesting seabird, PloS one, 13, e0202094, https://doi.org/10.1371/journal.pone.0202094, 2018.

Anache, J. A.A., Wendland, E. C., Oliveira, P. T.S., Flanagan, D. C., and Nearing, M. A.: Runoff and soil erosion plot-scale studies under natural rainfall: A meta-analysis of the Brazilian experience, CATENA, 152, 29–39, https://doi.org/10.1016/j.catena.2017.01.003, 2017.

Bernhard, N., Moskwa, L.-M., Schmidt, K., Oeser, R. A., Aburto, F., Bader, M. Y., Baumann, K., Blanckenburg, F. von, Boy, J., van den Brink, L., Brucker, E., Büdel, B., Canessa, R., Dippold, M. A., Ehlers, T. A., Fuentes, J. P., Godoy, R., Jung, P., Karsten, U., Köster, M., Kuzyakov, Y., Leinweber, P., Neidhardt, H., Matus, F., Mueller, C. W., Oelmann, Y., Oses, R., Osses, P., Paulino, L., Samolov, E., Schaller, M., Schmid, M., Spielvogel, S., Spohn, M., Stock, S., Stroncik, N., Tielbörger, K., Übernickel, K., Scholten, T., Seguel, O., Wagner, D., and Kühn, P.: Pedogenic and microbial interrelations to regional climate and local topography: New insights from a climate gradient (arid to humid) along the Coastal Cordillera of Chile, CATENA, 170, 335–355, https://doi.org/10.1016/j.catena.2018.06.018, 2018.

Black, T. A. and Montgomery, D. R.: Sediment transport by burrowing mammals, Marin County, California, Earth Surf. Process. Landforms, 16, 163–172, https://doi.org/10.1002/esp.3290160207, 1991.

Borgatti, L., Forte, E., Mocnik, A., Zambrini, R., Cervi, F., Martinucci, D., Pellegrini, F., Pillon, S., Prizzon, A., and Zamariolo, A.: Detection and characterization of animal burrows within river embankments by means of coupled remote sensing and geophysical techniques: Lessons from River Panaro (northern Italy), Engineering Geology, 226, 277–289, https://doi.org/10.1016/j.enggeo.2017.06.017, 2017.

Borrelli, P., Alewell, C., Alvarez, P., Anache, J. A. A., Baartman, J., Ballabio, C., Bezak, N., Biddoccu, M., Cerdà, A., Chalise, D., Chen, S., Chen, W., Girolamo, A. M. de, Gessesse, G. D., Deumlich, D., Diodato, N., Efthimiou, N., Erpul, G., Fiener, P., Freppaz, M., Gentile, F., Gericke, A., Haregeweyn, N., Hu, B., Jeanneau,

A., Kaffas, K., Kiani-Harchegani, M., Villuendas, I. L., Li, C., Lombardo, L., López-Vicente, M., Lucas-Borja, M. E., Märker, M., Matthews, F., Miao, C., Mikoš, M., Modugno, S., Möller, M., Naipal, V., Nearing, M., Owusu, S., Panday, D., Patault, E., Patriche, C. V., Poggio, L., Portes, R., Quijano, L., Rahdari, M. R., Renima, M., Ricci, G. F., Rodrigo-Comino, J., Saia, S., Samani, A. N., Schillaci, C., Syrris, V., Kim, H. S., Spinola, D. N., Oliveira, P. T., Teng, H., Thapa, R., Vantas, K., Vieira, D., Yang, J. E., Yin, S., Zema, D. A., Zhao, G., and Panagos, P.: Soil erosion modelling: A global review and statistical analysis, The Science of the total environment, 780, 146494, https://doi.org/10.1016/j.scitotenv.2021.146494, 2021.

Boudreau, B. P.: Mathematics of tracer mixing in sediments; I, Spatially-dependent, diffusive mixing, American Journal of Science, 286, 161–198, https://doi.org/10.2475/ajs.286.3.161, 1986.

Boudreau, B. P.: The diffusion and telegraph equations in diagenetic modelling, Geochimica et Cosmochimica Acta, 53, 1857–1866, https://doi.org/10.1016/0016-7037(89)90306-2, 1989.

Bowker, M. A., Eldridge, D. J., Val, J., and Soliveres, S.: Hydrology in a patterned landscape is co-engineered by soil-disturbing animals and biological crusts, Soil Biology and Biochemistry, 61, 14–22, https://doi.org/10.1016/j.soilbio.2013.02.002, 2013.

Bycroft, R., Leon, J. X., and Schoeman, D.: Comparing random forests and convoluted neural networks for mapping ghost crab burrows using imagery from an unmanned aerial vehicle, Estuarine, Coastal and Shelf Science, 224, 84–93, https://doi.org/10.1016/j.ecss.2019.04.050, 2019.

Cerqueira, R.: The Distribution of Didelphis in South America (Polyprotodontia, Didelphidae), Journal of Biogeography, 12, 135, https://doi.org/10.2307/2844837, 1985.

Chen, M., Ma, L., Shao, M.'a., Wei, X., Jia, Y., Sun, S., Zhang, Q., Li, T., Yang, X., and Gan, M.: Chinese zokor (Myospalax fontanierii) excavating activities lessen runoff but facilitate soil erosion – A simulation experiment, CATENA, 202, 105248, https://doi.org/10.1016/j.catena.2021.105248, 2021.

Coombes, M. A.: Biogeomorphology: diverse, integrative and useful, Earth Surf. Process. Landforms, 41, 2296–2300, https://doi.org/10.1002/esp.4055, 2016.

Corenblit, D., Corbara, B., and Steiger, J.: Biogeomorphological eco-evolutionary feedback between life and geomorphology: a theoretical framework using fossorial mammals, Die Naturwissenschaften, 108, 55, https://doi.org/10.1007/s00114-021-01760-y, 2021.

Culbert, P. D., Radeloff, V. C., St-Louis, V., Flather, C. H., Rittenhouse, C. D., Albright, T. P., and Pidgeon, A. M.: Modeling broad-scale patterns of avian species richness across the Midwestern United States with measures of satellite image texture, Remote Sensing of Environment, 118, 140–150, https://doi.org/10.1016/j.rse.2011.11.004, 2012.

Don, A., Hagen, C., Grüneberg, E., and Vos, C.: Simulated wild boar bioturbation increases the stability of forest soil carbon, Biogeosciences, 16, 4145–4155, https://doi.org/10.5194/bg-16-4145-2019, 2019.

Eccard, J. A. and Herde, A.: Seasonal variation in the behaviour of a short-lived rodent, BMC ecology, 13, 43, https://doi.org/10.1186/1472-6785-13-43, 2013.

Eitel, J. U.H., Williams, C. J., Vierling, L. A., Al-Hamdan, O. Z., and Pierson, F. B.: Suitability of terrestrial laser scanning for studying surface roughness effects on concentrated flow erosion processes in rangelands, CATENA, 87, 398–407, https://doi.org/10.1016/j.catena.2011.07.009, 2011.

Eltner, A., Schneider, D., and Maas, H.-G.: Integrated processing of high resolution topographic data for soil erosion assessment considering data acquisition schemes and surface properties, Int. Arch. Photogramm. Remote Sens. Spatial Inf. Sci., XLI-B5, 813–819, https://doi.org/10.5194/isprsarchives-XLI-B5-813-2016, 2016a.

Eltner, A., Kaiser, A., Castillo, C., Rock, G., Neugirg, F., and Abellán, A.: Image-based surface reconstruction in geomorphometry – merits, limits and developments, Earth Surf. Dynam., 4, 359–389, https://doi.org/10.5194/esurf-4-359-2016, 2016b.

Ferro, L. I. and Barquez, R. M.: Species Richness of Nonvolant Small Mammals Along Elevational Gradients in Northwestern Argentina, Biotropica, 41, 759–767, https://doi.org/10.1111/j.1744-7429.2009.00522.x, 2009.

Foster, D. W.: BIOTURB: A FORTRAN program to simulate the effects of bioturbation on the vertical distribution of sediment, Computers & Geosciences, 11, 39–54, https://doi.org/10.1016/0098-3004(85)90037-8, 1985.

François, F., Poggiale, J.-C., Durbec, J.-P., and Stora, G.: A New Approach for the Modelling of Sediment Reworking Induced by a Macrobenthic Community, Acta Biotheoretica, 45, 295–319, https://doi.org/10.1023/A:1000636109604, 1997.

Fritz, A., Li, L., Storch, I., and Koch, B.: UAV-derived habitat predictors contribute strongly to understanding avian species-habitat relationships on the Eastern Qinghai-Tibetan Plateau, Remote Sens Ecol Conserv, 4, 53–65, https://doi.org/10.1002/rse2.73, 2018.

Frouz, J., Pižl, V., Cienciala, E., and Kalčík, J.: Carbon storage in post-mining forest soil, the role of tree biomass and soil bioturbation, Biogeochemistry, 94, 111–121, https://doi.org/10.1007/s10533-009-9313-0, 2009.

Gabet, E. J., Reichman, O. J., and Seabloom, E. W.: The Effects of Bioturbation on Soil Processes and Sediment Transport, Annu. Rev. Earth Planet. Sci., 31, 249–273, https://doi.org/10.1146/annurev.earth.31.100901.141314, 2003.

García-Ruiz, J. M., Beguería, S., Lana-Renault, N., Nadal-Romero, E., and Cerdà, A.: Ongoing and Emerging Questions in Water Erosion Studies, Land Degrad. Dev., 28, 5–21, https://doi.org/10.1002/ldr.2641, 2017.

Gholizadeh, A., Žižala, D., Saberioon, M., and Borůvka, L.: Soil organic carbon and texture retrieving and mapping using proximal, airborne and Sentinel-2 spectral imaging, Remote Sensing of Environment, 218, 89–103, https://doi.org/10.1016/j.rse.2018.09.015, 2018.

Gray, H. J., Keen-Zebert, A., Furbish, D. J., Tucker, G. E., and Mahan, S. A.: Depth-dependent soil mixing persists across climate zones, Proceedings of the National Academy of Sciences of the United States of America, 117, 8750–8756, https://doi.org/10.1073/pnas.1914140117., 2020.

Guo, Z. G., Zhou, X. R., and Hou, Y.: Effect of available burrow densities of plateau pika (Ochotona curzoniae) on soil physicochemical property of the bare land and vegetation land in the Qinghai-Tibetan Plateau, Acta Ecologica Sinica, 32, 104–110, https://doi.org/10.1016/j.chnaes.2012.02.002, 2012.

Hakonson, T. E.: The Effects of Pocket Gopher Burrowing on Water Balance and Erosion from Landfill Covers, J. environ. qual., 28, 659–665, https://doi.org/10.2134/jeq1999.00472425002800020033x, 1999.

Hall, K., Boelhouwers, J., and Driscoll, K.: Animals as Erosion Agents in the Alpine Zone: Some Data and Observations from Canada, Lesotho, and Tibet, Arctic, Antarctic, and Alpine Research, 31, 436–446, https://doi.org/10.1080/15230430.1999.12003328, 1999.

Hancock, G. and Lowry, J.: Quantifying the influence of rainfall, vegetation and animals on soil erosion and hillslope connectivity in the monsoonal tropics of northern Australia, Earth Surf. Process. Landforms, 46, 2110–2123, https://doi.org/10.1002/esp.5147, 2021.

Hänsel, P., Schindewolf, M., Eltner, A., Kaiser, A., and Schmidt, J.: Feasibility of High-Resolution Soil Erosion Measurements by Means of Rainfall Simulations and SfM Photogrammetry, Hydrology, 3, 38, https://doi.org/10.3390/hydrology3040038, 2016.

Hazelhoff, L., van Hoof, P., Imeson, A. C., and Kwaad, F. J. P. M.: The exposure of forest soil to erosion by earthworms, Earth Surf. Process. Landforms, 6, 235–250, https://doi.org/10.1002/esp.3290060305, 1981.

Horn, B.K.P.: Hill shading and the reflectance map, Proc. IEEE, 69, 14–47, https://doi.org/10.1109/PROC.1981.11918, 1981.

Imeson, A. C. and Kwaad, F. J. P. M.: Some Effects of Burrowing Animals on Slope Processes in the Luxembourg Ardennes, Geografiska Annaler: Series A, Physical Geography, 58, 317–328, https://doi.org/10.1080/04353676.1976.11879941, 1976.

Jacob, J.: Response of small rodents to manipulations of vegetation height in agro-ecosystems, Integrative zoology, 3, 3–10, https://doi.org/10.1111/j.1749-4877.2008.00078.x, 2008.

Jimenez, J. E., Feinsinger, P., and Jaksi, F. M.: Spatiotemporal Patterns of an Irruption and Decline of Small Mammals in Northcentral Chile, Journal of Mammalogy, 73, 356–364, https://doi.org/10.2307/1382070, 1992.

Jones, C. G., Gutiérrez, J. L., Byers, J. E., Crooks, J. A., Lambrinos, J. G., and Talley, T. S.: A framework for understanding physical ecosystem engineering by organisms, Oikos, 119, 1862–1869, https://doi.org/10.1111/j.1600-0706.2010.18782.x, 2010.

Jumars, P. A., Nowell, A. R.M., and Self, R. F.L.: A simple model of flow—Sediment—Organism interaction, Marine Geology, 42, 155–172, https://doi.org/10.1016/0025-3227(81)90162-6, 1981.

Katzman, E. A., Zaytseva, E. A., Feoktistova, N. Y., Tovpinetz, N. N., Bogomolov, P. L., Potashnikova, E. V., and Surov, A. V.: Seasonal Changes in Burrowing of the Common Hamster (Cricetus cricetus L., 1758) (Rodentia: Cricetidae) in the City, PJE, 17, 251–258, https://doi.org/10.18500/1684-7318-2018-3-251-258, 2018.

Kinlaw, A. and Grasmueck, M.: Evidence for and geomorphologic consequences of a reptilian ecosystem engineer: The burrowing cascade initiated by the Gopher Tortoise, Geomorphology, 157-158, 108–121, https://doi.org/10.1016/j.geomorph.2011.06.030, 2012.

Koshkina, A., Grigoryeva, I., Tokarsky, V., Urazaliyev, R., Kuemmerle, T., Hölzel, N., and Kamp, J.: Marmots from space: assessing population size and habitat use of a burrowing mammal using publicly available satellite images, Remote Sens Ecol Conserv, 6, 153–167, https://doi.org/10.1002/rse2.138, 2020.

Kügler, M., Hoffmann, T. O., Beer, A. R., Übernickel, K., Ehlers, T. A., Scherler, D., and Eichel, J.: (LiDAR) 3D Point Clouds and Topographic Data from the Chilean Coastal Cordillera, 2022.

Larsen, A., Nardin, W., Lageweg, W. I., and Bätz, N.: Biogeomorphology, quo vadis? On processes, time, and space in biogeomorphology, Earth Surf. Process. Landforms, 46, 12–23, https://doi.org/10.1002/esp.5016, 2021.

Le Hir, P., Monbet, Y., and Orvain, F.: Sediment erodability in sediment transport modelling: Can we account for biota effects?, Continental Shelf Research, 27, 1116–1142, https://doi.org/10.1016/j.csr.2005.11.016, 2007.

Lehnert, L. W., Thies, B., Trachte, K., Achilles, S., Osses, P., Baumann, K., Schmidt, J., Samolov, E., Jung, P., Leinweber, P., Karsten, U., Büdel, B., and Bendix, J.: A Case Study on Fog/Low Stratus Occurrence at Las Lomitas, Atacama Desert (Chile) as a Water Source for Biological Soil Crusts, Aerosol Air Qual. Res., 18, 254-26, https://doi.org/10.4209/aaqr.2017.01.0021, 2018.

Li, G., Li, X., Li, J., Chen, W., Zhu, H., Zhao, J., and Hu, X.: Influences of Plateau Zokor Burrowing on Soil Erosion and Nutrient Loss in Alpine Meadows in the Yellow River Source Zone of West China, Water, 11, 2258, https://doi.org/10.3390/w11112258, 2019a.

Li, T. C., Shao, M. A., Jia, Y. H., Jia, X. X., Huang, L. M., and Gan, M.: Small-scale observation on the effects of burrowing activities of ants on soil hydraulic processes, Eur J Soil Sci, 70, 236–244, https://doi.org/10.1111/ejss.12748, 2019b.

Li, T., Jia, Y., Shao, M.'a., and Shen, N.: Camponotus japonicus burrowing activities exacerbate soil erosion on bare slopes, Geoderma, 348, 158–167, https://doi.org/10.1016/j.geoderma.2019.04.035, 2019c.

Li, T., Shao, M.'a., Jia, Y., Jia, X., and Huang, L.: Small-scale observation on the effects of the burrowing activities of mole crickets on soil erosion and hydrologic processes, Agriculture, Ecosystems & Environment, 261, 136–143, https://doi.org/10.1016/j.agee.2018.04.010, 2018.

Li, Z. and Zhang, J.: Calculation of Field Manning's Roughness Coefficient, Agricultural Water Management, 49, 153–161, https://doi.org/10.1016/S0378-3774(00)00139-6, 2001.

Longoni, L., Papini, M., Brambilla, D., Barazzetti, L., Roncoroni, F., Scaioni, M., and Ivanov, V.: Monitoring Riverbank Erosion in Mountain Catchments Using Terrestrial Laser Scanning, Remote Sensing, 8, 241, https://doi.org/10.3390/rs8030241, 2016.

Louw, M. A., Haussmann, N. S., and Le Roux, P. C.: Testing for consistency in the impacts of a burrowing ecosystem engineer on soil and vegetation characteristics across biomes, Scientific reports, 9, 19355, https://doi.org/10.1038/s41598-019-55917-x, 2019.

Malizia, A. I.: Population dynamics of the fossorial rodent Ctenomys talarum (Rodentia: Octodontidae), Journal of Zoology, 244, 545–551, https://doi.org/10.1111/j.1469-7998.1998.tb00059.x, 1998.

Meserve, P. L.: Trophic Relationships among Small Mammals in a Chilean Semiarid Thorn Scrub Community, Journal of Mammalogy, 62, 304–314, https://doi.org/10.2307/1380707, 1981.

Milstead, W. B., Meserve, P. L., Campanella, A., Previtali, M. A., Kelt, D. A., and Gutiérrez, J. R.: Spatial Ecology of Small Mammals in North-central Chile: Role of Precipitation and Refuges, Journal of Mammalogy, 88, 1532–1538, https://doi.org/10.1644/16-MAMM-A-407R.1, 2007.

Monteverde, M. J. and Piudo, L.: Activity Patterns of the Culpeo Fox (Lycalopex Culpaeus Magellanica) in a Non-Hunting Area of Northwestern Patagonia, Argentina, Mammal Study, 36, 119–125, https://doi.org/10.3106/041.036.0301, 2011.

Morgan, R. P. C. and Duzant, J. H.: Modified MMF (Morgan–Morgan–Finney) model for evaluating effects of crops and vegetation cover on soil erosion, Earth Surf. Process. Landforms, 33, 90–106, https://doi.org/10.1002/esp.1530, 2008.

Muñoz-Pedreros, A., Yáñez, J., Norambuena, H. V., and Zúñiga, A.: Diet, dietary selectivity and density of South American grey fox, Lycalopex griseus, in Central Chile, Integrative zoology, 13, 46–57, https://doi.org/10.1111/1749-4877.12260, 2018.

Nasermoaddeli, M. B. and Pasche, E.: Application of terrestrial 3D scanner in quantification of the riverbank erosion and deposition, https://www.tuhh.de/t3resources/wb/Publikationen/MA-Veroeffentlichungen/nasermoaddelli/riverflow2008.pdf, last access: 22 December 2021, 2008.

Nkem, J. N., Lobry de Bruyn, L. A., Grant, C. D., and Hulugalle, N. R.: The impact of ant bioturbation and foraging activities on surrounding soil properties, Pedobiologia, 44, 609–621, https://doi.org/10.1078/S0031-4056(04)70075-X, 2000.

Oeser, R. A., Stroncik, N., Moskwa, L.-M., Bernhard, N., Schaller, M., Canessa, R., van den Brink, L., Köster, M., Brucker, E., Stock, S., Fuentes, J. P., Godoy, R., Matus, F. J., Oses Pedraza, R., Osses McIntyre, P., Paulino, L., Seguel, O., Bader, M. Y., Boy, J., Dippold, M. A., Ehlers, T. A., Kühn, P., Kuzyakov, Y., Leinweber, P., Scholten, T., Spielvogel, S., Spohn, M., Übernickel, K., Tielbörger, K., Wagner, D., and Blanckenburg, F. von: Chemistry and microbiology of the Critical Zone along a steep climate and vegetation gradient in the Chilean Coastal Cordillera, CATENA, 170, 183–203, https://doi.org/10.1016/j.catena.2018.06.002, 2018.

Old, J. M., Lin, S. H., and Franklin, M. J. M.: Mapping out bare-nosed wombat (Vombatus ursinus) burrows with the use of a drone, BMC ecology, 19, 39, https://doi.org/10.1186/s12898-019-0257-5, 2019.

Olsoy, P. J., Shipley, L. A., Rachlow, J. L., Forbey, J. S., Glenn, N. F., Burgess, M. A., and Thornton, D. H.: Unmanned aerial systems measure structural habitat features for wildlife across multiple scales, Methods Ecol Evol, 9, 594–604, https://doi.org/10.1111/2041-210X.12919, 2018.

Pelletier, J. D., Barron-Gafford, G. A., Breshears, D. D., Brooks, P. D., Chorover, J., Durcik, M., Harman, C. J., Huxman, T. E., Lohse, K. A., Lybrand, R., Meixner, T., McIntosh, J. C., Papuga, S. A., Rasmussen, C., Schaap, M., Swetnam, T. L., and Troch, P. A.: Coevolution of nonlinear trends in vegetation, soils, and topography with elevation and slope aspect: A case study in the sky islands of southern Arizona, J. Geophys. Res. Earth Surf., 118, 741–758, https://doi.org/10.1002/jgrf.20046, 2013.

Platt, B. F., Kolb, D. J., Kunhardt, C. G., Milo, S. P., and New, L. G.: Burrowing Through the Literature, Soil Science, 181, 175–191, https://doi.org/10.1097/SS.0000000000000150, 2016.

Qin, Y., Yi, S., Ding, Y., Qin, Y., Zhang, W., Sun, Y., Hou, X., Yu, H., Meng, B., Zhang, H., Chen, J., and Wang, Z.: Effects of plateau pikas' foraging and burrowing activities on vegetation biomass and soil organic carbon of alpine grasslands, Plant Soil, 458, 201–216, https://doi.org/10.1007/s11104-020-04489-1, 2021.

Reichman, O. J. and Seabloom, E. W.: The role of pocket gophers as subterranean ecosystem engineers, Trends in Ecology & Evolution, 17, 44–49, https://doi.org/10.1016/S0169-5347(01)02329-1, 2002.

Richards, P. J. and Humphreys, G. S.: Burial and turbulent transport by bioturbation: a 27-year experiment in southeast Australia, Earth Surf. Process. Landforms, 21, n/a-n/a, https://doi.org/10.1002/esp.2007, 2010.

Ridd, P. V.: Flow Through Animal Burrows in Mangrove Creeks, Estuarine, Coastal and Shelf Science, 43, 617–625, https://doi.org/10.1006/ecss.1996.0091, 1996.

Sandino, J., Wooler, A., and Gonzalez, F.: Towards the Automatic Detection of Pre-Existing Termite Mounds through UAS and Hyperspectral Imagery, Sensors (Basel, Switzerland), 17, https://doi.org/10.3390/s17102196, 2017.

Sarbolandi, H., Plack, M., and Kolb, A.: Pulse Based Time-of-Flight Range Sensing, Sensors (Basel, Switzerland), 18, https://doi.org/10.3390/s18061679, 2018.

Shipitalo, M. and Le Bayon, R.-C.: Quantifying the Effects of Earthworms on Soil Aggregation and Porosity, in: Earthworm Ecology, edited by: Edwards, C., CRC Press, 183–200, https://doi.org/10.1201/9781420039719.pt5, 2004.

Shull, D. H.: Transition-matrix model of bioturbation and radionuclide diagenesis, Limnol. Oceanogr., 46, 905–916, https://doi.org/10.4319/lo.2001.46.4.0905, 2001.

Simonetti, J. A.: Microhabitat Use by Small Mammals in Central Chile, Oikos, 56, 309, https://doi.org/10.2307/3565615, 1989.

Soetaert, K., Herman, P. M. J., Middelburg, J. J., Heip, C., deStigter, H. S., van Weering, T. C. E., Epping, E., and Helder, W.: Modeling ^{210}Pb-derived mixing activity in ocean margin sediments: Diffusive versus nonlocal mixing, J Mar Res, 54, 1207–1227, https://doi.org/10.1357/0022240963213808, 1996.

St-Louis, V., Pidgeon, A. M., Radeloff, V. C., Hawbaker, T. J., and Clayton, M. K.: High-resolution image texture as a predictor of bird species richness, Remote Sensing of Environment, 105, 299–312, https://doi.org/10.1016/j.rse.2006.07.003, 2006.

Szantoi, Z., Smith, S. E., Strona, G., Koh, L. P., and Wich, S. A.: Mapping orangutan habitat and agricultural areas using Landsat OLI imagery augmented with unmanned aircraft system aerial photography, International Journal of Remote Sensing, 38, 2231–2245, https://doi.org/10.1080/01431161.2017.1280638, 2017.

Tajik, S., Ayoubi, S., and Lorenz, N.: Soil microbial communities affected by vegetation, topography and soil properties in a forest ecosystem, Applied Soil Ecology, 149, 103514, https://doi.org/10.1016/j.apsoil.2020.103514, 2020.

Tang, Z., Zhang, Y., Cong, N., Wimberly, M., Wang, L., Huang, K., Li, J., Zu, J., Zhu, Y., and Chen, N.: Spatial pattern of pika holes and their effects on vegetation coverage on the Tibetan Plateau: An analysis using unmanned aerial vehicle imagery, Ecological Indicators, 107, 105551, https://doi.org/10.1016/j.ecolind.2019.105551, 2019.

Temme, A. J.A.M. and Vanwalleghem, T.: LORICA – A new model for linking landscape and soil profile evolution: Development and sensitivity analysis, Computers & Geosciences, 90, 131–143, https://doi.org/10.1016/j.cageo.2015.08.004, 2016.

Tews, J., Brose, U., Grimm, V., Tielbörger, K., Wichmann, M. C., Schwager, M., and Jeltsch, F.: Animal species diversity driven by habitat heterogeneity/diversity: the importance of keystone structures, Journal of Biogeography, 31, 79–92, https://doi.org/10.1046/j.0305-0270.2003.00994.x, 2004.

Trauth, M. H.: TURBO: a dynamic-probabilistic simulation to study the effects of bioturbation on paleoceanographic time series, Computers & Geosciences, 24, 433–441, https://doi.org/10.1016/S0098-3004(98)00019-3, 1998.

Turnock, B. Y., Litt, A. R., Vore, J. M., and Hammond, C. A. M.: Habitat characteristics of the hoary marmot: assessing distribution limitations in Montana, Ecosphere, 8, e01977, https://doi.org/10.1002/ecs2.1977, 2017.

Übernickel, K., Pizarro-Araya, J., Bhagavathula, S., Paulino, L., and Ehlers, T. A.: Reviews and syntheses: Composition and characteristics of burrowing animals along a climate and ecological gradient, Chile, Biogeosciences, 18, 5573–5594, https://doi.org/10.5194/bg-18-5573-2021, 2021a.

Übernickel, K., Pizarro-Araya, J., Bhagavathula, S., Paulino, L., and Ehlers, T. A.: Reviews and Syntheses: Composition and Characteristics of Burrowing Animals along a Climate and Ecological Gradient, Chile, 2021b.

Übernickel, K., Ehlers, T. A., Paulino, L., and Fuentes Espoz, J.-P.: Time series of meteorological stations on an elevational gradient in National Park La Campana, Chile, 2021c.

Übernickel, K., Ehlers, T. A., Ershadi, M. R., Paulino, L., Fuentes Espoz, J.-P., Maldonado, A., Oses-Pedraza, R., and Blanckenburg, F. von: Time series of meteorological station data in the EarthShape study areas of in the Coastal Cordillera, Chile, 2020.

Vanwalleghem, T., Stockmann, U., Minasny, B., and McBratney, A. B.: A quantitative model for integrating landscape evolution and soil formation, J. Geophys. Res. Earth Surf., 118, 331–347, https://doi.org/10.1029/2011JF002296, 2013.

Voiculescu, M., Ianăş, A.-N., and Germain, D.: Exploring the impact of snow vole (Chionomys nivalis) burrowing activity in the Făgăraș Mountains, Southern Carpathians (Romania): Geomorphic characteristics and sediment budget, CATENA, 181, 104070, https://doi.org/10.1016/j.catena.2019.05.016, 2019.

Wallis, C. I.B., Brehm, G., Donoso, D. A., Fiedler, K., Homeier, J., Paulsch, D., Süßenbach, D., Tiede, Y., Brandl, R., Farwig, N., and Bendix, J.: Remote sensing improves prediction of tropical montane species diversity but performance differs among taxa, Ecological Indicators, 83, 538–549, https://doi.org/10.1016/j.ecolind.2017.01.022, 2017.

Wei, X., Li, S., Yang, P., and Cheng, H.: Soil erosion and vegetation succession in alpine Kobresia steppe meadow caused by plateau pika—A case study of Nagqu County, Tibet, Chin. Geograph.Sc., 17, 75–81, https://doi.org/10.1007/s11769-007-0075-0, 2007.

Wheatcroft, R. A., Jumars, P. A., Smith, C. R., and Nowell, A. R. M.: A mechanistic view of the particulate biodiffusion coefficient: Step lengths, rest periods and transport directions, J Mar Res, 48, 177–207, https://doi.org/10.1357/002224090784984560, 1990.

Wilkinson, M. T., Richards, P. J., and Humphreys, G. S.: Breaking ground: Pedological, geological, and ecological implications of soil bioturbation, Earth-Science Reviews, 97, 257–272, https://doi.org/10.1016/j.earscirev.2009.09.005, 2009.

Wu, C., Wu, H., Liu, D., Han, G., Zhao, P., and Kang, Y.: Crab bioturbation significantly alters sediment microbial composition and function in an intertidal marsh, Estuarine, Coastal and Shelf Science, 249, 107116, https://doi.org/10.1016/j.ecss.2020.107116, 2021.

Xiong, M., Sun, R., and Chen, L.: A global comparison of soil erosion associated with land use and climate type, Geoderma, 343, 31–39, https://doi.org/10.1016/j.geoderma.2019.02.013, 2019.

Yair, A.: Short and long term effects of bioturbation on soil erosion, water resources and soil development in an arid environment, Geomorphology, 13, 87–99, https://doi.org/10.1016/0169-555X(95)00025-Z, 1995.

Yoo, K. and Mudd, S. M.: Toward process-based modeling of geochemical soil formation across diverse landforms: A new mathematical framework, Geoderma, 146, 248–260, https://doi.org/10.1016/j.geoderma.2008.05.029, 2008.

Young, M. H., Andrews, J. H., Caldwell, T. G., and Saylam, K.: Airborne LiDAR and Aerial Imagery to Assess Potential Burrow Locations for the Desert Tortoise (Gopherus agassizii), Remote Sensing, 9, 458, https://doi.org/10.3390/rs9050458, 2017.

Yu, C., Zhang, J., Pang, X. P., Wang, Q., Zhou, Y. P., and Guo, Z. G.: Soil disturbance and disturbance intensity: Response of soil nutrient concentrations of alpine meadow to plateau pika bioturbation in the Qinghai-Tibetan Plateau, China, Geoderma, 307, 98–106, https://doi.org/10.1016/j.geoderma.2017.07.041, 2017.

Zhang, Q., Li, J., Hu, G., and Zhang, Z.: Bioturbation potential of a macrofaunal community in Bohai Bay, northern China, Marine pollution bulletin, 140, 281–286, https://doi.org/10.1016/j.marpolbul.2019.01.063, 2019.

Zhang, S., Fang, X., Zhang, J., Yin, F., Zhang, H., Wu, L., and Kitazawa, D.: The Effect of Bioturbation Activity of the Ark Clam Scapharca subcrenata on the Fluxes of Nutrient Exchange at the Sediment-Water Interface, J. Ocean Univ. China, 19, 232–240, https://doi.org/10.1007/s11802-020-4112-2, 2020.

3. Area-Wide Prediction of Vertebrate and Invertebrate Hole Density and Depth Across a Climate Gradient in Chile Based on UAV and Machine Learning

Paulina Grigusova [1]*, Annegret Larsen [2], Sebastian Achilles [1], Alexander Klug[1], Robin Fischer [1], Diana Kraus [3], Kirstin Übernickel [4], Leandro Paulino [5], Patricio Pliscoff [6,7,8], Roland Brandl [9], Nina Farwig [3] and Jörg Bendix [1]

[1] Laboratory for Climatology and Remote Sensing, Department of Geography, University of Marburg, 35037 Marburg, Germany; achilles@geo.uni-marburg.de (S.A.); fischer.robin92@gmail.com (R.F.); kluga@students.uni-marburg.de (A.K.); bendix@geo.uni-marburg.de (J.B.)

[2] Soil Geography and Landscape, Department of Environmental Sciences, Wageningen University & Research, 6700 AA Wageningen, The Netherlands; annegret.larsen@wur.nl

[3] Conservation Ecology, Department of Biology, University of Marburg, 35032 Marburg, Germany; diana.kraus@biologie.uni-marburg.de (D.K.); nina.farwig@biologie.uni-marburg.de (N.F.)

[4] Earth System Dynamics, Department of Geosciences, University of Tübingen, 72076 Tübingen, Germany; kirstin.uebernickel@uni-tuebingen.de

[5] Facultad de Agronomía, Universitad de Concepción, 3780000 Chillán, Chile; lpaulino@udec.cl

[6] Facultad de Historia, Geografía y Ciencia Política, Instituto de Geografía, Pontificia Universidad Católica de Chile, 782-0436 Santiago, Chile; pliscoff@uc.cl

[7] Facultad de Ciencias Biológicas, Departamento de Ecología, Pontificia Universidad Católica de Chile, 8331150 Santiago, Chile; pliscoff@uc.cl

[8] Center of Applied Ecology and Sustainability (CAPES), Pontificia Universidad Católica de Chile, 8331150 Santiago, Chile; pliscoff@uc.cl

[9] Animal Ecology, Department of Biology, University of Marburg, 35032 Marburg, Germany; brandlr@biologie.uni-marburg.de

Published in Drones (2021): https://doi.org/10.3390/drones5030086

Abstract

Burrowing animals are important ecosystem engineers affecting soil properties, as their burrowing activity leads to the redistribution of nutrients and soil carbon sequestration. The magnitude of these effects depends on the spatial density and depth of such burrows, but a method to derive this type of spatially explicit data is still lacking. In this study, we test the potential of using consumer-oriented UAV RGB imagery to determine the density and depth of holes created by burrowing animals at four study sites along a climate gradient in Chile, by combining UAV data with empirical field plot observations and machine learning techniques. To enhance the limited spectral information in RGB imagery, we derived spatial layers representing vegetation type and height and used landscape textures and diversity to predict hole parameters. Across-site models for hole density generally performed better than those for depth, where the best-performing model was for the invertebrate hole density (R^2 = 0.62). The best models at individual study sites were obtained for hole density in the arid climate zone (R^2 = 0.75 and 0.68 for invertebrates and vertebrates, respectively). Hole depth models only showed good to fair performance. Regarding predictor importance, the models heavily relied on vegetation height, texture metrics, and diversity indices.

Keywords: UAV; machine learning; burrowing animals; climate gradient; Chile; vegetation patterns; heterogeneity

3.1. Introduction

Terrestrial burrowing vertebrates and invertebrates are important ecosystem engineers. Through their burrowing activity, they increase soil porosity and permeability, thus affecting the infiltration and erosion rates (Shipitalo and Le Bayon, 2004; Bowker et al., 2013; Wilkinson et al., 2009; Gabet et al., 2003; Nkem et al., 2000). The construction of underground burrows leads to the redistribution and concentration of nutrients (Platt et al., 2016; Zhang et al., 2020; Yu et al., 2017). Their burrowing positively influences soil carbon storage (Frouz et al., 2009; Qin et al., 2021) and decreases the ratio of sTable 3.and unsTable 3.carbonate aggregates in the soil (Don et al., 2019). The mixing of soil shifts the soil horizons and drives soil production and pedogenesis on a long-term basis (Wilkinson and Humphreys, 2005; Cunha et al., 2016; JOECKEL and TUCKER, 2013). To understand the abundance of burrowing animals, their burrowing behavior and their potential distribution patterns is thus of importance.

The habitat preferences of burrowing animals in regard to the vegetation distribution were shown to be species dependent (Qin et al., 2021; Turnock et al., 2017; Tang et al., 2019; Tajik et al., 2020; Jacob, 2008) The distribution of single burrowing animal species was associated with cacti (Milstead et al., 2007) , herbs (Meserve, 1981) , perennial grass or dense shrubs (Ferro and Barquez, 2009; Tews et al., 2004) , skeleton (Simonetti, 1989) or increased landscape heterogeneity (Louw et al., 2019). Due to the important role of burrowing animals as ecosystem engineers and the contradictory habitat preferences of burrowing animals, a spatial analysis showing the dependence of the burrowing intensity on vegetation patterns across the species and climate zones is needed. For this, a suiTable 3.approach for the area-wide prediction of burrowing intensity, which can be expressed by the density and depth of holes created by all present burrowing animals, must be developed.

As taking in situ hole density and depth measurements is labor-intensive, remote sensing can serve as a more practical approach, as it provides opportunities for effective area-wide spatial estimates. Previous studies have used UAVs to directly map the burrows and mounds created by burrowing animals. However, these studies were conducted in areas where the burrows could be directly recognized in images, were limited to vertebrates, and focused on single species. The burrows were then mapped using image segmentation (Sandino et al., 2017) or classification approaches (Bycroft et al., 2019; Old et al., 2019; Albores-Barajas et al., 2018; Tang et al., 2019). The detection success predominantly depended on the vegetation density and height. Even within grassland areas with low vegetation cover, significantly more burrows were counted in ground-truth surveys than were detected in UAV-obtained orthomosaic images (Old et al., 2019). If burrows were not visible in the images because they were partly or completely overlaid by vegetation, previous authors did not estimate the density and depth of burrows, but only defined areas with or without burrows. In these cases, MaxEnt models (Koshkina et al., 2020) based on predictors from vegetation (Young et al., 2017) or Digital Surface Models (DSMs) generated from UAV images (Borgatti et al., 2017) have been applied. However, beyond hole detection, none of the previous studies has estimated the area-wide density and depth of holes created by all vertebrate and invertebrate burrowing animals, regardless of the vegetation coverage and taxa, or tested their approach in several climate zones. As demonstrated in this study, a combination of ecological in situ measurements, geospatial information, and application of machine learning techniques offers possibilities for the prediction of the area-wide hole density and depth, even in areas with dense vegetation coverage.

UAVs offer here a suiTable 3.solution to identify environmental parameters which might be linked to the animal burrowing intensity. UAV-estimated vegetation height and volume have previously been used as predictors to delineate vertebrate habitats (Olsoy et al., 2018). Similarly, land-use and the distribution of single vegetation types have been derived from UAV images and were associated with animal distribution (Fritz et al., 2018; Szantoi et al., 2017) or used as predictors for the estimation of population sizes (Guo et al., 2012). In cases where the landscape structure is of major importance, texture metrics and diversity indices have been shown to be suiTable 3.predictors for area-wide predictions of species richness in diverse ecosystems (St-Louis et al., 2006; Culbert et al., 2012; Wallis et al., 2017; Gholizadeh et al., 2018). The texture metrics obtained from high-resolution UAV images notably improved the estimation of habitat structures (Bourgoin et al., 2020; Fu et al., 2021).

For this study, we developed, applied, and tested machine learning approaches based on consumer-oriented UAV RGB (Red–Green–Blue spectral range) imagery, in order to predict the density and depth of holes created by all present burrowing vertebrates and invertebrates. We tested several predictor sets and included 3D landscape structures, their textures, land-cover fractions, and diversity as predictors, in addition to spectral bands, topography, and climate, which can only be obtained by UAVs at such high resolution. We analyzed the model performance and identified the most important predictors, and the performance of models trained for the vertebrate and invertebrate hole density and depth was determined across a climate gradient and at individual climate sites. Finally, we present the area-wide prediction of hole density and depth along the climate gradient.

3.2. Materials and Methods

We hypothesize that the animal burrowing intensity is dependent on vegetation patterns and can be spatially predicted by UAV-obtained data. We measured the density and depth of holes within plots created by local communities of vertebrate and invertebrate burrowing animals across four study sites in Chile. We first tested if there is a high correlation between in situ vegetation patterns and our targeted variables by setting up linear models and using data from ground vegetation survey as predictors. We then collected high-resolution UAV imagery of the study sites and trained machine learning models to predict the density and depth of holes (Figure 3.1). We used climate, topography, spectral bands, vegetation indices, land-cover fractions and diversity indices derived from land-cover classification, vegetation height, texture metrics derived from vegetation height, and texture metrics derived from spectral bands as predictors in our models. Then, we fitted one random forest (RF) model for the whole study area and one RF model per study site, and estimated the most important predictors. To test the impact of various predictor sets on the model performance, we separately tested models using different predictor sets consisting of several predictors describing similar environmental parameters. We present the predicted hole density and depth across the four study sites and their association with the estimated land-cover and vegetation height diversity.

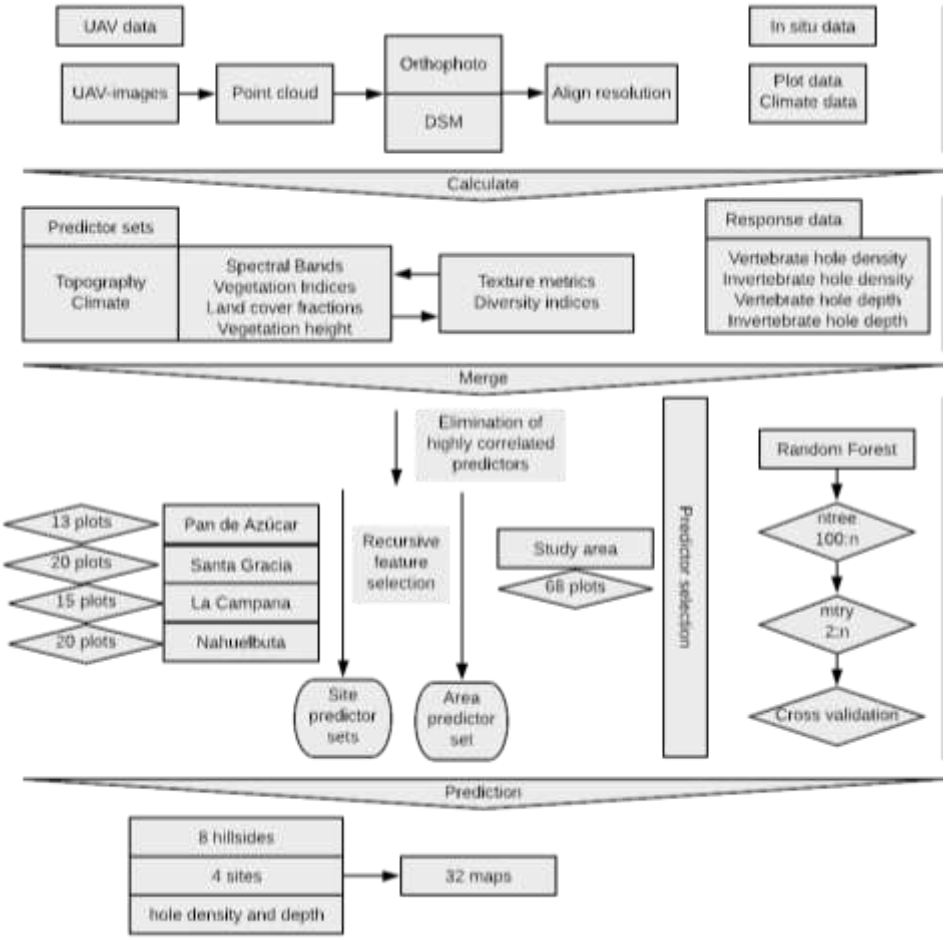

Figure 3.1. Workflow. Pre-processing comprises the acquisition and preparation of in situ and remote sensing data. Model input describes the calculated predictors and response data. Predictor selection describes the estimation of the predictors used in the final models. Hyperparameter tuning describes the tuned parameters and validation techniques. DSM = digital surface model; ntree = optimal number of trees after each split; mtry = optimal number of predictors randomly selected at each split.

3.2.1. Study Area

Our study was performed along a climate and vegetation gradient in Chile, comprising four study sites in the Chilean Coastal Cordillera: Pan de Azúcar (PdA) National Park (NP), Santa Gracia (SG), La Campana (LC) NP, and Nahuelbuta (NA) NP (Figure 3.2). PdA NP is located in the arid zone in a fog-laden environment in the southern part of the Atacama Desert, with almost no precipitation. The vegetation cover is less than 5% and dominated by small desert shrubs, several types of cacti and biocrusts (Lehnert et al., 2018). SG is a natural reserve located in the semi-arid zone near La Serena, which is dominated by goat grazing. The vegetation consists of shrubs and cacti, covering up to 40% of the study area. LC NP is part of the Mediterranean-type climatezone in the Valparaiso Region and is also affected by cattle. The study site is dominated by an evergreen sclerophyllous forest with endemic palms. The canopy reaches a height of up to 9 m, and the understory consists of deciduous shrubs and herbs. NA is located in the humid-temperate zone and characterized by a dense evergreen Araucaria forest comprising broadleaved trees with heights of up to 14 m. The ground is covered by

bamboo, shrubs, and herbs (Bernhard et al., 2018; Oeser et al., 2018). There are at least 45 vertebrate and 345 invertebrate species in Chile which exhibit burrowing behavior (Übernickel et al., 2021). The most common vertebrate burrowing animals are in PdA carnivores (Lycalopex culpaeus, Lycalopex griseus); marsupials (Didelphis marsupialis, Didelphis albiventris) and rodents (Phyllotis xanthopygus, Phyllotis limatus, Abrothrix andinus) (Jimenez et al., 1992; Cerqueira, 1985); in SG marsupials (Thylamys elegans) and rodents (Phyllotis darwini, Abrothrix olivaceus, Octodon degus, Abrocoma bennetti, Rattus rattus) (Milstead et al., 2007); in LC and NA rodents (Octodon degus, Rattus norvegicus and Phyllotis darwini) and carnivores (Lycalopex griseus) (Muñoz-Pedreros et al., 2018). The most commoninvertebrate burrowing animals are in PdA Curculionida and Tenebrionidae (Pizarro-Araya and JEREZ, 2004); in SG Araucomyrmex goetschi, Brachymyrmex giardia and Solenopsis gayi (Medel and Vásquez, 1994); in LC Arthroconus elongates and Nycterinus rugicep (Pizarro-Araya and JEREZ, 2004); and in NA Staphylinidae, Curculionidae and Cerambycidae (VERGARA et al., 2006).

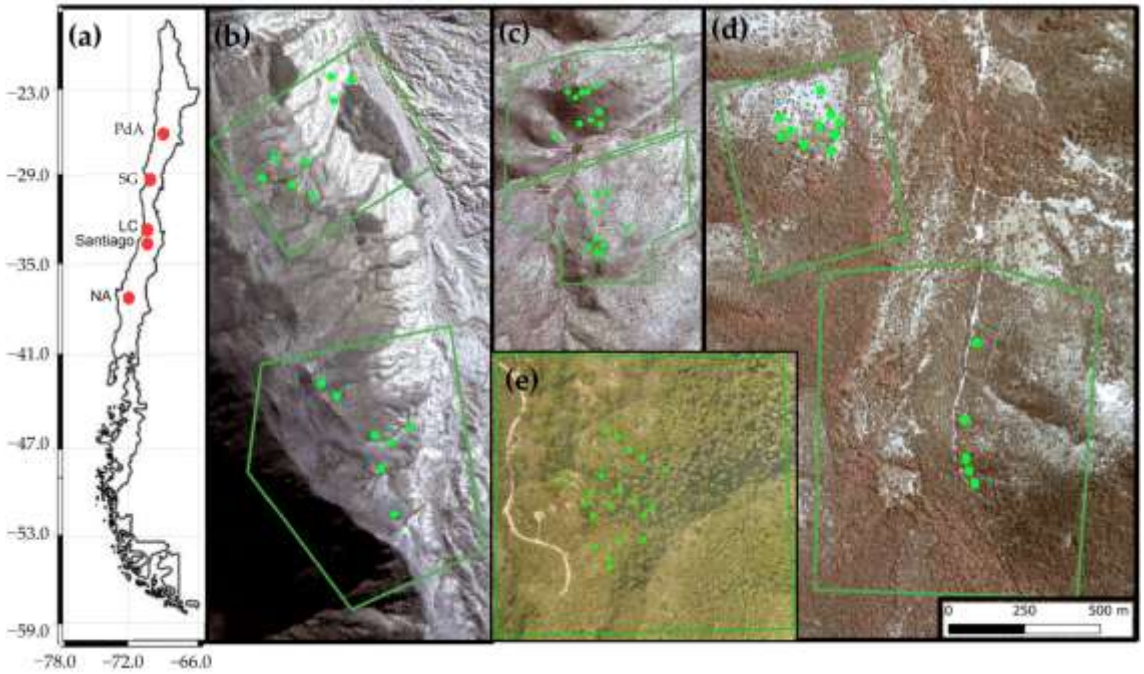

Figure 3.2. Study area and study sites. Green dots indicate the positions of plots. The green lines outline the UAV orthophotos: (**a**) Position of the study sites along the climate gradient. PdA = Pan de Azúcar, SG = Santa Gracia, LC = La Campana, NA = Nahuelbuta; Positions of plots in (**b**) PdA; (**c**) SG; (**d**) LC; and (**e**) NA. The background image is an RGB-composite calculated from WorldView-2 satellite imagery with applied hillshade.

3.2.2. In Situ Data

The response data were collected during a field campaign from September to November 2019 in 13–20 10 m × 10 m plots dispersed randomly on one north-facing and one south-facing hillside per study site (68 plots in total, Figure 3.1). The distance between the plots was at least 20 m. Within each plot, we counted the number of holes created by burrowing animals and measured the diameter and depth (tunnel length until first obstacle) of each hole (Table 3.S1, Figure 3.S7). We assumed that holes with a diameter equal to or greater than 2.5 cm were created by vertebrates and that holes with a diameter less than 2.5 cm were created by invertebrates (Übernickel et al., 2021). We created four response data sets: Density of vertebrate holes, density of invertebrate holes, depth of vertebrate holes, and depth of invertebrate holes.

Additionally, we mapped the ground land cover within each plot. We estimated the abundance, coverage, size (diameter and height) and position of all vegetation individuals and skeleton. We classified the mapped vegetation into herbs, shrubs, cacti and trees. We mapped only the skeleton with a diameter of 0.20 m and above. For trees, we measured the diameter of the stem and the height to the top of the crown. The height of vegetation individuals below 2.5 m was measured. Ten plots included at least one individual with a height of above 2.5 m. In this case, we guessed the height of the individual. The coverage of each class was estimated by multiplying the average cover by the number of individuals for each class. The vegetation cover was the sum of the calculated cover of each class. Additionally, we calculated the average vegetation height of each class and of all vegetation.

The climate data were measured in project-specific climate stations, located either directly on the studied hillsides or within a 1 km distance (Lehnert et al., 2018; Übernickel et al., 2020). The average air temperature [°C], average soil temperature [°C], and cumulative precipitation [mm] for the year 2019 were calculated for each site.

3.2.3. Linear Regression Models

We first tested if the response data sets can be predicted by the in situ measured vegetation patterns. We calculated 24 predictors from the land cover data estimated in plots. We used the soil, vegetation and skeleton coverage, average vegetation height as well as the coverage, height, diameter and abundance of individuals for each class as predictors. Additionally, we calculated the heterogeneity of each plot, by estimating the variance of measured vegetation height, abundance, size and coverage between the classes. Lastly, we included the site as a predictor, to be able to examine the predictor strength on the response variable per site.

We first applied a backward stepwise elimination to remove the redundant predictors and then fitted linear mixed effect regression models (Bates et al., 2015) . We validated the models by implemented Leave-One-Out cross validation (Sammut and Webb, 2010).

3.2.4. UAV Data

The UAV flights were conducted during the same field campaign from September to November 2019. We obtained UAV images of one north-facing and one south-facing hillside per study site, which included the 68 plots (Figure 3.3) . We used a 3D Robotics SOLO quadrocopter equipped with a GoPRO Hero 4 Black RGB camera. Eight flights were conducted for each hillside (total of 64 flights). The flight plans were created using the Mission Planner version 1.3.700 software (Gandor et al., 2015). Flight altitude was set at 20 m above the drone starting and landing points, and the flights were conducted downward from this point. The width and length of the overflown areas were set with respect to the hillside inclination and canopy level, in order to ensure that the maximum drone altitude above the ground did not exceed 40 m. Two flights were performed with opposite flying angles over every area, in order to ensure full coverage and to create a 3D model of the landscape afterwards. The flying speed was 5 m/s, the overlap was set to 90%, and the site overlap was at least 70%. The camera angle was

Table 3.1. List of the calculated predictors.

Predictor set	Number of Predictors	Description
Climate	3	Mean annual air temperature [°C] Mean annual soil temperature [°C] Mean annual precipitation [mm]
Topography	3	Elevation [m.a.s.l] Inclination [°] (Horn, 1981) Aspect [°] (Horn, 1981)
Spectral bands	3	Red band Green band Blue band
Vegetation indices	7	Red–green–blue vegetation index (RGBVI) (Bendig et al., 2015), green-leaf-index (GLI) (Canham, 1988), visible atmospherically resistant index (VARI) (Gitelson et al., 2002), normalized green–red difference index (NGRDI) (Tucker, 1979), vegetation dryness index (VDI) (Rahimzadeh-Bajgiran et al., 2012), excess green vegetation index (EXG) (Woebbecke et al., 1995), and green chromatic coordinate (GCC) (Gillespie et al., 1987)
Land-cover fractions per 10 m × 10 m	7	Soil, skeleton, herbs, shrubs, cacti, trees, all vegetation
Average vegetation height per 10 m × 10 m	5	Herbs, shrubs, cacti, trees, all vegetation
Texture metrics calculated from the spectral bands + vegetation indices + vegetation height with a surrounding of 10 m × 10 m or 108 × 108 pixels (Haralick et al., 1973)	21 + 14 + 7	Variance, entropy, homogeneity, second moment, correlation, dissimilarity, contrast
Diversity indices (calculated from land-cover classification using a moving	7	Shannon's Diversity (Shannon, 1948), Pielou's Evenness (Pielou,

window of 108 × 108 pixels) (Rocchini et al., 2021)	1966), the Berger–Parker Index (Berger and Parker, 1970), Rao's quadratic entropy (Rao, 1982), Cumulative Residual Entropy (Rao et al., 2004), Hill's numbers (Hill, 1973), Rényi's Index

10°, and a photo was taken every 0.74 s during the mission. The photos were geo-tagged using CAM messages from the data-flash protocol. The images were then used to create an orthophoto and a Digital Surface Model (DSM) of each hillside. The processing was carried out using the Agisoft Metashape Professional version 1.5.5.9097 software. The photos were aligned using a generic pre-selection method, and a point cloud was created. The DSM was calculated from the point cloud, and the orthophotos were built from the aligned photos. The ground sampling distance of the DSM and orthophotos varied between 1.76 and 3.7 cm. The orthophotos were resampled to a uniform ground sampling distance of 3.7 cm, in order to allow for a comparison of model performance between the study sites (Table 3.S2).

3.2.5. Calculation of the Predictors

We used several predictor sets in the models to determine spatial hole densities and depths (Table 3.1). The predictor sets included climate, topography, spectral bands, vegetation indices, land-cover, vegetation height, texture metrics (calculated from two vegetation indices, spectral bands and vegetation height), and diversity indices calculated from land-cover classification.

The 'red' (R), 'green' (G), and 'blue' (B) spectral bands were extracted from orthophotos. The following vegetation indices were calculated using the relative data extracted directly from GoPro: The red–green–blue vegetation index (RGBVI) (Bendig et al., 2015), green-leaf-index (GLI) (Canham, 1988), visible atmospherically resistant index (VARI) (Gitelson et al., 2002), normalized green-red difference index (NGRDI) (Tucker, 1979), vegetation dryness index (VDI) (Rahimzadeh-Bajgiran et al., 2012), excess green vegetation index (EXG) (Woebbecke et al., 1995), and green chromatic coordinate (GCC) (Gillespie et al., 1987). These indices were selected due to their various vegetation detection abilities under diverse environmental conditions, which are possibly related to the disturbances caused by burrowing animals (Bendig et al., 2015; Canham, 1988; Gitelson et al., 2002; Tucker, 1979; Rahimzadeh-Bajgiran et al., 2012; Gillespie et al., 1987; Woebbecke et al., 1995).

The land-cover fractions were obtained through land-cover classification. The basis for calculating the fractions of land-cover per 10 m × 10 m pixels was the land-cover classification at 3.7 ground sampling distance. One pixel-based supervised classification per study site was conducted using Random Forest Classification from the R 'caret' package (Kuhn, 2008). The RF algorithm is based on building several uncorrelated decision trees during training, then merging them together and providing an output, which is calculated as the mean predicted value of the individual trees (Breiman, 2001). We used the DSM, RGB bands, and vegetation indices as predictors. We specified six main classes and divided them into sub-classes. The main classes were soil, skeleton, herbs, shrubs, cacti, and trees. The sub-classes varied between sites (Table 3.S3). In PdA, soil was sub-divided into soil largely covered by soil crusts, weathered granite soil, and saprolite soil, while cacti were

sub-divided into classes of the genera Copiapoa and Eulychnia. In SG, the soil was sub-divided into two sub-classes, and cacti were classified into the genus Eulychnia and other genera. In NA, skeleton was classified into rocks (equal to or less than 25.5 cm in diameter) and boulders (greater than 25.5 cm in diameter), while trees were sub-divided into the genera Araucaria and others. No trees were classified in PdA, and no cacti in LC and NA. Training areas for the land-cover classification were visually identified in the orthophotos. Approximately 200 pixels per land-cover class per site were tagged, in order to create the training/testing data set. This data set was randomly split into 70% training and 30% testing data. The land-cover classification model was trained using the 70% training data and validated using 30% test pixels. Classification performance was estimated by Cohen's Kappa and Sensitivity. Sensitivity was calculated separately for each land-cover class. The performance of the land-cover models varied along the climate gradient (in PdA: $\kappa = 0.81$; in SG: $\kappa = 0.72$; in LC: $\kappa = 0.81$; in NA: $\kappa = 0.76$). The highest sensitivity was observed for the classes soil, cacti, and trees (Table 3.S4), which were correctly classified in more than 80% of cases. In SG, all soil pixels were classified accordingly. The sensitivity was lower for the class skeleton, which was often misclassified as soil. Cacti were misclassified as shrubs or herbs in roughly 10% of all cases, but the model almost always correctly differentiated between the various types of cacti. The predictability of the shrubs and herbs classes varied. Overall, the sensitivity of both was 70%. However, in NA, the model misclassified 40% of herbs as shrubs; meanwhile, in SG, 75% of shrubs were classified as herbs. The study sites were then classified using the trained models. The resolution of the classification output layer was downscaled to 10 m, and the soil fraction, herb fraction, shrub fraction, tree fraction, cacti fraction, and skeleton fraction were calculated as the percent coverage per pixel. Additionally, the vegetation fraction was calculated as the percent coverage of any vegetation type per pixel.

The elevation predictor was obtained by calculating the digital elevation model (DEM) using the DSM and the land-cover classification. A masked DSM layer was created by removing all pixels classified as any class other than soil or skeleton in the corresponding land-cover classification. The remaining pixels were used to fit a thin plate spline (TPS) model, by applying the TPS regression algorithm from the 'fields' R package (Nychka, 2016). The distribution of pixels used for the regression fit was uniform across the elevation gradient on hillsides in PdA, SG, and LC. However, in NA, most of the pixels at lower altitudes were masked. The TPS models were trained separately for each site. The smoothing parameter was chosen using generalized cross-validation. The mean absolute error (MAE) of the regression model was the lowest in NA (MAE = 0.05), SG (MAE = 0.08), and PdA (MAE = 0.11), and the highest in LC (MAE = 0.41). The DEM was created by applying the fitted TPS models for the interpolation of the masked DSM using the function 'interpolate' from the R 'raster' package (Hijmans et al.). The inclination and aspect predictors were calculated from the DEM (Horn, 1981). The number of neighbors was 8.

The vegetation height predictor was calculated by subtracting the DEM from the DSM. The height was additionally calculated for each vegetation type (herbs, shrubs, trees, and cacti) separately. For this, the corresponding difference values classified as the respective vegetation type in the land-cover classification were used, while all other values were set to zero.

As burrowing animals are expected to increase landscape heterogeneity (Ballová et al., 2019; Valkó et al., 2021), we calculated several texture metrics and diversity indices. The texture metrics were calculated from the spectral bands, two vegetation indices, and the vegetation height predictor, and were derived from gray-level co-occurrence matrices using the 'glcm' R-package (Zvoleff). We used a moving window of 108 × 108 pixels,

which is equal to 10 m x 10 m, corresponding to the size of the plots. The texture metrics applied were ‘variance’, ‘entropy’, ‘homogeneity’, ‘second moment’, ‘correlation’, ‘dissimilarity’, and ‘contrast’ (Haralick et al., 1973) (Table 3.S7). These metrics determine the heterogeneity of habitats (Tuanmu and Jetz, 2015; Regolin et al., 2020), particularly in relation to vegetation structure (Wood et al., 2012). The texture metrics mean, variance, and correlation were least correlated with each other. There was a higher positive correlation between the entropy, dissimilarity, and contrast metrics, which were negatively correlated with homogeneity and second moment (Hall-Beyer, 2017). We calculated several diversity indices from the land-cover classifications using the ‘rasterDiv’ package (Rocchini et al., 2021); namely, Shannon’s Diversity (Shannon, 1948), Pielou’s Evenness (Pielou, 1966), the Berger–Parker Index (Berger and Parker, 1970), Cumulative Residual Entropy (Rao et al., 2004), Rao’s quadratic entropy (Rao, 1982), Hill’s number (Hill, 1973), and Rényi’s index (Rényi, 1961). The window size was also 10 m x 10 m (or 108 × 108 pixels), corresponding to the size of the plots. These indices were selected due to their various representations of diversity (in our case, the land-cover class diversity), which is expected to be largely affected by burrowing animals (Louw et al., 2019; Parsons et al., 2016).

A cumulative error developed during the calculation of the predictors. The DEM layers were created with an $R^2 = 0.95$. The land cover classifications had an average $R^2 = 0.80$. The vegetation height layers thus have a cumulative error of $R^2 = 0.95 \times 0.80 = 0.76$. The diversity predictors have $R^2 = 0.76$ (when derived from vegetation height) till $R^2 = 0.80$ (when derived from land cover classification).

3.2.6. Model Setup

To obtain the best-fit models for the whole study area for each response data set, we first selected the predictors, then tuned the hyperparameters and, finally, trained the models.

To select the predictors, we first calculated Pearson’s correlation between all predictors and removed all redundant predictors with an absolute correlation of ≥0.75. Using the remaining predictors with an absolute correlation of <0.75, we applied a recursive feature elimination algorithm (RFE). The RFE first trains a model and estimates the importance of the predictors. Then, the RFE iteratively removes predictors with the least importance and trains the models using the remaining predictors. The outcome of the RFE is the number and composition of predictors that were used in the best-performing model, based on the specified model performance metrics (Kuhn, 2008). Within the RFE, we used an RF selection function and validated the models by performing repeated 5-fold cross-validation. We selected the predictors used in the model through use of the lowest root-mean-square error (RMSE).

After the RFE, hyperparameter tuning was conducted. We used the ‘tuneRF’ function, which enables the training of several RF models with varying hyperparameter values, and then examined the performance of the models. The tuning consisted of selecting the optimal number of trees after each split (ntree) and the optimal number of predictors randomly selected at each split (mtry) (Kuhn, 2008). We gradually tested ‘ntree’ with values between 50 and 1000 (in steps of 50) and selected the ‘ntree’ value leading to the highest model performance. We selected the ideal ‘mtry’ by selecting the model with the lowest Out-of-bag Error (OOB Error). We started at mtry = 1 and increased it stepwise by 1, and continued as long as the OOB Error decreased by at least 1e-5 [64].

Additionally, we trained models for each response data set separately for each study site. We followed the same predictor selection and parameter tuning workflow. To test the impact of individual predictor sets on model performance, we trained models using only spectral bands, vegetation indices, topography, climate, texture metrics, diversity indices, land-cover fractions, and vegetation height predictors.

The models were validated by independent data (data not used for the model training). We implemented a Leave-One-Out cross validation. During this validation, the model step-wise uses one instance of the dataset for testing and the remaining instances for training. This validation method was used due to limited number of plots (Sammut and Webb, 2010).

We used the models trained for the whole study area for the prediction. As the plots had a size of 10 m × 10 m, we aggregated the predictors to a spatial resolution of 10 m. We predicted the vertebrate and invertebrate hole density and depth on all eight hillsides and present 32 maps.

3.3. Results

3.3.1. Model Performance

The linear mixed effect regression models trained using in situ measured vegetation patterns achieved high accuracy. The best results were obtained for vertebrate hole depth ($R^2 = 0.84$, $p < 0.001$) and vertebrate hole density ($R^2 = 0.83$, $p < 0.001$). The models for the invertebrate hole density ($R^2 = 0.76$, $p < 0.001$) and hole depth ($R^2 = 0.64$, $p < 0.001$) achieved good performance.

The random forest models trained using vegetation patterns obtained by UAV achieved varying performances. Of the models trained for the whole study area, the highest performance was achieved by the invertebrate hole density prediction model ($R^2 = 0.62$, $p < 0.001$, MAE = 4.05), followed by the invertebrate hole depth model ($R^2 = 0.44$, $p < 0.001$, MAE = 0.3). The model for the vertebrate hole density had a similar performance ($R^2 = 0.43$, $p < 0.01$, MAE = 3.79). The model for the vertebrate hole depth performed worse than the other three models ($R^2 = 0.22$, $p < 0.05$, MAE = 2.23; Figure 3.3, Table 3.2).

The performance of the significant models trained for the study sites varied strongly (from $R^2 = 0.29$ to $R^2 = 0.75$). The best results were obtained in the models trained for PdA, in terms of vertebrate hole density ($R^2 = 0.75$, $p < 0.001$, MAE = 1.29) and invertebrate hole density ($R^2 = 0.68$, $p < 0.001$, MAE = 4.5). In SG, none of the models reached an R^2 above 0.30; while, in LC, only the model for the vertebrate hole depth reached an R^2 exceeding 0.30 ($R^2 = 0.66$, $p < 0.001$, MAE = 0.81). In NA, all models showed a significant relationship between the predicted and measured data. The highest performance was achieved by the model for the prediction of vertebrate hole density ($R^2 = 0.46$, $p < 0.01$; Table 3.2.

The performance of the models trained separately with each of the predictor sets ranged from $R^2 = 0.05$ to $R^2 = 0.32$. For all response variables, the best results were achieved with the following predictor sets: Vegetation height (for the invertebrate hole depth), diversity indices (for the vertebrate hole depth), land-cover fractions (for the invertebrate hole density), and texture metrics (for the vertebrate hole density); see Table 3.S5.

The models underestimate the hole density and depth for plots with higher hole density and deeper holes and overestimate the hole density and depth for the plots with lower hole density and less deep holes.

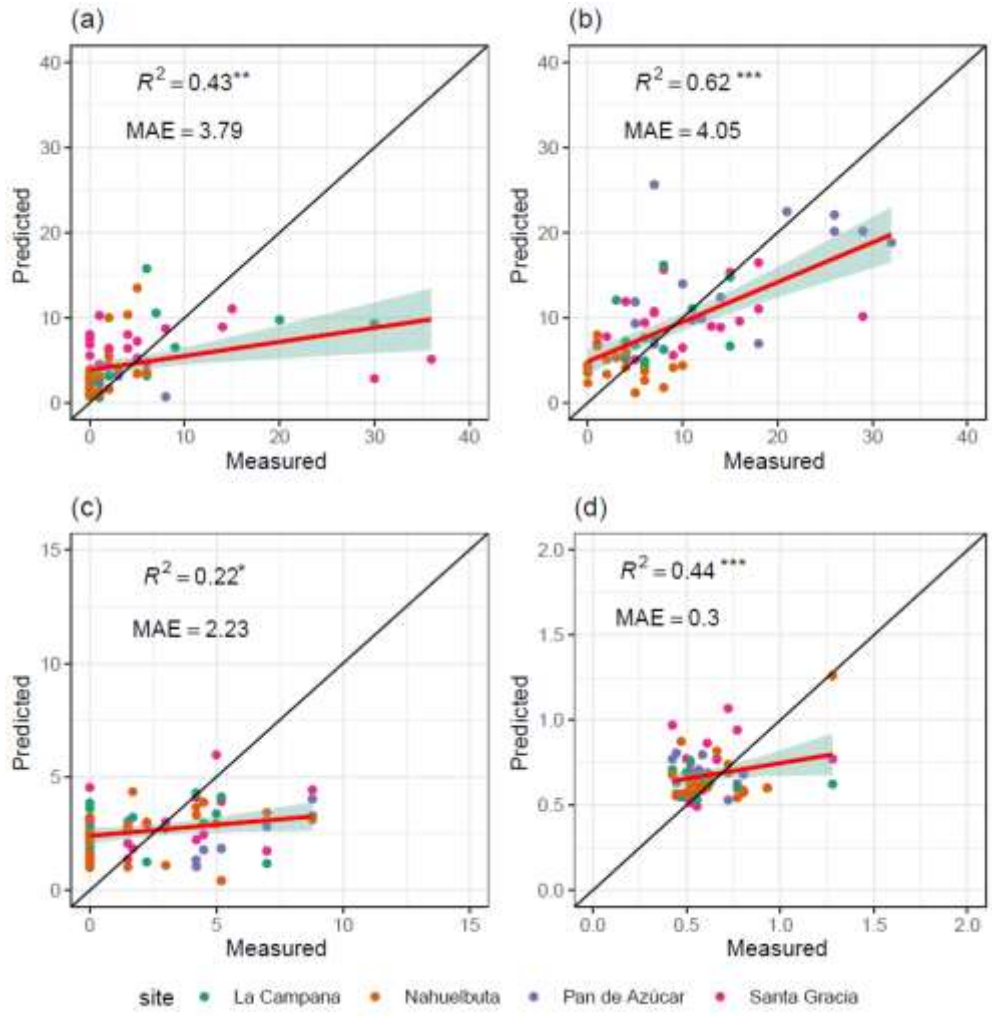

Figure 3.3. Performance of the models trained for the whole study area. The red line is the linear regression line. The green shadow is the confidence interval. MAE = mean absolute error: (**a**) Vertebrate hole density/10 m × 10 m; (**b**) invertebrate hole density/10 m × 10 m; (**c**) vertebrate hole depth [cm]/10 m × 10 m; and (**d**) invertebrate hole depth [cm]/10 m × 10 m. Significance level: p *** ≤ 0.001; p ** ≤ 0.01; p * ≤ 0.05.

Table 3.2. Performance of models trained for individual study sites and for the whole study area (all study sites). 'mtry' is the optimal number of predictors randomly selected at each split. PdA = Pan de Azúcar, SG = Santa Gracia, LC = La Campana, NA = Nahuelbuta.; p *** ≤ 0.001; p ** ≤ 0.01; p * ≤ 0.05.

Unit	Animals	Study Site	Number of Selected Predictors	Mtry	R^2
Hole density	Vertebrates	All	23	5	0.43 **
		PdA	2	1	0.75 ***
		SG	5	1	0.04
		LC	2	1	0.11
		NA	2	1	0.46 ***
	Invertebrates	All	13	3	0.62 ***
		PdA	10	3	0.68 ***

		SG	20	6	0.15
		LC	26	8	0.10
		NA	6	2	0.29 *
Hole depth	Vertebrates	All	5	2	0.22 *
		PdA	7	2	0.01
		SG	33	11	0.01
		LC	8	2	0.66 ***
		NA	4	1	0.36 **
	Invertebrates	All	3	1	0.44 ***
		PdA	34	11	0.07
		SG	15	5	0.19
		LC	30	10	0.01
		NA	6	2	0.31 *

3.3.2. Predictor Selection and Importance

The significant predictors describing in situ measured vegetation patterns which were selected during backward feature selection and used in the linear regression models varied between the models (Tables S6–S9). For the hole density, site SG was not selected as significant while for hole depth, all sites were significant. The significant predictors for the vertebrate hole density were vegetation cover, skeleton cover and diameter of shrubs. The significant predictors for the invertebrate hole density were cacti height, cacti abundance and the vegetation cover in PdA. The significant predictors for vertebrate hole depth were vegetation cover and the cover of the single classes as well as heterogeneity. Lastly, the significant predictors for invertebrate hole depth were heterogeneity, shrub height and diameter.

Following predictors calculated from the UAV-data and used in random forest models were selected. Of 76 predictors, 40 were highly correlated with each other and were removed before further analysis. The retained indices were all land-cover fractions, most of the diversity indices, texture metrics, and vegetation height predictors, all spectral bands and topographic indices, one vegetation index, and one climate predictor. The number of selected predictors and their composition varied from 2 to 34 for the different responses (Figure 3.S1, Table 3.2). The RFE conducted using data from the whole study area retained between 3 and 23 predictors (Table 3.2). For the individual study sites, the number of chosen predictors varied between 2 and 34.

For the vertebrate hole density, the most important predictors were the texture metric dissimilarity calculated from the vegetation height; the texture metrics-based contrast, variance, and second moment calculated from the blue or red band; and several land-cover fractions and diversity indices (Figure 3.4). For the invertebrate hole density, the Berger–Parker diversity index was the most important, followed by the land-cover fractions rocks, soil, and shrubs (Figure 3.4). In terms of vertebrate hole depth, the aspect and tree fraction, and the variance and dissimilarity calculated from the vegetation height were important (Figure 3.4). For the invertebrate hole depth, the contrast texture metrics calculated from the red band and cacti height were the most important (Figure 3.4).

For the individual study sites, the selected predictors varied. In PdA, the texture metrics calculated from the vegetation height and the NGRDI were the most important for the vertebrate and invertebrate hole density.

In LC, for the vertebrate hole depth, the soil and tree fraction and inclination were the most important. In NA, the correlation texture metric calculated from the green band was the most important for the invertebrate hole density and depth.

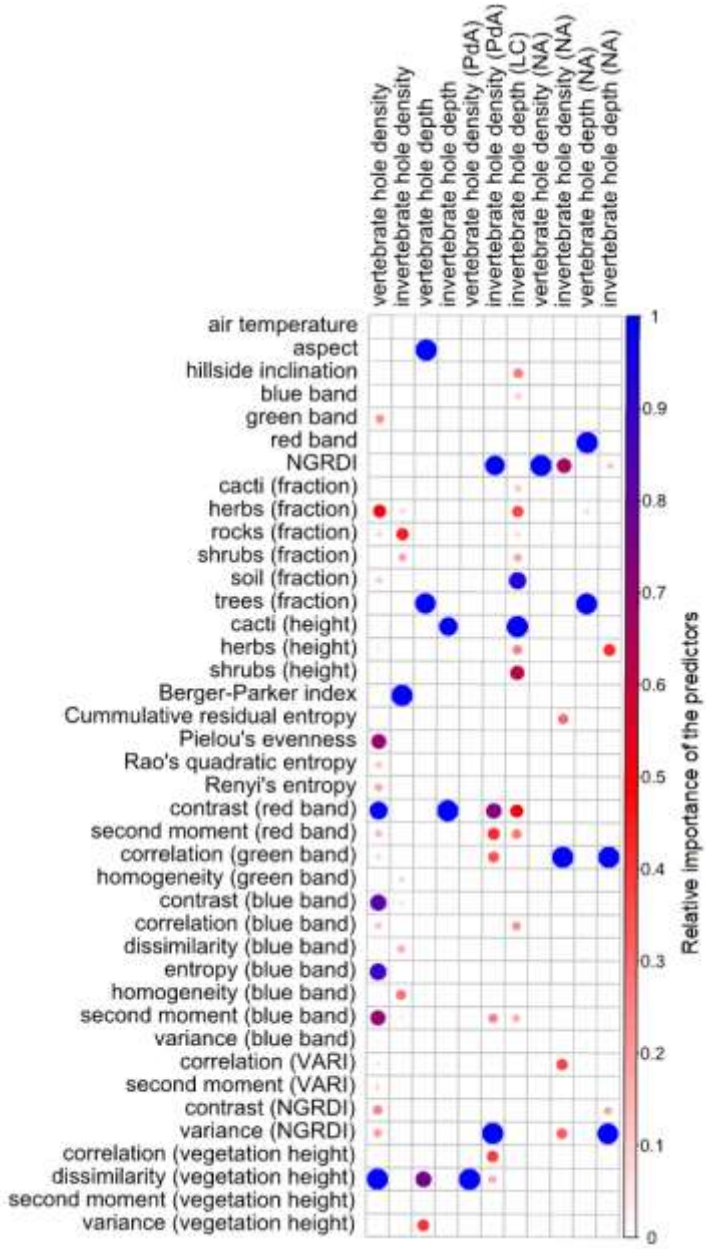

Figure 3.4. Predictor importance in the models fitted for the whole study area and the individual study sites. Only statistically significant models are shown. The importance of all predictors estimated by RFE was normalized from 0 to 1 separately for each model. The predictors not selected by the RFE were assigned a value of 0. PdA = Pan de Azúcar, SG = Santa Gracia, LC = La Campana, NA = Nahuelbuta, VARI = visible atmospherically resistant index (Gitelson et al., 2002), NGRDI = normalized green–red difference index (Tucker, 1979).

3.3.3. Prediction

We used the models trained for the whole study area for the prediction. The predicted hole density and depth varied across sites and hillsides (Figures 5, S2–S6). The highest vertebrate hole density was predicted in SG, with an average of 6.1 holes per 10 m × 10 m, followed by LC with 5.3 holes per 10 m × 10 m. The average vertebrate hole density was 3 holes per 10 m × 10 m in PdA and 4.1 holes per 10 m × 10 m in NA. In SG, on average, 1.5 more holes per 10 m × 10 m were predicted on south-facing than north-facing hillsides. In LC, five more holes, on average, were predicted on the north-facing than south-facing hillsides. There was no difference between the hillsides in PdA and NA. The highest invertebrate hole density was predicted in PdA (13 holes per 10 m × 10 m), followed by SG and LC (ca. 10 holes per 10 m × 10 m), and the lowest density was predicted in NA (4.1 holes per 10 m × 10 m). A higher density was predicted on north-facing than south-facing hillsides in PdA and LC (up to five more holes per 10 m × 10 m), while a lower hole density was predicted on north-facing than south-facing hillsides in SG (up to three fewer holes per 10 m × 10 m).

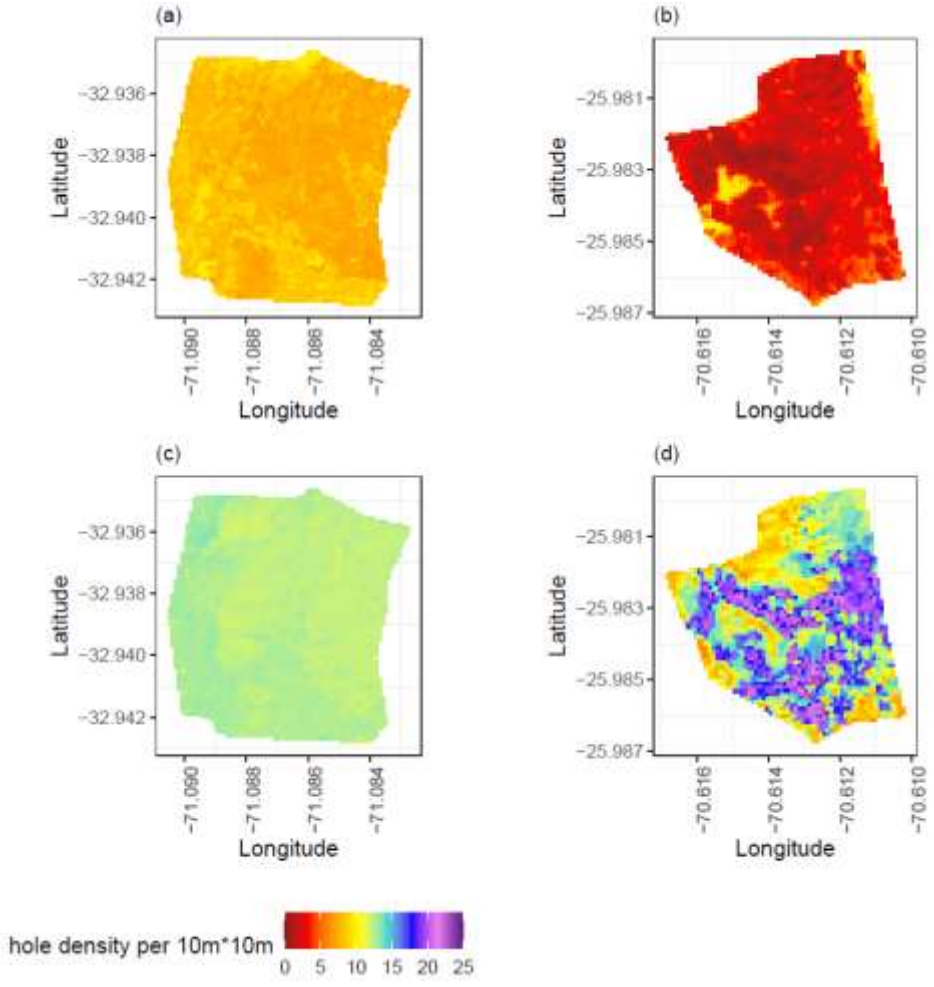

Figure 3.5. Predicted hole density per 10 m × 10 m across north-facing hillsides using models trained for the whole study area: (**a**) Vertebrate hole density in LC; (**b**) vertebrate hole density in PdA; (**c**) invertebrate hole density in LC; and (**d**) invertebrate hole density in PdA.

The distribution of holes and their depth was not uniform along the hillsides and depended on vegetation patterns and inclination of the hillside (Figures S3–S6). The dependencies varied between the sites. In general,

higher density of vertebrate holes was predicted in areas with lower density of invertebrate holes. The density and depth of the holes increased with decreasing hillside inclination and slope.

More vertebrate holes were predicted within the hillside rills. The vertebrate hole density was rather positively associated with the shrub, herb and cacti cover in all climate zones and negatively with the tree cover in the humid-temperate climate zone. It was positively associated with vegetation height in all climate zones except for the humid-temperate zone. The density of invertebrate holes was higher in areas with less vegetation cover and more skeleton within all sites. It was also negatively associated with vegetation height in all climate zones.

The depth of the holes was positively associated with vegetation cover and vegetation height in the arid and semi-arid zone and negatively in the Mediterranean-type and humid-temperate zone. The depth of all holes in arid and semi-arid climate zone was higher in areas with a higher density of vertebrate holes. Deeper holes were predicted near shrubs and herbs. In the Mediterranean-type and humid-temperate climate zone, the depth of vertebrate holes is higher in areas with higher density of vertebrate holes and vice versa. Deeper vertebrate holes were here predicted near herbs, deeper invertebrate holes near skeleton.

3.4. Discussion

We analyzed the potential use of UAV data for the area-wide prediction of the density and depth of holes created by vertebrates and invertebrates in several climate zones. The results demonstrated the importance of including texture metrics, land-cover fractions, land-cover diversity indices, and vegetation height in models. Most of our models achieved a good to moderate performance.

3.4.1. Model Performance

In comparison to models not predicting the density of burrows but only the presence or absence of burrows and mounds (Koshkina et al., 2020), the occurrence of burrowing animals (Valerio et al., 2020), or their species richness (Wallis et al., 2016), our models performed lower. This might be due to the burrowing patterns being dependent on the behavior of individual animals. Animal behavior cannot be predicted by strict physical processes, and is not necessarily the same under similar habitat conditions. On the contrary, it depends on a large variety of factors, such as small-scale soil and vegetation conditions, (Deacon, 2006), intra-species competition, or even the well-being of every individual (Jirkof, 2014).

The models trained using plots from all 4 sites (Figure 3.3) underestimate higher hole density and deeper hole depth. These errors more likely occurred due to response data variability and possible range of predictor values describing environmental parameters. The predictor values described the vegetation patterns per 10 m. This might lead to a lower accuracy especially in the semi-arid and Mediterranean-type climate with homogenous vegetation patterns within the site. The models could not distinguish small-scale changes and aptitudes in hole density and depth in dependence on these parameters and thus the model predicts very similar values for these sites. Another reason might be the data variability. Due to random resampling of the data during the training, the models might capture the changing hole density and depth tendencies between the sites but not the magnitudes within the sites. This explanation is supported by the higher accuracy of models trained separately for the arid and humid-temperate sites, in comparison to models trained for the whole study area and for the semi-arid and Mediterranean-type climate zone (Table 3.2).

The lower model accuracy can furthermore be caused by error propagation, as the models trained using same predictors estimated in situ achieved higher accuracy. The uncertainties accumulated during the calculation of predictors vegetation cover and vegetation height might cause lower model accuracy. However, the models trained separately for the arid zone PdA, in which the UAVs captured the ground vegetation in comparison to Mediterranean-type and humid-temperate areas where the ground vegetation is covered by tree canopy, did still achieve the highest accuracy.

The models trained for invertebrates outperformed those trained for vertebrates. The reason for this may be due to the differences in habitat preferences between vertebrates and invertebrates. In the case of vertebrates, limitations of remote sensing-based predictors have been attributed to the unpredictability of vertebrate behavior and the number of suitable, yet unoccupied areas (Leyequien et al., 2007). Furthermore, the applicability of remote sensing predictors depends on the vertebrate trophic level, as the distribution of herbivore species is more likely to correlate with various vegetation characteristics, while predator and generalist habitat characteristics are not associated with variables directly measurable by remote sensing (Leyequien et al., 2007; Cowley et al., 2000). In contrast, the distribution of all soil-living invertebrates has been shown to be highly associated with vegetation diversity and soil properties, which directly affect vegetation distribution (Tajik et al., 2020).

The models for predicting hole density outperformed those for hole depth. The worst result was obtained when predicting vertebrate hole depth. For invertebrates, the measured hole depth presumably determines the maximum depth that they have reached, whereas vertebrate burrows are more complex (Mukherjee et al., 2017). As we measured only the depth of the hole leading to the burrow, and not the complexity of the underground burrow, this may explain the poorer model performance.

Among the models trained for each of the study sites, the models for the arid PdA and humid-temperate NA performed better than those for LC and SG. In the arid climate zone, a strong link between burrowing and vegetation distribution can be expected, as the habitat choice has been shown to be associated with water and nutrient supply, due to limited resources (Cerqueira, 1985). No such clear relationship can be applied to semi-arid and Mediterranean-type climate zones, where the distribution of burrowing animals has been found to be both positively (Milstead et al., 2007) and negatively (Meserve, 1981; Cramer and Willig, 2005) associated with vegetation distribution. Thus, it is not surprising that the models for study sites performed better where a clear positive relationship between vegetation distribution and burrowing animals can be expected.

3.4.2. Predictor Importance

The predictor importance varied between the models. The texture metrics were more important in the models for the whole study area, while land-cover fractions were more important in the models trained for individual sites. Our results indicate that the level of spatial heterogeneity determines the difference in burrowing patterns between sites. At the same time, small-scale differences within sites were dependent on specific vegetation distribution and vegetation types. Previous studies have shown a strong link between biodiversity and spectral heterogeneity (Rocchini et al., 2004; Rocchini et al., 2010; Rocchini et al., 2018; Oldeland et al., 2010). Although we did not predict the biodiversity of burrowing animals, the burrowing patterns were shown to be species-dependent (Platt et al., 2016).

Predictors selected for the hole density were mostly the texture metrics calculated from the NGRDI and VARI. These indices have been shown to correlate with plant biomass and the vegetation fraction, and were

able to detect small-scale patterns of biomass variability (Bendig et al., 2015; Gitelson et al., 2002). Burrowing animals have an impact on the vegetation coverage (Davidson and Lightfoot, 2007; Pang et al., 2021; Zhang et al., 2017; Zhao et al., 2021); however, the specific impacts seem to vary between species, with some species mainly being affecting the distribution of cacti (Milstead et al., 2007), thorn shrubs (Turnock et al., 2017), or herbs (Contreras and Gutiérrez, 1991). Therefore, it is no surprise that the indices describing variation in vegetation biomass (Bendig et al., 2015; Gitelson et al., 2002), and not simple land-cover fractions, were identified as the most important predictors. Our results are furthermore in line with studies using satellite images which have identified indices related to vegetation density as being significant for the prediction of animal abundance (Chidodo et al., 2020; Andreo et al., 2019).

The diversity indices and texture metrics calculated from the vegetation height and vegetation indices were especially important predictors for vertebrate hole density and depth. The texture metrics entropy and dissimilarity and the diversity indices Shannon's and Rao's quadratic entropy were selected, which are all associated with a heterogeneous landscape (Shannon, 1948; Rao, 1982). Previous studies using heterogeneity and texture metrics in their models have identified them as significant for the prediction of the habitats of burrowing vertebrates (Valerio et al., 2020). An association between landscape heterogeneity and the distribution of animals has been shown in a number of ecological studies considering the long-term impacts of burrowing animals (Ballová et al., 2019; Valkó et al., 2021). Burrowing vertebrates, in particular, have been found to create dense vegetation patches due to the concentration of resources near burrows [18,24,25].

For invertebrates, the texture metrics homogeneity and correlation were identified as the most important predictors. In comparison to our results, a previous study (Wallis et al., 2017) found the diversity of invertebrate species to be associated with the texture entropy calculated from the NDVI and ARI. The habitat complexity has also been shown to be positively associated with invertebrate diversity and abundance (Mormul et al., 2011), possibly as the distribution of roots and stems creates suiTable 3.microhabitats (Thomaz, Sidinei,M. et al., 2007). Thus, the findings of previous studies support our results.

3.5. Conclusions

In this study, we demonstrated the potential of using UAV data to predict the density and depth of holes created by burrowing animals. Our models achieved moderate performance. Models trained for the study area outperformed models trained separately for the single study sites, except for the arid climate zone. Models for the invertebrates outperformed models for the vertebrates and models for the hole density outperformed models for the hole depth. The results furthermore show the importance of inclusion of vertical and horizontal landscape structures into the models, as the models mostly relied on the diversity indices, vegetation height and texture metrics calculated from the vegetation height.

The results furthermore showed the dependence of burrowing intensity on vegetation patterns. Vertebrate hole density and depth was rather positively associated with vegetation cover and height (especially of shrubs and herbs) in all except in the humid-temperate climate zone. Invertebrate hole density was negatively associated with the vegetation cover in all climate zones and with vegetation height in the Mediterranean-type climate zone.

Supplementary Materials: The following are available online at www.mdpi.com/xxx/s1, Table 3.S1: Mean density and depth of vertebrate and invertebrate holes per site, Table 3.S2: Summary of the collected UAV data sets, Table 3.S3: Hierarchy of classes for the land-cover classification, Table 3.S4: Sensitivity of individual land-cover classes of the land-cover classification models trained for each site separately, Table 3.S5: Performance of models trained with each predictor set separately, Table 3.S6: Significant variables selected by the linear mixed model for the vertebrate hole density, Table 3.S7: Significant variables selected by the linear mixed model for the invertebrate hole density, Table 3.S8: Significant variables selected by the linear mixed model for the vertebrate hole depth, Table 3.S9: Significant variables selected by the linear mixed model for the invertebrate hole depth, Figure 3.S1: Predictor selection by means of recursive feature, Figure 3.S2: Predicted hole density and depth across hillsides, Figure 3.S3: Predicted hole density and depth in PdA, Figure 3.S4: Predicted hole density and depth in SG, Figure 3.S5: Predicted hole density and depth in LC, Figure 3.S6: Predicted hole density and depth in NA, Figure 3.S7: Examples of measured holes.

Author Contributions: P.G. conducted the field research and UAV flights, processed and evaluated the data, and wrote the manuscript. S.A., R.F. and A.K. conducted field research and UAV flights. D.K. provided hole density field data. S.A. provided technical support. L.P., P.P. and K.Ü. supported the field research. J.B., A.L., N.F. and R.B. designed and supervised the project and supported the field research. All authors discussed the results and contributed to the final manuscript. All authors have read and agreed to the published version of the manuscript.

Funding: This study was funded by the German Research Foundation, DFG [grant numbers BE1780/52-1, LA3521/1-1, FA 925/12-1, BR 1293-18-1], and is part of the DFG Priority Programme SPP 1803: EarthShape: Earth Surface Shaping by Biota, sub-project “Effects of bioturbation on rates of vertical and horizontal sediment and nutrient fluxes”.

Institutional Review Board Statement: Not applicable

Informed Consent Statement: Not applicable

Data availability statement: The respective results can be accessed in Grigusova, P. (2021). Predicted density and depth of holes created by burrowing animals across 8 hillsides along Chilean climate gradient [Data set]. Laboratory for Climatology and Remote Sensing (LCRS), University of Marburg. DOI: 10.5678/lcrs/dat.433.

Acknowledgments: We further thank CONAF for the kind support provided during our field campaign.

Conflicts of Interest: There is no conflict of interest.

References

Albores-Barajas, Y. V., Soldatini, C., Ramos-Rodríguez, A., Alcala-Santoyo, J. E., Carmona, R., and Dell’Omo, G.: A new use of technology to solve an old problem: Estimating the population size of a burrow nesting seabird, PloS one, 13, e0202094, https://doi.org/10.1371/journal.pone.0202094, 2018.

Andreo, V., Belgiu, M., Hoyos, D. B., Osei, F., Provensal, C., and Stein, A.: Rodents and satellites: Predicting mice abundance and distribution with Sentinel-2 data, Ecological Informatics, 51, 157–167, https://doi.org/10.1016/j.ecoinf.2019.03.001, 2019.

Ballová, Z., Pekárik, L., Píš, V., and Šibík, J.: How much do ecosystem engineers contribute to landscape evolution? A case study on Tatra marmots, CATENA, 182, 104121, https://doi.org/10.1016/j.catena.2019.104121, 2019.

Bates, D., Mächler, M., Bolker, B., and Walker, S.: Fitting Linear Mixed-Effects Models Using lme4, J. Stat. Soft., 67, https://doi.org/10.18637/jss.v067.i01, 2015.

Bendig, J., Yu, K., Aasen, H., Bolten, A., Bennertz, S., Broscheit, J., Gnyp, M. L., and Bareth, G.: Combining UAV-based plant height from crop surface models, visible, and near infrared vegetation indices for biomass monitoring in barley, International Journal of Applied Earth Observation and Geoinformation, 39, 79–87, https://doi.org/10.1016/j.jag.2015.02.012, 2015.

Berger, W. H. and Parker, F. L.: Diversity of planktonic foraminifera in deep-sea sediments, Science (New York, N.Y.), 168, 1345–1347, https://doi.org/10.1126/science.168.3937.1345, 1970.

Bernhard, N., Moskwa, L.-M., Schmidt, K., Oeser, R. A., Aburto, F., Bader, M. Y., Baumann, K., Blanckenburg, F. von, Boy, J., van den Brink, L., Brucker, E., Büdel, B., Canessa, R., Dippold, M. A., Ehlers, T. A., Fuentes, J. P., Godoy, R., Jung, P., Karsten, U., Köster, M., Kuzyakov, Y., Leinweber, P., Neidhardt, H., Matus, F., Mueller, C. W., Oelmann, Y., Oses, R., Osses, P., Paulino, L., Samolov, E., Schaller, M., Schmid, M., Spielvogel, S., Spohn, M., Stock, S., Stroncik, N., Tielbörger, K., Übernickel, K., Scholten, T., Seguel, O., Wagner, D., and Kühn, P.: Pedogenic and microbial interrelations to regional climate and local topography: New insights from a climate gradient (arid to humid) along the Coastal Cordillera of Chile, CATENA, 170, 335–355, https://doi.org/10.1016/j.catena.2018.06.018, 2018.

Borgatti, L., Forte, E., Mocnik, A., Zambrini, R., Cervi, F., Martinucci, D., Pellegrini, F., Pillon, S., Prizzon, A., and Zamariolo, A.: Detection and characterization of animal burrows within river embankments by means of coupled remote sensing and geophysical techniques: Lessons from River Panaro (northern Italy), Engineering Geology, 226, 277–289, https://doi.org/10.1016/j.enggeo.2017.06.017, 2017.

Bourgoin, C., Betbeder, J., Couteron, P., Blanc, L., Dessard, H., Oszwald, J., Le Roux, R., Cornu, G., Reymondin, L., Mazzei, L., Sist, P., Läderach, P., and Gond, V.: UAV-based canopy textures assess changes in forest structure from long-term degradation, Ecological Indicators, 115, 106386, https://doi.org/10.1016/j.ecolind.2020.106386, 2020.

Bowker, M. A., Eldridge, D. J., Val, J., and Soliveres, S.: Hydrology in a patterned landscape is co-engineered by soil-disturbing animals and biological crusts, Soil Biology and Biochemistry, 61, 14–22, https://doi.org/10.1016/j.soilbio.2013.02.002, 2013.

Breiman, L.: Random Forests, Machine Learning, 45, 5–32, https://doi.org/10.1023/A:1010933404324, 2001.

Bycroft, R., Leon, J. X., and Schoeman, D.: Comparing random forests and convoluted neural networks for mapping ghost crab burrows using imagery from an unmanned aerial vehicle, Estuarine, Coastal and Shelf Science, 224, 84–93, https://doi.org/10.1016/j.ecss.2019.04.050, 2019.

Canham, C. D.: An Index For Understory Light Levels in and Around Canopy Gaps, Ecology, 69, 1634–1638, https://doi.org/10.2307/1941664, 1988.

Cerqueira, R.: The Distribution of Didelphis in South America (Polyprotodontia, Didelphidae), Journal of Biogeography, 12, 135, https://doi.org/10.2307/2844837, 1985.

Chidodo, D. J., Kimaro, D. N., Hieronimo, P., Makundi, R. H., Isabirye, M., Leirs, H., Massawe, A. W., Mdangi, M. E., Kifumba, D., and Mulungu, L. S.: Application of normalized difference vegetation index (NDVI) to forecast rodent population abundance in smallholder agro-ecosystems in semi-arid areas in Tanzania, Mammalia, 84, 136–143, https://doi.org/10.1515/mammalia-2018-0175, 2020.

Contreras, L. C. and Gutiérrez, J. R.: Effects of the subterranean herbivorous rodent Spalacopus cyanus on herbaceous vegetation in arid coastal Chile, Oecologia, 87, 106–109, https://doi.org/10.1007/BF00323787, 1991.

Cowley, M. J. R., Wilson, R. J., Leon-Cortes, J. L., Gutierrez, D., Bulman, C. R., and Thomas, C. D.: Habitat-based statistical models for predicting the spatial distribution of butterflies and day-flying moths in a fragmented landscape, J Appl Ecology, 37, 60–72, https://doi.org/10.1046/j.1365-2664.2000.00526.x, 2000.

Cramer, M. J. and Willig, M. R.: Habitat heterogeneity, species diversity and null models, Oikos, 108, 209–218, https://doi.org/10.1111/j.0030-1299.2005.12944.x, 2005.

Culbert, P. D., Radeloff, V. C., St-Louis, V., Flather, C. H., Rittenhouse, C. D., Albright, T. P., and Pidgeon, A. M.: Modeling broad-scale patterns of avian species richness across the Midwestern United States with measures of satellite image texture, Remote Sensing of Environment, 118, 140–150, https://doi.org/10.1016/j.rse.2011.11.004, 2012.

Cunha, L., Brown, G. G., Stanton, D. W. G., Da Silva, E., Hansel, F. A., Jorge, G., McKey, D., Vidal-Torrado, P., Macedo, R. S., Velasquez, E., James, S. W., Lavelle, P., and Kille, P.: Soil Animals and Pedogenesis, Soil Science, 181, 110–125, https://doi.org/10.1097/SS.0000000000000144, 2016.

Davidson, A. D. and Lightfoot, D. C.: Interactive effects of keystone rodents on the structure of desert grassland arthropod communities, Ecography, 30, 515–525, https://doi.org/10.1111/j.0906-7590.2007.05032.x, 2007.

Deacon, R. M. J.: Assessing nest building in mice, Nature protocols, 1, 1117–1119, https://doi.org/10.1038/nprot.2006.170, 2006.

Don, A., Hagen, C., Grüneberg, E., and Vos, C.: Simulated wild boar bioturbation increases the stability of forest soil carbon, Biogeosciences, 16, 4145–4155, https://doi.org/10.5194/bg-16-4145-2019, 2019.

Ferro, L. I. and Barquez, R. M.: Species Richness of Nonvolant Small Mammals Along Elevational Gradients in Northwestern Argentina, Biotropica, 41, 759–767, https://doi.org/10.1111/j.1744-7429.2009.00522.x, 2009.

Fritz, A., Li, L., Storch, I., and Koch, B.: UAV-derived habitat predictors contribute strongly to understanding avian species-habitat relationships on the Eastern Qinghai-Tibetan Plateau, Remote Sens Ecol Conserv, 4, 53–65, https://doi.org/10.1002/rse2.73, 2018.

Frouz, J., Pižl, V., Cienciala, E., and Kalčík, J.: Carbon storage in post-mining forest soil, the role of tree biomass and soil bioturbation, Biogeochemistry, 94, 111–121, https://doi.org/10.1007/s10533-009-9313-0, 2009.

Fu, Y., Yang, G., Song, X., Li, Z., Xu, X., Feng, H., and Zhao, C.: Improved Estimation of Winter Wheat Aboveground Biomass Using Multiscale Textures Extracted from UAV-Based Digital Images and Hyperspectral Feature Analysis, Remote Sensing, 13, 581, https://doi.org/10.3390/rs13040581, 2021.

Gabet, E. J., Reichman, O. J., and Seabloom, E. W.: The Effects of Bioturbation on Soil Processes and Sediment Transport, Annu. Rev. Earth Planet. Sci., 31, 249–273, https://doi.org/10.1146/annurev.earth.31.100901.141314, 2003.

Gandor, F., Rehak, M., and Skaloud, J.: PHOTOGRAMMETRIC MISSION PLANNER FOR RPAS, Int. Arch. Photogramm. Remote Sens. Spatial Inf. Sci., XL-1/W4, 61–65, https://doi.org/10.5194/isprsarchives-XL-1-W4-61-2015, 2015.

Gholizadeh, A., Žižala, D., Saberioon, M., and Borůvka, L.: Soil organic carbon and texture retrieving and mapping using proximal, airborne and Sentinel-2 spectral imaging, Remote Sensing of Environment, 218, 89–103, https://doi.org/10.1016/j.rse.2018.09.015, 2018.

Gillespie, A. R., Kahle, A. B., and Walker, R. E.: Color enhancement of highly correlated images. II. Channel ratio and "chromaticity" transformation techniques, Remote Sensing of Environment, 22, 343–365, https://doi.org/10.1016/0034-4257(87)90088-5, 1987.

Gitelson, A. A., Kaufman, Y. J., Stark, R., and Rundquist, D.: Novel algorithms for remote estimation of vegetation fraction, Remote Sensing of Environment, 80, 76–87, https://doi.org/10.1016/S0034-4257(01)00289-9, 2002.

Guo, Z. G., Zhou, X. R., and Hou, Y.: Effect of available burrow densities of plateau pika (Ochotona curzoniae) on soil physicochemical property of the bare land and vegetation land in the Qinghai-Tibetan Plateau, Acta Ecologica Sinica, 32, 104–110, https://doi.org/10.1016/j.chnaes.2012.02.002, 2012.

Hall-Beyer, M.: Practical guidelines for choosing GLCM textures to use in landscape classification tasks over a range of moderate spatial scales, International Journal of Remote Sensing, 38, 1312–1338, https://doi.org/10.1080/01431161.2016.1278314, 2017.

Haralick, R. M., Shanmugam, K., and Dinstein, I.'H.: Textural Features for Image Classification, IEEE Trans. Syst., Man, Cybern., SMC-3, 610–621, https://doi.org/10.1109/TSMC.1973.4309314, 1973.

Hijmans, R. J., van Etten, J., Sumner, M., Cheng, J., Baston, D., Bevan, A., Bivand, R., Busetto, L., Canty, M., Fasoli, B., Forrest, D., Ghosh, A., Golicher, D., Gray, J., Greenberg, J. A., Hiemstra, P., Hingee, K., Karney, C., Mattiuzi, M., Mosher, S., Naimi, B., Nowosad, J., Pebesma, E., Lamigueiro, O. P., Racine, E. B., Rowlingson, B., Shortridge, A., Venables, B., and Wueest, R.: raster: Geographic Data Analysis and Modeling. https://rspatial.org/raster .

Hill, M. O.: Diversity and Evenness: A Unifying Notation and Its Consequences, Ecology, 54, 427–432, https://doi.org/10.2307/1934352, 1973.

Horn, B.K.P.: Hill shading and the reflectance map, Proc. IEEE, 69, 14–47, https://doi.org/10.1109/PROC.1981.11918, 1981.

Jacob, J.: Response of small rodents to manipulations of vegetation height in agro-ecosystems, Integrative zoology, 3, 3–10, https://doi.org/10.1111/j.1749-4877.2008.00078.x, 2008.

Jimenez, J. E., Feinsinger, P., and Jaksi, F. M.: Spatiotemporal Patterns of an Irruption and Decline of Small Mammals in Northcentral Chile, Journal of Mammalogy, 73, 356–364, https://doi.org/10.2307/1382070, 1992.

Jirkof, P.: Burrowing and nest building behavior as indicators of well-being in mice, Journal of neuroscience methods, 234, 139–146, https://doi.org/10.1016/j.jneumeth.2014.02.001, 2014.

JOECKEL, R. M. and TUCKER, S. T.: Exceptionally well preserved latest Miocene (Hemphillian) rodent burrows from Eastern Great Plains, United States, and a review of the burrows of North American rodents., PALAIOS, 28, 793–824, https://doi.org/10.2110/palo.2014.042, 2013.

Koshkina, A., Grigoryeva, I., Tokarsky, V., Urazaliyev, R., Kuemmerle, T., Hölzel, N., and Kamp, J.: Marmots from space: assessing population size and habitat use of a burrowing mammal using publicly available satellite images, Remote Sens Ecol Conserv, 6, 153–167, https://doi.org/10.1002/rse2.138, 2020.

Kuhn, M.: Building Predictive Models in R Using the caret Package, J. Stat. Soft., 28, https://doi.org/10.18637/jss.v028.i05, 2008.

Lehnert, L. W., Thies, B., Trachte, K., Achilles, S., Osses, P., Baumann, K., Bendix, J., Schmidt, J., Samolov, E., Jung, P., Leinweber, P., Karsten, U., and Büdel, B.: A Case Study on Fog/Low Stratus Occurrence at Las Lomitas, Atacama Desert (Chile) as a Water Source for Biological Soil Crusts, Aerosol Air Qual. Res., 18, 254–269, https://doi.org/10.4209/aaqr.2017.01.0021, 2018.

Leyequien, E., Verrelst, J., Slot, M., Schaepman-Strub, G., Heitkönig, I. M.A., and Skidmore, A.: Capturing the fugitive: Applying remote sensing to terrestrial animal distribution and diversity, International Journal of Applied Earth Observation and Geoinformation, 9, 1–20, https://doi.org/10.1016/j.jag.2006.08.002, 2007.

Louw, M. A., Haussmann, N. S., and Le Roux, P. C.: Testing for consistency in the impacts of a burrowing ecosystem engineer on soil and vegetation characteristics across biomes, Scientific reports, 9, 19355, https://doi.org/10.1038/s41598-019-55917-x, 2019.

Medel, R. G. and Vásquez, R. A.: Comparative analysis of harvester ant assemblages of Argentinian and Chilean arid zones, Journal of Arid Environments, 26, 363–371, https://doi.org/10.1006/jare.1994.1038, 1994.

Meserve, P. L.: Trophic Relationships among Small Mammals in a Chilean Semiarid Thorn Scrub Community, Journal of Mammalogy, 62, 304–314, https://doi.org/10.2307/1380707, 1981.

Milstead, W. B., Meserve, P. L., Campanella, A., Previtali, M. A., Kelt, D. A., and Gutiérrez, J. R.: Spatial Ecology of Small Mammals in North-central Chile: Role of Precipitation and Refuges, Journal of Mammalogy, 88, 1532–1538, https://doi.org/10.1644/16-MAMM-A-407R.1, 2007.

Mormul, R. P., Thomaz, S. M., Takeda, A. M., and Behrend, R. D.: Structural Complexity and Distance from Source Habitat Determine Invertebrate Abundance and Diversity, Biotropica, 43, 738–745, https://doi.org/10.1111/j.1744-7429.2011.00762.x, 2011.

Mukherjee, A., Pilakandy, R., Kumara, H. N., Manchi, S. S., and Bhupathy, S.: Burrow characteristics and its importance in occupancy of burrow dwelling vertebrates in Semiarid area of Keoladeo National Park, Rajasthan, India, Journal of Arid Environments, 141, 7–15, https://doi.org/10.1016/j.jaridenv.2017.02.003, 2017.

Muñoz-Pedreros, A., Yáñez, J., Norambuena, H. V., and Zúñiga, A.: Diet, dietary selectivity and density of South American grey fox, Lycalopex griseus, in Central Chile, Integrative zoology, 13, 46–57, https://doi.org/10.1111/1749-4877.12260, 2018.

Nkem, J. N., Lobry de Bruyn, L. A., Grant, C. D., and Hulugalle, N. R.: The impact of ant bioturbation and foraging activities on surrounding soil properties, Pedobiologia, 44, 609–621, https://doi.org/10.1078/S0031-4056(04)70075-X, 2000.

Nychka, D.: fields: Tools for Spatial Data, UCAR/NCAR - Computational and Information Systems Laboratory (CISL), 2016.

Oeser, R. A., Stroncik, N., Moskwa, L.-M., Bernhard, N., Schaller, M., Canessa, R., van den Brink, L., Köster, M., Brucker, E., Stock, S., Fuentes, J. P., Godoy, R., Matus, F. J., Oses Pedraza, R., Osses McIntyre, P., Paulino, L., Seguel, O., Bader, M. Y., Boy, J., Dippold, M. A., Ehlers, T. A., Kühn, P., Kuzyakov, Y., Leinweber, P., Scholten, T., Spielvogel, S., Spohn, M., Übernickel, K., Tielbörger, K., Wagner, D., and Blanckenburg, F. von: Chemistry and microbiology of the Critical Zone along a steep climate and vegetation gradient in the Chilean Coastal Cordillera, CATENA, 170, 183–203, https://doi.org/10.1016/j.catena.2018.06.002, 2018.

Old, J. M., Lin, S. H., and Franklin, M. J. M.: Mapping out bare-nosed wombat (Vombatus ursinus) burrows with the use of a drone, BMC ecology, 19, 39, https://doi.org/10.1186/s12898-019-0257-5, 2019.

Oldeland, J., Wesuls, D., Rocchini, D., Schmidt, M., and Jürgens, N.: Does using species abundance data improve estimates of species diversity from remotely sensed spectral heterogeneity?, Ecological Indicators, 10, 390–396, https://doi.org/10.1016/j.ecolind.2009.07.012, 2010.

Olsoy, P. J., Shipley, L. A., Rachlow, J. L., Forbey, J. S., Glenn, N. F., Burgess, M. A., and Thornton, D. H.: Unmanned aerial systems measure structural habitat features for wildlife across multiple scales, Methods Ecol Evol, 9, 594–604, https://doi.org/10.1111/2041-210X.12919, 2018.

Pang, X. P., Yang, H., Wei, X. X., and Guo, Z. G.: Effect of plateau pika (Ochotona curzoniae) bioturbation on soil C-N-P stoichiometry in alpine meadows, Geoderma, 397, 115098, https://doi.org/10.1016/j.geoderma.2021.115098, 2021.

Parsons, M. A., Barkley, T. C., Rachlow, J. L., Johnson-Maynard, J. L., Johnson, T. R., Milling, C. R., Hammel, J. E., and Leslie, I.: Cumulative effects of an herbivorous ecosystem engineer in a heterogeneous landscape, Ecosphere, 7, 388, https://doi.org/10.1002/ecs2.1334, 2016.

Pielou, E. C.: The measurement of diversity in different types of biological collections, Journal of Theoretical Biology, 13, 131–144, https://doi.org/10.1016/0022-5193(66)90013-0, 1966.

Pizarro-Araya, J. and JEREZ, V.: Distribución geográfica del género Gyriosomus Guérin-Méneville, 1834 (Coleoptera: Tenebrionidae): una aproximación biogeográfica, Rev. chil. hist. nat., 77, https://doi.org/10.4067/S0716-078X2004000300008, 2004.

Platt, B. F., Kolb, D. J., Kunhardt, C. G., Milo, S. P., and New, L. G.: Burrowing Through the Literature, Soil Science, 181, 175–191, https://doi.org/10.1097/SS.0000000000000150, 2016.

Qin, Y., Yi, S., Ding, Y., Qin, Y., Zhang, W., Sun, Y., Hou, X., Yu, H., Meng, B., Zhang, H., Chen, J., and Wang, Z.: Effects of plateau pikas' foraging and burrowing activities on vegetation biomass and soil organic carbon of alpine grasslands, Plant Soil, 458, 201–216, https://doi.org/10.1007/s11104-020-04489-1, 2021.

Rahimzadeh-Bajgiran, P., Omasa, K., and Shimizu, Y.: Comparative evaluation of the Vegetation Dryness Index (VDI), the Temperature Vegetation Dryness Index (TVDI) and the improved TVDI (iTVDI) for water stress detection in semi-arid regions of Iran, ISPRS Journal of Photogrammetry and Remote Sensing, 68, 1–12, https://doi.org/10.1016/j.isprsjprs.2011.10.009, 2012.

Rao, C.R.: Diversity and dissimilarity coefficients: A unified approach, Theoretical Population Biology, 21, 24–43, https://doi.org/10.1016/0040-5809(82)90004-1, 1982.

Rao, M., Chen, Y., Vemuri, B. C., and Wang, F.: Cumulative Residual Entropy: A New Measure of Information, IEEE Trans. Inform. Theory, 50, 1220–1228, https://doi.org/10.1109/TIT.2004.828057, 2004.

Regolin, A. L., Ribeiro, M. C., Martello, F., Melo, G. L., Sponchiado, J., Campanha, L. F. d. C., Sugai, L. S. M., Silva, T. S. F., and Cáceres, N. C.: Spatial heterogeneity and habitat configuration overcome habitat composition influences on alpha and beta mammal diversity, Biotropica, 52, 969–980, https://doi.org/10.1111/btp.12800, 2020.

Rényi, A.: On Measures of Entropy and Information, Berkeley Symposium on Mathematical Statistics and Probability, 547–561, 1961.

Rocchini, D., Thouverai, E., Marcantonio, M., Iannacito, M., Da Re, D., Torresani, M., Bacaro, G., Bazzichetto, M., Bernardi, A., Foody, G. M., Furrer, R., Kleijn, D., Larsen, S., Lenoir, J., Malavasi, M., Marchetto, E., Messori, F., Montaghi, A., Moudrý, V., Naimi, B., Ricotta, C., Rossini, M., Santi, F., Santos, M. J., Schaepman, M. E., Schneider, F. D., Schuh, L., Silvestri, S., Šímová, P., Skidmore, A. K., Tattoni, C., Tordoni, E., Vicario, S., Zannini, P., and Wegmann, M.: rasterdiv—

An Information Theory tailored R package for measuring ecosystem heterogeneity from space: To the origin and back, Methods Ecol Evol, 12, 1093–1102, https://doi.org/10.1111/2041-210X.13583, 2021.

Rocchini, D., Bacaro, G., Chirici, G., Da Re, D., Feilhauer, H., Foody, G. M., Galluzzi, M., Garzon-Lopez, C. X., Gillespie, T. W., He, K. S., Lenoir, J., Marcantonio, M., Nagendra, H., Ricotta, C., Rommel, E., Schmidtlein, S., Skidmore, A. K., van de Kerchove, R., Wegmann, M., and Rugani, B.: Remotely sensed spatial heterogeneity as an exploratory tool for taxonomic and functional diversity study, Ecological Indicators, 85, 983–990, https://doi.org/10.1016/j.ecolind.2017.09.055, 2018.

Rocchini, D., Balkenhol, N., Carter, G. A., Foody, G. M., Gillespie, T. W., He, K. S., Kark, S., Levin, N., Lucas, K., Luoto, M., Nagendra, H., Oldeland, J., Ricotta, C., Southworth, J., and Neteler, M.: Remotely sensed spectral heterogeneity as a proxy of species diversity: Recent advances and open challenges, Ecological Informatics, 5, 318–329, https://doi.org/10.1016/j.ecoinf.2010.06.001, 2010.

Rocchini, D., Chiarucci, A., and Loiselle, S. A.: Testing the spectral variation hypothesis by using satellite multispectral images, Acta Oecologica, 26, 117–120, https://doi.org/10.1016/j.actao.2004.03.008, 2004.

Sammut, C. and Webb, G. I. (Eds.): Encyclopedia of Machine Learning, Springer US, Boston, MA, 2010.

Sandino, J., Wooler, A., and Gonzalez, F.: Towards the Automatic Detection of Pre-Existing Termite Mounds through UAS and Hyperspectral Imagery, Sensors (Basel, Switzerland), 17, https://doi.org/10.3390/s17102196, 2017.

Shannon, C. E.: A Mathematical Theory of Communication, Bell System Technical Journal, 27, 379–423, https://doi.org/10.1002/j.1538-7305.1948.tb01338.x, 1948.

Shipitalo, M. and Le Bayon, R.-C.: Quantifying the Effects of Earthworms on Soil Aggregation and Porosity, in: Earthworm Ecology, edited by: Edwards, C., CRC Press, 183–200, https://doi.org/10.1201/9781420039719.pt5, 2004.

Simonetti, J. A.: Microhabitat Use by Small Mammals in Central Chile, Oikos, 56, 309, https://doi.org/10.2307/3565615, 1989.

St-Louis, V., Pidgeon, A. M., Radeloff, V. C., Hawbaker, T. J., and Clayton, M. K.: High-resolution image texture as a predictor of bird species richness, Remote Sensing of Environment, 105, 299–312, https://doi.org/10.1016/j.rse.2006.07.003, 2006.

Szantoi, Z., Smith, S. E., Strona, G., Koh, L. P., and Wich, S. A.: Mapping orangutan habitat and agricultural areas using Landsat OLI imagery augmented with unmanned aircraft system aerial photography, International Journal of Remote Sensing, 38, 2231–2245, https://doi.org/10.1080/01431161.2017.1280638, 2017.

Tajik, S., Ayoubi, S., and Lorenz, N.: Soil microbial communities affected by vegetation, topography and soil properties in a forest ecosystem, Applied Soil Ecology, 149, 103514, https://doi.org/10.1016/j.apsoil.2020.103514, 2020.

Tang, Z., Zhang, Y., Cong, N., Wimberly, M., Wang, L., Huang, K., Li, J., Zu, J., Zhu, Y., and Chen, N.: Spatial pattern of pika holes and their effects on vegetation coverage on the Tibetan Plateau: An analysis using unmanned aerial vehicle imagery, Ecological Indicators, 107, 105551, https://doi.org/10.1016/j.ecolind.2019.105551, 2019.

Tews, J., Brose, U., Grimm, V., Tielbörger, K., Wichmann, M. C., Schwager, M., and Jeltsch, F.: Animal species diversity driven by habitat heterogeneity/diversity: the importance of keystone structures, Journal of Biogeography, 31, 79–92, https://doi.org/10.1046/j.0305-0270.2003.00994.x, 2004.

Thomaz, Sidinei,M., Dibble, E,D., EVANGELISTA, L. R., HIGUTI, J., and BINI, L. M.: Influence of aquatic macrophyte habitat complexity on invertebrate abundance and richness in tropical lagoons, Freshwater Biol, 0, 071116231725007-???, https://doi.org/10.1111/j.1365-2427.2007.01898.x, 2007.

Tuanmu, M.-N. and Jetz, W.: A global, remote sensing-based characterization of terrestrial habitat heterogeneity for biodiversity and ecosystem modelling, Global Ecology and Biogeography, 24, 1329–1339, https://doi.org/10.1111/geb.12365, 2015.

Tucker, C. J.: Red and photographic infrared linear combinations for monitoring vegetation, Remote Sensing of Environment, 8, 127–150, https://doi.org/10.1016/0034-4257(79)90013-0, 1979.

Turnock, B. Y., Litt, A. R., Vore, J. M., and Hammond, C. A. M.: Habitat characteristics of the hoary marmot: assessing distribution limitations in Montana, Ecosphere, 8, e01977, https://doi.org/10.1002/ecs2.1977, 2017.

Übernickel, K., Pizarro-Araya, J., Bhagavathula, S., Paulino, L., and Ehlers, T. A.: Reviews and Syntheses: Composition and Characteristics of Burrowing Animals along a Climate and Ecological Gradient, Chile, 2021.

Übernickel, K., Ehlers, T. A., Ershadi, M. R., Paulino, L., Fuentes Espoz, J.-P., Maldonado, A., Oses-Pedraza, R., and Blanckenburg, F. von: Time series of meteorological station data in the EarthShape study areas of in the Coastal Cordillera, Chile, 2020.

Valerio, F., Ferreira, E., Godinho, S., Pita, R., Mira, A., Fernandes, N., and Santos, S. M.: Predicting Microhabitat Suitability for an Endangered Small Mammal Using Sentinel-2 Data, Remote Sensing, 12, 562, https://doi.org/10.3390/rs12030562, 2020.

Valkó, O., Tölgyesi, C., Kelemen, A., Bátori, Z., Gallé, R., Rádai, Z., Bragina, T. M., Bragin, Y. A., and Deák, B.: Steppe Marmot (Marmota bobak) as ecosystem engineer in arid steppes, Journal of Arid Environments, 184, 104244, https://doi.org/10.1016/j.jaridenv.2020.104244, 2021.

VERGARA, O. E., JEREZ, V., and PARRA, L. E.: Diversidad y patrones de distribución de coleópteros en la Región del Biobío, Chile: una aproximación preliminar para la conservación de la diversidad, Rev. chil. hist. nat., 79, https://doi.org/10.4067/S0716-078X2006000300008, 2006.

Wallis, C. I.B., Brehm, G., Donoso, D. A., Fiedler, K., Homeier, J., Paulsch, D., Süßenbach, D., Tiede, Y., Brandl, R., Farwig, N., and Bendix, J.: Remote sensing improves prediction of tropical montane species diversity but performance differs among taxa, Ecological Indicators, 83, 538–549, https://doi.org/10.1016/j.ecolind.2017.01.022, 2017.

Wallis, C. I.B., Paulsch, D., Zeilinger, J., Silva, B., Curatola Fernández, G. F., Brandl, R., Farwig, N., and Bendix, J.: Contrasting performance of Lidar and optical texture models in predicting avian diversity in a tropical mountain forest, Remote Sensing of Environment, 174, 223–232, https://doi.org/10.1016/j.rse.2015.12.019, 2016.

Wilkinson, M. T. and Humphreys, G. S.: Exploring pedogenesis via nuclide-based soil production rates and OSL-based bioturbation rates, Soil Res., 43, 767, https://doi.org/10.1071/SR04158, 2005.

Wilkinson, M. T., Richards, P. J., and Humphreys, G. S.: Breaking ground: Pedological, geological, and ecological implications of soil bioturbation, Earth-Science Reviews, 97, 257–272, https://doi.org/10.1016/j.earscirev.2009.09.005, 2009.

Woebbecke, D. M., Meyer, G. E., Bargen, K. V., and Mortensen, D. A.: Color Indices for Weed Identification Under Various Soil, Residue, and Lighting Conditions, Transactions of the ASAE, 38, 259–269, https://doi.org/10.13031/2013.27838, 1995.

Wood, E. M., Pidgeon, A. M., Radeloff, V. C., and Keuler, N. S.: Image texture as a remotely sensed measure of vegetation structure, Remote Sensing of Environment, 121, 516–526, https://doi.org/10.1016/j.rse.2012.01.003, 2012.

Young, M. H., Andrews, J. H., Caldwell, T. G., and Saylam, K.: Airborne LiDAR and Aerial Imagery to Assess Potential Burrow Locations for the Desert Tortoise (Gopherus agassizii), Remote Sensing, 9, 458, https://doi.org/10.3390/rs9050458, 2017.

Yu, C., Zhang, J., Pang, X. P., Wang, Q., Zhou, Y. P., and Guo, Z. G.: Soil disturbance and disturbance intensity: Response of soil nutrient concentrations of alpine meadow to plateau pika bioturbation in the Qinghai-Tibetan Plateau, China, Geoderma, 307, 98–106, https://doi.org/10.1016/j.geoderma.2017.07.041, 2017.

Zhang, L.-J., Qi, Y.-A., Buatois, L. A., Mángano, M. G., Meng, Y., and Li, D.: The impact of deep-tier burrow systems in sediment mixing and ecosystem engineering in early Cambrian carbonate settings, Scientific reports, 7, 45773, https://doi.org/10.1038/srep45773, 2017.

Zhang, S., Fang, X., Zhang, J., Yin, F., Zhang, H., Wu, L., and Kitazawa, D.: The Effect of Bioturbation Activity of the Ark Clam Scapharca subcrenata on the Fluxes of Nutrient Exchange at the Sediment-Water Interface, J. Ocean Univ. China, 19, 232–240, https://doi.org/10.1007/s11802-020-4112-2, 2020.

Zhao, J., Tian, L., Wei, H., Zhang, T., Bai, Y., Li, R., and Tang, Y.: Impact of plateau pika (Ochotona curzoniae) burrowing-induced microtopography on ecosystem respiration of the alpine meadow and steppe on the Tibetan plateau, Plant Soil, 458, 217–230, https://doi.org/10.1007/s11104-019-04122-w, 2021.

Zvoleff, A.: Package 'glcm'. Calculate Textures from Grey-Level Co-Occurence Matrices (GLCMs). https://CRAN.R-project.org/package=glcm.

Supplementary material

Table 3.S1: Mean density and depth of vertebrate and invertebrate holes per site. N = number of plots.

Unit	Animals	PdA	SG	LC	NA
Mean density	Vertebrates	1.46	6.75	5.60	1.70
	Invertebrates	16.3	9.90	7.07	3.20
Mean depth	Vertebrates	2.84	2.44	2.87	2.44
	Invertebrates	0.74	0.73	0.76	0.72

Table 3.S2: Summary of the collected UAV data sets (PdA = Pan de Azúcar, SG = Santa Gracia, LC = La Campana, NA = Nahuelbuta; Aspect = the average direction that hillsides are facing counterclockwise from the east; Extent = the minimum and maximum longitude and latitude values of the generated orthophotos of the hillsides [EPSG:4326WGS 84]; Inclination = mean inclination of the hillsides in degrees; Altitude range [a.s.l.] = minimum and maximum altitudes of the hillsides in meters above sea level).

Site	**Aspect [°]**	**Extent**	**Inclination [°]**	**Altitude range [m a.s.l.]**	**Ground Sampling Distance [cm]**	**Covered area [km^2]**
PdA	173.10	-70.61875999999 -25.97690569047 -70.61122717402 -25.97072500000	16.42	485–760	2.57	0.34
	73.10	-70.61747800000 -25.98792750527 -70.61004863371 -25.97936899999	6.62	633–720	3.07	0.58
SG	204.84	-71.169226580458 -29.758944299143 -71.162390068944 -29.754619999691	11.73	630–740	2.57	0.27
	86.76	-71.167225099000 -29.764107785292	4.18	611–723	1.76	0.28

		-71.162634910771				
		-29.758786575999				
		-71.09082499999				
LC	225.36	-32.94316192996 -71.08180970164	11.09	433–591	2.74	0.67
		-32.93423200000 -71.09315231476				
	87.84	-32.93436314092 -71.08806183080	17.01	399–541	1.58	0.30
		-32.92908755615 -73.01619835389				
NA	65.90	-37.80900328612 -73.00848544256	10.50	1190–1248	2.59	0.31
		-37.80456593102 -73.01734991663				
	185.00	-37.811992231189 -73.01034841517 -37.80787731366	5.04	1190–1240	2.59	0.33

Table 3.S3: Hierarchy of classes for the land-cover classification (PdA = Pan de Azúcar, SG = Santa Gracia,

LC = La Campana, NA = Nahuelbuta, X = class represented within the site).

Main class	**Sub-class**	**PdA**	**SG**	**LC**	**NA**
Soil	Soil			X	X
	Weathered granite soil	X	X		
	Saprolite	X	X		
	Soil covered by soil crusts	X			
Cacti	Copiapoa	X			
	Eulychnia	X	X		
	Other cacti		X		
Shrubs	Shrubs	X	X	X	X
Herbs	Herbs	X	X	X	X
Skeleton	Skeleton	X	X	X	
	Rocks				X

	Boulders				X
Trees	Trees	X	X		
	Araucaria				X
	Other genera				X

Table 3.S4: Sensitivity of individual land-cover classes of the land-cover classification models trained for each site separately. Sensitivity = the proportion [%] of positives that are correctly identified.

Main class	**Sub-class**	**PdA**	**SG**	**LC**	**NA**
Soil	Soil	94		94	78
	Granite	87	83		
	Saprolite	86	1		
	Soil crusts	95			
Cacti	Copiapoa	77			
	Eulychnia	84	85		
	Other cacti		92		
Shrubs	Shrubs	82	47	84	68
Herbs	Herbs	53	79	83	60
Skeleton	Skeleton	90	58	72	
	Rocks				59
	Boulders				69
Trees	Trees			81	
	Araucaria				80
	Other genera				92

Table 3.S5: Performance of models trained with each predictor set separately.

	Hole density				**Hole depth**			
	Vertebrates		Invertebrate		Vertebrates		Invertebrate	
Predictor sets	R^2	MAE	R^2	MAE	R^2	MAE	R^2	MAE
Spectral bands	0.08	4.6	0.01	6.4	0.13	2.25	0.23	0.27
Climate	0.10	4.2	0.36	5.2	0.18	2.52	0.13	0.29
Land-cover fractions	0.10	4.3	0.50	4.1	0.05	2.38	0.10	0.28
Diversity indices	0.28	4.0	0.16	5.7	0.16	2.3	0.10	0.31
Vegetation height	0.24	3.8	0.33	5.0	0.14	2.2	0.29	0.25
Vegetation indices	0.28	3.7	0.26	5.4	0.08	2.2	0.03	0.32
Texture metrics	0.28	3.8	0.31	5.3	0.07	2.4	0.10	0.30
Topography	0.06	4.4	0.33	5.1	0.06	2.4	0.01	0.39

Table 3.S6: Significant variables selected by the linear mixed model for the vertebrate hole density (R^2 = 0.83; p <

0.0001). p-value* < 0.05. p-value** < 0.01. p-value*** < 0.001.

Predictors	Estimate	Error	t value	p-value
(Intercept)	1.06027	1.74163	0.609	0.546291
Vegetation cover	0.43305	0.03806	11.377	8.41e-14 ***
Skeleton	-0.45436	0.22290	-2.038	0.048510 *
Shrub diameter	-4.20671	1.17676	-3.575	0.000974 ***
Site LC	6.24868	2.43901	2.562	0.014497 *
Vegetation cover at site LC	-0.50120	0.04753	-10.546	7.64e-13 ***
Vegetation cover at site PdA	-0.48401	0.04961	-9.755	6.76e-12 ***
Shrub diameter at site LC	4.10939	1.22249	3.361	0.001778 **

Table 3.S7: Significant variables selected by the linear mixed model for the invertebrate hole density (R^2 = 0.76; p <

0.0001). p-value* < 0.05; p-value** < 0.01; p-value*** < 0.001.

Predictors	Estimate	Error	t value	p-value
(Intercept)	9.21479	2.21611	4.158	0.000183 ***
Cacti height	-7.87052	2.33218	-3.375	0.001746 **
Cacti abundance	-0.43325	0.08503	-5.095	1.05e-05 ***
Site PdA	13.96073	3.27388	4.264	0.000133 ***
Vegetation cover at site PdA	0.19026	0.09018	2.110	0.041715 *

Table 3.S8: Significant variables selected by the linear mixed model for the vertebrate hole depth (R^2 = 0.84; p <

0.0001) p-value* < 0.05; p-value** < 0.01; p-value*** < 0.001.

Predictors	Estimate	Error	t value	p-value
(Intercept)	4.628e+00	2.013e+00	2.299	0.029762 *
Vegetation cover	-4.134e-01	1.847e-01	-2.238	0.033974 *
Shrub cover	-5.319e-01	2.110e-01	-2.521	0.018179 *
Cacti cover	-1.911e+00	5.529e-01	-3.456	0.001895 **
Trees cover	-4.609e-01	1.508e-01	-3.056	0.005136 **
Trees diameter	3.595e+00	1.529e+00	2.351	0.026570 *
Cacti abundance	7.804e-01	3.292e-01	2370	0.025467 *
Tree abundance	6.068e-01	1.714e-01	3540	0.001532 **

Skeleton abundance	2.984e-01	7.706e-02	3873	0.000651 ***
Cover heterogeneity	2.172e-01	8.778e-02	2474	0.020196 *
Site SG	-3.475e+01	5.572e+00	-6237	1.34e-06 ***
Site LC	-5.881e+00	2.632e+00	-2235	0.034260 *
Vegetation cover at site SG	5.890e-01	1.900e-01	3099	0.004617 **
Shrub diameter at site SG	6.031e+01	2.632e+00	2476	0.020108 *
Cover heterogeneity at site SG	-2.696e-01	8.794e-02	-3066	0.005015 **
Cover heterogeneity at site LC	-1.878e-01	8.524e-02	-2203	0.036630 *
Cover heterogeneity at site NA	-1.823e-01	8.518e-02	-2141	0.041846 *
Abundance heterogeneity at site SG	-4.936e-02	2.182e-02	-2263	0.032247 *

Table 3.S9: Summary of the linear mixed model for the invertebrate hole depth ($R^2 = 0.64$; $p < 0.01$). p-value* < 0.05;

p-value** < 0.01; p-value*** < 0.001.

	Estimate	**Error**	**t value**	**p-value**
(Intercept)	-1.648610	0.712062	-2.315	0.026095 *
Cacti cover	-0.228478	0.077160	-2.961	0.005260 **
Soil cover	0.015397	0.006048	2.546	0.015081 *
Shrub diameter	-11.838280	2.812155	-4.210	0.000151 ***
Cacti diameter	0.609415	0.232873	2.617	0.012664 *
Shrub height	12.358300	2.907531	4.250	0.000133 ***
Shrubs abundance	0.056238	0.011687	4.812	2.38e-05 ***
Cacti abundance	0.064426	0.016059	4.012	0.000273 ***
Trees abundance	0.048822	0.001302	4.086	0.000219 ***
Cover heterogeneity	-0.038438	0.016170	-2.377	0.022586 *
Abundance heterogeneity	-0.004589	0.001302	-3.525	0.001123 **
Site SG	-1.687547	0.784658	-2.151	0.037926 *
Site NA	1.361993	0.586687	2.321	0.025720 *
Vegetation cover at site NA	-0.054720	0.026520	-2.063	0.045961 *
Shrub diameter at site SG	13.354248	2.946862	4.532	5.67e-05 ***
Shrub diameter at site LC	11.910892	2.817994	4.227	0.000143 ***
Shrub diameter at site NA	11.735616	2.818636	4.164	0.000173 ***
Shrub height at site SG	-12.367284	2.939758	-4.207	0.000152 ***
Shrub height at site LC	-12.819465	2.936441	-4.392	8.68e-05 ***
Shrub height at site NA	-12.718590	2.936441	-4.331	0.000104 ***
Cover heterogeneity at site LC	0.035311	0.016198	2.180	0.035529 *
Cover heterogeneity at site NA	0.040147	0.016192	2.479	0.017710 *
Abundance heterogeneity at site NA	0.004269	0.001525	2.800	0.007988 **

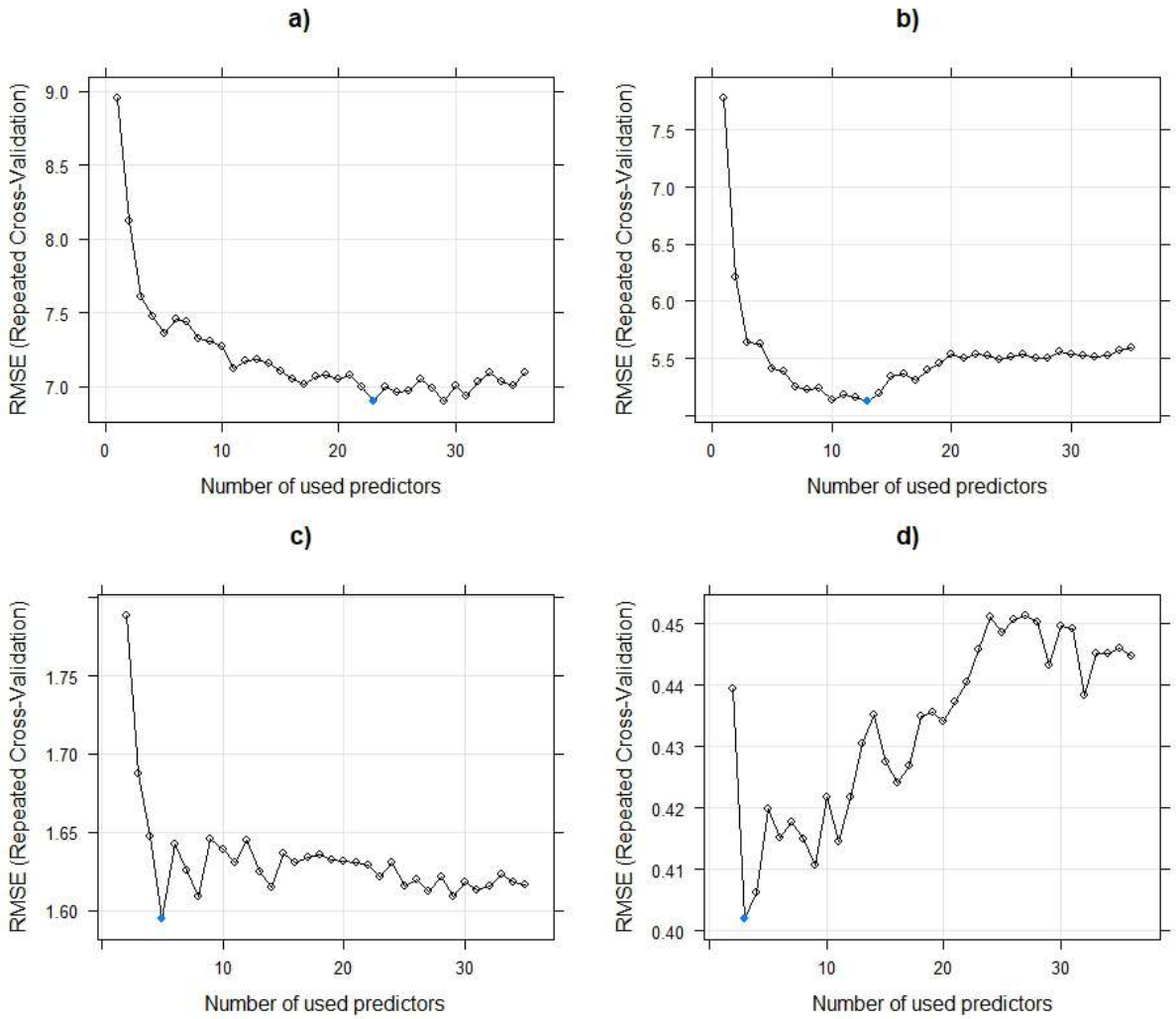

Figure 3.S1. Predictor selection by means of recursive feature elimination (RFE). The blue points show the number of selected predictors with the lowest achieved RMSE: **(a)** Vertebrate hole density; **(b)** Invertebrate hole density; **(c)** Vertebrate hole depth; and **(d)** Invertebrate hole depth.

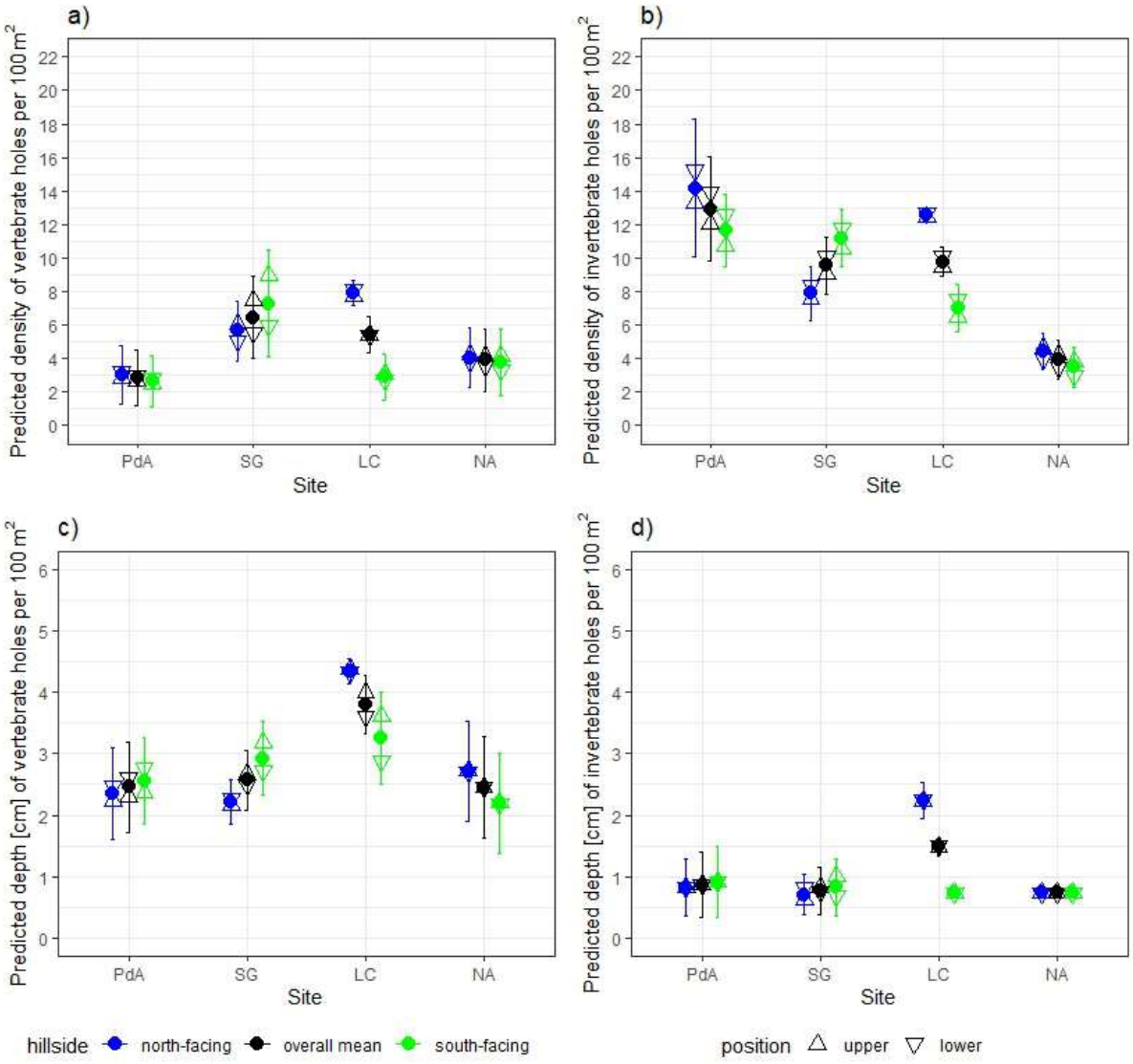

Figure 3.S2. Predicted hole density and depth across hillsides. The position refers to the position on either the upper or lower part of the hillside. The upper part of the hillside is the convex part of the hillside, while the lower part of the hillside is the concave part of the hillside. The points represent the mean overall value, the triangles are the mean overall values on the upper or lower part of the hillside, and the error bars are the standard deviations. **(a)** Predicted vertebrate hole density; **(b)** predicted invertebrate hole density**; (c)** predicted vertebrate hole depth; and **(d)** predicted invertebrate hole depth.

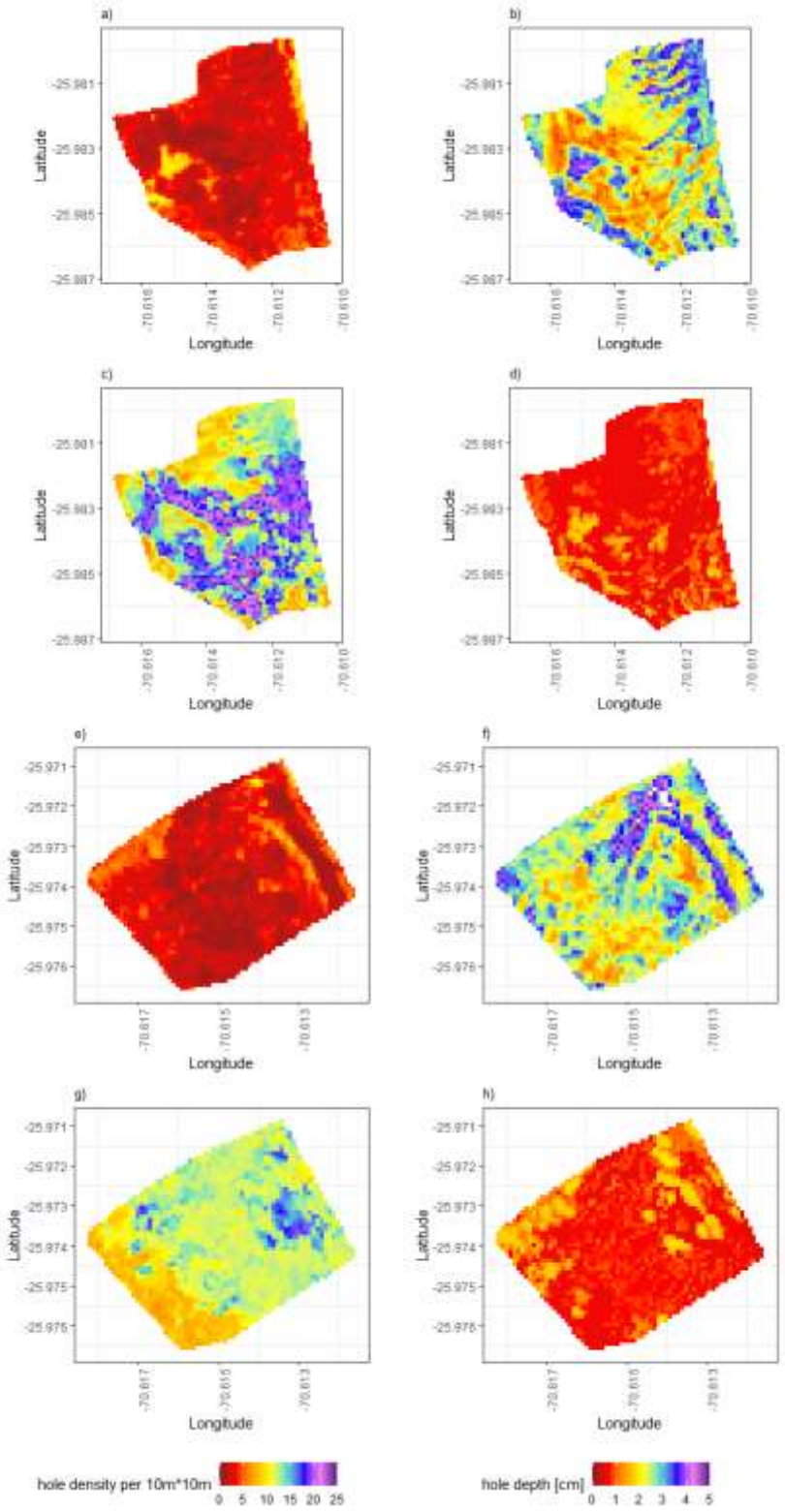

Figure 3.S3. Predicted hole density and depth in PdA (arid climate zone). **(a)** Vertebrate hole density on the north-facing hillside; **(b)** Vertebrate hole depth on the north-facing hillside; **(c)** Invertebrate hole density on the north-facing hillside; **(d)** Invertebrate hole depth on the north-facing hillside; **(e)** Vertebrate hole density on the south-facing hillside; (**f)** Vertebrate hole depth on the south-facing hillside; **(g)** Invertebrate hole density on the south-facing hillside; **(h)** Invertebrate hole depth on the south-facing hillside.

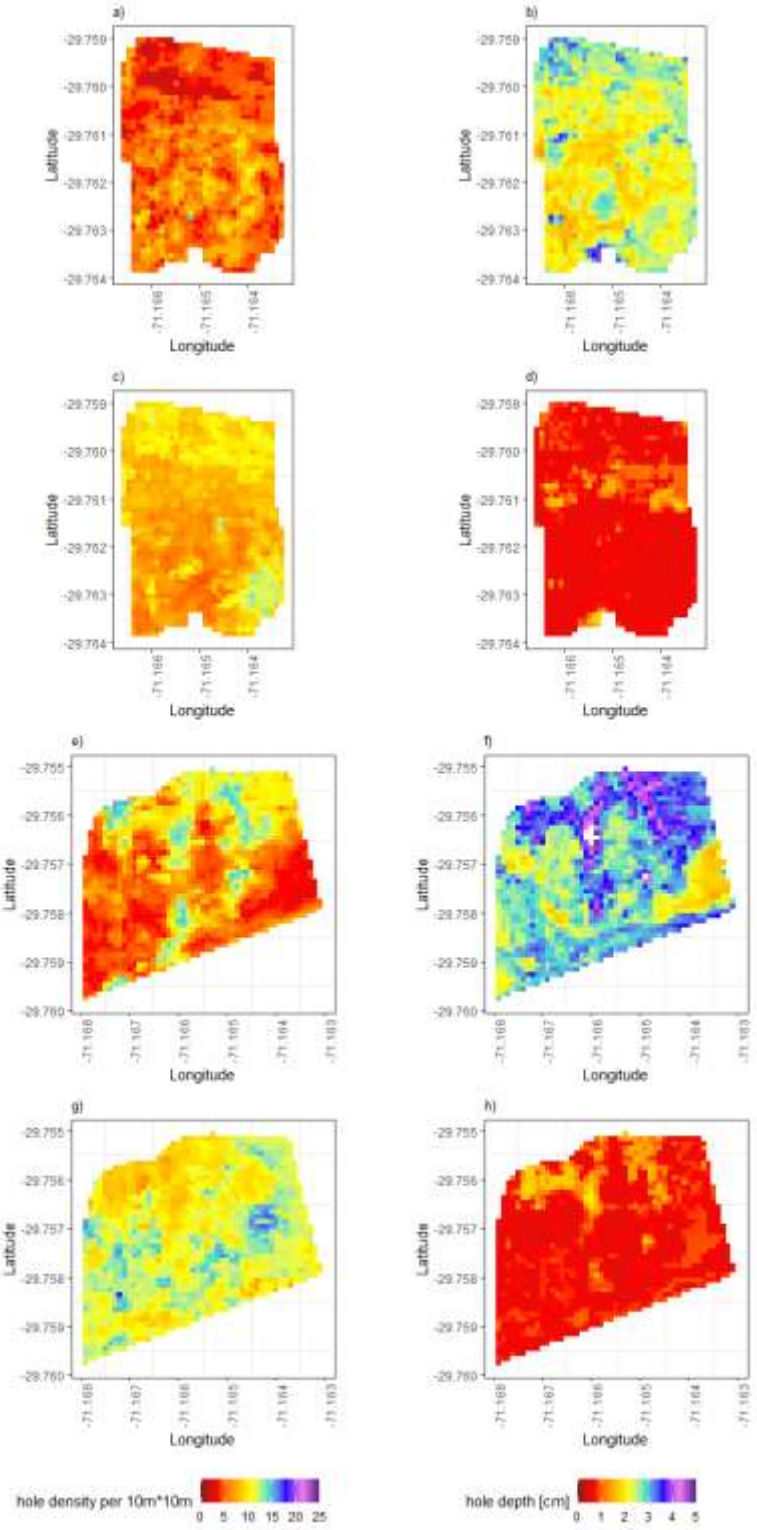

Figure 3.S4. Predicted hole density and depth in SG (semi-arid climate zone). **(a)** Vertebrate hole density on the north-facing hillside; **(b)** Vertebrate hole depth on the north-facing hillside; **(c)** Invertebrate hole density on the north-facing hillside; **(d)** Invertebrate hole depth on the north-facing hillside; **(e)** Vertebrate hole density on the south-facing hillside; (**f)** Vertebrate hole depth on the south-facing hillside; **(g)**

Invertebrate hole density on the south-facing hillside; **(h)** Invertebrate hole depth on the south-facing hillside.

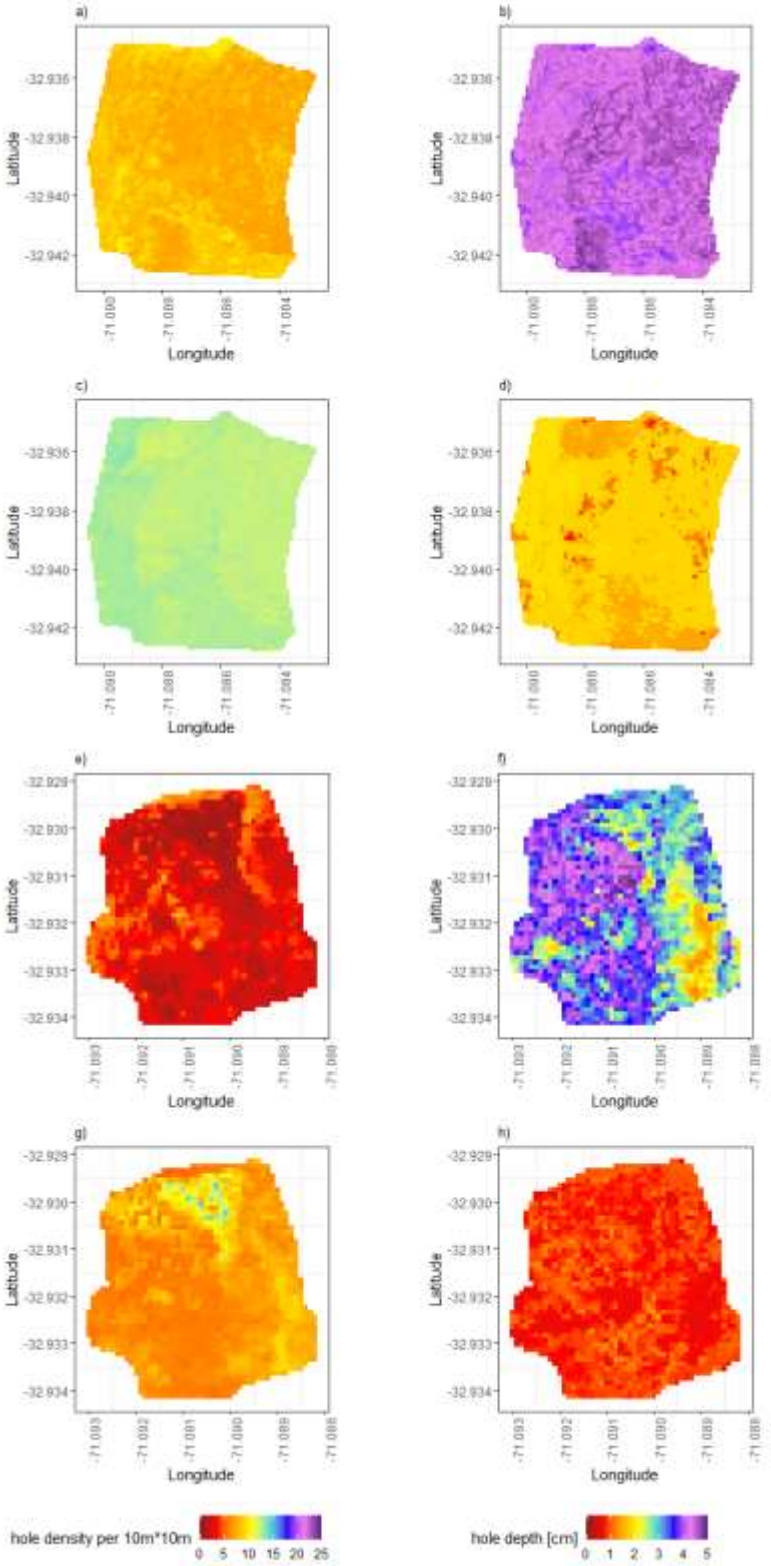

Figure 3.S5. Predicted hole density and depth in LC (Mediterranean-type climate zone). **(a)** Vertebrate hole density on the north-facing hillside; **(b)** Vertebrate hole depth on the north-facing hillside; **(c)** Invertebrate hole density on the north-facing hillside; **(d)** Invertebrate hole depth on the north-facing

hillside; **(e)** Vertebrate hole density on the south-facing hillside; (**f)** Vertebrate hole depth on the south-facing hillside; **(g)** Invertebrate hole density on the south-facing hillside; **(h)** Invertebrate hole depth on the south-facing hillside.

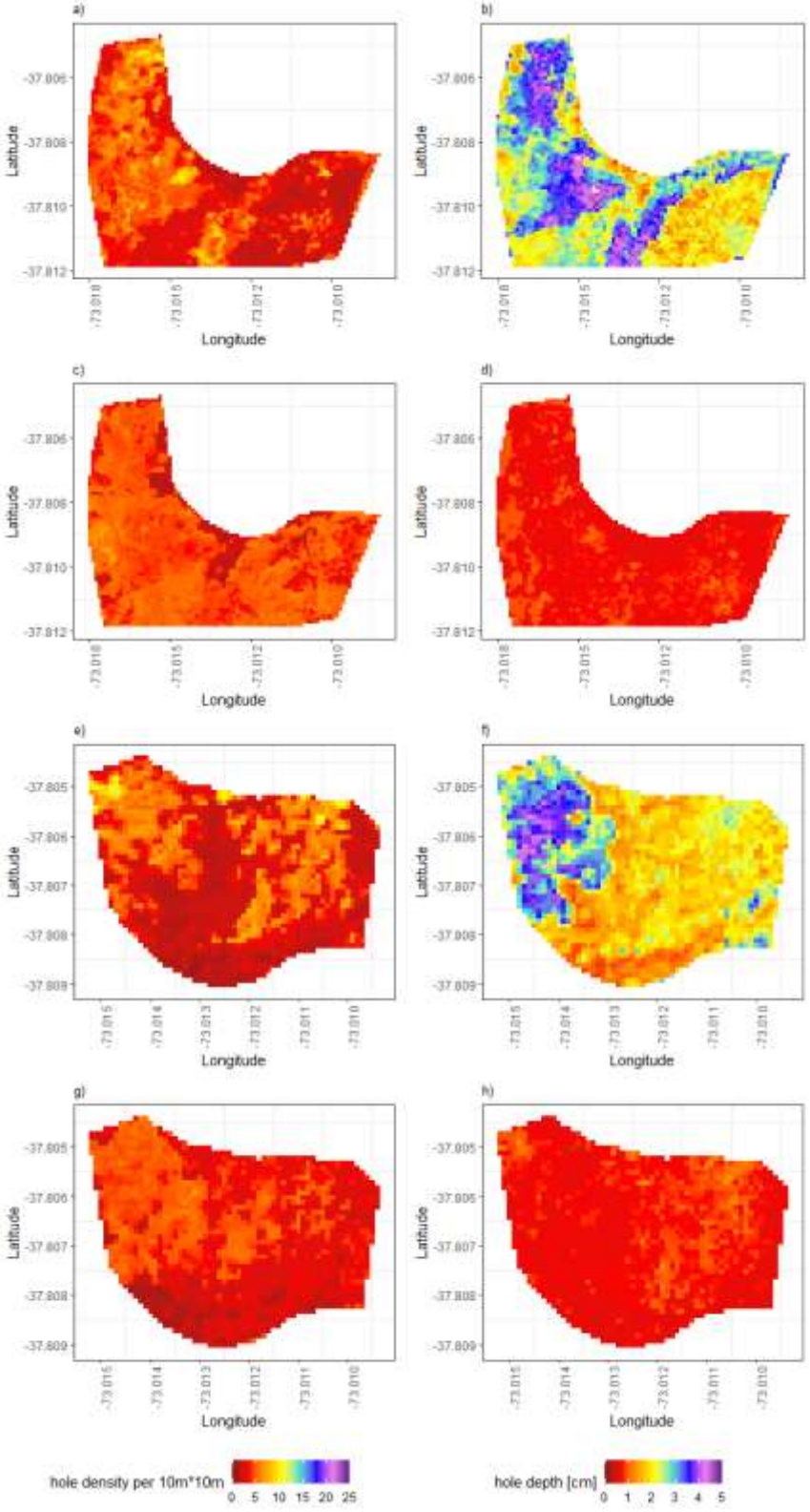

Figure 3.S6. Predicted hole density and depth in NA (humid-temperate climate zone). **(a)** Vertebrate hole density on the north-facing hillside; **(b)** Vertebrate hole depth on the north-facing hillside; **(c)** Invertebrate hole density on the north-facing hillside; **(d)** Invertebrate hole depth on the north-facing hillside; **(e)** Vertebrate hole density on the south-facing hillside; (**f)** Vertebrate hole depth on the south-facing hillside; **(g)** Invertebrate hole density on the south-facing hillside; **(h)** Invertebrate hole depth on the south-facing hillside.

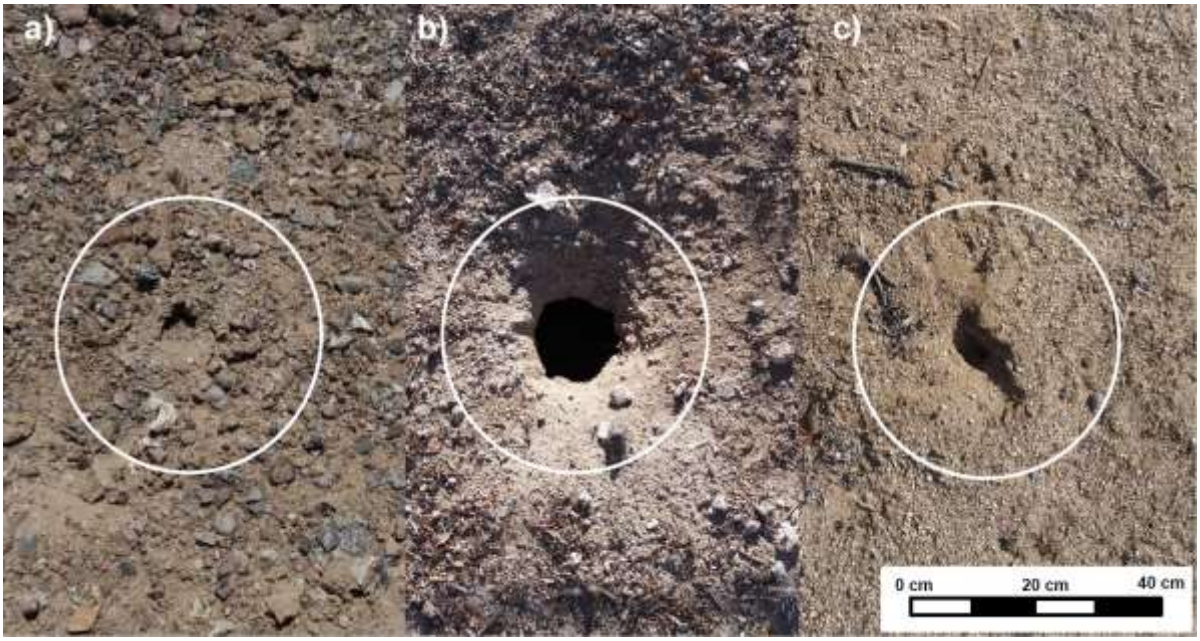

Figure 3.S7. Examples of measured holes. **(a)** in PdA; **(b)** in SG; **(c)** in LC.

4. Higher sediment redistribution rates related to burrowing animals than previously assumed as revealed by Time-Of-Flight based monitoring

Paulina Grigusova[1], Annegret Larsen[2], Sebastian Achilles[1], Roland Brandl[3], Camilo del Río[4,5], Nina Farwig[6], Diana Kraus[6], Leandro Paulino[7], Patricio Pliscoff[4,8,9], Kirstin Übernickel[10], Jörg Bendix[1]

[1] Laboratory for Climatology and Remote Sensing, Department of Geography, University of Marburg, 35037 Marburg, Germany; paulina.grigusova@staff.uni-marburg.de (P.G.); bendix@geo.uni-marburg.de (J.B.)

[2] Soil Geography and Landscape, Department of Environmental Sciences, Wageningen University & Research, 6700 AA Wageningen, The Netherlands; annegret.larsen@wur.nl

[3] Animal Ecology, Department of Biology, University of Marburg, 35032 Marburg, Germany; brandlr@biologie.uni-marburg.de

[4] Facultad de Historia, Geografía y Ciencia Política, Instituto de Geografía, Pontificia Universidad Católica de Chile, 782-0436 Santiago, Chile; pliscoff@uc.cl; cdelriol@uc.cl

[5] Centro UC Desierto de Atacama, Pontificia Universidad Católica de Chile, 782-0436 Santiago, Chile; cdelriol@uc.cl

[6] Conservation Ecology, Department of Biology, University of Marburg, 35047 Marburg, Germany; diana.kraus@biologie.uni-marburg.de (D.K.); nina.farwig@biologie.uni-marburg.de (N.F.)

[7] Facultad de Agronomía, Universidad de Concepción, 3780000 Chillán, Chile; lpaulino@udec.cl

[8] Facultad de Ciencias Biológicas, Departamento de Ecología, Pontificia Universidad Católica de Chile, 8331150 Santiago, Chile; pliscoff@uc.cl

[9] Center of Applied Ecology and Sustainability (CAPES), Pontificia Universidad Católica de Chile, 8331150 Santiago, Chile; pliscoff@uc.cl

[10] Earth System Dynamics, Department of Geosciences, University of Tübingen, 72076 Tübingen, Germany; kirstin.uebernickel@uni-tuebingen.de

Published in Earth Surface Dynamics (2022): 10.5194/esurf-10-1273-2022

Abstract

Burrowing animals influence surface microtopography and hillslope sediment redistribution, but changes often remain undetected due to a lack of automated high resolution field monitoring techniques. In this study, we present a new approach to quantify microtopographic variations and surface changes caused by burrowing animals and rainfall-driven erosional processes applied to remote field plots in arid and Mediterranean Chile. We compared the mass balance of redistributed sediment between burrow and burrow embedding area, quantified the cumulative sediment redistribution caused by animals and rainfall, and upscaled the results to a hillslope scale. The newly developed instrument, a Time-of-Flight camera, showed a very good detection accuracy. The animal-caused cumulative sediment excavation was 14.6 $cm^3\ cm^{-2}\ year^{-1}$ in the Mediterranean, and 16.4 $cm^3\ cm^{-2}\ year^{-1}$ in the arid climate zone. The rainfall-caused cumulative sediment erosion within burrows was higher (10.4 $cm^3\ cm^{-2}\ year^{-1}$) in the Mediterranean than the arid climate zone (1.4 $cm^3\ cm^{-2}\ year^{-1}$). Daily sediment redistribution during rainfall within burrow areas were up to 350% / 40% higher in the mediterranean / arid zone compared to burrow embedding areas, and much higher than previously reported in studies which were not based on continuous microtopographic monitoring. 38% of the sediment eroding from burrows accumulated within the burrow entrance while 62% was incorporated into hillslope sediment flux, which exceeds previous estimations two-fold. Animals burrowed between on average 1.2 – 2.3 times a month, and the burrowing intensity increased after rainfall. This revealed a newly detected feedback mechanism between rainfall, erosion, and animal burrowing activity, likely leading to an underestimation of animal-triggered hillslope sediment flux in wetter climates. Our findings hence show that the rate of sediment redistribution due to animal burrowing is climate dependant, and that animal burrowing plays a larger than previously expected role in hillslope sediment redistribution. Subsequently, animal burrowing activity should be incorporated into soil erosion and landscape evolution models that rely on soil processes but do not yet include animal-induced surface processes on microtopographical scales in their algorithms.

Keywords: Biogeomorphology, bioturbation, sediment transport, burrowing animals, rainfall, Time-of-Flight camera, Chile

4.1. Introduction

Animal burrowing activity affects surface microtopography (Reichman and Seabloom, 2002; Kinlaw and Grasmueck, 2012), surface roughness (Yair, 1995; Jones et al., 2010; Hancock and Lowry, 2021), and soil physical properties (Ridd, 1996; Yair, 1995; Hall et al., 1999; Reichman and Seabloom, 2002; Hancock and Lowry, 2021; Coombes, 2016; Larsen et al., 2021; Corenblit et al., 2021). Previous studies estimated both positive as well as negative impacts of burrowing animals on sediment redistribution rates. These studies relied on applying tests under laboratory conditions using rainfall simulators, conducting several field campaigns weeks to months apart, or by measuring the volume of excavated or eroded sediment in the field using instruments such as erosion pins, splash boards, or simple rulers (Imeson and Kwaad, 1976; Reichman and Seabloom, 2002; Wei et al., 2007; Le Hir et al., 2007; Li et al., 2018; Li et al., 2019b; Li et al., 2019c; Voiculescu et al., 2019; Chen et al., 2021; Übernickel et al., 2021a; Li et al., 2019a). Although burrowing animals are generally seen as ecosystem engineers (Gabet et al., 2003; Wilkinson et al., 2009), their role in soil erosion in general, and for numerical soil erosion models in particular, is to date limited to predictions of burrow locations and particle mixing (Black and Montgomery, 1991; Meysman et al., 2003; Yoo et al., 2005; Schiffers et al., 2011). The complex interaction of sediment excavation and accumulation, and erosion processes at the burrow and hillslope scale are not yet included in earth-surface-models.

The reason for this knowledge gap is that previous studies have not provided data on low magnitude but frequently occurring sediment redistribution due to a lack of spatio-temporal high-resolution microtopographic surface monitoring techniques which can also measure continuously in the field. Field experiments with, for example, rainfall simulators can unveil processes but cannot cover the time-dependant natural dynamics of sediment redistribution. When using erosion pins or splash boards, the sites had to be revisited each time and the data were thus obtained only sporadically (Imeson and Kwaad, 1976; Hazelhoff et al., 1981; Richards and Humphreys, 2010). This limited all previous studies in their explanatory power, because biotic-driven processes are typically characterised by small quantity and a frequent re-occurrence (Larsen et al., 2021). It is hence likely that previous studies based on non-continuously conducted measurements or rainfall experiments underestimated the role of burrowing animals on rates of hillslope sediment flux.

High-resolution, ground-based imaging sensing techniques have the potential to overcome limitations of previous surface monitoring techniques. Terrestrial laser scanner systems have been shown to be a suiTable 4.tool for the estimation of sediment redistribution and erosion processes (Nasermoaddeli and Pasche, 2008; Afana et al., 2010; Eltner et al., 2016a; Eltner et al., 2016b; Longoni et al., 2016). However, these instruments are expensive and labour-intensive. Hence, a simultaneous, continuous, and automated monitoring of several animal burrows is for this reason not possible. Time-lapse photogrammetry is a low-cost (up to 5000 USD), topographic monitoring technique, which can be applied at variable observation distances and scales (e.g. (James and Robson, 2014; Galland et al., 2016; Eltner et al., 2017; MALLALIEU et al., 2017; Kromer et al., 2019; Blanch et al., 2021). However, several cameras are needed to monitor the surface under various angles, which makes the field installation difficult and yields the large potential to disturb the animals and lead to behavioural changes.

Another high resolution surface monitoring technique is based on Time-of-Flight (ToF) technology. ToF-based cameras illuminate the targeted object with a light source for a known amount

of time and then estimate the distance between the camera and the object by measuring the time needed for the reflected light to reach the camera sensor (Sarbolandi et al., 2018). ToF cameras exhibit lower spatial resolution and aerial coverage compared to time-lapse photogrammetry. But, the technique also has several advantages: as an active remote sensing tool it is able to monitor surface change at night, the processing is less complex compared to photogrammetry because the distance values are immediately received in a local coordinate system, and the field installation is much smaller and less invasive. ToF offers hence a new possibility for surface monitoring, as a technique for a cost-effective, high-resolution monitoring of sediment redistribution (Eitel et al., 2011; Hänsel et al., 2016), which can be achieved by a simple installation of only one device in the field.

In this study we developed, tested and applied a cost-effective Time-of-Flight camera for automated monitoring of the rainfall and burrowing animal-driven sediment redistribution of burrows and burrow embedding areas with a high temporal (four times a day) and spatial (6 mm) resolution. For this, we equipped several plots in remote field study sites in the Chilean arid and mediterranean climate zone. The selected field sites had a variable rainfall regime and sunlight exposure, and were all affected by burrowing activity (Grigusova et al., 2021). After 7 month of field monitoring including wet and dry season, we estimated burrowing intensity and its dependence on rainfall. Then, we quantified the daily sediment redistribution within the burrow and its embedding area, which enabled us to better understand the impacts of animal burrowing activity, and rainfall, on the local sediment redistribution. This allowed us to quantify the volume of burrow sediment which was incorporated into the hillslope sediment flux. Finally, we upscaled sediment redistribution rates to the entire hillslope.

4.2. Study area

Our study sites were located in the Chilean Coastal Cordillera in two climate zones (Fig. 4.1): in the National Park Pan de Azúcar (further as Pan de Azúcar or PdA) and the National Park La Campana (further as La Campana or LC). The Las Lomitas site in PdA is located in the arid climate zone of the Atacama Desert with a precipitation rate of 12 mm year^{-1}, and it has a mean annual temperature of 16.8 °C (Übernickel et al., 2021b). Here, the vegetation cover is below 5%, and it is dominated by small desert shrubs, several species of cacti (*Eulychnia breviflora, Copiapoa atacamensis)* and biocrusts (Lehnert et al., 2018). LC is located in the mediterranean climate zone with a precipitation rate of 367 mm year^{-1} and a mean annual temperature of 14.1 °C (Übernickel et al., 2021b). LC is dominated by an evergreen sclerophyllous forest with endemic palm trees, *Jubaea chilensis*. Both research sites have a granitic rock base, and the dominating soil texture is sandy loam (Bernhard et al., 2018). In PdA, the study setup consisted of one north-facing and one south-facing hillslope. The hillslope inclinations were ~20°, and a climate station was located ~15 km from the camera sites. In LC, the setup consisted of two north-facing and one south-facing hillslopes. The hillslope inclinations were ~25°, and a climate station was located ~250 m from the south-facing hillslope (Übernickel et al., 2021b).

Figure 4.1. Location of the cameras and climate stations on which this study was based. Black points show the location of the research sites in Chile. The green points represent the camera plots, and the blue points the climate stations: (a) Location of study sites in Chile: PdA stands for Pan de Azúcar, LC for La Campana; (b) Study setup in Pan de Azúcar; (c) Study setup in LC. The background images in (b) and (c) are orthophotos created from WorldView-2 data from 19 July 2019. For exact latitude and longitude see Table 4.A2.

4.2.1 Local burrowing animals

In order to assess which animal species burrowed at both study sites, we adapted a two-step approach. First, we used motion-activated camera traps to capture animals during the borrowing process at our field sites. Then, we complimented the list of identified species by a literature review. We found that the most common vertebrate animal species which burrow in PdA were carnivores of the family Canidae (*Lycalopex culpaeus*, *Lycalopex griseus*) as well as rodents of the families Abrocomidae (*Abrocoma bennetti)*, Chnichillidae (*Lagidium viscacia)*, Cricetidae (*Abrothrix andinus, Phyllotis xanthopygus*, *Phyllotis limatus, Phyllotis darwini*) and Octogontidae (Cerquiera 1985, Jimenéz et al. 1992, Übernickel et al. 2021) (Table 4.1). In LC, the most common burrowing vertebrate animal species were the carnivores of the family Canidae, Lagomorpha of the family Leporidae (*Oryctolagus cuniculus*), and rodents of the families Cricetidae (*Abrothrix longipilis, Abrothrix olivaceus, Phyllotis darwini*), Muridae (*Mus musculus*) and Octogontidae (*Octogon degus, Spalacopus cyanus*) (Munoz-Pedreros et al. 2018, Übernickel et al. 2021) (Table 4.1. The motion-activated camera traps recorded several burrowing animals which all agreed with the list of burrowing vertebrate animals collected from literature: *Lycalopex culpaeus*, *Oryctolagus cunniculus* and *Abrocoma bennettii*) (Figure 4.2)

Table 4.1. Most common burrowing animals in the study sites. The list includes both, animal species recorded with our motion-activated wildlife traps and those from the review by Übernickel et al. 2021,

Cerquiera 1985, Jimenéz et al. 1992, Munoz-Pedreros et al. 2018). “X” indicates at which site the species can be found.

Order	Family	Species	Common name	Site	
				PdA	LC
Carnivora	Canidae	*Lycalopex culpaeus*	Culpeo	X	X
Carnivora	Canidae	*Lycalopex griseus*	South-American grey fox	X	X
Carnivora	Methitidae	*Conepatus chinga*	Molina’s Hog noised skunk		X
Lagomorpha	Leporidae	*Oryctolagus cuniculus*	European rabbit		X
Rodentia	Abrocomidae	*Abrocoma bennetti*	Bennett’s chinchilla rat	X	X
Rodentia	Chinchillidae	*Lagidium viscacia*	Southern mountain vischacha	X	
Rodentia	Cricetidae	*Abrothrix andinus*	Andean grass mouse	X	
Rodentia	Cricetidae	*Abrothrix longipilis*	Long-haired mouse	X	X
Rodentia	Cricetidae	*Abrothrix olivaceus*	Olive grass mouse	X	X
Rodentia	Cricetidae	*Phyllotis darwini*	Darwin’s leaf-eared mouse	X	X
Rodentia	Cricetidae	*Phyllotis xanthopygus*	Yellow leaf-eared mouse	X	
Rodentia	Cricetidae	*Phyllotis limatus*	Lima leaf-eared mouse	X	
Rodentia	Muridae	*Mus musculus*	Common house mouse	X	X
Rodentia	Octogontidae	*Octogon degus*	Degu (rat)	X	X
Rodentia	Octogontidae	*Spalacopus cyanus*	Coruro (rat)	X	X

Figure 4.2. Examples of burrowing vertebrate animals recorded by motion-activated camera traps. (a) Set-up of motion-activated camera trap. (b) and (c) European rabbit (*Oryctolagus cunniculus*). (d) and (e) Culpeo (*Lycalopex culpaeus*). (f) Bennett’s chinchilla rat *(Abrocoma bennettii)*. The yellow box highlights the position of the animal on the photo. Photo courtesy: Diana Kraus.

4.3. Methodology

4.3.1 Time-of-Flight (ToF) principle

A Time-of-Flight-based camera illuminates an object with a light source, usually in a non-visible spectrum, such as near-infrared, for a precise length of time. ToF cameras rely on the principle of measuring the phase shift, with different options to modulate the light source to be able to measure the phase shift. The here employed cameras used pulse-based modulation, meaning the light pulse was first emitted by the camera, then reflected from the surface, and finally measured by the camera using two temporary windows. The opening of the first window is synchronized with the pulse emission i.e. the receiver opens the window with the same Δt as the emitted pulse. Then, the second window is opened, for the same duration Δt, which is synchronised with the closing of the first window. The first temporary window thus measures the incoming reflected light while the light pulse is also still emitting from the camera. The second temporary window measures the incoming reflected light when no pulse is emitting from the camera. The captured photon number (i.e. measured by electrical charge) in both windows can be related according to equation 1 and the distance from the camera to the object can then be calculated as follows:

$$d = \frac{1}{2} * c * t * \left(\frac{g1}{g1+g2}\right) \quad . \tag{1}$$

In Eq. (1), d (m) is the distance from the camera to the object, c (m s^{-1}) is the speed of light (299,792,458 m s^{-1}), t (s) is the overall time of the illumination and measurement, g_1 is the ratio of the reflected photons to all photons accumulated in the first window, and g_2 the ratio of the reflected photons to all photons accumulated in the second window (Sarbolandi et al., 2018; Li, 2014).

The sensor in our camera came from Texas Instruments and the data scan contained information on 320 x 240 points. The camera field of view (FOV) and the spatial resolution of the scans depended on the height of the camera above the surface and camera orientation. The distance was calculated for every point, and the object was saved in binary format as a collection of 3D points with *x*-, *y*- and *z*-coordinates. The point clouds taken by the camera were transformed from the binary format to an ASCII format. Each point in the point cloud was assigned to an *x*-, *y*- and *z*-coordinate. The coordinates were distributed within a three-dimensional Euclidian space, with the point at the camera nadir (the centre of the camera sensor) being the point of origin of the 3D Cartesian coordinate system. *x*- and *y*-coordinates describe the distance to the point of origin (m). *z*-coordinate describes the distance (m) from the object to the camera. The lowest point of the scanned surface thus has the highest *z*-coordinate value.

4.3.2 Data processing

The distortion caused by the hillslope and the camera angle was corrected for each point cloud as follows:

$$z_{cor} = z_{uncor} - \tan(\alpha + \beta) * (y_1 - y_i) \quad . \tag{2}$$

In Eq. (2), z_{cor} is the corrected distance (m) between the camera and surface (m), z_{uncor} is the uncorrected *z*-coordinate (m), α is the tilt angle of the camera (°), β is the surface inclination (°), and y_i (m) is the distance between each point, and the point with i) an y-coordinate = 0 and ii) the same x-coordinate as the respective point. The most frequent errors were identified and treated as follows. Due to the ambient

light reaching the camera sensor, the *z*-coordinate values of some of the points were incorrect (scattering error). To remove this error, a threshold value was calculated for each point cloud:

$$\Omega = mean_{zcor-coordinates} \pm sd_{zcor-coordinates} \quad . \tag{3}$$

In Eq. (3), Ω is the threshold value, $mean_{zcor\text{-}coordinate}$ is the average value, and $sd_{zcor\text{-}coordinate}$ is the standard deviation of the corrected *z*-coordinates (m). Then, all points with a *z*-coordinate above and below this value were deleted. Point clouds with more than 50% of points above the threshold value Ω were also not considered for further processing. A drift error occurred when the *z*-coordinate values of around one-third of the point clouds decreased by several centimetres from one point cloud to another. Here, the average *z*-coordinate of ten point clouds before and after the drift were calculated, and the difference was added to *z*-coordinates of the points affected by the drift. The corrected height values were then transformed into a digital surface model (DSM).

4.3.3 Accuracy of the ToF cameras

The accuracy of the ToF camera was tested under laboratory conditions by recreating similar surface conditions as in the field (sloping surface, covered by sediment). An artificial mound using sediment extracted from a riverbank in central Germany was used, mimicking a mound created by a burrowing animal. During the test, the camera was installed 100 cm above the surface. The camera FOV was 3 m^2 and the scan spatial resolution was 6 mm. The surface was scanned twice by the ToF camera. Then 100 – 450 cm^3 of sediment was manually extracted from the mound. The volume of the extracted sediment was measured by a measuring cup. After extraction, the surface was again scanned twice by the camera. The experiment was repeated 45 times with varying amounts of extracted sediment. The scans were transformed to point clouds in VoxelViewer-0.9.10, and the point clouds were corrected according to Eq. (2) and (3). The *z*-coordinates of the two point clouds before and two point clouds after the extraction were averaged. The standard deviation of the z-coordinate of the two scans was 0.06 cm. Figure 4.A1 shows the spatially distributed standard deviation. The deviation increases from the centre towards the corners of the scan. The mound was outlined and only the points representing the mound were used in the further analysis. The point clouds were then transformed into DSMs, and the differences between the time steps were calculated. A scan was taken of a smooth surface (linoleum floor) and a point cloud was created from the data. Then, we fitted a plane into the point cloud and calculated the distance between the plane and the camera sensor. The standard variation (0.17 cm) in the distance measurements was saved. Solely, the differences between the DSMs below this variation were considered in the calculation of the detected sediment extraction. The detected extracted sediment volume was then calculated for each experiment as follows:

$$Vol_{detected} = \sum_{p}^{1}\left(DSM_{before} - DSM_{after}\right) * res^2 \quad , \tag{4}$$

In Eq. (4), $Vol_{detected}$ is the volume of the extracted sediment as detected by the camera (cm^3), p is the number of pixels, DSM_{before} (cm) is the DSM calculated from the scan taken before the extraction, DSM_{after} (cm) is the DSM calculated from the scan taken after the extraction, res (cm) is the resolution of the scan, which was 0.6 cm. To evaluate the camera's accuracy, the measured volume of the extracted sediment was compared to the volume detected by the camera. The camera's accuracy was estimated between the detected volume and measured volume as follows:

$$MAE = \sum_1^n \frac{(Vol_{detected} - Vol_{measured})}{area} \quad . \qquad (5)$$

In Eq. (5), MAE (cm^3/cm^2) is the mean absolute error, n is the number of scans, $Vol_{measured}$ (cm^3) is the volume of the extracted sediment measured by the measuring cup, and the area is the total surface area monitored by the camera (cm^2).

4.3.4 Installation of the cameras in the field

We installed 8 custom-tailored ToF-based cameras on 4 hillslopes in two climate zones in areas including visible signs of bioturbation activity (burrows) and areas without visible signs of bioturbation (Fig. 4.3). The cameras were installed in LC on the north-facing upper hillslope (LC-NU), north-facing lower hillslope (LC-NL), south-facing upper hillslope (LC-SU) and the south-facing lower hillslope (LC-SL); in PdA on the north-facing upper hillslope (PdA-NU), north-facing lower hillslope (PdA-NL), south-facing upper hillslope (PdA-SU) and south-facing lower hillslope (PdA-SL). The custom-tailored cameras were installed during a field campaign in March 2019, the monitoring took place for seven months, and the data were collected in October 2019. The construction consisted of a 3D ToF-based sensor from Texas Instruments (Li, 2014), a RasperryPi single board computer (SBC), a timer, a 12 V 12 Ah battery and three 20 W solar panels for unattended operation (Fig. 4.2). Solar panels were located at the camera pole and were recharging the battery via a charge controller. The camera was located approximately one meter above the surface, facing the surface with a tilt angle of 10 degrees. The timer was set to close the electric circuit 4 times a day: at 1 a.m., 5 a.m., 8 a.m. and 10 p.m. At these times, the camera and the computer were turned on for 15 minutes. The camera turned on and took five scans delayed one second from each other and sent them to the SBC. Each camera had its own WiFi (Wireless Fidelity) and the data could be read from the SBC via Secure Shell (SSH). The cameras collected the data for the time period of 7 months.

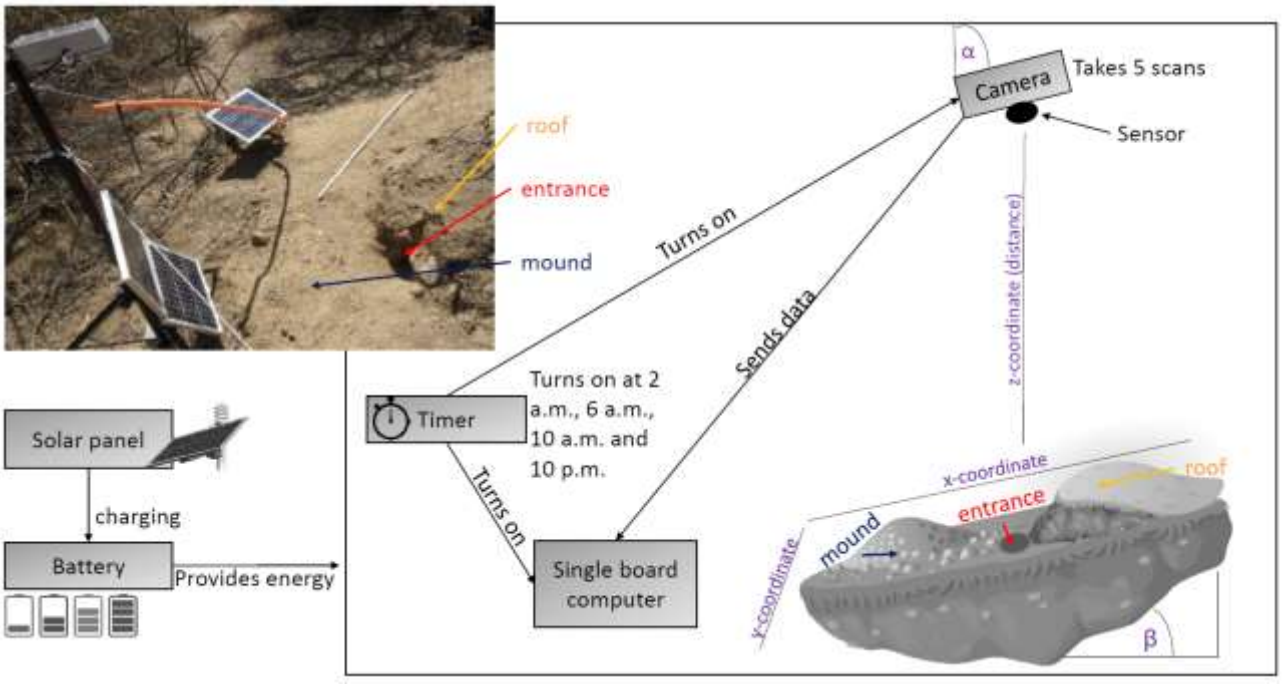

Figure 4.3. Scheme and photo example of a Time-of-Flight-based camera installation in the field. The photo example is from upper north-facing hillslope in La Campana. Black boxes describe single installation parts. Purple descriptions are the variables needed for the correction of the scans. Roof, entrance and mound describe parts of the burrow. The *x*-, *y*- and *z*-coordinates are 3D coordinates identifying the position of each point in space, where the *x*-coordinate is the length, *y*-coordinate is the width and the *z*-coordinate is the distance between the camera sensor and the surface. α is the inclination of the camera, and β is the surface inclination.

4.3.5 Delineation of burrows and burrow embedding areas

The surface area scanned by the cameras was divided by a delineation scheme into burrows (B) and burrow embedding areas (EM). The burrows included three sub-areas: (i) mound (M), (ii) entrance (E) and (iii) burrow roof (R). “Mound” describes the sediment excavated by the animal while digging the burrow. “Entrance” describes the entry to the animal burrow up to the depth possible to obtain via the camera. “Burrow roof” describes the part of the sediment above and uphill the burrow entrance (BANCROFT and Hill, D. and Roberts, J.D., 2004). During the burrow’s creation, sediment was not only excavated but also pushed aside and uphill the entrance, which created the burrow roof. We assume that this elevated microtopographical feature then forms an obstacle for sediment transported from uphill, which leads to its accumulation in this area. The remaining surface within the camera’s FOV was burrow embedding area. Please note, that this area may still be affected by the burrowing activity of the animal and is not completely unaffected by the animal.

For the delineation, we used the DSM calculated from the point cloud, and a slope layer calculated from the DSM (Horn, 1981). The DSM had a size of 4 m^2 a resolution of 0.6 cm. Entrance was assigned to an area determined by a search algorithm starting at the lowest point of the DSM (pixel with the highest *z*-coordinate value). We increased the circular buffer around the starting point by one pixel until the average depth of the new buffer points was not higher than the height of the camera above the surface, or until the slope of at least 50% of the new buffer points was not 0. Then, we masked all pixels within the buffer with a depth lower than the average depth of the points within the buffer, which had a slope that was 0. The remaining pixels belonged to the entrance area. Then, the surface scan was divided into an uphill and downhill part with regards to the entrance position. Both the uphill and the downhill parts were subdivided into 16 squares, so that each of the four quadrants within the 2D grid (x- and y-axis) contained four squares. The squares had size of 0.5 m^2.

To delineate the mound in the downhill part, we first identified the highest points (pixel with the lowest *z*-coordinate value) within all 16 squares. We then calculated the distance of these maxima to the entrance, and the pixel located nearest to the entrance was identified as the highest point of the mound (i.e., seed point). Consecutively, we increased the circular buffer around the seed point by one pixel until the average depth of the new buffer points was not lower than the height of the camera above the surface, or until the slope of at least 50% of the new buffer points was not 0. Then, we masked all pixels within the buffer with a depth higher than the average depth of the points within the buffer, which had a slope that was 0. The remaining pixels were classified as mound area. To delineate burrow roof, we used the same approach as for the delineation of mound and applied it on the uphill part of the surface

scan. We used the DEM and slope layers for the delineation for several reasons. The distance from the surface to the camera was the most important parameter to derive (i) the deepest point of the entrance and (ii) the highest point of the mound or burrow roof, as this was (mostly) the closest point to the camera. After the angle correction of the z-coordinate according to chapter 3.2., the surface inclination of the areas without burrow was 0°, while the angle between the border of the burrow entrance or mound and the burrow embedding surface was above 0°. Because neither the entrance nor the mound have a perfect circular form, we would largely overestimate or underestimate the entrance or mound size. Overestimate by not stopping the search algorithm until the angle between all new points of the buffer to the rest of the buffer was 0°. Underestimate by stopping the algorithm when the angle of one point of the buffer to the nearest point of the buffer was 0°. The value of 50% thus minimized the error. All pixels that were not classified during the entire delineation process were treated as burrow embedding areas. The position and the boundaries of entrance, mound and burrow roof were validated visually (Fig. 4.4 and A2).

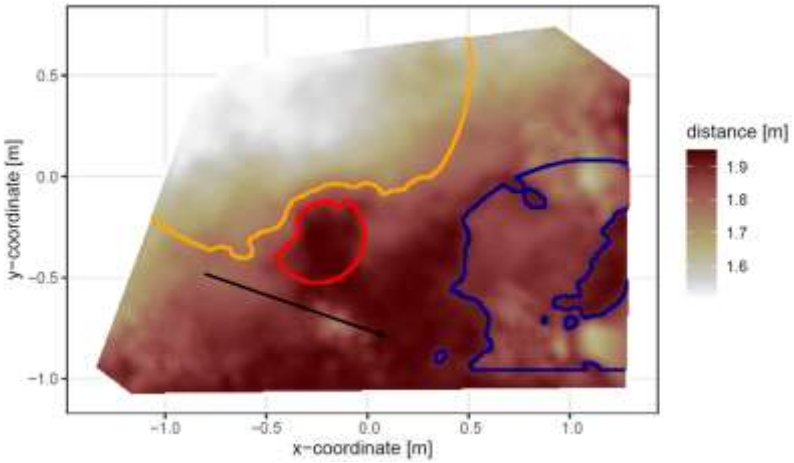

Figure 4.4. Corrected digital surface model of the camera on the upper north-facing hillslope in La Campana with delineated areas. The point of origin of the coordinate system is at the camera nadir. Distance refers to the distance between surface and camera. The red line delineates the burrow entrance, blue the mound and orange the burrow roof. The area which was outside of any delineated area was classified as burrow embedding area. The arrow indicates a downhill direction of the hillslope.

In LC, the burrows always consisted of an entrance, mound and burrow roof. In PdA, there was no burrow roof on the upper hillslopes. Burrows without a burrow roof were located on shallower parts of the hillslopes (up to an inclination of 5°), and the angle of the burrow entrance to the ground was ~90°. Burrows with a burrow roof were located on steeper parts of the hillslopes (with an inclination above 5°), and the angle of the burrow entrance to the ground was ~45°.

4.3.6 Calculation of animal-caused and rainfall-caused sediment redistribution

We pairwise compared the DSMs of each scan with the scan saved before and identified 3 types of sediment redistribution which occurred in the time period between these images. The 3 types of redistribution were: a) animal caused; b) rainfall-caused; c) both animal and rainfall caused.

The animal-caused sediment redistribution occurred when the animal actively reworked sediment within its burrow. Following five prerequisites had to be met when the sediment redistribution

was caused solely by the animal: (i) as the animal excavates sediment from the entrance, the depth of the entrance must increase in the second scan; (ii) as the excavated sediment accumulates on the mound, the height of the mound must increase in the second scan; (iii) as the burrowing might lead to an expansion or a collapse of the burrow roof, an increase or decrease of the burrow roof must occur between the scans; (iv) as the animal only digs within his burrow, no changes must occur between the two scans within the burrow embedding area by the animal; (v) no rainfall occurred during this period.

The rainfall-caused sediment redistribution was calculated as follows: From the data from the climate stations (Übernickel et al., 2021b), we calculated the daily precipitation in mm. The sediment redistribution recorded immediately and within five scans before and after a rainfall event is defined to be the result of the rainfall event. This was necessary as the climate stations are located up to a 15 km distance from the cameras (Fig. 4.1). To attribute sediment redistribution to rainfall event, three preconditions had to be met: (i) A rainfall event occurred; (ii) sediment is eroded from burrow roof, mound and the embedding area; (iii) sediment is accumulated within the burrow entrance.

To attribute sediment redistribution to a combination of animal activity and rainfall, four preconditions had to be met: (i) A rainfall event occurred; (ii) sediment is eroded from embedding area; (iii) the height of burrow roof and mound decreased or increased; (iv) the depth of burrow entrance increased.

The animal-caused sediment redistribution was calculated as the sediment volume excavated from the entrance. Animal excavation always increased depth of the burrow entrance. The rainfall-caused sediment redistribution was calculated as the sediment volume which eroded from the burrow roof and mound. During a rainfall event, sediment eroding from burrow roof might accumulate within burrow entrances. In this case, the depth of the burrow entrance decreased. No sediment could erode from the entrance during a rainfall event. Decreased depth of a burrow entrance always points to sediment redistribution caused by rainfall, increased depth of burrow entrance always means redistribution by animals. Rainfall-caused redistribution always occurred before animal-caused redistribution, as without erosion caused by rainfall, the animals did not need to reconstruct their burrows.

4.3.7 Calculation of daily sediment mass balance budget

The volume of the redistributed sediment was calculated daily and was then cumulated from the first day of monitoring. For the calculation of the daily sediment redistribution, the change in the surface level detected by the camera was calculated first. For each day, the scans from the day before and after the respective day were averaged and subtracted. The average standard deviation of the z-coordinate of these scans was 0.06 cm. As described in Section 2.2., all values with a difference below and above the threshold value of 0.2 cm were set to 0. The redistributed sediment volume was then calculated from the surface change for each pixel as follows:

$$Vol_{redistributed} = (S_b - S_a) * res^2 \quad . \tag{6}$$

In Eq. (6), $Vol_{redistributed}$ (cm^3 $pixel^{-1}$) is the volume of the calculated redistributed sediment, S_b (cm) the scan before, S_a (cm) the scan after the rainfall event and *res* is the spatial resolution (cm). Using the daily volume of the redistributed sediment per pixel, we calculated the daily mass balance budget by summing the volume of sediment eroding or accumulating within each delineated area.

4.3.8 Calculation of the overall volume of redistributed sediment after the period of 7 months

From the camera data, we calculated the average cumulative volume of redistributed sediment for the period of 7 months within burrows ($Vol_{burrows}$ ($cm^3\ cm^{-2}\ year^{-1}$)) and burrow embedding ($Vol_{embedding}$ ($cm^3\ cm^{-2}\ year^{-1}$)) areas and the average sediment volume redistributed (excavated) by the animal (Vol_{exc} ($cm^3\ cm^{-2}\ year^{-1}$)), separately for each site. We estimated the volume of sediment that was redistributed during rainfall events due to the presence of the burrow (Vol_{add} ($cm^3\ cm^{-2}\ year^{-1}$)). Vol_{add} was calculated as the difference in the redistributed sediment volume between burrows and burrow embedding areas according to Eq. (7).

$$Vol_{add} = \left(Vol_{affected} - Vol_{unaffected}\right) * 1.71 \quad , \quad (7)$$

Additionally, we calculated the average volume of the redistributed sediment per burrow ($Vol_{per\ burrow}$ [$cm^3\ burrow^{-1}\ year^{-1}$]).

$$Vol_{per\ burrow} = (Area_{burrow} * Vol) * 1.71 \quad (8)$$

In Eq. (8), $Area_{burrow}$ (cm^2) is the average size of the burrows that are monitored by the cameras; Vol is Vol_{burrow} ($cm^3\ cm^{-2}\ year^{-1}$), Vol_{exc} ($cm^3\ cm^{-2}\ year^{-1}$) or Vol_{add} ($cm^3\ cm^{-2}\ year^{-1}$).

We then upscaled the Vol_{burrow} ($cm^3\ cm^{-2}\ year^{-1}$), Vol_{exc} ($cm^3\ cm^{-2}\ year^{-1}$)) and Vol_{add} ($cm^3\ cm^{-2}\ year^{-1}$)) to the hillslope using the following approach. Hillslope-wide upscaling of the results generated in this study was performed by using a previous estimation of vertebrate burrow density (Grigusova et al., 2021). In this study, the density of burrows was measured in situ within eighty 100 m^2 plots and then upscaled to the same hillslopes on which the cameras were located by applying machine-learning methods, using the UAV-data as predictors. For upscaling, we applied a random forest model with recursive feature elimination. The model was validated by a repeated Leave-One-Out cross validation. The density of vertebrate burrows was between 6 and 12 100 m^2 in LC and between 0 and 12 100 m^{-2} in Pan de Azúcar. Using the hillslope-wide predicted vertebrate burrow densities ($Dens_{burrow}$ (number of burrows 100 m^{-2})) from Grigusova et al. 2021, we estimated the volume of redistributed sediment for each pixel of the raster layers ($Vol_{per\ pixel}$ ($cm^3\ m^{-2}\ year^{-1}$)) according to Eq. (9):

$$Vol_{per\ pixel} = Vol_{per\ burrow} * \ Dens_{burrow} * 1.71 \quad (9)$$

The average hillslope-wide volume of redistributed sediment ($Vol_{hillslope\text{-}wide}$ ($m^3\ ha^{-1}\ year^{-1}$)) was then estimated as follows:

$$Vol_{hillslope-wide} = \sum_1^m Vol_{per\ pixel} * 0.001 * 1.71 \quad , \quad (10)$$

In Eq (10), m is the number of pixels.

4.4. Results

4.4.1 Camera accuracy and data availability

The accuracy between the measured extracted sediment volume and sediment volume calculated from the camera scans was very high (MAE = 0.023 $cm^3\ cm^{-2}$, R^2 = 0.77, SD = 0.02 $cm^3\ cm^{-2}$, Fig. 4.A3). The accuracy between the calculated and measured extracted sediment was higher when the two scans taken before as well as after the extraction of the sediment were averaged and the sediment volume was estimated using these averaged scans. When calculating the redistributed

sediment from solely one scan before and after extraction, the accuracy slightly decreased (MAE = 0.081 cm^3 cm^{-2}, R^2 = 0.64). The cameras tended to overestimate the volume of redistributed sediment. Six out of eight custom-tailored cameras collected data over the seven-month period (Table 4.A2). One camera collected data for a period of three months and one camera stopped working a few days after installation. The quantity of usable point clouds taken at 1 a.m., 5 a.m. and 10 p.m. was higher than of point clouds taken at 8 a.m. Approximately 20% of points was removed from the point clouds before final analysis due to the high scattering at the point cloud corners. After data filtering (see Section 3.2.), 1326 scans were usable and for 86% of the days, at least one usable scan was available. The usable scans were distributed continuously within the monitoring period.

4.4.3 Mass balance of redistributed sediment

The cameras detected (i) sediment redistribution directly following rainfall events and (ii) due to the burrowing activity in times without rainfall (Fig. 4.5, A4 and A5). In all cases, burrows (entrance, burrow roof and mound) exhibited higher sediment redistribution rates than burrow embedding areas. In addition, the volume of redistributed sediment by animal activity was higher after a rainfall event occurred.

In the following, the dynamics are exemplary explained for four cameras. Animal burrowing activity was detected seven times by the camera LC NU (Fig. 4.5a, A4, A5) during the monitoring period, by an increase in sediment volume in the area delineated as mound. Simultaneously, the burrow entrance showed signs of modification and sediment accumulation, but these changes were less clear. Overall, the volume of the excavated soil varied. From April until June, up to 0.5 cm^3 cm^{-2} of sediment was excavated by the animal and accumulated on the mound. From June until September, animal burrowing activity was detected at four time slots (5 June 2019, 9 June 2019, 1 July 2019 and 18 August 2019) and sediment volume of up to 2 cm^3 cm^{-2} accumulated each time on the mound, burrow roof and within the entrance. During the rainfall events of up to 20 mm day^{-1} on 16 June 2019, 27 mm day^{-1} on 29 June 2019 and 7 mm day^{-1} on 13 July 2019, sediment volume of up to 4 cm^3 cm^{-2} eroded, especially from the burrow roof and the mound while a sediment volume of up to 1 cm^3 cm^{-2} accumulated within the entrance during each rainfall event. Camera LC-SL (Fig. 4.A4, A5) showed burrowing activities eight times and sediment volumes of up to 3 cm^3 cm^{-2} accumulated within the entrance and burrow roof. The camera detected sediment erosion of up to 2 cm^3 cm^{-2} after a rainfall event of 27 mm day^{-1} on 27 July 2019. On the south-upper hillslope, the camera detected animal burrowing activity six times, with a sediment accumulation of up to 3 cm^3 cm^{-2} (Fig. 4.A2 and A3).

In contrast, camera PdA-NU pointed to animal burrowing activity up to 15 times where up to 1 cm^3 cm^{-2} of sediment volume was redistributed from the entrance to the mound (Fig. 4.5b, A4, A5). At the end of June on 27 June 2019, a rainfall event of 1.5 mm day^{-1} occurred and up to 2 cm^3 cm^{-2} of sediment eroded from the burrow roof and accumulated within the burrow entrance. We observed increased sediment redistribution by the animal after the rainfall events. Camera PdA-SL evenly revealed animal burrowing activity up to 15 times ((Fig. 4.A4, A5)). The burrowing had a strong effect on the sediment redistribution. The rainfall event of 1.5 mm day^{-1} on 27 June 2019 did not cause any detecTable 4.surface change.

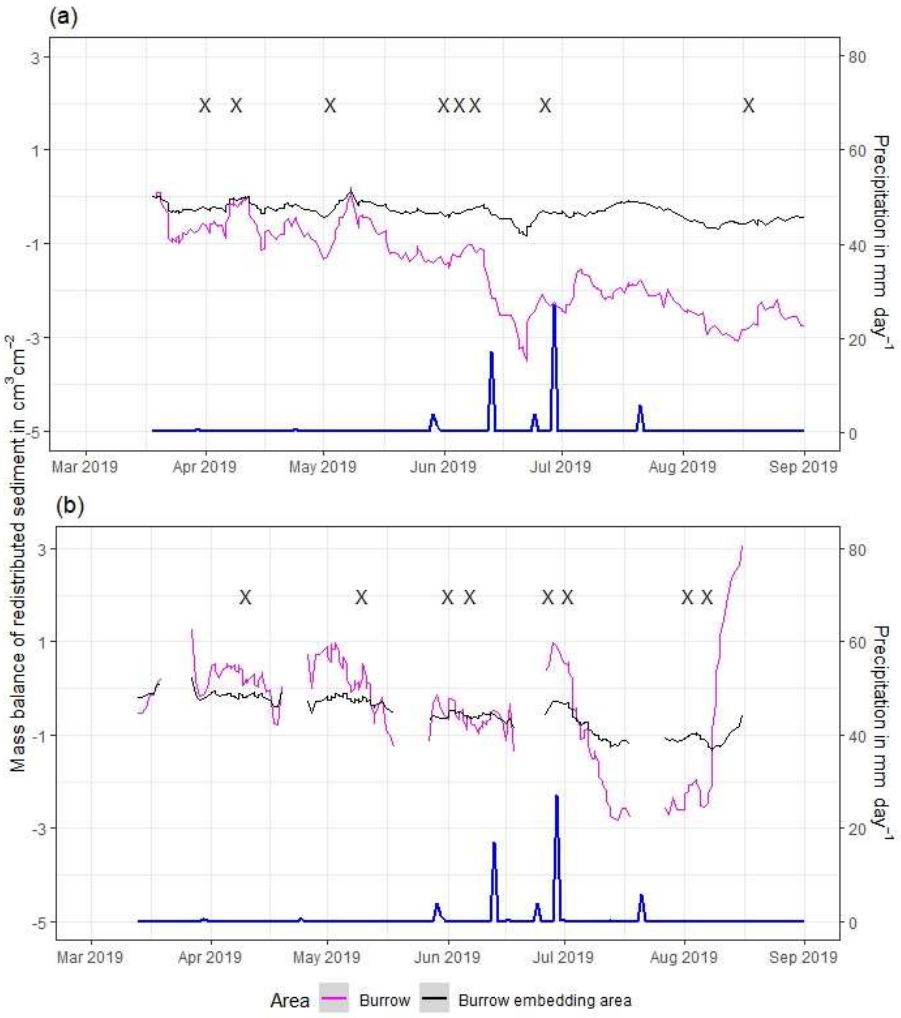

Figure 4.5. Examples of the mass balance of redistributed sediment for burrows and burrow embedding areas (**a**) The record of the camera on the upper north-facing hillslope in La Campana showed that larger rainfall events cause a negative sediment balance (sediment loss), followed by a phase of positive sediment mass balance after approximately 3 days due to sediment excavation; (**b**) The record of the camera on the upper north-facing in Pan de Azúcar hillslope showed a similar pattern to the camera on the upper north-facing hillslope, but the phase of positive mass balance was delayed in comparison. The blue line is the daily precipitation in mm day^{-1}, and "X" marks the days at which animal burrowing activity was detected. Positive values indicate sediment accumulation. Negative values indicate sediment erosion. Mass balances for all cameras are displayed in Fig. 4.A2 and A3.

The analysis of cumulative volume of the redistributed sediment caused by burrowing animal activity and rainfall over the monitored period of seven months for all eight cameras showed a heterogeneous pattern.

In LC, the cumulative volume of the sediment excavated by the animal within the burrow roof and mound increased continuously (Fig. 4.6, A7). Especially between the rainfall events from June until August, a cumulative volume of on average 6.5 cm^3 cm^{-2} was excavated by the animal. We calculated that, on average, 8.53 cm^3 cm^{-2} cumulatively eroded from the burrow roof and mound; while 2.44 cm^3

cm^{-2} sediment volume accumulated within the entrance (Fig. 4.6, A7). These results indicate that 28% of sediment eroding from the burrow roof accumulated within the entrance, while over 62% of sediment eroded downhill. Averaged over all camera scans, 338% more sediment was redistributed by rain within burrow compared to the burrow embedding area (Fig. 4.7).

In PdA, cameras continuously detected animal burrowing activity and excavation of the sediment (Fig. 4.A7). The volume of the detected excavated sediment increased steadily within all cameras. The cumulative sediment accumulation surpasses the sediment eroded due to the rainfall. The volume of the sediment eroded within the burrows was 40% higher than within the burrow embedding areas. The results show that approximately 50% of the eroded sediment accumulated within the entrance (Fig. 4.7).

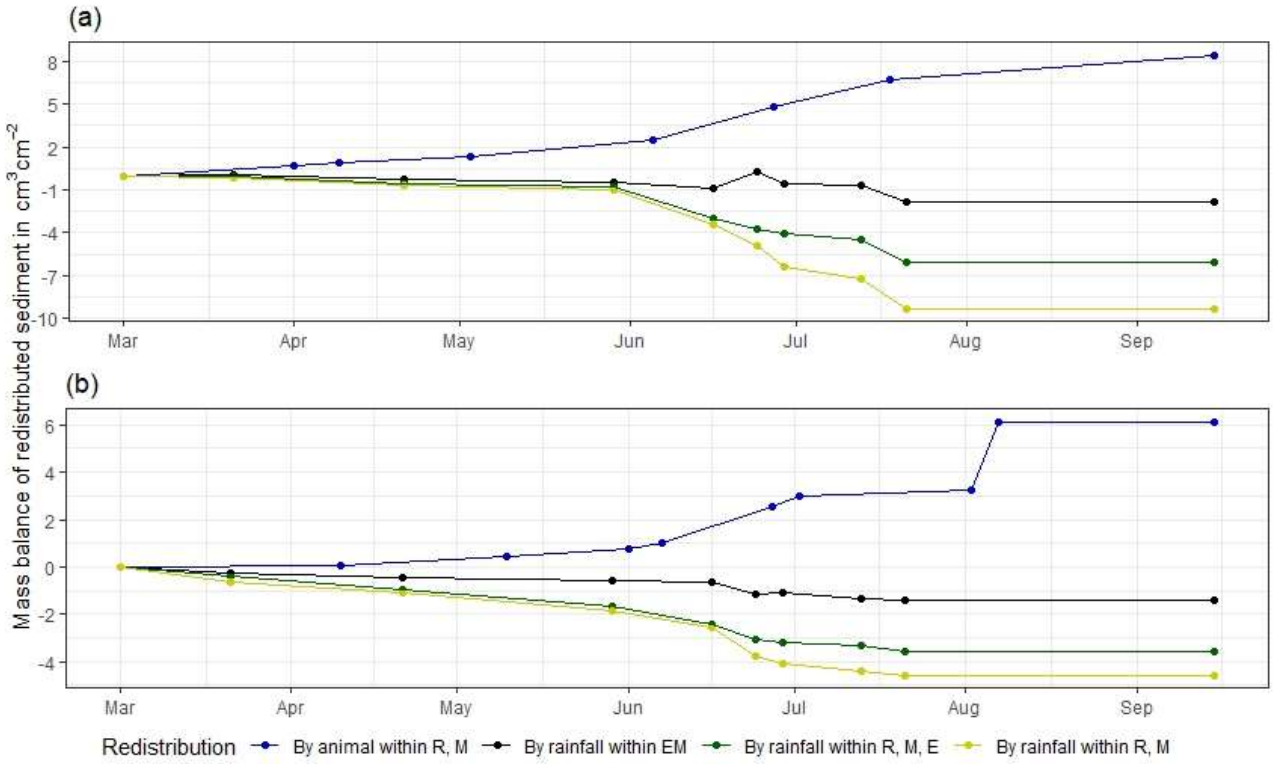

Figure 4.6. Examples of the cumulative volume of redistributed sediment within burrows and burrow embedding areas caused by animal burrowing activity or rainfall in mediterranean La Campana: (**a**) Upper north-facing hillslope; (**b**) Lower south-facing hillslope. Positive values indicate sediment accumulation. Negative values indicate sediment erosion. E is the burrow entrance; M is the mound; R is burrow roof; EM is the burrow embedding area. Cumulative volumes for all cameras are in Fig. 4.A7.

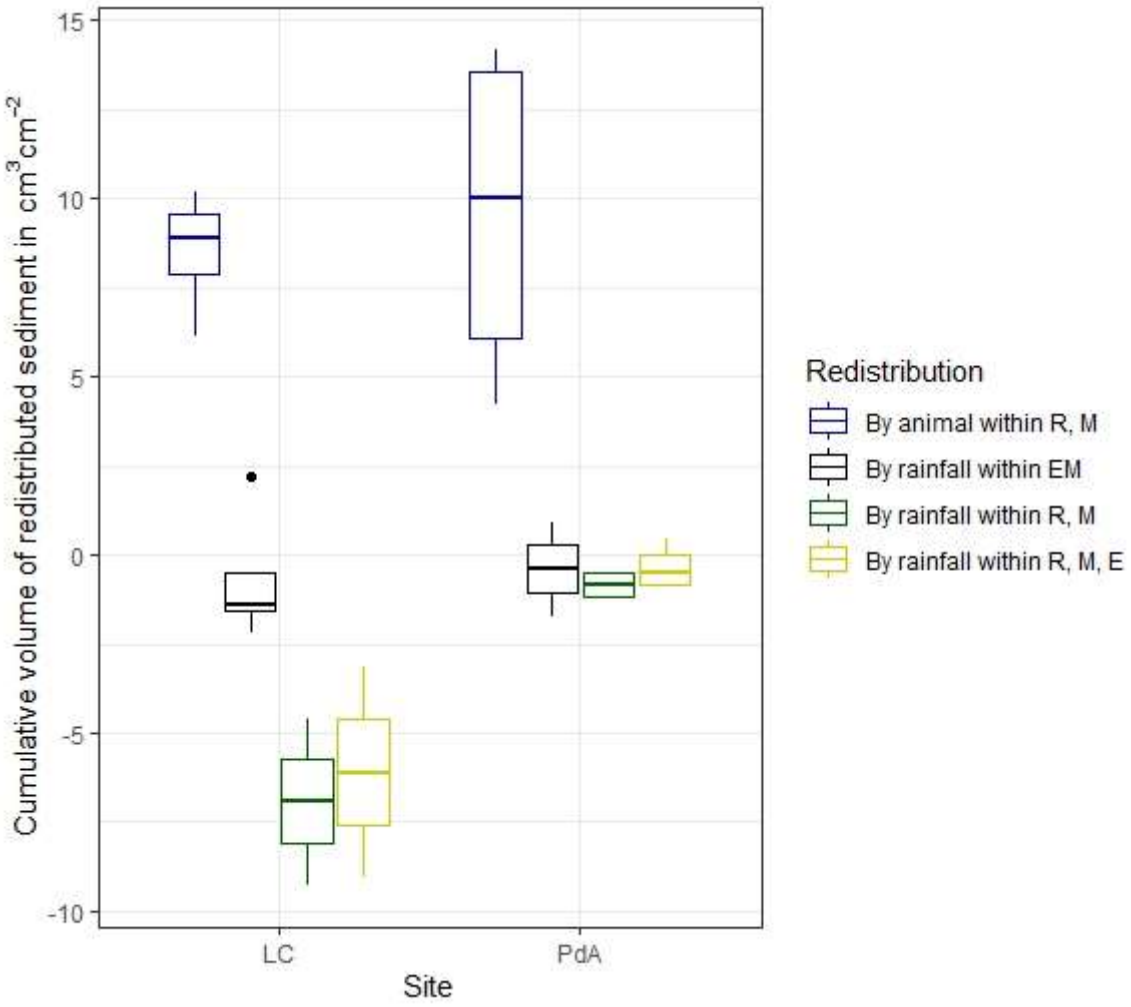

Figure 4.7. Cumulative volume of the redistributed sediment for the time period of 7 months for all cameras. Positive values indicate sediment accumulation. Negative values indicate sediment erosion. Whiskers indicate the median of sediment redistribution. E is the burrow entrance; M the mound; R is the burrow roof; EM is burrow embedding area; LC stands for National Park La Campana in the mediterranean climate zone; PdA stands for National Park PdA in the arid climate zone.

4.4.4 Volume of redistributed sediment

The average size of the burrows was 84.3 cm^2 (SD = 32.5 cm^2) in LC and 91.3 cm^2 in PdA (SD = 8.5 cm^2). The animals burrowed on average 1.2 times $month^{-1}$ in LC and 2.3 times $month^{-1}$ in PdA. The volume of the excavated sediment was 102.2 cm^{-3} $month^{-1}$ in LC and 124.8 cm^3 $month^{-1}$ in PdA. Each time the animals burrowed, they excavated 42 cm^3 sediment volume in LC and 14.3 cm^3 sediment volume in PdA. The burrowing intensity increased in winter after the rainfall occurrences in LC and stayed constant during the whole monitoring period in PdA. The burrows deteriorate after rainfall events with a rate of 73.0 cm^3 $month^{-1}$ or 63.9 cm^3 $event^{-1}$ in LC and 10.5 cm^{-3} month or 24.5 cm^3 $event^{-1}$.

The overall volume of the sediment excavated by the animal and redistributed during rainfall events varied between the sites (Table 4.1). The volume of the sediment redistributed by the animal was lower in LC than in PdA. However, on the hillslope scale, a higher total area-wide volume of excavation was calculated for LC compared to PdA, due to the higher burrow density in LC. The volume of the

sediment redistributed within burrows during rainfall events was higher in LC than in PdA. The volume of additionally redistributed sediment due to the presence of burrows was higher in LC than in PdA (Table 4.2, Fig. 4.8).

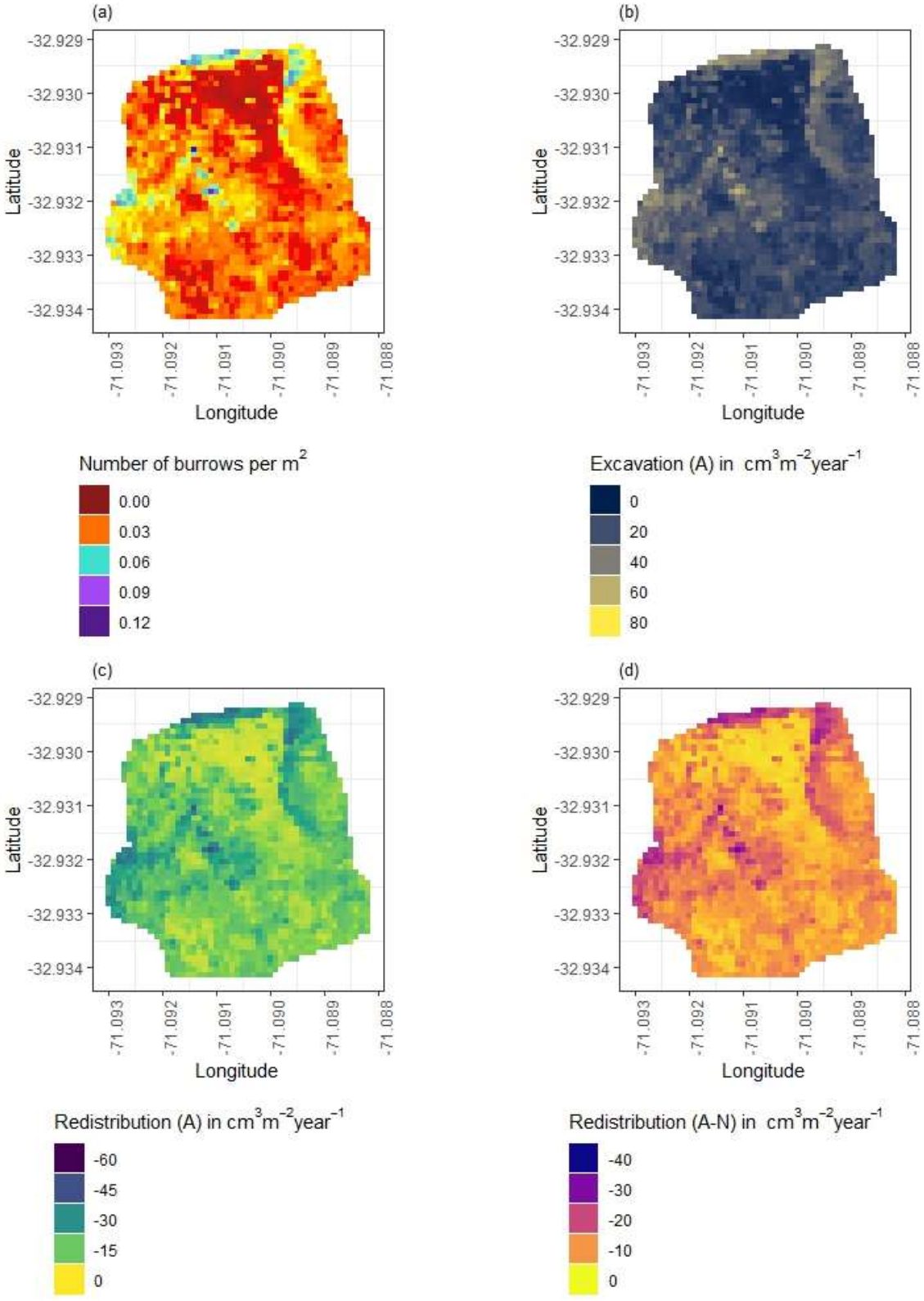

Figure 4.8. Example of the hillslope-wide volume of redistributed sediment on the south-facing hillslope in La Campana: (a) Density of burrows as estimated by Grigusova et al. (2021); (b) Volume of the

sediment excavated by the animals; (c) Volume of the sediment redistributed during rainfall events within burrows; (d) Volume of additionally redistributed sediment during rainfall events due to the presence of the burrows. The values were calculated per burrow as stated in Section 3.7. by subtracting the sediment volume redistributed within burrows from the sediment volume redistributed within burrow embedding area and then upscaled. The letters in brackets indicate if the upscaling was conducted using data from burrows or burrow embedding areas. “B” stands for burrow. By “EM-B”, the redistribution calculated within burrow embedding areas was subtracted from the redistribution calculated within burrows to obtain the additional volume of redistributed sediment due to the burrows’ presence. Positive values indicate sediment accumulation. Negative values indicate sediment erosion.

Table 4.2. Summary of the volume of redistributed sediment, according to area and disturbance type. Vol_{exc} describes volume of the sediment excavated by the animals. Vol_{burrow} describes volume of the sediment redistributed during rainfall events within burrows. Vol_{add} describes the difference in redistributed sediment volume within burrows and burrow embedding areas during rainfall. Positive values indicate sediment accumulation; negative values indicate sediment erosion.

Disturbance	Area	PdA	LC
Vol_{exc}	Burrow	16.4 cm^3 cm^{-2} $year^{-1}$	14.6 cm^3 cm^{-2} $year^{-1}$
	Per burrow	1498.6 cm^3 $burrow^{-1}$ $year^{-1}$	1226.1 cm^3 $burrow^{-1}$ $year^{-1}$
	Hillslope-wide	0.8 m^3 ha^{-1} $year^{-1}$	0.7 m^3 ha^{-1} $year^{-1}$
$Vol_{affected}$	Burrow	-1.9 cm^3 cm^{-2} $year^{-1}$	-10.4 cm^3 cm^{-2} $year^{-1}$
	Per burrow	-126.3 cm^3 $burrow^{-1}$ $year^{-1}$	-876.8 cm^3 $burrow^{-1}$ $year^{-1}$
	Hillslope-wide	-0.1 m^3 ha^{-1} $year^{-1}$	-0.4 m^3 ha^{-1} $year^{-1}$
Vol_{add}	Burrow	-1.1 cm^3 cm^{-2} $year^{-1}$	-7.3 cm^3 cm^{-2} $year^{-1}$
	Per burrow	-48.3 cm^3 $burrow^{-1}$ $year^{-1}$	-619.2 cm^3 $burrow^{-1}$ $year^{-1}$
	Hillslope-wide	-0.1 m^3 ha^{-1} $year^{-1}$	-0.3 m^3 ha^{-1} $year^{-1}$

4.5. Discussion

Our results showed that the custom-made ToF device is a suiTable 4.tool for high-resolution, automated monitoring of surface changes, applicable also in remote areas. The continuous observation of sediment redistribution over a longer time period provided new insights into the relative importance of burrowing animals for hillslope sediment flux. Our research revealed that the presence of vertebrate burrows increases hillslope sediment redistribution rates much more than previously assumed (increase of up to 208%). We showed that the quantity of animal-related sediment redistribution, however, varied with rainfall occurrence, with an increase in sediment redistribution between 40% in the arid research area and 338% percent in the mediterranean research area.

4.5.1 Suitability of the ToF - cameras for surface monitoring

The newly introduced monitoring technique ToF enables an automatic monitoring of surface changes on a microtopographic scale, and is less costly and invasive than other techniques. The measurement continuity of the device also allows for the analysis of ongoing biogeomorphological processes in high temporal and spatial resolution.

With regard to the costs, measurement frequency and sampling autonomy, the custom-made ToF device constitutes an improvement to earlier studies which used laser scanning technology to monitor microtopographic changes (Table 4.A5). This is because previous studies applied expensive laser scanning for the estimation of sediment redistribution, and due to the costs of the instrument it was not left in the field for continuous measurements, and hence research sites had to be revisited for each measurement (Nasermoaddeli and Pasche, 2008; Eltner et al., 2016a; Eltner et al., 2016b; Hänsel et al., 2016). The estimated costs in studies using time-lapse photogrammetry were similar to our study (up to 5000 USD) (James and Robson, 2014; Galland et al., 2016; MALLALIEU et al., 2017; Eltner et al., 2017; Kromer et al., 2019; Blanch et al., 2021). However, time-lapse monitoring needs several devices set up in different viewing angles, which increases installation efforts and disturbance significantly.

In terms of data quality, our ToF device is more precise or comparable to those employed in earlier studies using ToF. The accuracy of the camera (R^2 = 0.77) was in the range of previous studies (R^2 = 0.26–0.83 (Eitel et al., 2011), Table 4.A5). The horizontal point spacing of our cameras was 0.32 cm, and the maximum number of points per cm^2 was 8.5. These values are similar to previous studies in which the used devices had a horizontal point spacing in the range of 0.25–0.57 cm (Kaiser et al., 2014; Nasermoaddeli and Pasche, 2008)) (Table 4.A5), and the maximum number of points per cm^2 in a range of 1 point–25 points cm^{-2} (Eitel et al., 2011; Longoni et al., 2016) (Table 4.A5).

Our cameras tended to slightly overestimate or underestimate the volume of redistributed sediment. This error occurs when the pulse reflects from several vertical objects such as walls or, in our case, branches or stones and then enters the camera sensor. This phenomenon was also observed in previous studies applying laser scanners and is ineviTable 4.if the goal is to study surface changes under natural field conditions (Kukko and Hyyppä, 2009; Ashcroft et al., 2014). During operation of the cameras, we learnt that our newly developed instruments are particularly capable of delivering usable scans at night. This is likely due to the strong scattered sunlight reaching the camera sensor during the day, blurring the data (Li, 2014). Thus, in future studies, we recommend focusing on nocturnal operation to prevent light contamination.

4.5.2 The role of climate variability and burrowing cycles

We have found that rainfall plays a key role in triggering burrowing activity, which means that wet seasons experience higher sediment redistribution rates than dry seasons. In the year of investigation (2019), the dry season lasted from January until April, and from September until December (8 months), and the wet season lasted from May until August (4 months). The monitoring period lasted from March until October which covered 3 dry and 4 wet months (7 months in total). A yearly rate of sediment redistribution can be calculated by simply averaging the redistribution rate of the 7 monitored

months and multiplying this result by 12 months, which results in an average redistribution rate of 0.4 m^2 ha^{-1} $year^{-1}$ for LC and 0.1 m^2 ha^{-1} $year^{-1}$ for PdA. However, because burrowing activity and rain-driven sediment redistribution is mainly determined by rainfall, this method might have led to an overestimation of the annual redistribution rate based on averaging, because the unmonitored part of the year 2019 was predominantly dry (Übernickel et al., 2021b). This can be accounted for by adding five times the dry month redistribution rate to the monitored 7 months, which leads to a lower annual redistribution rates for LC of 0.3 m^2 ha^{-1} $year^{-1}$ and for PdA of 0.1 m^2 ha^{-1} $year^{-1}$. Our values might thus overestimate sediment redistribution for the year 2019. This difference between both values (0.1 m^2 ha^{-1} $year^{-1}$ for LC and under 0.1 m^2 ha^{-1} $year^{-1}$ for PdA) can be interpreted as the uncertainty range for the year of observation.

However, decadal rainfall variability indicates that the year of monitoring (2019) was among the drier years of the last 30 years (Yáñez et al., 2001; Valdés-Pineda et al., 2016; Garreaud et al., 2002; Wilcox et al., 2016)). The amount of precipitation since 1980 ranges from 200 mm until 800 mm per year (https://climatologia.meteochile.gob.cl/application/requerimiento/producto/RE3005) while the amount of precipitation in 2019 was just above 100 mm. This means, our results might underestimate sediment redistribution on a longer time perspective by 2 - 7 times.

Furthermore, the phenology of the burrowing animals is an additional source for uncertainty when calculating annual rates. The most common burrowing animal families in the area are active for three months of the year. The months in which they are active, are between April and September. None of the most common burrowing animal families were reported to be active from November until February. (Eccard and Herde, 2013; Jimenez et al., 1992; Katzman et al., 2018; Malizia, 1998; Monteverde and Piudo, 2011). This is also in line with our observations, because burrowing intensity increased from March until May, reached its peak between May and June and declined until September (Figure 4.6). By extrapolating from 7 months to one-year period, our estimated excavation was 0.7 m^2 ha^{-1} $year^{-1}$ in LC and 0.8 m^2 ha^{-1} $year^{-1}$ in PdA. By adding five times the low active months to the 7 months of observation, the estimated excavation would be 0.6 m^2 ha^{-1} $year^{-1}$ in LC and 0.6 m^2 ha^{-1} $year^{-1}$ in PdA. Our values might thus overestimate the sediment excavation and the excavation uncertainty range is 0.1 m^2 ha^{-1} $year^{-1}$ for LC and 0.2 m^2 ha^{-1} $year^{-1}$ for PdA.

4.5.3. Sediment Redistribution

Our research reveals that the presence of vertebrate burrows generally increases hillslope sediment redistribution. We show, however, that the ratio between the sediment redistribution caused by rainfall within burrow and burrow embedding areas varies between climate zones. Sediment redistribution within burrow areas was 40% higher at the arid research site, and at the mediterranean research site, it was 338% higher when compared to burrow embedding area (Table 4.A6).

By monitoring microtopographical changes in a high spatio-temporal resolution, we found that the occurrence of larger rainfall events played a two-fold, accelerating role in influencing sediment redistribution (Fig. 4.9). Firstly, rainfall-runoff eroded burrow material caused increased sediment loss. This was followed by animal burrowing activity after the rainfall. This means that rainfall triggered animal burrowing activity which was very likely related to a lower burrowing resistance of the soil due to the increased soil moisture (Rutin, 1996; Romañach et al., 2005; Herbst and Bennett, 2006). This double

feedback led to frequently occurring but small redistribution rates. However, cumulatively, the mechanism increased downhill sediment fluxes. Previous studies most likely missed this low magnitude but frequent surface processes due to a lower monitoring duration and frequency, or artificial laboratory conditions, and thus, did not quantify the full volume of redistributed sediment associated with burrowing activity. To quantify all occurred sediment redistribution processes, a continuous surface monitoring, like the here presented, is needed.

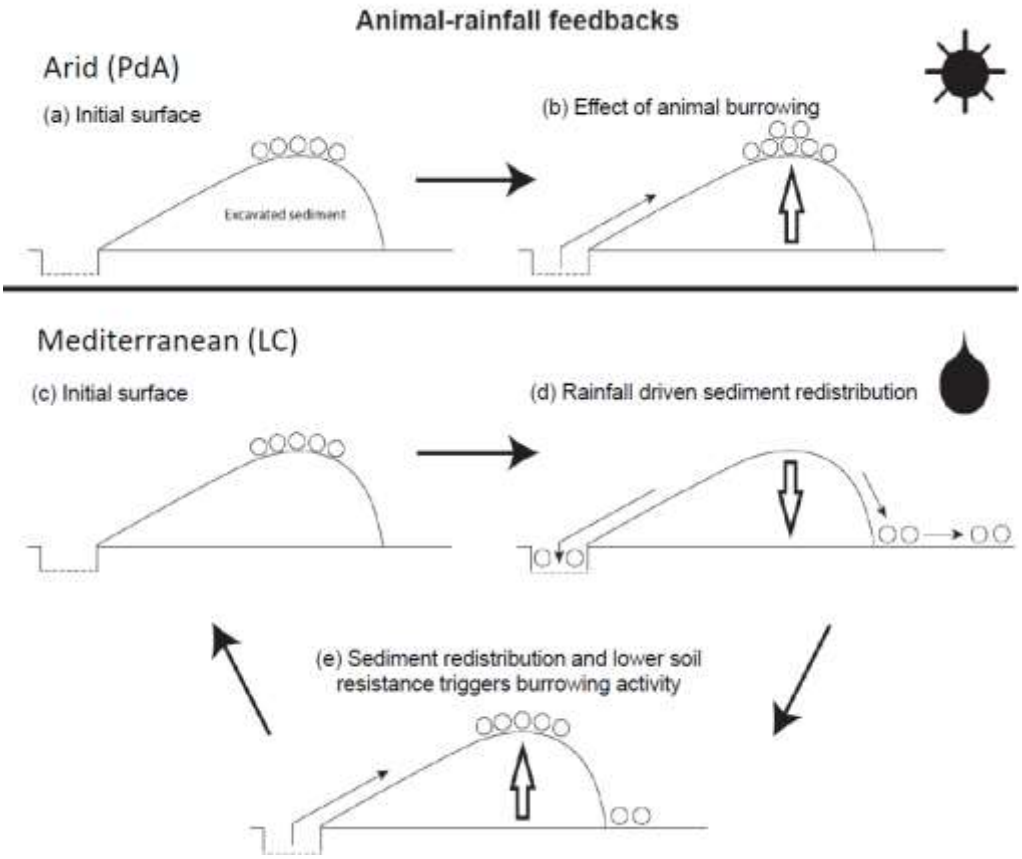

Figure 4.9. Scheme of animal-driven and rainfall-driven sediment redistribution processes in both investigated climate zones: (**a**) Describes the initial surface of the burrow before the start of a sediment redistribution process, and (**b**) the animal excavation process in the arid climate zone. Here, due to rarely occurring rainfall events, sediment redistribution is mostly controlled by the animal burrowing activity; (**c**) describes the initial burrow surface in the mediterranean climate zone, (**d**) the process of sediment redistribution during a rainfall event and (**e**) the subsequent animal burrowing activity. Burrowing is triggered by decreased soil resistance due to the increased soil moisture after rainfall as well as by sediment accumulation within the burrow's entrance. Burrowing activity leads to a new supply of sediment being excavated to the surface. In the mediterranean climate zone, sediment redistribution is controlled by both animal burrowing activity and rainfall. The alternating excavation and erosion process ultimately lead to an increase in redistribution rates.

Our results indicate an up to 338% increase in the sediment volume redistributed during rainfall events measured within burrows when compared to burrow embedding areas. In contrast to our result, the maximum increase estimated in previous studies was 208% (Table 4.A6, (Imeson and Kwaad, 1976). The two climate zones also show different patterns: In the mediterranean climate, the contribution of animals' (vertebrates') burrowing activity appear larger than previously observed by using field methods such as erosion pins or splash traps (from –3% until – 208%, Table 4.A6, (Imeson and Kwaad, 1976; Hazelhoff et al., 1981; Black and Montgomery, 1991). In contrast, in arid PdA, our study found a much smaller increase (40%, Table 4.A6) in the sediment volume redistributed during rainfall events measured within burrows when compared to burrow embedding areas. This is lower than previously estimated (125%, Table 4.A6, (Black and Montgomery, 1991). However, solely one rainfall event above 0.2 mm day^{-1} occurred during our monitoring period. Hence, we conclude that the contribution of burrowing activity of animals to hillslope sediment transport is much larger in areas with frequent rainfall events than previously thought, while it has been realistically estimated by previous studies for areas with rare rainfall events (Table 4.A6).

Magnitudes of sediment volume redistributed within burrows similar to our results were previously obtained solely in studies applying rainfall simulators. These studies estimated an increase in the volume of sediment redistributed during rainfall events, measured within burrows when compared to burrow embedding areas, to be between 205% and 473% (Table 4.A6, (Li et al., 2018; Chen et al., 2021). However, a rainfall simulator can only provide data on surface processes within a plot of a few m^2 in size and under ideal laboratory conditions while ignoring the uphill microtopography, vegetation cover and distribution (Iserloh et al., 2013), which were shown to reduce erosion rates. More importantly, the rainfall intensity on hillslopes decreases with (i) the angle of incidence of the rain, (ii) the inclination of the surface and iii) the relative orientation of the sloping surface to the rain vector (Sharon, 1980). When simulating a rainfall event with the same rainfall volume as in the field, the rain is induced directly over the treated surface and has thus a higher velocity which leads to an increased splash erosion than under natural conditions (Iserloh et al., 2013). We thus propose that the rainfall experiments overestimate the erosion rate while the correct erosion rate can be measured solely under field conditions.

Cumulative sediment redistribution within burrow roof, mound and entrance was, on average, 28% lower than cumulative sediment redistribution only within the mound and the burrow roof (Figure 4.A7). These results suggest that 28% of the eroded sediment from animal mounds and burrow roofs is re-accumulated within the burrow entrance during rainfall-runoff events, and the remaining 62% is incorporated into overall hillslope sediment flux. Our numbers contrast with previous studies, which quantified that about 58% of the sediment excavated by animals will accumulate back in the burrow entrance and only 42% is incorporated to downhill sediment flux (Andersen, 1987; Reichman and Seabloom, 2002). Hence, our results indicate not only higher redistribution rates within burrows by burrowing animals but also point to much higher supply of sediment to the downhill sediment flux than previously thought.

Our cost-effective ToF device provides data on surface changes in a high spatio-temporal resolution. The high temporal resolution was able to unravel ongoing low magnitude but frequent animal

excavation and erosion processes. The high spatial resolution enabled us to estimate the exact volume of sediment fluxes from the burrows downhill. The here presented results indicate that the contribution of burrowing animals on the burrow as well as on the hillslope scale was much higher than previously assumed. Our results can be integrated into long-term soil erosion models that rely on soil processes and improve their accuracy by including animal-induced surface processes on microtopographical scales in their algorithms.

Funding: This study was funded by the German Research Foundation, DFG [grant numbers BE1780/52-1, LA3521/1-1, FA 925/12-1, BR 1293-18-1], and is part of the DFG Priority Programme SPP 1803: EarthShape: Earth Surface Shaping by Biota, sub-project “Effects of bioturbation on rates of vertical and horizontal sediment and nutrient fluxes”.

Institutional Review Board Statement: Not applicable.

Informed Consent Statement: Not applicable.

Acknowledgments: We thank CONAF for the kind support provided during our field campaign.

Competing interests: There is no conflict of interest.

Author contribution: JB, AL and SA planned the campaign; PG and SA performed the measurements; PG analysed the data and wrote the manuscript draft; AL, JB, NF, RB, KÜ, LP, CR, DK and PP reviewed and edited the manuscript.

Code/Data availability: Code and all raw data can be provided by the corresponding author upon request.

References

Afana, A., Solé-Benet, A., and Pérez, J. L.: Determination of Soil Erosion Using Laser Scanners, last access: 22 December 2021, 2010.

Andersen, D. C.: Geomys Bursarius Burrowing Patterns: Influence of Season and Food Patch Structure, Ecology, 68, 1306–1318, https://doi.org/10.2307/1939215, 1987.

Ashcroft, M. B., Gollan, J. R., and Ramp, D.: Creating vegetation density profiles for a diverse range of ecological habitats using terrestrial laser scanning, Methods Ecol Evol, 5, 263–272, https://doi.org/10.1111/2041-210X.12157, 2014.

BANCROFT, W. J. and Hill, D. and Roberts, J.D.: A new method for calculating volume of excavated burrows: the geomorphic impact of Wedge-Tailed Shearwater burrows on Rottnest Island, Funct Ecology, 18, 752–759, https://doi.org/10.1111/j.0269-8463.2004.00898.x, 2004.

Bernhard, N., Moskwa, L.-M., Schmidt, K., Oeser, R. A., Aburto, F., Bader, M. Y., Baumann, K., Blanckenburg, F. von, Boy, J., van den Brink, L., Brucker, E., Büdel, B., Canessa, R., Dippold, M. A., Ehlers, T. A., Fuentes, J. P., Godoy, R., Jung, P., Karsten, U., Köster, M., Kuzyakov, Y., Leinweber, P., Neidhardt, H., Matus, F., Mueller, C. W., Oelmann, Y., Oses, R., Osses, P., Paulino, L., Samolov, E., Schaller, M., Schmid, M., Spielvogel, S., Spohn, M., Stock, S., Stroncik, N., Tielbörger, K., Übernickel, K., Scholten, T., Seguel, O., Wagner, D., and Kühn, P.: Pedogenic and microbial interrelations to regional climate and local topography: New insights from a climate gradient (arid to humid) along the Coastal Cordillera of Chile, CATENA, 170, 335–355, https://doi.org/10.1016/j.catena.2018.06.018, 2018.

Black, T. A. and Montgomery, D. R.: Sediment transport by burrowing mammals, Marin County, California, Earth Surf. Process. Landforms, 16, 163–172, https://doi.org/10.1002/esp.3290160207, 1991.

Blanch, X., Eltner, A., Guinau, M., and Abellan, A.: Multi-Epoch and Multi-Imagery (MEMI) Photogrammetric Workflow for Enhanced Change Detection Using Time-Lapse Cameras, Remote Sensing, 13, 1460, https://doi.org/10.3390/rs13081460, 2021.

Castner, J. L. and Fowler, H. G.: Distribution of Mole Crickets (Orthoptera: Gryllotalpidae: Scapteriscus) and the Mole Cricket Parasitoid Larra bicolor (Hymenoptera: Sphecidae) in Puerto Rico, The Florida Entomologist, 67, 481, https://doi.org/10.2307/3494730, 1984.

Chen, M., Ma, L., Shao, M.'a., Wei, X., Jia, Y., Sun, S., Zhang, Q., Li, T., Yang, X., and Gan, M.: Chinese zokor (Myospalax fontanierii) excavating activities lessen runoff but facilitate soil erosion – A simulation experiment, CATENA, 202, 105248, https://doi.org/10.1016/j.catena.2021.105248, 2021.

Coombes, M. A.: Biogeomorphology: diverse, integrative and useful, Earth Surf. Process. Landforms, 41, 2296–2300, https://doi.org/10.1002/esp.4055, 2016.

Corenblit, D., Corbara, B., and Steiger, J.: Biogeomorphological eco-evolutionary feedback between life and geomorphology: a theoretical framework using fossorial mammals, Die Naturwissenschaften, 108, 55, https://doi.org/10.1007/s00114-021-01760-y, 2021.

Eccard, J. A. and Herde, A.: Seasonal variation in the behaviour of a short-lived rodent, BMC ecology, 13, 43, https://doi.org/10.1186/1472-6785-13-43, 2013.

Eitel, J. U.H., Williams, C. J., Vierling, L. A., Al-Hamdan, O. Z., and Pierson, F. B.: Suitability of terrestrial laser scanning for studying surface roughness effects on concentrated flow erosion processes in rangelands, CATENA, 87, 398–407, https://doi.org/10.1016/j.catena.2011.07.009, 2011.

Eltner, A., Schneider, D., and Maas, H.-G.: Integrated processing of high resolution topographic data for soil erosion assessment considering data acquisition schemes and surface properties, Int. Arch. Photogramm. Remote Sens. Spatial Inf. Sci., XLI-B5, 813–819, https://doi.org/10.5194/isprsarchives-XLI-B5-813-2016, 2016a.

Eltner, A., Mulsow, C., and Maas, H.-G.: QUANTITATIVE MEASUREMENT OF SOIL EROSION FROM TLS AND UAV DATA, Int. Arch. Photogramm. Remote Sens. Spatial Inf. Sci., XL-1/W2, 119–124, https://doi.org/10.5194/isprsarchives-XL-1-W2-119-2013, 2013.

Eltner, A., Kaiser, A., Abellan, A., and Schindewolf, M.: Time lapse structure-from-motion photogrammetry for continuous geomorphic monitoring, Earth Surf. Process. Landforms, 42, 2240–2253, https://doi.org/10.1002/esp.4178, 2017.

Eltner, A., Kaiser, A., Castillo, C., Rock, G., Neugirg, F., and Abellán, A.: Image-based surface reconstruction in geomorphometry – merits, limits and developments, Earth Surf. Dynam., 4, 359–389, https://doi.org/10.5194/esurf-4-359-2016, 2016b.

Gabet, E. J., Reichman, O. J., and Seabloom, E. W.: The Effects of Bioturbation on Soil Processes and Sediment Transport, Annu. Rev. Earth Planet. Sci., 31, 249–273, https://doi.org/10.1146/annurev.earth.31.100901.141314, 2003.

Galland, O., Bertelsen, H. S., Guldstrand, F., Girod, L., Johannessen, R. F., Bjugger, F., Burchardt, S., and Mair, K.: Application of open-source photogrammetric software MicMac for monitoring surface deformation in laboratory models, J. Geophys. Res. Solid Earth, 121, 2852–2872, https://doi.org/10.1002/2015JB012564, 2016.

Garreaud, R., Rutllant, J., and Fuenzalida, H.: Coastal Lows along the Subtropical West Coast of South America: Mean Structure and Evolution, Mon. Wea. Rev., 130, 75–88, https://doi.org/10.1175/1520-0493(2002)130<0075:CLATSW>2.0.CO;2, 2002.

Grigusova, P., Larsen, A., Achilles, S., Klug, A., Fischer, R., Kraus, D., Übernickel, K., Paulino, L., Pliscoff, P., Brandl, R., Farwig, N., and Bendix, J.: Area-Wide Prediction of Vertebrate and Invertebrate Hole Density and Depth across a Climate Gradient in Chile Based on UAV and Machine Learning, Drones, 5, 86, https://doi.org/10.3390/drones5030086, 2021.

Hakonson, T. E.: The Effects of Pocket Gopher Burrowing on Water Balance and Erosion from Landfill Covers, J. environ. qual., 28, 659–665, https://doi.org/10.2134/jeq1999.00472425002800020033x, 1999.

Hall, K., Boelhouwers, J., and Driscoll, K.: Animals as Erosion Agents in the Alpine Zone: Some Data and Observations from Canada, Lesotho, and Tibet, Arctic, Antarctic, and Alpine Research, 31, 436–446, https://doi.org/10.1080/15230430.1999.12003328, 1999.

Hancock, G. and Lowry, J.: Quantifying the influence of rainfall, vegetation and animals on soil erosion and hillslope connectivity in the monsoonal tropics of northern Australia, Earth Surf. Process. Landforms, 46, 2110–2123, https://doi.org/10.1002/esp.5147, 2021.

Hänsel, P., Schindewolf, M., Eltner, A., Kaiser, A., and Schmidt, J.: Feasibility of High-Resolution Soil Erosion Measurements by Means of Rainfall Simulations and SfM Photogrammetry, Hydrology, 3, 38, https://doi.org/10.3390/hydrology3040038, 2016.

Hazelhoff, L., van Hoof, P., Imeson, A. C., and Kwaad, F. J. P. M.: The exposure of forest soil to erosion by earthworms, Earth Surf. Process. Landforms, 6, 235–250, https://doi.org/10.1002/esp.3290060305, 1981.

Herbst, M. and Bennett, N. C.: Burrow architecture and burrowing dynamics of the endangered Namaqua dune mole rat (Bathyergus janetta) (Rodentia: Bathyergidae), Journal of Zoology, 270, 420–428, https://doi.org/10.1111/j.1469-7998.2006.00151.x, 2006.

Horn, B.K.P.: Hill shading and the reflectance map, Proc. IEEE, 69, 14–47, https://doi.org/10.1109/PROC.1981.11918, 1981.

Imeson, A. C.: Splash erosion, animal activity and sediment supply in a small forested Luxembourg catchment, Earth Surf. Process. Landforms, 2, 153–160, https://doi.org/10.1002/esp.3290020207, 1977.

Imeson, A. C. and Kwaad, F. J. P. M.: Some Effects of Burrowing Animals on Slope Processes in the Luxembourg Ardennes, Geografiska Annaler: Series A, Physical Geography, 58, 317–328, https://doi.org/10.1080/04353676.1976.11879941, 1976.

Iserloh, T., Ries, J. B., Arnáez, J., Boix-Fayos, C., Butzen, V., Cerdà, A., Echeverría, M. T., Fernández-Gálvez, J., Fister, W., Geißler, C., Gómez, J. A., Gómez-Macpherson, H., Kuhn, N. J., Lázaro, R., León, F. J., Martínez-Mena, M., Martínez-Murillo, J. F., Marzen, M., Mingorance, M. D., Ortigosa, L., Peters, P., Regüés, D., Ruiz-Sinoga, J. D., Scholten, T., Seeger, M., Solé-Benet, A., Wengel, R., and Wirtz, S.: European small porTable 4.rainfall simulators: A comparison of rainfall characteristics, CATENA, 110, 100–112, https://doi.org/10.1016/j.catena.2013.05.013, 2013.

James, M. R. and Robson, S.: Sequential digital elevation models of active lava flows from ground-based stereo time-lapse imagery, ISPRS Journal of Photogrammetry and Remote Sensing, 97, 160–170, https://doi.org/10.1016/j.isprsjprs.2014.08.011, 2014.

Jimenez, J. E., Feinsinger, P., and Jaksi, F. M.: Spatiotemporal Patterns of an Irruption and Decline of Small Mammals in Northcentral Chile, Journal of Mammalogy, 73, 356–364, https://doi.org/10.2307/1382070, 1992.

Jones, C. G., Gutiérrez, J. L., Byers, J. E., Crooks, J. A., Lambrinos, J. G., and Talley, T. S.: A framework for understanding physical ecosystem engineering by organisms, Oikos, 119, 1862–1869, https://doi.org/10.1111/j.1600-0706.2010.18782.x, 2010.

Kaiser, A., Neugirg, F., Rock, G., Müller, C., Haas, F., Ries, J., and Schmidt, J.: Small-Scale Surface Reconstruction and Volume Calculation of Soil Erosion in Complex Moroccan Gully Morphology Using Structure from Motion, Remote Sensing, 6, 7050–7080, https://doi.org/10.3390/rs6087050, 2014.

Katzman, E. A., Zaytseva, E. A., Feoktistova, N. Y., Tovpinetz, N. N., Bogomolov, P. L., Potashnikova, E. V., and Surov, A. V.: Seasonal Changes in Burrowing of the Common Hamster (Cricetus cricetus

L., 1758) (Rodentia: Cricetidae) in the City, PJE, 17, 251–258, https://doi.org/10.18500/1684-7318-2018-3-251-258, 2018.

Kinlaw, A. and Grasmueck, M.: Evidence for and geomorphologic consequences of a reptilian ecosystem engineer: The burrowing cascade initiated by the Gopher Tortoise, Geomorphology, 157-158, 108–121, https://doi.org/10.1016/j.geomorph.2011.06.030, 2012.

Kromer, R., Walton, G., Gray, B., Lato, M., and Group, R.: Development and Optimization of an Automated Fixed-Location Time Lapse Photogrammetric Rock Slope Monitoring System, Remote Sensing, 11, 1890, https://doi.org/10.3390/rs11161890, 2019.

Kukko, A. and Hyyppä, J.: Small-footprint Laser Scanning Simulator for System Validation, Error Assessment, and Algorithm Development, photogramm eng remote sensing, 75, 1177–1189, https://doi.org/10.14358/PERS.75.10.1177, 2009.

Larsen, A., Nardin, W., Lageweg, W. I., and Bätz, N.: Biogeomorphology, quo vadis? On processes, time, and space in biogeomorphology, Earth Surf. Process. Landforms, 46, 12–23, https://doi.org/10.1002/esp.5016, 2021.

Le Hir, P., Monbet, Y., and Orvain, F.: Sediment erodability in sediment transport modelling: Can we account for biota effects?, Continental Shelf Research, 27, 1116–1142, https://doi.org/10.1016/j.csr.2005.11.016, 2007.

Lehnert, L. W., Thies, B., Trachte, K., Achilles, S., Osses, P., Baumann, K., Bendix, J., Schmidt, J., Samolov, E., Jung, P., Leinweber, P., Karsten, U., and Büdel, B.: A Case Study on Fog/Low Stratus Occurrence at Las Lomitas, Atacama Desert (Chile) as a Water Source for Biological Soil Crusts, Aerosol Air Qual. Res., 18, 254–269, https://doi.org/10.4209/aaqr.2017.01.0021, 2018.

Li, G., Li, X., Li, J., Chen, W., Zhu, H., Zhao, J., and Hu, X.: Influences of Plateau Zokor Burrowing on Soil Erosion and Nutrient Loss in Alpine Meadows in the Yellow River Source Zone of West China, Water, 11, 2258, https://doi.org/10.3390/w11112258, 2019a.

Li, L.: Time-of-Flight Camera – An Introduction, Technical White Paper, https://www.ti.com/lit/wp/sloa190b/sloa190b.pdf, last access: 22 December 2021, 2014.

Li, T. C., Shao, M. A., Jia, Y. H., Jia, X. X., Huang, L. M., and Gan, M.: Small-scale observation on the effects of burrowing activities of ants on soil hydraulic processes, Eur J Soil Sci, 70, 236–244, https://doi.org/10.1111/ejss.12748, 2019b.

Li, T., Jia, Y., Shao, M.'a., and Shen, N.: Camponotus japonicus burrowing activities exacerbate soil erosion on bare slopes, Geoderma, 348, 158–167, https://doi.org/10.1016/j.geoderma.2019.04.035, 2019c.

Li, T., Shao, M.'a., Jia, Y., Jia, X., and Huang, L.: Small-scale observation on the effects of the burrowing activities of mole crickets on soil erosion and hydrologic processes, Agriculture, Ecosystems & Environment, 261, 136–143, https://doi.org/10.1016/j.agee.2018.04.010, 2018.

Longoni, L., Papini, M., Brambilla, D., Barazzetti, L., Roncoroni, F., Scaioni, M., and Ivanov, V.: Monitoring Riverbank Erosion in Mountain Catchments Using Terrestrial Laser Scanning, Remote Sensing, 8, 241, https://doi.org/10.3390/rs8030241, 2016.

Malizia, A. I.: Population dynamics of the fossorial rodent Ctenomys talarum (Rodentia: Octodontidae), Journal of Zoology, 244, 545–551, https://doi.org/10.1111/j.1469-7998.1998.tb00059.x, 1998.

MALLALIEU, J., CARRIVICK, J. L., QUINCEY, D. J., SMITH, M. W., and William H.M.: An integrated Structure-from-Motion and time-lapse technique for quantifying ice-margin dynamics, J. Glaciol., 63, 937–949, https://doi.org/10.1017/jog.2017.48, 2017.

Meysman, F. J. R., Boudreau, B. P., and Middelburg, J. J.: Relations between local, nonlocal, discrete and continuous models of bioturbation, Journal of Marine Research, 61, 391–410, https://doi.org/10.1357/002224003322201241, 2003.

Monteverde, M. J. and Piudo, L.: Activity Patterns of the Culpeo Fox (Lycalopex Culpaeus Magellanica) in a Non-Hunting Area of Northwestern Patagonia, Argentina, Mammal Study, 36, 119–125, https://doi.org/10.3106/041.036.0301, 2011.

Morris, R. H., Buckman, S., Connelly, P., Dragovich, D., Ostendorf, B., and and Bradstock, R. A.: The dirt on assessing post-fire erosion in the Mount Lofty Ranges: comparing methods, 2011.

Nasermoaddeli, M. B. and Pasche, E.: Application of terrestrial 3D scanner in quantification of the riverbank erosion and deposition, https://www.tuhh.de/t3resources/wb/Publikationen/MA-Veroeffentlichungen/nasermoaddelli/riverflow2008.pdf, last access: 22 December 2021, 2008.

Pang, X. P. and Guo, Z. G.: Plateau pika disturbances alter plant productivity and soil nutrients in alpine meadows of the Qinghai-Tibetan Plateau, China, Rangel. J., 39, 133, https://doi.org/10.1071/RJ16093, 2017.

Reichman, O. J. and Seabloom, E. W.: The role of pocket gophers as subterranean ecosystem engineers, Trends in Ecology & Evolution, 17, 44–49, https://doi.org/10.1016/S0169-5347(01)02329-1, 2002.

Richards, P. J. and Humphreys, G. S.: Burial and turbulent transport by bioturbation: a 27-year experiment in southeast Australia, Earth Surf. Process. Landforms, 21, n/a-n/a, https://doi.org/10.1002/esp.2007, 2010.

Ridd, P. V.: Flow Through Animal Burrows in Mangrove Creeks, Estuarine, Coastal and Shelf Science, 43, 617–625, https://doi.org/10.1006/ecss.1996.0091, 1996.

Romañach, S. S., Reichman, O. J., and Seabloom, E. W.: Seasonal influences on burrowing activity of a subterranean rodent, Thomomys bottae, Journal of Zoology, 266, 319–325, https://doi.org/10.1017/S0952836905006941, 2005.

Rutin, J.: The burrowing activity of scorpions (Scorpio maurus palmatus) and their potential contribution to the erosion of Hamra soils in Karkur, central Israel, Geomorphology, 15, 159–168, https://doi.org/10.1016/0169-555X(95)00120-T, 1996.

Sarbolandi, H., Plack, M., and Kolb, A.: Pulse Based Time-of-Flight Range Sensing, Sensors (Basel, Switzerland), 18, https://doi.org/10.3390/s18061679, 2018.

Schiffers, K., Teal, L. R., Travis, J. M. J., and Solan, M.: An open source simulation model for soil and sediment bioturbation, PloS one, 6, e28028, https://doi.org/10.1371/journal.pone.0028028, 2011.

Sharon, D.: The distribution of hydrologically effective rainfall incident on sloping ground, Journal of Hydrology, 46, 165–188, https://doi.org/10.1016/0022-1694(80)90041-4, 1980.

Thomsen, L. M., Baartman, J. E. M., Barneveld, R. J., Starkloff, T., and Stolte, J.: Soil surface roughness: comparing old and new measuring methods and application in a soil erosion model, SOIL, 1, 399–410, https://doi.org/10.5194/soil-1-399-2015, 2015.

Übernickel, K., Pizarro-Araya, J., Bhagavathula, S., Paulino, L., and Ehlers, T. A.: Reviews and syntheses: Composition and characteristics of burrowing animals along a climate and ecological gradient, Chile, Biogeosciences, 18, 5573–5594, https://doi.org/10.5194/bg-18-5573-2021, 2021a.

Übernickel, K., Ehlers, T. A., Paulino, L., and Fuentes Espoz, J.-P.: Time series of meteorological stations on an elevational gradient in National Park La Campana, Chile, 2021b.

Valdés-Pineda, R., Valdés, J. B., Diaz, H. F., and Pizarro-Tapia, R.: Analysis of spatio-temporal changes in annual and seasonal precipitation variability in South America-Chile and related ocean-atmosphere circulation patterns, Int. J. Climatol., 36, 2979–3001, https://doi.org/10.1002/joc.4532, 2016.

Voiculescu, M., Ianăş, A.-N., and Germain, D.: Exploring the impact of snow vole (Chionomys nivalis) burrowing activity in the Făgăraș Mountains, Southern Carpathians (Romania): Geomorphic characteristics and sediment budget, CATENA, 181, 104070, https://doi.org/10.1016/j.catena.2019.05.016, 2019.

Wei, X., Li, S., Yang, P., and Cheng, H.: Soil erosion and vegetation succession in alpine Kobresia steppe meadow caused by plateau pika—A case study of Nagqu County, Tibet, Chin. Geograph.Sc., 17, 75–81, https://doi.org/10.1007/s11769-007-0075-0, 2007.

Wilcox, A. C., Escauriaza, C., Agredano, R., Mignot, E., Zuazo, V., Otárola, S., Castro, L., Gironás, J., Cienfuegos, R., and Mao, L.: An integrated analysis of the March 2015 Atacama floods, Geophys. Res. Lett., 43, 8035–8043, https://doi.org/10.1002/2016GL069751, 2016.

Wilkinson, M. T., Richards, P. J., and Humphreys, G. S.: Breaking ground: Pedological, geological, and ecological implications of soil bioturbation, Earth-Science Reviews, 97, 257–272, https://doi.org/10.1016/j.earscirev.2009.09.005, 2009.

Yair, A.: Short and long term effects of bioturbation on soil erosion, water resources and soil development in an arid environment, Geomorphology, 13, 87–99, https://doi.org/10.1016/0169-555X(95)00025-Z, 1995.

Yáñez, E., Barbieri, M.A., Silva, C., Nieto, K., and Espíndola, F.: Climate variability and pelagic fisheries in northern Chile, Progress in Oceanography, 49, 581–596, https://doi.org/10.1016/S0079-6611(01)00042-8, 2001.

Yoo, K., Amundson, R., Heimsath, A. M., and Dietrich, W. E.: Process-based model linking pocket gopher (Thomomys bottae) activity to sediment transport and soil thickness, Earth Surf. Process. Landforms, 33, 917, https://doi.org/10.1130/G21831.1, 2005.

Supplementary Material

Table 4.A1. List of abbreviations

α [°]	**Tilt angle of the camera**
b [°]	Surface inclination
Ω	Threshold value for the scan scattering error
B	Burrow
$Area_{burrow}$	mean in the field measured size of the burrows which are monitored
Area	total surface area monitored by the camera
BD	Bulk density
c [m/s]	Speed of light
D	Distance from the camera to the object
$Dens_{burrow}$	Burrow density
DSM	Digital surface model
DSM_{after}	DSM calculated from the scan taken after the extraction
DSM_{before}	DSM calculated from the scan taken before the extraction
EM	Burrow embedding area
Entrance	entrance to the animal burrow
g [-]	ratio [-] of the reflected photons to all photons
LC	National Park LC
LC-NL	Camera in LC on the lower north-facing hillslope
LC-NU	Camera in LC on the upper north-facing hillslope
LC-SL	Camera in LC on the lower south-facing hillslope
LC-SU	Camera in LC on the upper south-facing hillslope
MAE	Mean absolute error
MAP [°]	Mean annual precipitation
m.a.s.l.	Meters above sea level
MAT	Mean annual temperature

mClay [%]	Mean content of clay
$mean_{z\text{-coordinate}}$	Mean value of the z-coordinates
Mound	the sediment excavated by the animal while digging the burrow
mSand [%]	Mean content of sand
mSilt [%]	Mean content of silt
n	Number of scans
PdA	National Park Pan de Azúcar
PdA-NL	Camera in PdA on the lower north-facing hillslope
PdA-NU	Camera in PdA on the upper north-facing hillslope
PdA-SL	Camera in PdA on the lower south-facing hillslope
PdA-SU	Camera in PdA on the upper south-facing hillslope
Res	Resolution
Roof	sediment pushed aside and uphill the entrance during burrow creation
S_a	scan after the rainfall event
S_b	scan before the rainfall event
SBC	Single board computer
$sd_{z\text{-coordinate}}$	standard deviation of the z-coordinates
SSH	Secure shell
t [s]	Overall time of camera illumination
TOC [%]	Total organic carbon
ToF	Time-of-Flight
Vol_{burrow}	volume of redistributed sediment within burrow
$Vol_{detected}$	volume of the extracted sediment as detected by the camera
Vol_{add}	difference in redistributed sediment volume between burrows and burrow embedding areas
Vol_{exc}	Volume of the sediment excavated by the animal
$Vol_{hillslope\text{-}wide}$	Hillslope-wide volume of redistributed sediment
$Vol_{measured}$	volume of the extracted sediment measured by the measuring cup
$Vol_{per\ burrow}$	Volume of redistributed sediment per burrow
$Vol_{per\ pixel}$	Volume of redistributed sediment per pixel
$Vol_{redistributed}$	volume of the calculated redistributed sediment
$Vol_{embedding}$	volume of redistributed sediment within burrow embedding area
y_i	distance of the point to the point of origin at the camera nadir
z_{cor}	Corrected z-coordinate
z_{uncor}	Uncorrected z-coordinate

Table 4.A2. Number of usable scans for each camera

Camera	Latitude	Longitude	Number of scans	Percentage of usable scans taken at 1am / 5am / 8am / 10pm	Time period

PdA-NU	-25.98131	-70.6166	238	29 / 27 / 20 / 24	18.3.-18.9.
PdA-NL	-25.98277	-70.61278	52	24 / 0 / 40 / 36	27.3.-31.5
PdA-SU	-25.97477	-70.61641	351	30 / 26 / 32 / 11	16.3.-19.9.
PdA-SL	-25.97177	-70.61409	167	48 / 38 / 7 / 8	16.3.-19.9.
LC-NU	-32.95230	-71.06231	215	37 / 20 / 8 / 33	9.3.-9.9.
LC-NL	-32.93928	-71.08613	3	-	6.3.-12.9
LC-SU	-32.93078	-71.09066	160	22 / 28 / 26 / 25	28.3.-22.5
LC-SL	-32.93110	-71.08987	167	27 / 25 / 22 / 26	16.3.-19.9.

Table 4.A3. Summary of the volume of redistributed sediment, according to area and disturbance type. Vol_{exc} describes volume of the sediment excavated by the animals. Vol_{burrow} describes volume of the sediment redistributed during rainfall events within burrows. Vol_{add} describes the difference in redistributed sediment volume within burrows and burrow embedding area during rainfall.

Disturbance	**Area**	**PdA**	**LC**
Vol_{exc}	Burrow	16.41 cm^3 cm^{-2} $year^{-1}$	14.62 cm^3 cm^{-2} $year^{-1}$
	Per burrow	1498.66 cm^3 $burrow^{-1}$ $year^{-1}$	1226.61 cm^3 $burrow^{-1}$ $year^{-1}$
	Hillslope-wide	0.18 m^3 ha^{-1} $year^{-1}$	0.67 m^3 ha^{-1} $year^{-1}$
Vol_{burrow}	Burrow	-1.97 cm^3 cm^{-2} $year^{-1}$	-10.44 cm^3 cm^{-2} $year^{-1}$
	Per burrow	-126.36 cm^3 $burrow^{-1}$ $year^{-1}$	-876.38 cm^3 $burrow^{-1}$ $year^{-1}$
	Hillslope-wide	-0.05 m^3 ha^{-1} $year^{-1}$	-0.48 m^3 ha^{-1} $year^{-1}$
Vol_{add}	Burrow	-1.18 cm^3 cm^{-2} $year^{-1}$	-7.37 cm^3 cm^{-2} $year^{-1}$
	Per burrow	-48.36 cm^3 $burrow^{-1}$ $year^{-1}$	-619.2 cm^3 $burrow^{-1}$ $year^{-1}$
	Hillslope-wide	-0.02 m^3 ha^{-1} $year^{-1}$	-0.34 m^3 ha^{-1} $year^{-1}$

Table 4.A4. Summary of the volume of redistributed sediment, according to area and disturbance type. Vol_{exc} describes volume of the sediment excavated by the animals. Vol_{burrow} describes volume of the sediment redistributed during rainfall events within burrows. Vol_{add} describes the difference in redistributed sediment volume within burrows and burrow embedding areas during rainfall.

Disturbance	**Area**	**PdA**	**LC**
Vol_{exc}	Burrow	9.57 cm^3 cm^{-2} 7 $months^{-1}$	8.53 cm^3 cm^{-2} 7 $months^{-1}$
	Per burrow	874.22 cm^3 $burrow^{-1}$ 7 $months^{-1}$	715.52 cm^3 $burrow^{-1}$ 7 $months^{-1}$
	Hillslope-wide	0.11 m^3 ha^{-1} 7 $months^{-1}$	0.39 m^3 ha^{-1} 7 $months^{-1}$
Vol_{burrow}	Burrow	-1.15 cm^3 cm^{-2} 7 $months^{-1}$	-6.09 cm^3 cm^{-2} 7 $months^{-1}$

	Per burrow	-73.71 cm^3 $burrow^{-1}$ 7 $months^{-1}$	-511.22 cm^3 $burrow^{-1}$ 7 $months^{-1}$
	Hillslope-wide	-0.03 m^3 ha^{-1} 7 $months^{-1}$	-0.28 m^3 ha^{-1} 7 $months^{-1}$
Vol_{add}	Burrow	-0.69 cm^3 cm^{-2} 7 $months^{-1}$	-4.30 cm^3 cm^{-2} 7 $months^{-1}$
	Per burrow	-28.21 cm^3 $burrow^{-1}$ 7 $months^{-1}$	-361.20 cm^3 $burrow^{-1}$ 7 $months^{-1}$
	Hillslope-wide	-0.01 m^3 ha^{-1} 7 $months^{-1}$	-0.2 m^3 ha^{-1} 7 $months^{-1}$

Table 4.A5. Review of studies which used laser scanners for the estimation of surface processes.

Reference	**R^2**	**Error**	**Horizontal point spacing**	**Points per cm^{-2}**	**Model**	**Price**
Our results	0.77	0.15 cm	0.32 cm	8.5	Texas Instruments OPT3101	900 USD
(Eitel et al., 2011)	0.23-0.86	0.07 cm	NA	25	Leica ScanStation 2	102 375 USD
(Eltner et al., 2013)	NA	0.4 cm	NA	6.4	Riegl LMS-Z420i	16 795 USD
(Kaiser et al., 2014)	NA	NA	0.57 cm	NA	Riegl LMS-Z420i	16 795 USD
(Longoni et al., 2016)	NA	NA	NA	1	Riegl LMS-Z420i	16 795 USD
(Morris et al., 2011)	NA	0.5 cm	NA	NA	Maptek I-Site 4400LR	240 000 USD
(Nasermoaddeli and Pasche, 2008)	NA	0.2 cm	0.25 cm	NA	Leica Cyrax HDS 2500	4500 USD
(Thomsen et al., 2015)	NA	NA	0.4 cm	NA	Leica ScanStation 2	102 375 USD

Table 4.A6. Review of studies which estimated the sediment redistribution within burrows and burrow embedding areas and the proposed impact.

Reference	**Climate**	**Animals**	**Method**	**Monitoring period**	**Frequency**	**Burrows**	**Burrow embedding area**	**impact**
(Imeson and	continental	Rodents	erosion pins	15 months	monthly	20 mm		NA

Kwaad, 1976)								
(Imeson and Kwaad, 1976)	continental	Rodents	splash boards	15 months	monthly	91.75g 24.49 cm^{-2} = 3.75 cm^3 cm^{-2}	94g	-3%
(Imeson and Kwaad, 1976)	continental	Rodents	rainfall simulation (7.5 cm / hour intensity)	One-time measurement	NA	0.2 g – 0.73 g	0.009 g – 0.23 g	+208 %
(Imeson, 1977)	continental	Vertebrates	rainfall simulation	One-time measurement	NA	0.18-0.3 100 J^{-1} m^{-2} rain	0.146 100 J^{-1} m^{-2} rain	+123 %
(Hazelhoff et al., 1981)	continental	Earthworms	splash traps	12 months	monthly	NA	NA	+180 %
(Black and Montgomery, 1991)	arid	pocket gopher	erosion pins	10 months	2 months	NA	NA	+125 %
(Hakonson, 1999)	temperate	pocket gophers	rainfall simulator (60 mm / hour)	2 years	2 – 3 weeks	2.4 – 8.7 mg ha^{-1}	4.4 – 15 mg ha^{-1}	-43%
(Li et al., 2018)	temperate	mole crickets	rainfall simulation (36 mm / hour)	One time measurement	15 measurements	22.1 g 115 cm^{-2} = 5.2 cm^3 cm^{-2}	5 g 123 cm^{-2} = 1.09 cm^3 cm^{-2}	+473 %
(Li et al., 2018)	temperate	mole crickets	rainfall simulation (36 mm / hour)	One time measurement	15 measurements	35.3 g 220.5 cm^{-2} = 6.24 cm^3 cm^{-2}	5 g 123 cm^{-2} = 1.09 cm^3 cm^{-2}	+473 %
(Chen et al., 2021)	lab	chinese zocor	rainfall simulation (80	One-time measurement	3 measurements	2,69 g cm^{-2} = 2.69 cm^3 cm^{-2}	0,88 g cm^{-2} = 0.88 cm^3 cm^{-2}	+205 %

		mm / hour)				

Table 4.A7. Review of studies which estimated the sediment redistribution within burrows, average burrow density as found in the literature and area-wide yearly contribution of burrowing animals to sediment redistribution.

Climate	Animals	Burrows	Average burrow density	Average burrow size	Area-wide redistribution
Continental	Rodents	91.75g 24.49 cm^{-2} = 3.75 cm^3 cm^{-2} (Imeson and Kwaad, 1976)	14 625 m^{-2} = 0.02 m^{-2} (Pang and Guo, 2017)	24.49 cm^2 (Imeson and Kwaad, 1976)	0.183 m^3 ha^{-1} $year^{-1}$
Temperate	mole crickets	22.1 g 115 cm^{-2} = 5.2 cm^3 cm^{-2} (Li et al., 2018)	405 ha^{-1} (Castner and Fowler, 1984)	115 cm^2 (Li et al., 2018)	0.24 m^3 ha^{-1} $year^{-1}$
Temperate	mole crickets	35.3 g 220.5 cm^{-2} = 6.24 cm^3 cm^{-2} (Li et al., 2018)	405 ha^{-1} (Castner and Fowler, 1984)	220.5 cm^2 (Li et al., 2018)	0.56 m^3 ha^{-1} $year^{-1}$
Lab	chinese zocor	2,69 g cm^{-2} = 2.69 cm^3 cm^{-2} (Chen et al., 2021)	94.69 2500m^{-2} = 0.04 m^{-2} = 400 ha^{-1}	1256 cm^2	1.35 m^3 ha^{-1} $year^{-1}$

Table 4.A8. Review of studies which estimated the volume of sediment excavated by burrowing animals.

	Climate	Animals	Method	Monitoring period	Frequency	volume of the excavated sediment
(Black and Montgomery, 1991)	Arid	porcupines	mound volume	3 years	yearly	0.2 m^3 ha^{-1} $year^{-1}$
(Black and Montgomery, 1991)	Arid	isopods	mound volume	3 years	yearly	0.11 m^3 ha^{-1} $year^{-1}$

(Black and Montgomery, 1991)	Arid	pocket gopher	mound volume	2 years	3 model runs	0.05 – 0.11 m^3 ha^{-1} $year^{-1}$
(Rutin, 1996)	Subtropical	scorpions	mound volume	6 months	2-29 days	0.42 m^3 ha^{-1} $year^{-1}$
(Hall et al., 1999)	Alpine	rodents	mound volume	1 year	yearly	0.02 m^3 ha^{-1} $year^{-1}$
(Hall et al., 1999)	Alpine	bears	mound volume	1 year	yearly	0.49 m^3 ha^{-1} $year^{-1}$
(Yoo et al., 2005)	Arid	pocket gopher	mound volume	1 year	One model run	0.1-0.2 m^3 ha^{-1} $year^{-1}$

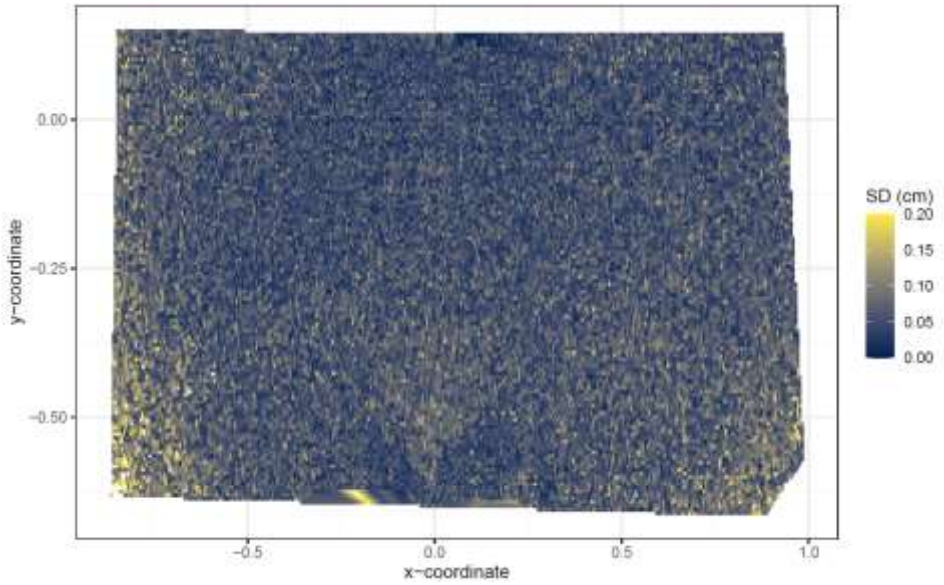

Figure 4.A1. Standard deviation of the z-coordinate of unprocessed five scans showed exemplary for the camera on the upper north-facing hillside. SD is standard deviation. The error increases with distance from the camera nadir point. The standard deviation was here calculated from scans before any corrections.

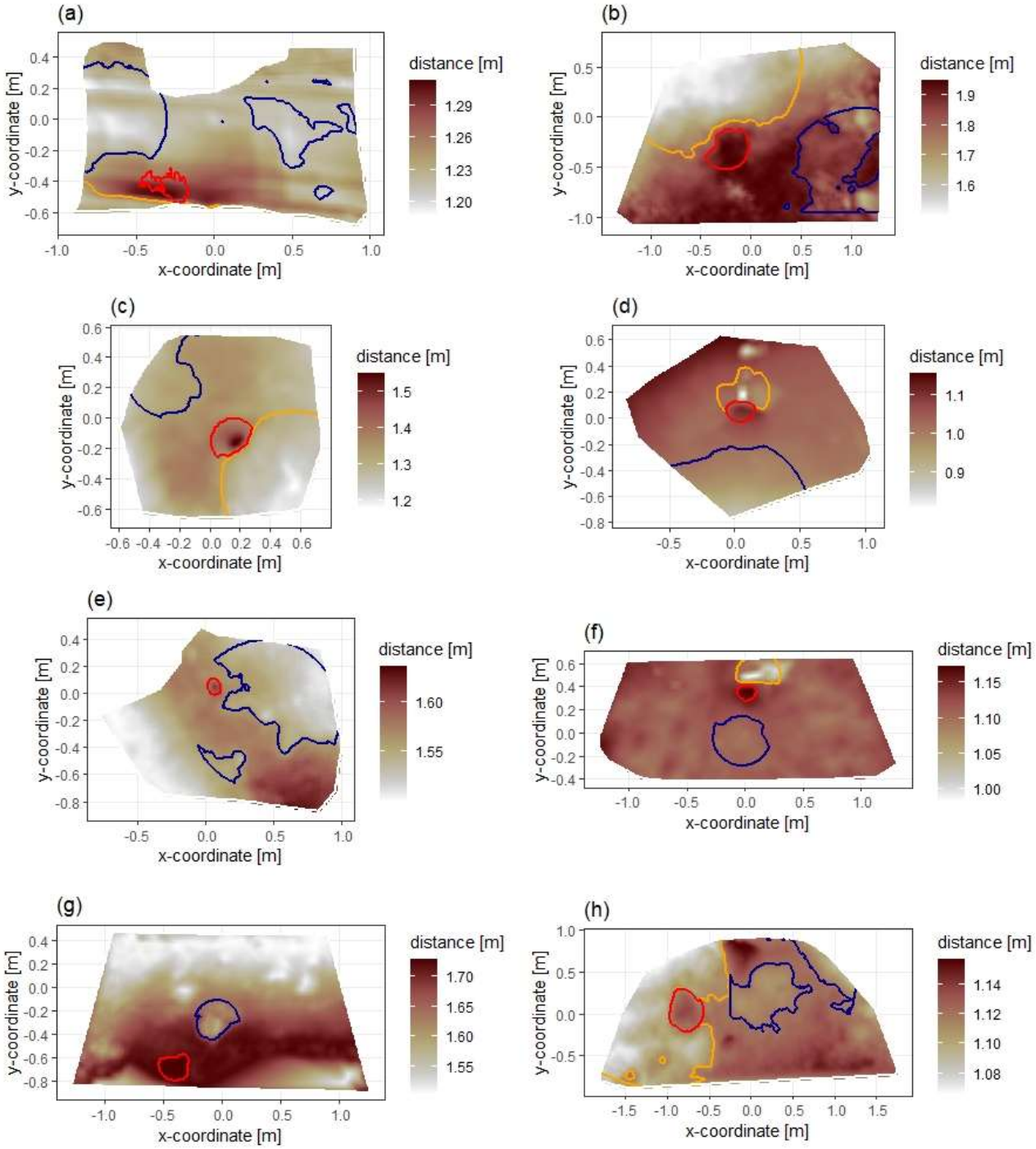

Figure 4.A2. Delineation of the areas. The point of origin of the coordinate system is at the camera nadir. Depth is the distance between the surface and the camera. Red is the outline of the burrow entrance. Green is the outline of mound. Orange is the outline of burrow roof. Area which is not outlined is burrow embedding area. Arrow indicates downhill direction of the hillslope. (a) LC-NU. (b) LC-NL (c) LC-SU. (d) LC-SL. (e) PdA-NU. (f) PdA-NL. (g) PdA-SU. (h) PdA-SL.

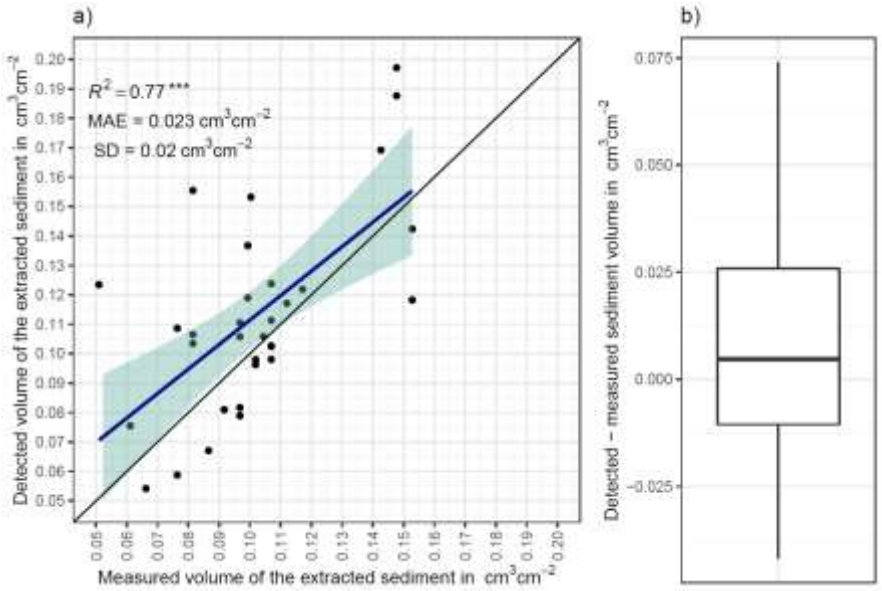

Figure 4.A3. a) Estimation of Time-of-Flight camera accuracy based on averaging two surface scans before and after the sediment extraction under controlled conditions. The *x*-axis shows the exact sediment volume measured with a cup. The *y*-axis represents the volume of the sediment calculated from the camera scans (according to Equation (4)). The blue line is the linear regression calculated from the measured and detected volume. The green shadow shows the confidence interval of 95% for the linear regression slope. ***$p \leq 0.001$. MAE is the mean absolute error, SD is standard deviation and R^2 the coefficient of determination. b) Measured sediment volume subtracted from the detected sediment volume for all measurements.

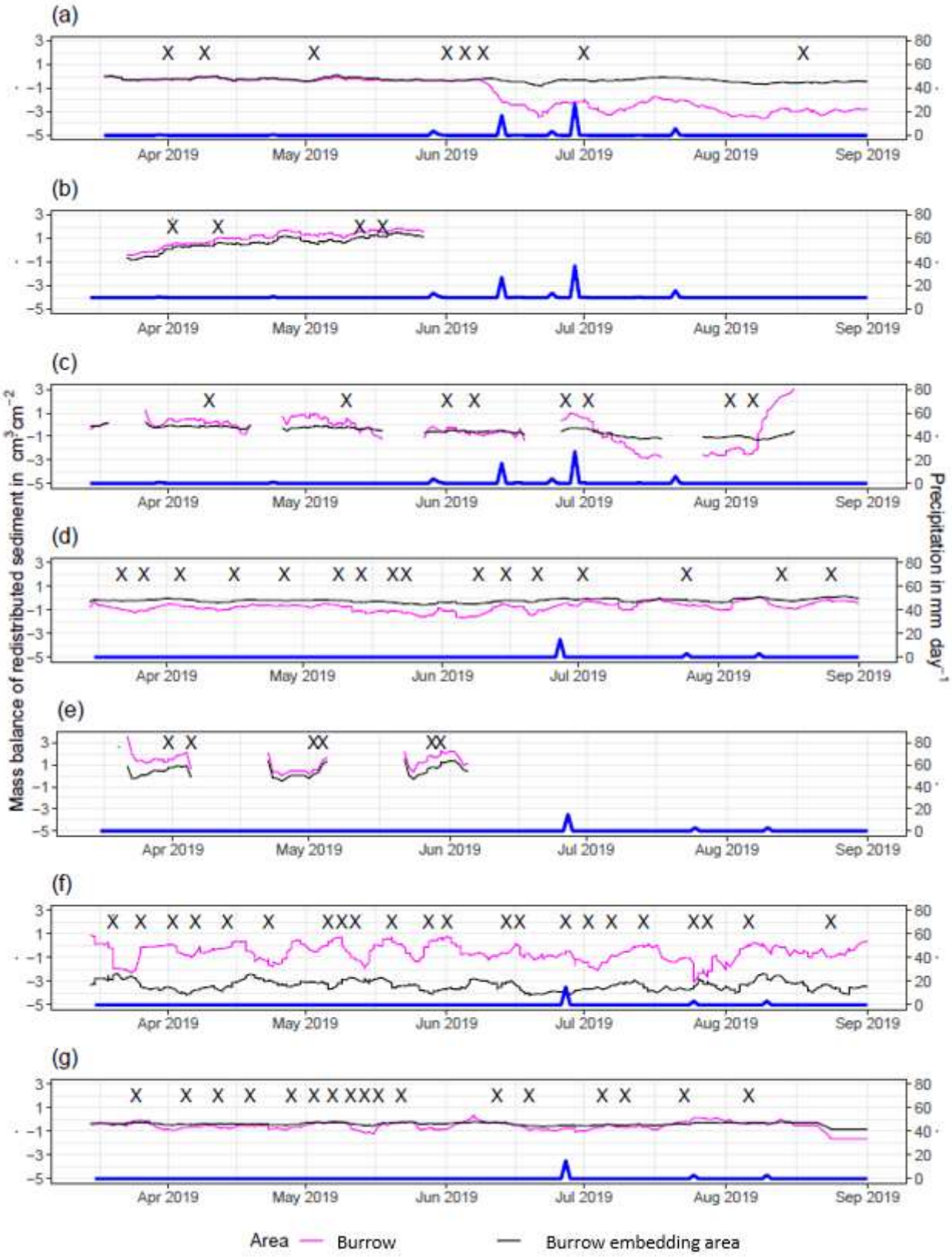

Figure 4.A4. Sediment mass balance for the period of 7 months separately for burrows and burrow embedding areas as measured by the cameras. (a) LC-NU. (b) LC-SU. (c) LC-SL. (d) PdA-NU. (e) PdA-NL.
(f) PdA-SU. (g) PdA-SL. For abbreviations see Table 4.A1.

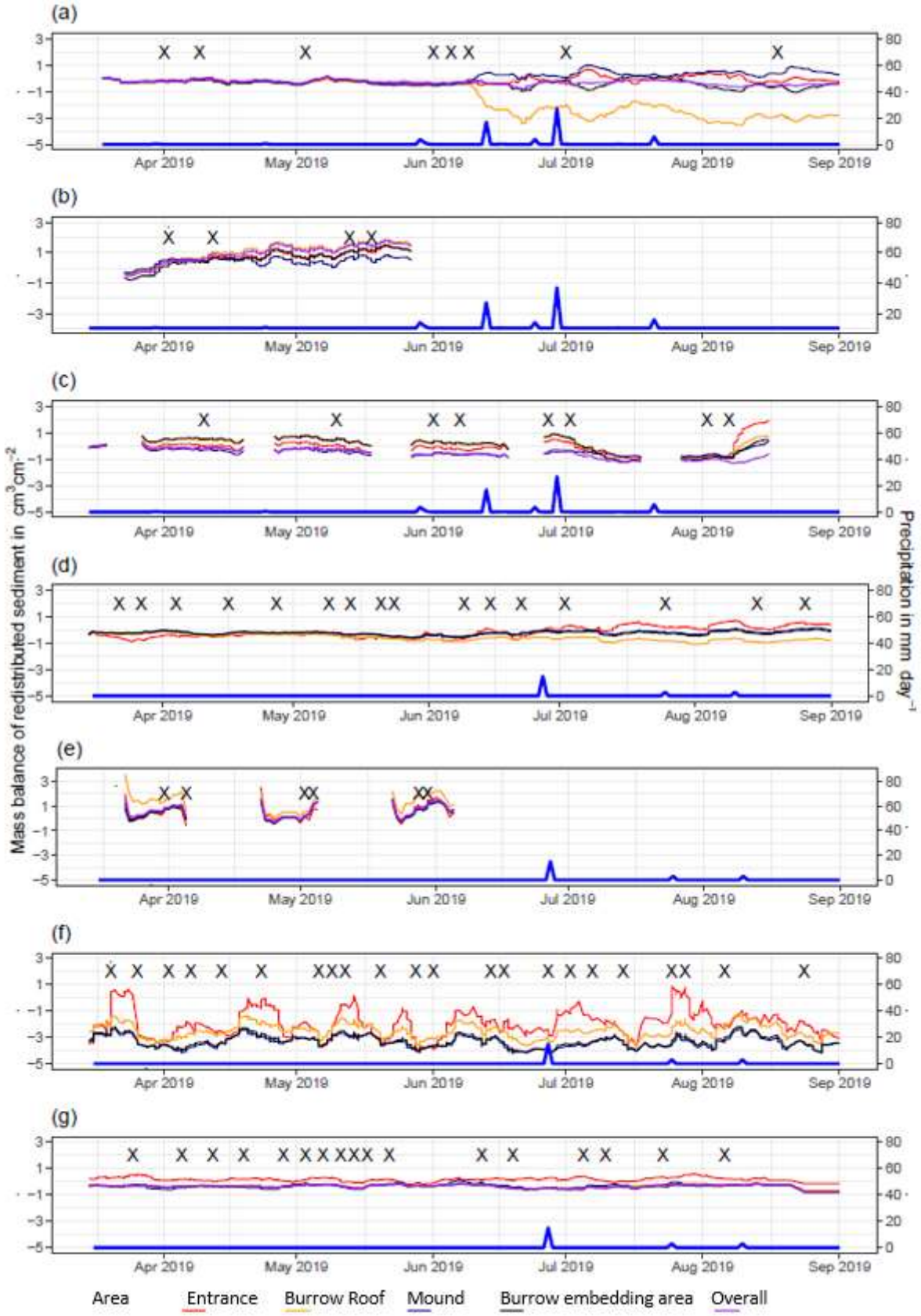

Figure 4.A5. Sediment mass balance for the period of 7 months separately for all delineated areas as measured by the cameras. (a) LC-NU. (b) LC-SU. (c) LC-SL. (d) PdA-NU. (e) PdA-NL. (f) PdA-SU. (g) PdA-SL. For abbreviations see Table 4.A1.

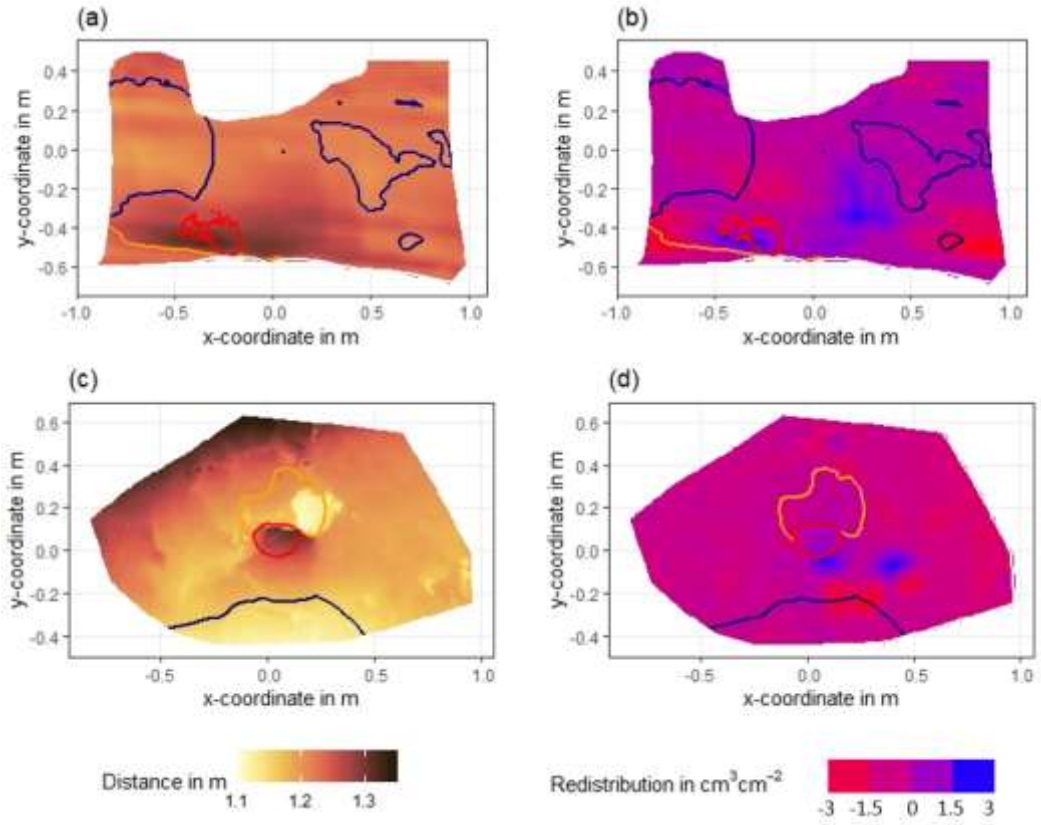

Figure 4.A6. Examples of surface scans showing the digital surface model (DSM) before a rainfall event (**a**, **c**) at two camera locations in La Campana, and the calculated volume of redistributed sediment (**b**, **d**) after the rainfall event: (**a**) DSM of a scan from the camera on the upper north-facing hillslope in La Campana; (**b**) Detected sediment redistribution (cm^3 cm^{-2}) on the upper north-facing hillslope in La Campana after a rainfall event of 17.2 mm day^{-1}; (**c**) DSM of a scan from the camera on the upper south-facing hillslope in La Campana; (**d**) Detected sediment redistribution (cm^3 cm^{-2}) on the upper south-facing hillslope after a rainfall event of 17.2 mm day^{-1}. Red is the outline of the burrow entrance. Green is the outline of mound. Orange is the outline of the burrow roof. The area which is not outlined is burrow embedding area. Redistribution is the volume of the redistributed sediment, either accumulated (positive value) or eroded (negative value) per cm^3 cm^{-2}. After the rainfall events, sediment mostly accumulated within the burrow entrance or near mounds and eroded from burrow roofs and mounds.

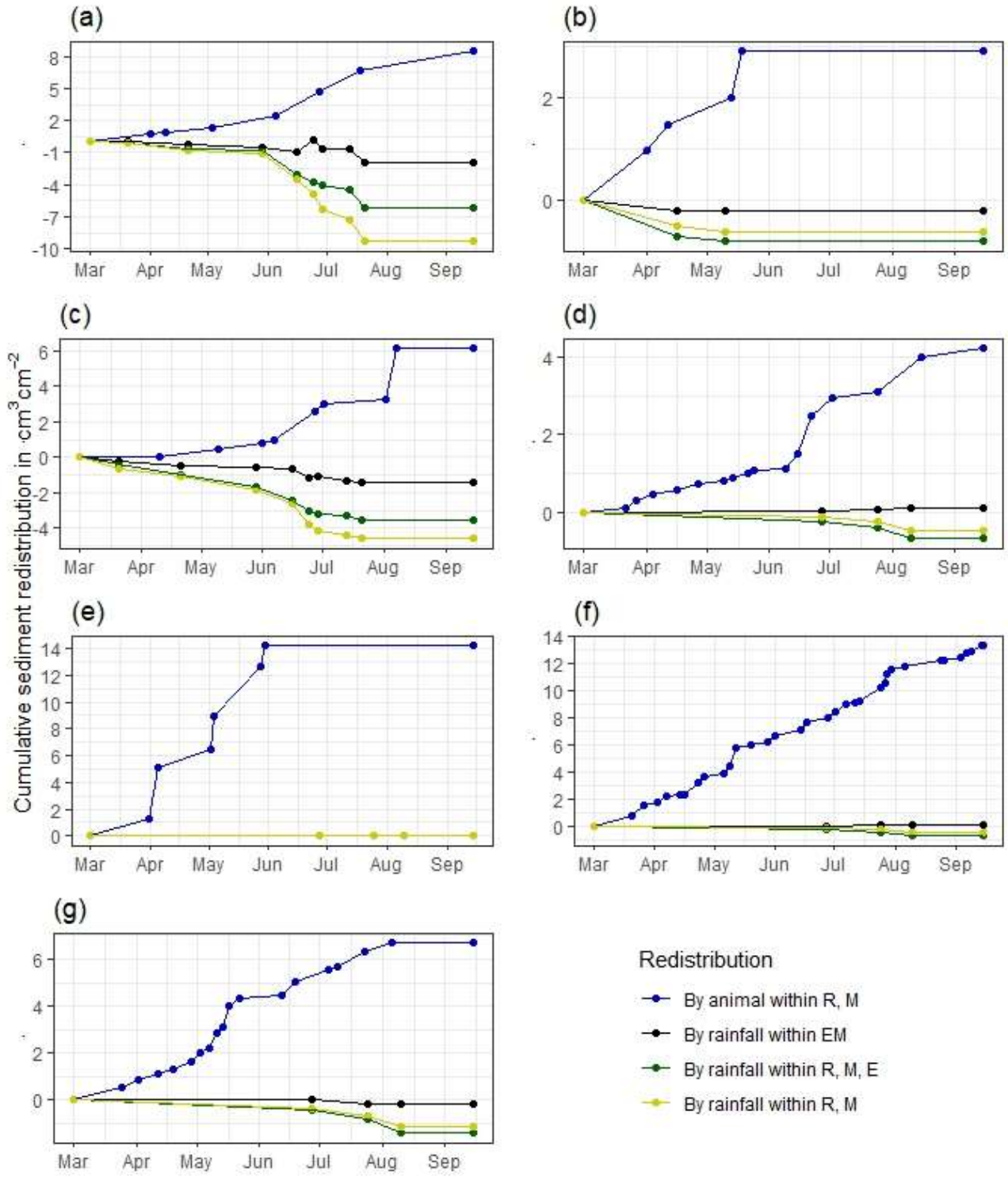

Figure 4.A7. Cumulative volume of redistributed sediment for all cameras. Positive values indicate sediment accumulation. Negative values indicate sediment erosion. Whiskers are the median sediment redistribution. E is the burrow entrance. M is the mound. R is burrow roof. EM is burrow embedding area. LC is mediterranean climate zone. PdA is arid climate zone. (a) LC-NU. (b) LC-SU. (c) LC-SL. (d) PdA-NU. (e) PdA-NL. (f) PdA-SU. (g) PdA-SL. For abbreviations see Table 4.A1.

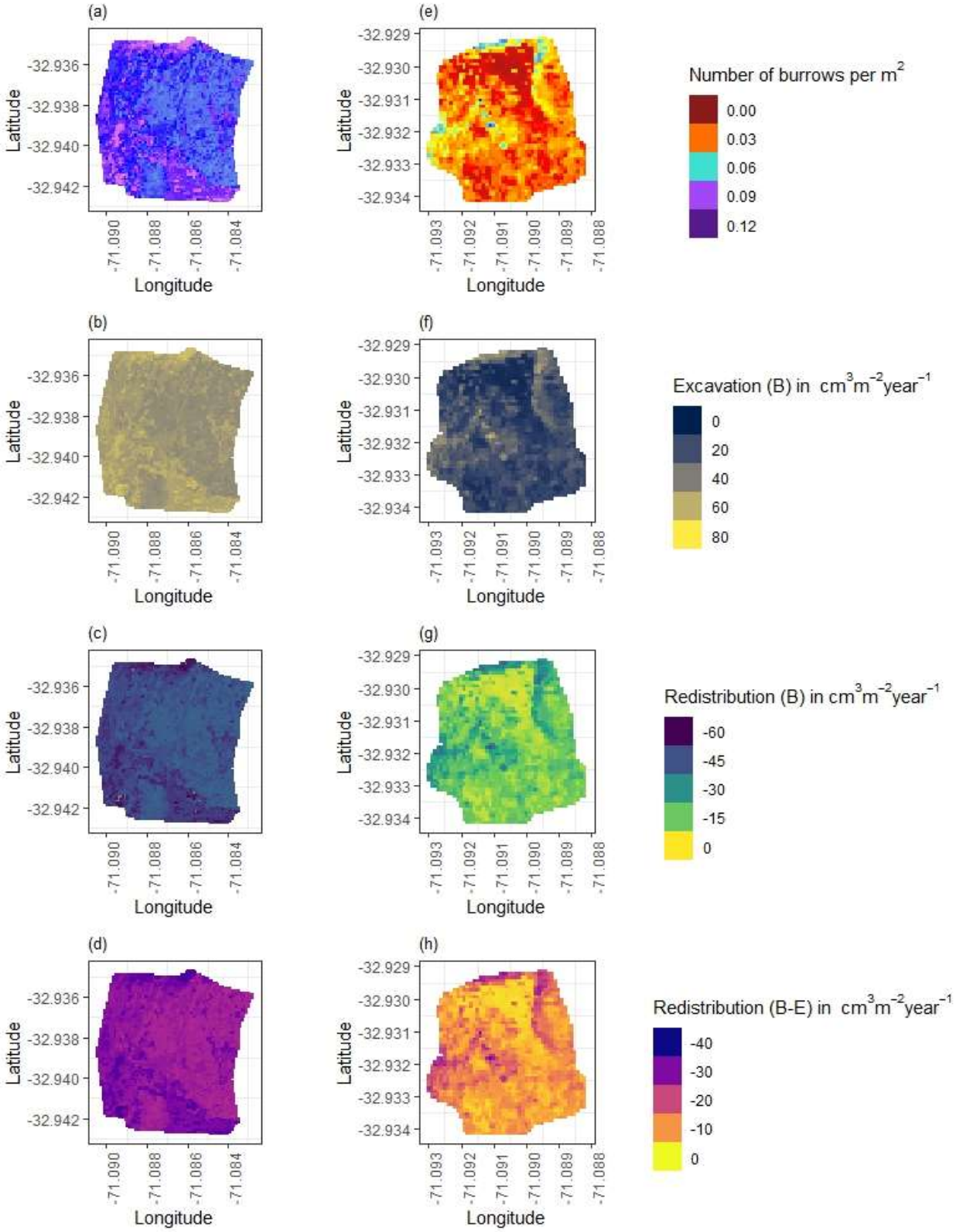

Figure 4.A8. Hillslope-wide volume of redistributed sediment for a time period of one year in LC. (a-d) North-facing hillslope. (e-h) South-facing hillslope. (a) and (e) Density of burrows as estimated by Grigusova et al. 2021. (b) and (f) Volume of the sediment excavated by the animals. (c) and (g) Volume of the sediment redistributed during rainfall events within burrows. (d) and (h) Volume of additionally redistributed sediment during rainfall events due to presence of the burrows. The values were calculated per burrow as stated in section 3.7 by subtracting the sediment volume redistributed within burrows from

the sediment volume redistributed within burrow embedding area and then upscaled. B stays for burrow, EM stays for burrow embedding area.

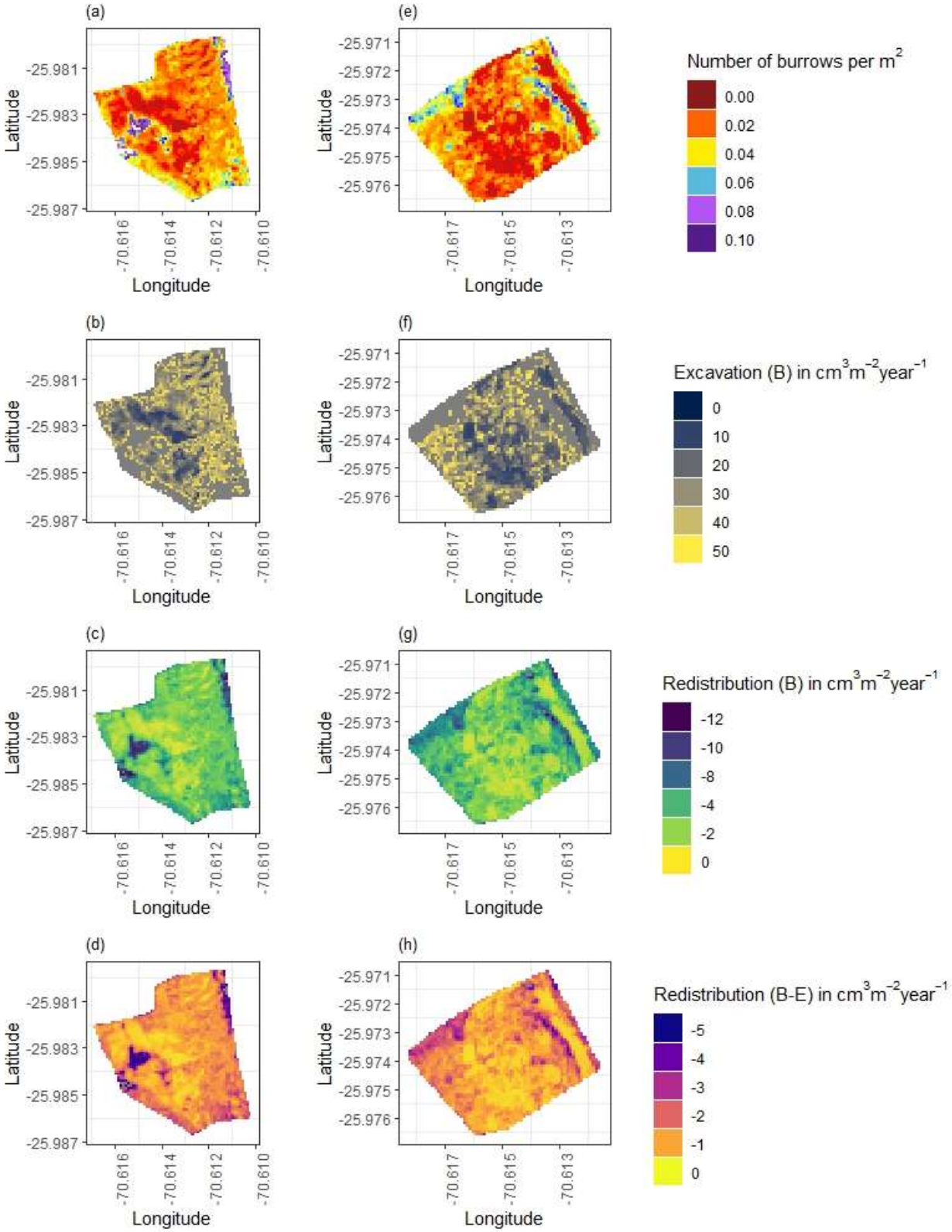

Figure 4.A9. Hillslope-wide volume of redistributed sediment for a time period of one year in Pan de Azúcar. (a-d) North-facing hillslope. (e-h) South-facing hillslope. (a) and (e) Density of burrows as estimated by Grigusova et al. 2021. (b) and (f) Volume of the sediment excavated by the animals. (c)

and (g) Volume of the sediment redistributed during rainfall events within burrows. (d) and (h) Volume of additionally redistributed sediment during rainfall events due to presence of the burrows. The values were calculated per burrow as stated in section 3.7 by subtracting the sediment volume redistributed within burrow from the sediment volume redistributed within burrow embedding area and then upscaled. B stays for burrow, EM stays for burrow embedding area by the burrowing animal.

5. Mammalian bioturbation amplifies rates of both, hillslope sediment erosion and accumulation, in coastal Chile

Paulina Grigusova[1], Annegret Larsen[2], Roland Brandl[3], Camilo del Río[4], Nina Farwig[6], Diana Kraus[6], Leandro Paulino[7], Patricio Pliscoff[4,8,9], Jörg Bendix[1]

[1] Laboratory for Climatology and Remote Sensing, Department of Geography, University of Marburg, 35037 Marburg, Germany; paulina.grigusova@staff.uni-marburg.de (P.G.); bendix@geo.uni-marburg.de (J.B.)

[2] Soil Geography and Landscape, Department of Environmental Sciences, Wageningen University & Research, 6700 AA Wageningen, The Netherlands; annegret.larsen@wur.nl

[3] Animal Ecology, Department of Biology, University of Marburg, 35032 Marburg, Germany; brandlr@biologie.uni-marburg.de

[4] Facultad de Historia, Geografía y Ciencia Política, Instituto de Geografía, Pontificia Universidad Católica de Chile, 782-0436 Santiago, Chile; cdelriol@uc.cl

[5] Centro UC Desierto de Atacama, Pontificia Universidad Católica de Chile, 782-0436 Santiago, Chile

[6] Conservation Ecology, Department of Biology, University of Marburg, 35047 Marburg, Germany; diana.kraus@biologie.uni-marburg.de (D.K.); nina.farwig@biologie.uni-marburg.de (N.F.)

[7] Facultad de Agronomía, Universidad de Concepción, 3780000 Chillán, Chile; lpaulino@udec.cl

[8] Facultad de Ciencias Biológicas, Departamento de Ecología, Pontificia Universidad Católica de Chile, 8331150 Santiago, Chile; pliscoff@uc.cl

[9] Center of Applied Ecology and Sustainability (CAPES), Pontificia Universidad Católica de Chile, 8331150 Santiago, Chile; pliscoff@uc.cl

Accepted as preprint for discussion in Biogeosciences (2023): 10.5194/egusphere-2023-84

Abstract

Soil bioturbation activity affects soil texture, bulk density, soil water content and redistribution of nutrients. All of these parameters influences sediment redistribution, which shapes the earth surface. Hence it is important to include bioturbation into erosion models. However, up to present, the inclusion of bioturbation into erosion models was limited. This is because to realistically include bioturbation into the modelling, the interplay between bioturbation, sediment redistribution and environmental parameters is not understood.

Here, we included bioturbation into a soil erosion model and interpreted the impacts of bioturbation on sediment redistribution. To do this, we measured the needed soil properties and location of burrows created by bioturbating animals in four research sites located along the Chilean climate gradient. Then, we parametrized a semi-empirical erosion model by applying machine learning algorithms to upscale soil properties and burrow distribution. We ran the model for a time period of 6 years under two conditions: With and without bioturbation. We validated the model using several sediment fences in the field. We estimated the modelled sediment redistribution and surface runoff in all climate zones. Lastly, we identified environmental parameters determining the positive or negative impact of bioturbation on sediment redistribution.

We found that the model with integrated bioturbation performed much better (R^2 = 0.71, RMSE = 0.63) than the model without integrated bioturbation (R^2 = 0.17, RMSE = 1.18), meaning that model runs which considered bioturbation predicted the sediment redistribution more realistically. Furthermore, bioturbation increased sediment redistribution in all but the humid climate zone, especially in the Mediterranean zone. The quantity of sediment redistributed due to bioturbation was reliant on an interplay between elevation, slope, surface roughness and sink connectivity. Overall, bioturbation enhances sediment erosion in areas where more erosion is expected, and enhances sediment accumulation in areas which are more prone to accumulate sediment. In other words, considering bioturbation when studying earth surface evolution means an amplification of existing tendencies in sediment redistribution, and leads to a faster hillslope relief equalisation.

5.1. Introduction

Bioturbation was shown to shape the land surface (Hazelhoff et al., 1981; Istanbulluoglu, 2005; Taylor et al., 2019; Tucker and Hancock, 2010; Whitesides and Butler, 2016; Wilkinson et al., 2009; Corenblit et al., 2021) by influencing surface microtopography (Reichman and Seabloom, 2002; Kinlaw and Grasmueck, 2012; Debruyn and Conacher, 1994), and soil properties such as soil porosity, permeability and infiltration (Reichman and Seabloom, 2002; Yair, 1995; Hancock and Lowry, 2021; Ridd, 1996; Hall et al., 1999; Coombes, 2016; Larsen et al., 2021). Cumulatively, these modifications lead to changes in sediment redistribution (Gabet et al., 2003; Nkem et al., 2000; Wilkinson et al., 2009) and hence have the potential to affect surface topography and nutrient redistribution on large spatial and temporal scale. To quantify these effects, the shared role of climate, landscape characteristics and burrowing dynamics on sediment redistribution needs to be understood.

On a local scale, currently used field methods to monitor sediment redistribution under real-life condition are mainly erosion pins, splash boards, or rainfall simulators (Imeson and Kwaad, 1976; Wei et al., 2007; Le Hir et al., 2007; Li et al., 2019a; Li et al., 2019b; Li et al., 2018; Voiculescu et al., 2019; Chen et al., 2021; Übernickel et al., 2021a). The monitoring of box experiments yields a high spatio-temporal resolution, and can also be linked with mathematical equations, such as random walks (Boudreau, 1986; Wheatcroft et al., 1990), stochastic differential equations (Boudreau, 1989; Milstead et al., 2007), finite difference mass balancing (Soetaert et al., 1996; François et al., 1997) or Markov chain theory (Jumars et al., 1981; Foster, 1985; Trauth, 1998; Shull, 2001) to describe sediment redistribution. Another approach offer raster-based soil erosion and landscape evolution models which integrate co-dependencies between bioturbation relevant environmental parameters (Black and Montgomery, 1991; Meysman et al., 2003; Yoo et al., 2005; Schiffers et al., 2011). Most common soil erosion models are empirical (Wischmeier and Smith, 1978; Williams, 1975; Renard et al., 1991), process-based (Morgan et al., 1998; ROO et al., 1996; Nearing et al., 1989; Beasley et al., 1980), or semi-empirical models, the latter of which are a combination of both (Morgan et al., 1984; BEVEN and KIRKBY, 1979). Empirical models are limited to one study site, but they provide highly accurate predictions at low computational costs, as they are based on simple mathematical equations. In contrast, process-based models require an intensive parametrisation and calibration process, however, once calibrated, they can be applied to almost any site (Lal, 2001; Merritt et al., 2003). Semi-empirical models combine semi-empirical equations with a physical basis and thus include the advantages of the both model types (Morgan et al., 1984; Morgan, 2001; Morgan and Duzant, 2008; Devia et al., 2015; Lilhare et al., 2015).

Previously used methods have, however, several limitations when studying bioturbation. Field measurements likely lead to an underestimation of sediment fluxes, as they are one-time or seasonal measurements, and thus do not capture the continuous excavation of the sediment by the animal (Grigusova et al., 2022) at a high temporal resolution. Box experiments and from them derived mathematical equations describe bioturbation as an isolated process and ignore surrounding environmental parameters (such as climate or vegetation). Most erosion or landscape evolution models do not yet implement impacts of bioturbators on water and sediment fluxes (Brosens et al., 2020; Anderson et al., 2019; Braun et al., 2016; Cohen et al., 2015; Cohen et al., 2010; Carretier et al., 2014; Welivitiya et al., 2019). Models which include bioturbation as an input factor still have large limitations. They predict landscape evolution on a millennial scale, but ignore processes acting on a daily basis.

This rather large spatio-temporal scale also means an omission of the natural variability in burrow sizes and densities, climate zones and seasonality (Temme and Vanwalleghem, 2016; Vanwalleghem et al., 2013; Yoo and Mudd, 2008; Pelletier et al., 2013). The most significant limitation is, however, that in all models bioturbation is hard-coded to have predefined effects on the environment: (i) soil erosion is proportionally increasing with increasing bioturbation, (ii) vertical soil mixing rates are uniform, and (iii) bioturbation is positively linked with vegetation cover. Thus, none of these models consider that the interaction of bioturbation with environmental parameters and the effect on sediment redistribution may not be uniform but context dependent. However, the field measurements showed both, positive (Hazelhoff et al., 1981; Black and Montgomery, 1991; Chen et al., 2021) and negative impact of bioturbation on erosion (Imeson and Kwaad, 1976; Hakonson, 1999). Also, previous field based studies observed an increased bioturbation activity with higher (Milstead et al., 2007; Meserve, 1981; Tews et al., 2004; Wu et al., 2021; Ferro and Barquez, 2009), but also with lower vegetation cover (Simonetti, 1989; Zhang et al., 2020; Zhang et al., 2019; Qin et al., 2021). Furthermore, soil mixing rates are not homogenous throughout the year but depend on the animal phenological cycles (Eccard and Herde, 2013; Jimenez et al., 1992; Katzman et al., 2018; Malizia, 1998; Morgan and Duzant, 2008; Monteverde and Piudo, 2011; Gray et al., 2020; Yu et al., 2017).

To improve this, bioturbation has to be included into erosion models at a high spatial and temporal resolution under real-life conditions across several climate zones. A suiTable 5.model which can be extended to include continuous bioturbating activity is the semi-empirical Morgan – Morgan – Finney soil erosion model (Morgan et al., 1984; Morgan, 2001). This model was successfully tested in several climate zones and land use types, such as Mediterranean sites (Jong et al., 1999), rainfed agrosystems, fields and pastures (López-Vicente et al., 2008), East-African Highlands (Vigiak et al., 2005) or humid forests (Vieira et al., 2014). One of the recently developed improvements of this model is the Daily Morgan – Morgan – Finney model (DMMF), which introduces subsurface flow, vegetation structures (type, size, height, root depth), and enables modelling at a high spatial (0.5 m) and temporal (daily) resolution (Choi et al., 2017). These improvements yield the potential to integrate the bioturbation into the model, as the burrowing activity is not constant and depends on vegetation structure (Tews et al., 2004; Ferro and Barquez, 2009).

To study the interplay between bioturbation, environmental parameters and sediment redistribution along a climate gradient, we (i) include bioturbation into a semi-empirical soil erosion model (DMMF) at a high temporal and spatial resolution. We specifically not presuppose a homogenous relationship between bioturbation, sediment transport and vegetation cover. Based on (i), we (ii) identify environmental parameters which determine if the bioturbation enhances sediment erosion or sediment accumulation. In order to do this, we included bioturbation into the DMMF while considering (i) variable co-dependency between bioturbation and vegetation type, density and height; (ii) various burrow sizes and burrow densities, (iii) variable soil mixing rates due to continuous reconstruction of the burrow by the animal depending on season and (iv) variable influence of bioturbation on litter and coarse grain size. Furthermore, we set up generalized additive models to unveil significant environmental parameters that determine the impact of bioturbation on sediment redistribution. Lastly, we analyse how the impact of bioturbation on sediment redistribution depends on the burrow structure, climate, topography and

surrounding vegetation. Our study shows the importance of including bioturbation into erosion modelling and the interplay between bioturbation, environmental parameters and sediment redistribution.

5.2. Study area

Our study was performed along a climate and vegetation gradient in Chile (Übernickel et al., 2021b), comprising four study sites in the Chilean Coastal Cordillera: Pan de Azúcar (PdA) National Park (NP), Santa Gracia (SG), La Campana (LC) NP, and Nahuelbuta (NA) NP (Fig. 5.1). PdA NP is located in the arid zone in a fog-laden environment in the southern part of the Atacama Desert, with almost no rainfall. The vegetation cover is less than 5 % and dominated by small desert shrubs, several types of cacti and biocrusts (Lehnert et al., 2018). SG is a natural reserve located in the semi-arid zone near La Serena, which is dominated by goat grazing. The vegetation consists of shrubs and cacti, covering up to 40 % of the study area. LC NP is part of the Mediterranean-type climate zone in the Valparaiso Region and is also affected by cattle. The study site is dominated by an evergreen sclerophyllous forest with endemic palms. The canopy reaches a height of up to 9 m, and the understory consists of deciduous shrubs and herbs. NA is located in the humid-temperate zone and characterized by a dense evergreen *Araucaria* forest comprising broadleaved trees with heights of up to 14 m. The ground is covered by bamboo, shrubs, and herbs (Bernhard et al., 2018; Oeser et al., 2018). The most common bioturbating vertebrate animal species recorded within these sites are carnivores of the family Canidae (*Lycalopex culpaeus*, *Lycalopex griseus*) as well as rodents of the families Abrocomidae (*Abrocoma bennetti)*, Chnichillidae (*Lagidium viscacia)*, Cricetidae (*Abrothrix andinus, Phyllotis xanthopygus*, *Phyllotis limatus, Phyllotis darwini*) and Octogontidae (Cerqueira, 1985; Jimenez et al., 1992; Übernickel et al., 2021a).

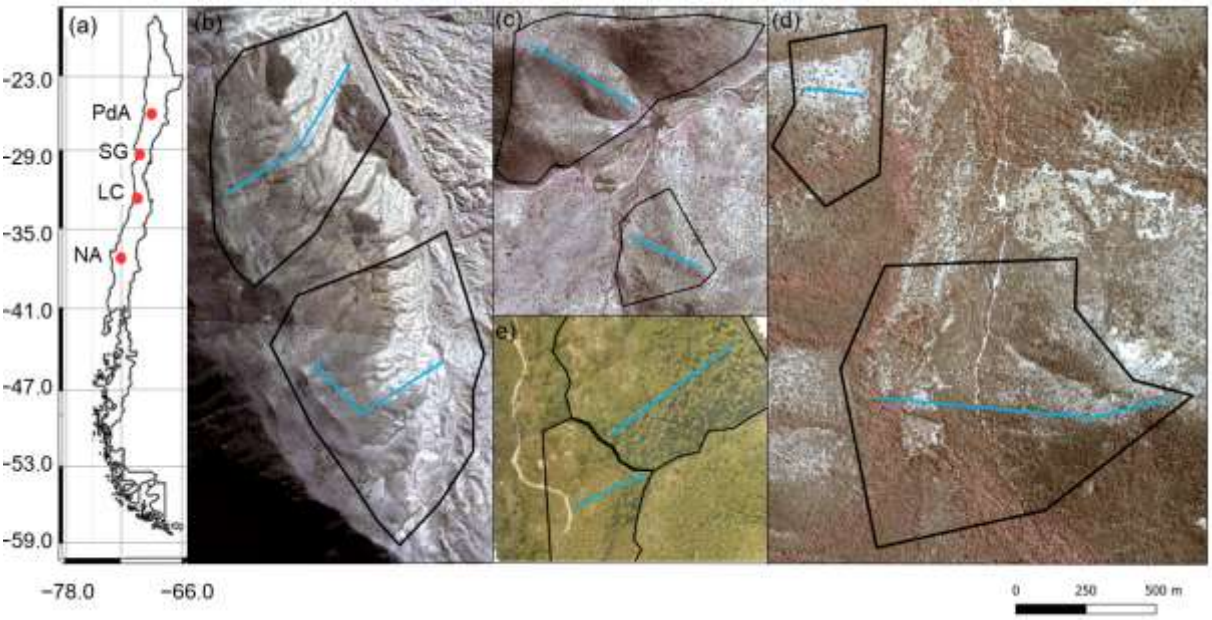

Figure 5.1. Study area and study sites. Black lines outline the catchments. Along the blue lines, the in situ data (mound locations, soil samples, vegetation mapping) were collected. (a) Position of the study sites along the climate gradient. PdA = Pan de Azúcar, SG = Santa Gracia, LC = La Campana, NA = Nahuelbuta; Positions of plots in (b) PdA; (c) SG; (d) LC; and (e) NA. The background image is an RGB-composite calculated from WorldView-2 satellite imagery.

5.3. Methodology

We combined semi-empirical soil erosion modelling with in-situ measurements, remote sensing data and machine learning methods (Fig. 5.2). Along 8 catchments within 4 climate zones we mapped locations of burrows, estimated the vegetation cover and extracted soil samples. We analyzed the soil samples in the laboratory. Then we used remote sensing datasets and machine learning to upscale burrow distribution, vegetation cover and soil properties into the catchments. The catchment-wide predictions, the topographical information retrieved from LiDAR data (Kügler et al., 2022) and the climate information retrieved from climate stations were the input parameters for our soil erosion model. We ran the model with and without bioturbation. We included the bioturbation into the model by adjusting the input parameters at the predicted burrow locations, by including the continuous burrowing activity and soil mixing (Grigusova et al., 2021), and the seasonality (Kraus et al., 2022).and the animal phenological cycle as found in (Jimenez et al., 1992). The models were validated using self-constructed sediment traps. We studied the modeled surface runoff and sediment redistribution. Lastly, we analyzed if and how the impact of bioturbation on sediment redistribution depends on environmental parameters (topography, landscape connectivity and vegetation).

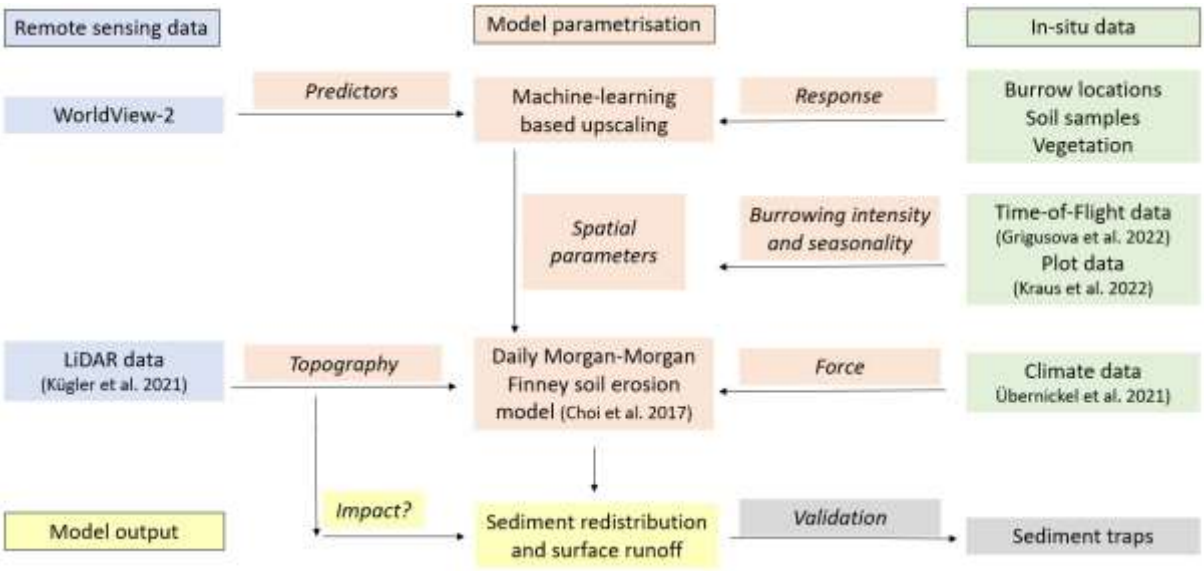

Figure 5.2. Flow chart of our study. Green color indicates in-situ input data, blue indicates remote sensing input data. Red indicates Model parametrization. Yellow indicates model output and analysis. Grey indicates model validation.

5.3.1 In-situ data

The study set-up consisted of eight hillside catchments: one north-facing and one south-facing hillside catchment per study site. We defined a line with a width of one meter from the top to the base of each hillside catchment (see blue line, Fig. 5.1). We subdivided the track into tiles of 1 m^2. We saved the GPS information of each tile.

Within each tile of the line, we mapped burrow presence, land cover and extracted soil samples. A burrow consisted of an entrance and a mound (Fig. 5.3a). Each 1 m^2 tile with a burrow was described

as a presence data point, tiles without a burrow as absence data points. We noted the size of the burrow, vegetation cover and land cover types (bare soil, herbs, shrubs, trees) within the tile. We extracted 162 soil samples from soil without a mound at a depth of 10 cm. Additionally, we took a photo of the surface every second tile along the track.

To validate the model output, we set up sediment traps (Fig. 5.3b), with six traps per site, two of which were located at the catchment base and four were located on two random positions within the catchment. The sediment traps consisted of geotextile vertically attached to wooden poles for stability. The traps had a length of 2 m – 5 m, a width of ~1.5 m and a height of ~1 m. 1.5 m of geotextile was laid down at the surface uphill the wooden poles to enable the collection of sediment. The sediment accumulated within the traps was collected after 1 year and its mass [cm^3] and dry weight [kg] were estimated.

Climate information was retrieved from climate stations located adjacent to the catchments which provide climate data in 5 minute intervals (Übernickel et al. 2021). To force the model on an hourly basis, hourly air temperature, precipitation total and intensity, wind speed, wind direction and humidity was calculated for the study period from 1st April 2016 to 1st December 2021. Evapotranspiration was estimated by the Penman-Monteith equation (Penman, 1948).

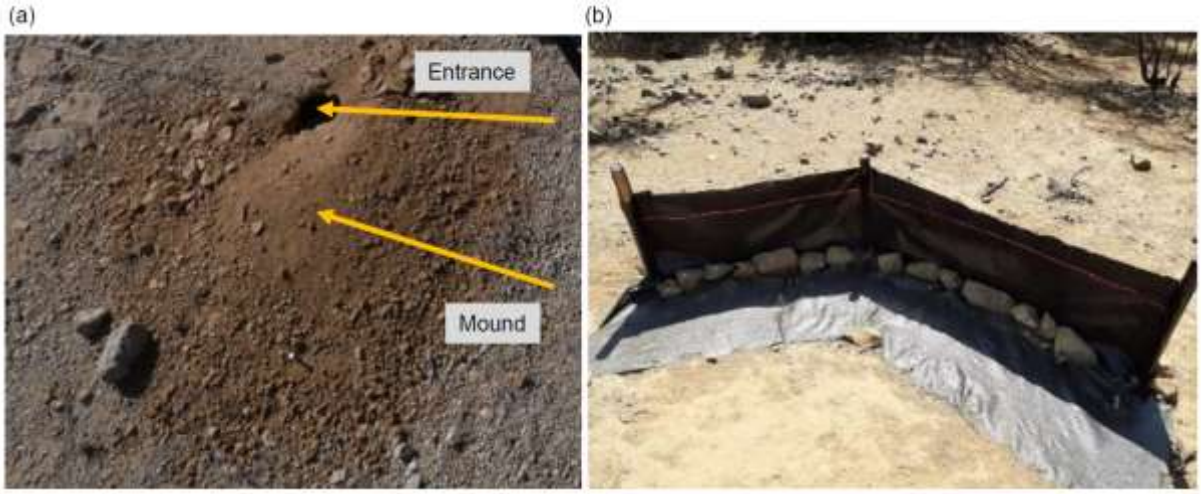

Figure 5.3. In-situ constructions. (a) Example of a burrow consisting of burrow entrance and mound. (b) Fence construction used for the collection of eroded sediment to validate the model.

5.3.2 Estimation of soil properties

We estimated several soil properties from the soil samples and photos collected in-situ ((Grigusova et al., 2022). We estimated above-ground skeleton and debris from the photos taken every second tile. For this, the photos were firstly classified into 5 classes. The classification was unsupervised using k-means (Fig. 5.A1). Then we calculated the ratio of pixels classified as skeleton and / or debris to the overall amount of all pixels to determine the amount of both parameters in percent.

In the lab, we estimated soil water content, bulk density, soil particle density, soil texture (sand, silt, clay, coarse / middle / fine sand, coarse / middle / fine silt), soil skeleton, organic matter and organic carbon. Gravimetric soil water content [%] (GSWC) described the mass of water within the soil sample and was estimated as in Eq (1):

$$GSWC = \frac{(Sm-Sd)}{Sd} * 100 \quad , \tag{1}$$

where Sm [g] is the mass of moist soil measured directly after the extraction and Sd [g] is the mass of soil dried at 105 °C for at least 24 hours. Bulk density [g cm^{-3}] (BD) was calculated as following:

$$BD = \frac{Sd}{Sv} \quad , \tag{2}$$

where Sv [cm^{-3}] is the volume of the sample. Soil particle density [g cm^{-3}] (SPD) was calculated as in Eq (3):

$$SPD = \frac{dm}{Sv} \quad , \quad , \tag{3}$$

where dm [g] is the dry mass of soil particles.

Particle size distribution [%] – clay (< 0.002 mm), coarse, middle and fine silt (0.002 mm to 0.02 mm), and coarse, middle and fine sand (0.02 mm to 2 mm) was estimated using a PARIO method (Durner et al., 2017). Soil skeleton was estimated as the ratio of particles with a diameter above 2 mm. Ratio of organic matter (OM) was estimated as in Eq. (4)

$$OM = \frac{Sc}{Sd} \quad , \tag{4}$$

where Sc is the weight [g] of the sample dried at 500 °C for 16 hours.

We used pedotransfer functions to determine porosity, saturated soil moisture, hydraulic conductivity, water content at field capacity, and permanent wilting point. Pore ratio (θs) was estimated from bulk and particle density as in Eq. (5):

$$\theta s = \frac{BD}{SPD} \tag{5}$$

Saturated water content [g g^{-1}] (Ws) was estimated as in Eq. (6):

$$Ws = \theta s \frac{pw}{BD} \quad , \tag{6}$$

where pw [g cm^{-3}] is the density of water which is set to be 1 g cm^{-3} (Pollacco, 2008).

Hydraulic conductivity Ks [m s^{-1}] was estimated as in Eq. (8):

$$Ks = 1.15741 * 0.0000001 * \exp(x) \quad , \tag{7}$$

where x for sandy soil is:

$$x = 9.5 - 1.471 * (BD * BD) - 0.688 * OM + 0.0369 * (OM * OM) - 0.332 * CS \quad , \tag{8}$$

and x for loamy and clayey soils is:

$$x = -43.1 + 64.8 * BD - 22.21 * (BD * BD) + 7.02 * OM - 0.1562 * (OM * OM) + 0.985 * \ln(OM) - 0.01332 * C * OM - 4.71 * BD * CS \quad , \tag{9}$$

where C is percentage of clay and CS is percentage of clay and silt (Wösten, 1997). To estimate water content at field capacity [%] (FC) and permanent wilting point (PWP), we applied functions by (Tomasella et al., 2000) as these were developed for South American soils:

$$FC = 4.046 + 0.426 * Si + 0.404 * C \quad , \tag{10}$$

$$PWP = 0.91 + 0.15 * Si + 0.396 * C \quad , \tag{11}$$

where Si is the percentage of silt.

5.3.3 Processing of remote sensing data

The digital elevation models (DEM) were calculated from the LiDAR data (Kügler et al., 2022; Horn, 1981) at a resolution of 0.5 m. Slope was calculated according to Horn (1981). Manning's surface roughness coefficient was estimated following (Li and Zhang, 2001). Topographic position index (TPI)

and Topographic ruggedness index were calculated according to (Wilson et al., 2007). Plan and profile curvature were determined after (Zevenbergen and Thorne, 1987). Connectivity indices, Sinks, Wetness index, Flow direction, Flow path, Catchment slope and Catchment were calculated in SAGA GIS.
Single license stereo WorldView-2 images with a resolution of 0.5 m were retrieved from GAF Munich GmbH. The topographic correction of WorldView-2 images was done using the LiDAR data, solar elevation angle, solar zenith angle and azimuth angle according to Goslee (2019). The digital surface models (DSMs) were calculated from the stereo images. Additionally, we extracted single bands and calculated the normalized difference vegetation index (NDVI).

5.3.4 The erosion model

5.3.4.1 Daily Morgan-Morgan-Finney model

The DMMF model is a combined soil erosion model used to estimate surface runoff and sediment flux on a field scale on a daily basis. Spatially, the DMMF model represents an area as several interconnected elements (e.g. pixels) of uniform topography, soil characteristics, land cover type, and vegetation structure. Through coupling, the model operates with flow direction algorithms: each element receives water and sediments from upslope elements and delivers the generated surface runoff and eroded soils to downslope elements. On a temporal scale, the model estimates surface runoff and sediment flux of each element on a daily basis. The model input parameters include climate, topography, soil properties and land cover information (Choi et al., 2017). Data pre-processing, modelling and analysis (see Fig. 5.2) was done in R statistic environment. The raster data were cropped to the size of the catchments (Fig. 5.1). Input parameters are listed in Table 5.1 and plotted in Fig. 5.A2.

5.3.4.2 Estimation of spatial parameters

For spatial parameterization of the DMMF model, we upscaled land cover, soil properties and burrow distribution onto the catchments using machine learning techniques. For each parameter, we trained one random forest (RF) model per site. The upscaling was done at 0.5 m spatial resolution. We used the WorldView-2 layers, NDVI, DEM, DSM, slope and roughness as predictors while the response data were the parameters which we measured in-situ (soil properties, vegetation, burrow locations). The most important predictors were selected by forward feature selection. The quality of the random forest models was assessed by Leave-Location-Out cross validation. We trained the model stepwise, using in-situ data collected from seven of the catchments and validated the model using in-situ data from the remaining catchment (Meyer et al., 2018).
For the area-wide upscaling of burrow locations across the catchments, we used the burrow presence and absence data (section 3.1) as the response data within the RF models. The accuracy was 0.82 for PdA, 0.77 for SG, 0.75 for LC and 0.85 for NA.
The upscaling of soil properties was done using soil properties estimated along the track line (see section 3.1) as response data within the RF models. All of the models reached a high accuracy (Table 5.A1).
To upscale the vegetation cover and type, we used as the response within the RF models the land cover measured in-situ. The classes were soil without rocks, rocks, biocrusts, grass/herbs, shrubs and trees. Predictor values for each class were extracted from at least 100 polygons per site and class. The

accuracy of the RF models was 0.71 for PdA, 0.81 for SG, 0.83 for LC and 0.75 for NA. The vegetation height measured in plots was averaged for each class per site. All pixels classified as respective class were assigned the same vegetation height information. Vegetation density was estimated per catchment as the amount of vegetation individuals per m^2. Vegetation diversity was calculated by Shannon index (Shannon, 1948). The interception area was the area not covered by vegetation (herbs, shrubs or trees).

5.3.4.3 Inclusion of bioturbation

In the grid cells with predicted burrow locations, we adapted the values of input parameters to include bioturbation. The adaptations varied with climate zone and burrow size. The size, geometric structure and excavation rates of burrowing animalswere previously estimated at a high spatial and temporal resolution (Grigusova et al., 2022). Based on this results, we firstly adjusted the microtopography. We modified the layer depth to represent burrow entrance and elevation to represent animal mound. Mounds were always located downslope of burrow entrances in the direction of flow.

Secondly, we adjusted the soil properties. Soil properties texture and organic carbon were estimated from soil extracted from mounds in Kraus et al. (in review). In this study we additionally estimated bulk density, initial water content, soil skeleton, porosity, saturated water content, available water capacity and water content at field capacity from the same dataset (see section 3.2). We calculated the median value of each property for the samples extracted from mounds and for the samples extracted from soil without mounds. Then, we estimated the change in percent between these two values. This was then used to adjust the soil property for each pixel including a mound.

Thirdly, modelled mound pixels had to be cleared from ground vegetation cover. For this, we removed ground vegetation cover from pixels with burrow locations and decreased ground vegetation cover, height, diameter and amount of ground vegetation individuals from surrounding pixels as measured in situ. Then, the amount of above-ground skeleton and debris was set as estimated from soil samples (section 3.2)

Animal activity has been found to be highly variable throughout the year (Grigusova et al., 2022; Kraus et al., 2022). The density of burrows does not stay sTable 5.throughout the year but increases or decreases depending on the season and climate zone. For this, we artificially removed or added burrows into the catchments at the particular seasons. Furthermore, the animals do not burrow at the same pace in the course of the year. There is a 3-month period, during which they are highly active.

Lastly, we also included the vertical movement of sediment particles from deeper soil layers to the surface in dependence on climate. The animals were found to reconstruct their burrows after each rainfall event (Grigusova et al., 2022). Corresponding with these findings, we increased the entrance depth and mound height by 30% after each rainfall event.

Table 5.1. Model input layers and respective changes to layer values at the predicted burrow locations. Ground vegetation was removed from the respective pixels, while tree canopy was not changed. The values were estimated as described in 3.5.2. Using the adjusted values, we calculated Evapotranspiration using Penman-Monteith equation, surface roughness from the elevation layer, and hydraulic conductivity, water content at field capacity and saturated water content using pedotransfer functions.

			Pixel value at burrow locations			
Parameter group	Parameter	Units	PdA	SG	LC	NA
Topography	Elevation	m asl	+0.24	+0.23	+0.36	+0.19
	Surface roughness	-	-	-	-	-
	Depth	m	-0.23	-0.41	-0.22	-0.04
Soil	Water content	%	+120	-6	-68	-62
	Bulk density	g cm^{-3}	-	-6	-17	-
	Sand	%	-29	-12	+57	-43
	Silt	%	+54	+22	+23	ns
	Clay	%	+145	+44	+19	-73
	Organic carbon	%	+168	+72	+105	+25
	Hydraulic conductivity	m s^{-1}	-	-	-	-
	Water content at field capacity	%	-	-	-	-
	Saturated water content	%	-	-	-	-
Cover	Ground vegetation cover	%	0	0	0	0
	Soil and debris	%	100	100	100	100
	Skeleton	%	0	0	0	0
	Average plant height	m	0	0	0	0
	Average plant diameter	m	0	0	0	0
	Number of plants	n m^{-2}	0	0	0	0

5.3.5 DMMF model sensitivity test and validation

We conducted a sensitivity test to identify the input parameters, which significantly influence the model output. For this, we estimated the mean, minimum and maximum values of each input parameter. For this, we first created an artificial catchment of 100 m * 100 m. Then, each pixel received a mean value of each parameter. We ran the model under these conditions. The model output described: (i) sediment erosion, (ii) sediment accumulation and (iii) surface runoff. We estimated sediment redistribution by subtracting the erosion from accumulation for each pixel. Then, we stepwise changed the input parameter values from their minimum to their maximum values while we did not adjust any other parameters. To quantify the significance of the input variations, we conducted a t-test (Fig A2). For this, we compared the amount of redistributed sediment of each model run to the first model run with homogeneous parameters.

For the validation, we ran the model for the time periods between the installation of sediment fences and the collections of sediment. We compared the mass and weight of modelled and collected sediment and estimated R^2 and RMSE. To test the importance of the inclusion of individual bioturbation parameters into the model, we ran the model under 4 conditions: (i) No burrows; (ii) Solely entrances; (iii) Solely mounds; (iv) Entire burrows (entrances and mounds).

5.3.6 Impact of burrows on surface processes

We estimated burrow density, as a ratio of pixels with predicted burrows to all pixels. Additionally, we calculated the ratio of pixels which are part of a burrow aggregation to all pixels which include a burrow. Burrow aggregation describes at least 4 neighboring pixels with predicted burrows. We calculated the amount of excavated sediment as a sum of burrow density and the burrow excavation rate as estimated in Grigusova et al. (2022).

To estimate the impact of burrows on sediment redistribution and surface runoff, we ran the DMMF model for the time period from 1st April 2016 until 31th December 2021 for all catchments. We ran the model (i) with no burrows and (ii) with entire burrows. We estimated (i) sediment redistribution (accumulation - erosion) and (ii) surface runoff. We analyzed the redistribution and runoff on the plot (1 m^2) and catchment (1 ha) scale.

Lastly, to analyze under which biotic and abiotic environmental parameters (topography, vegetation cover) the bioturbation enhances sediment erosion or accumulation, we set-up a generalized additive model (GAM) (Wood, 2006). For this, we first subtracted the output of the model with no burrows from the output of the model with entire burrows. Positive pixel values thus meant, bioturbation enhanced sediment accumulation, negative pixel values meant, bioturbation enhanced sediment erosion. We tested following environmental parameters: mound density, vegetation cover, elevation, slope, aspect, TRI, curvature and connectivity and wetness index. The model performance was evaluated by the percentage of explained data variance. We analyzed the impact of environmental parameters within 1-meter and within 10-meter distance from the burrows.

5.4 Results

5.4.1 Model sensitivity test and accuracy

Parameters which significantly influenced the model output were precipitation, slope, vegetation cover, surface roughness, silt content and water content (Table 5.A2). We quantified the model performance by comparing the modelled and measured sediment redistribution. The performance varied depending on the burrow inclusion (Figure 5.4). The performance of the model without any bioturbation was lower (R^2 = 0.73, RMSE = 1.50, MSE = 2.27), as when burrow entrances (R^2 = 0.81, RMSE = 1.34, MSE = 1.16) or mounds (R^2 = 0.83, RMSE = 1.10, MSE = 1.22) were included. The model had the highest performance when entire burrows were included (R^2 = 0.85, RMSE = 1.01, MSE = 1.01). However, as the scatterplots showed, the model performance seemed to be determined strongly by one measurement (Fig. 5.A3). For this reason, we calculated the metrics without this measurement (Fig. 5.A4). The model without any burrows (R^2 = 0.17, RMSE = 1.18, MSE = 1.39) in this case performed much lower than models with burrows. The model performance continuously strongly increased when burrow entrances (R^2 = 0.48, RMSE = 0.61, MSE = 0.78), mounds (R^2 = 0.51, RMSE = 0.75, MSE = 0.57) were included. The model with whole burrows reached the highest performance (R^2 = 0.71, RMSE = 0.63, MSE = 0.39). When we compare the modelled redistribution to the sediment redistribution estimated by Time-of-Flight cameras in Grigusova et al. (2022), then the differences are minor (R^2 = 0.62, RMSE = 0.12, MSE = 0.35).

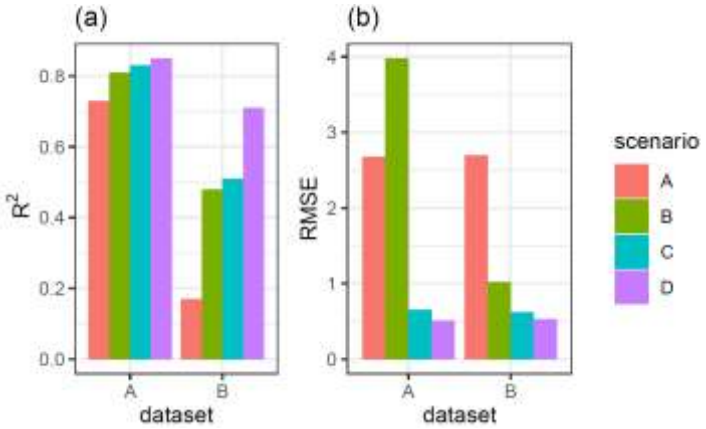

Figure 5.4. R^2 and RMSE of the Morgan-Morgan-Finney soil erosion model. For dataset A, we compared the amount of sediment collected in all sediment fences with the modelled eroded sediment (see Fig. 5.A3). For dataset B, we removed one measurement, as the R^2 seemed to be defined by this measurement (see Fig. 5.A4). For Scenario A, we did not include any burrows into the model. For scenario B, we included burrow entrances and for scenario C, we included mounds. For scenario D, we included whole burrows into the model. The adjustments made to include entrances, mounds and burrows into the model are described in section 3.5.2.

5.4.2 Model output: Surface runoff and sediment redistribution

Catchment – wide sediment redistribution (1 ha resolution) was the highest in humid NA, followed by Mediterranean LC, semi-arid SG and arid PdA (Fig. 5.5a, 5b, 6). In NA, LC and SG, the erosion processes dominated, while in PdA, more sediment accumulated than eroded. The impact of burrows on sediment redistribution was significant in PdA, SG and LC. Burrows increased sediment erosion by 137.8 % in PdA (3.53 kg ha^{-1} $year^{-1}$ vs. 48.79 kg ha^{-1} $year^{-1}$), by 6.5 % in SG (129.16 kg ha^{-1} $year^{-1}$ vs. 122.05 kg ha^{-1} $year^{-1}$) and by 15.6 % in LC (4602.69 kg ha^{-1} $year^{-1}$ vs. 3980.96 kg ha^{-1} $year^{-1}$).

Surface runoff was the highest in humid NA, followed by Mediterranean LC, arid PdA and semi-arid SG (Figure 5.5c). The impact of burrows on surface runoff was significant in all climate zones. Burrows increased surface runoff in PdA by 34 %, in SG by 40% and in LC by 4.1 %; and decreased surface runoff by 5.9 % in NA. Catchment-wide maps are shown in Fig. 5.A6-A8.

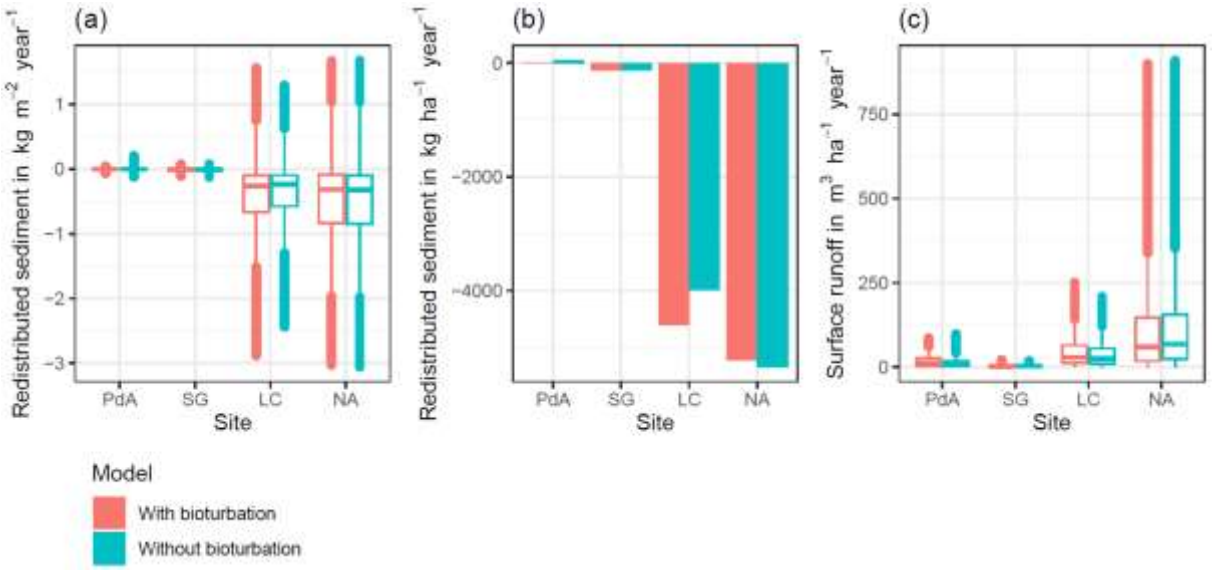

Figure 5.5. Summary of model outputs across the climate gradient. (a) and (b) Modelled sediment redistribution. Positive values indicate sediment accumulation; negative values indicate sediment erosion. (a) Sediment redistribution on a pixel scale in kg m^{-2} $year^{-1}$. (b) Sediment redistribution on the catchment scale in kg ha^{-1} $year^{-1}$. The impact of bioturbation on sediment redistribution was estimated by a t-test and was significant in PdA***, SG** and LC***. Bioturbation increased sediment erosion by 137.8 % in PdA, by 6.5 % in SG and by 15.6 % in LC. For catchment-wide maps see Fig. 5.A6-A8). (c) Modelled surface runoff on the catchment scale in m^3 ha^{-1} $year^{-1}$. Impact of bioturbation on surface runoff was estimated by a t-test and was significant at all sites. Bioturbation increased surface runoff in PdA by 34 %, in SG by 40 % and in LC by 4.1 %; and decreased surface runoff by 5.9 % in NA. For catchment-wide maps see Fig. 5.A6.

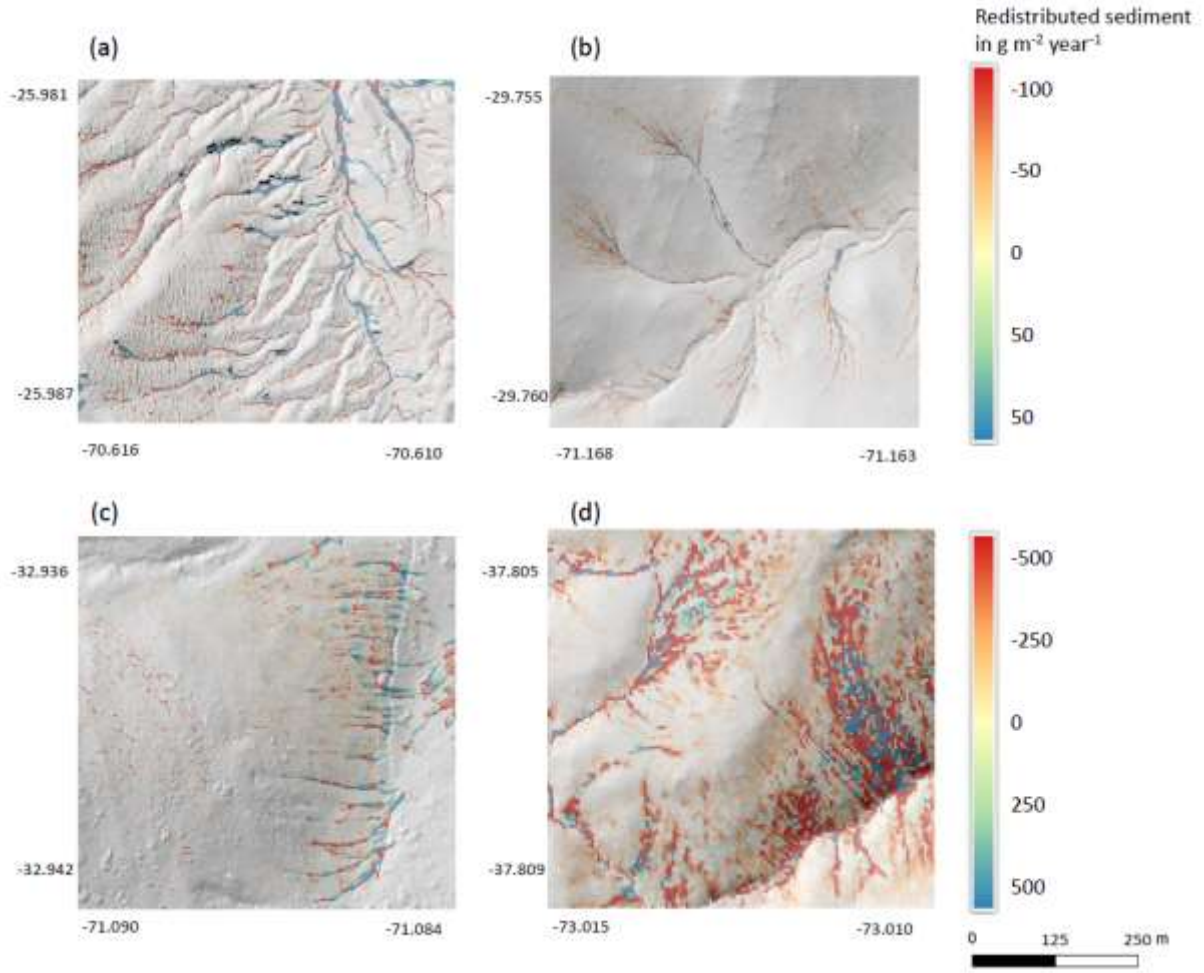

Figure 5.6. Catchment-wide predicted sediment redistribution. Colours indicate sediment redistribution. Positive values indicate sediment accumulation; negative values indicate sediment erosion. Grey shadows indicate the hill shading. (a) Pan de Azúcar, (b) Santa Gracia, (c) La Campana, (d) Nahuelbuta.

5.4.3 Role of continuous burrowing activity on sediment redistribution

We included the excavation of the sediment by the animal itself into the model. The density of burrows was the highest in PdA, then LC, SG and the lowest in NA (Table 5.2). The burrow aggregations were most predominant in LC and SG, almost non-existent in NA. The burrows were of largest size in LC, followed by PdA, SG and NA. Similarly, the highest volume of excavated sediment at the beginning of the modelling period was in LC and PdA. After each rainfall event, the animals reconstructed their burrows as described in Grigusova et al. 2022. Due to various number of rainfall events, the volume of excavated sediment during our modelling period was the highest in NA, followed by LC, SG and PdA. However, when the percentage of sediment which was excavated before and during the modelling to the amount of sediment redistributed during rainfall events was 47 % in PdA, 24 % in SG, 33.5 % in LC and 5.6 % in NA.

Table 5.2. Impact of animal bioturbation activity on overall sediment redistribution on various scales. The bioturbation activity was estimated using Time-of-Flight based cameras in Grigusova et al. 2022. This study showed that animals reconstruct their burrows after each rainfall events. During this process,

10 % of the overall sediment burrow volume is relocated from within the burrow to the surface. We integrated this process into our model and calculated the percentage of newly excavated sediment by the animals to the amount of sediment which was redistributed during rainfalls for the period of one year.

Parameter	**Units**	**PdA**	**SG**	**LC**	**NA**
Burrow density	ha^{-1}	91.35	71.50	84.36	13.30
Burrow aggregations	%	24	62	73	5
Burrow size	m^3	0.015	0.012	0.047	0.008
Sediment at the surface at the start of modelling	$m^3\ ha^{-1}$	1.35	0.88	4.11	0.10
Sediment excavated after each rainfall	$m^3\ ha^{-1}$	0.07	0.04	0.22	0.01
Number of rainfall events	$year^{-1}$	3	7	16	137
Sediment excavated by the animal after the rain	$m^3\ ha^{-1}\ year^{-1}$	0.21	0.28	3.52	0.69
Sediment redistributed due to rainfall	$m^3\ ha^{-1}\ year^{-1}$	0.44	1.17	10.51	12.21
Excavated sediment to redistributed sediment	%	47	24	33.5	5.6

5.4.4 Role of surrounding environment

We subtracted the output of the model with included burrows from the output of the model without burrows (Figure 5.A8). Although, the burrows on average enhanced sediment erosion on the catchment – scale, the high–resolution maps unveiled that burrows enhance sediment erosion within some pixels while they rather increased sediment accumulation within others.

The amount of data variance explained by the GAM models (see section 3.6.) differed between models (Table 5.A3). Models estimating the impact of environmental parameters on sediment redistribution within 1-meter distance from the burrows, explained 3.84 % of variance in PdA, 37.1 % in SG, 46 % in LC and 42. % in NA. Models estimating the impact of environmental parameters on sediment redistribution within 10-meter distance from the burrows, explained 1.99 % of variance in PdA, 12.8 % in SG, 52 % in LC and 72.9 % in NA. The parameters selected for SG were slope, roughness, curvature, TRI and NDVI. Parameters selected for LC were elevation, slope, NDVI, sinks and roughness. Parameters selected for NA were elevation, slope, aspect, TRI, sinks and roughness (Table 5.3).

Bioturbation strongly increased sediment redistribution (erosion and accumulation) at high values of elevation, slope, surface roughness TRI, sinks and topographic wetness index, at the middle values of elevation and aspect, and at low values of profile curvature and NDVI. From these parameters, bioturbation increased sediment erosion at high and middle values of elevation, at high values of slope, sinks and TRI, and at low values of profile curvature. Bioturbation increased sediment accumulation at high values of surface roughness and topographic wetness index and at low values of NDVI (Fig. 5.A9 – A14).

Bioturbation somewhat enhanced sediment erosion at medium values of surface roughness, NDVI and sinks, and at low values of topographic wetness index. Bioturbation somewhat increased sediment accumulation at low values of slope and TRI, at low and medium values of elevation and at high values of profile curvature.

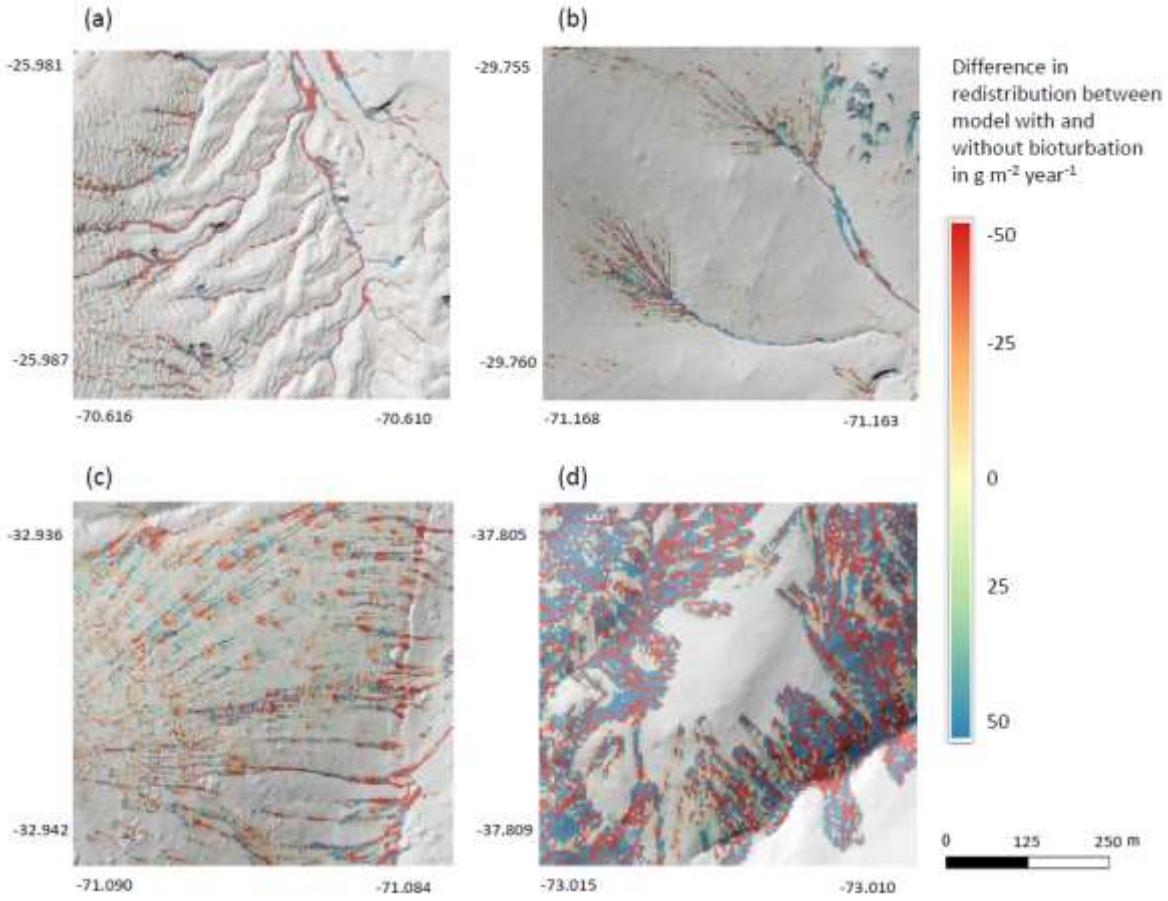

Figure 5.7. Catchment-wide impact of bioturbation on sediment redistribution. Colour indicates the impact. Positive values indicate bioturbation enhanced sediment accumulation, negative values indicate bioturbation enhanced sediment erosion. Grey shadows indicate the hill shading. (a) Pan de Azúcar, (b) Santa Gracia, (c) La Campana, (d) Nahuelbuta.

Table 5.3. Parameters influencing impact of bioturbation on sediment redistribution. The catchment-wide analysis showed that bioturbation has varying impact on sediment redistribution (see Fig. 5.5,7). The x-axis shows the parameter values. The y-axis shows the amount of sediment which was redistributed due to bioturbation. Red colour indicates that at these parameter values, bioturbation caused sediment accumulation. Blue colour indicates that at these parameter values, bioturbation enhanced sediment erosion. One GAM model was run per site. The lines are not smooth as this is a conceptual Figure 5.only. For regression fits as estimated by the GAMs see Fig. 5.A9-A14. For the amount of explained variance of each GAM model see Tab. A2.

Parameter	**Impact**

Elevation	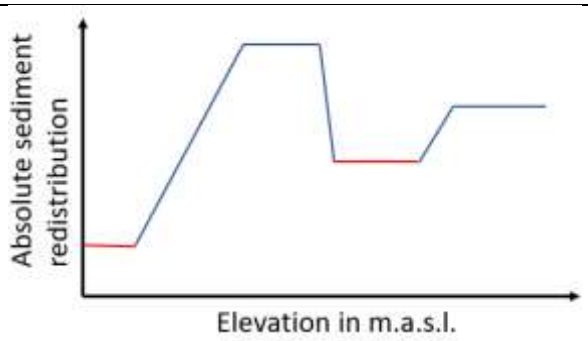
Slope	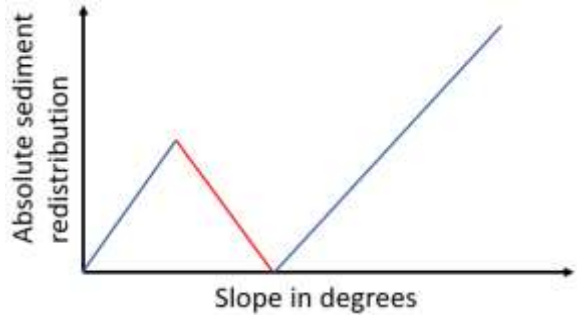
Surface roughness	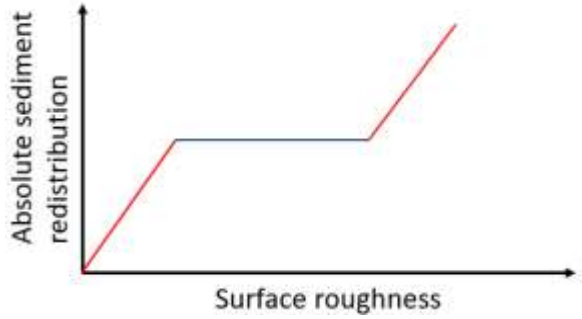
Aspect	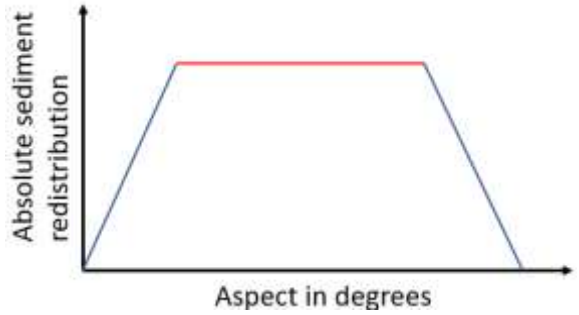
TRI	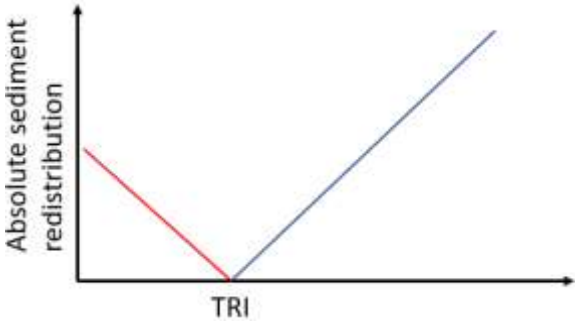

Profile curvature	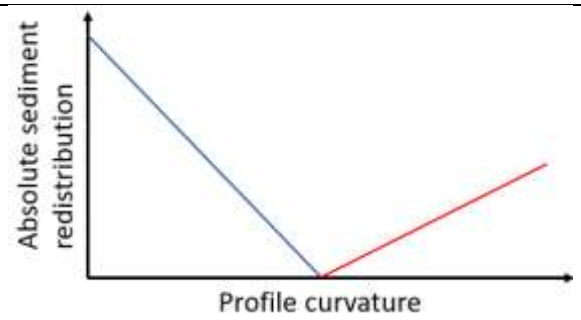
NDVI	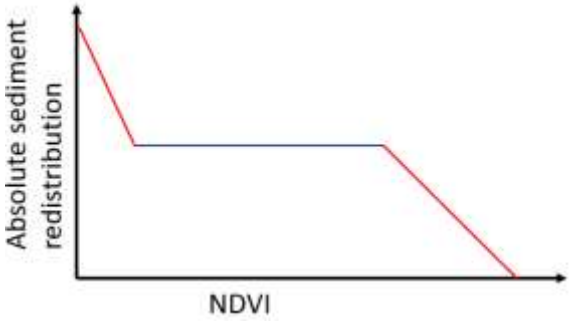
Sinks connectivity	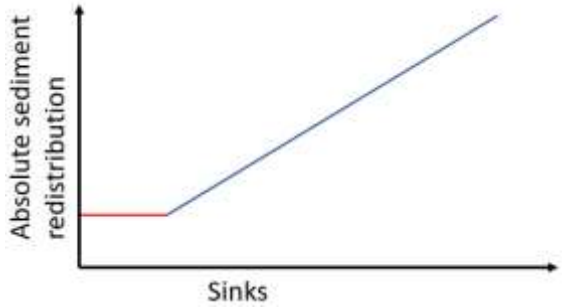
Topographic wetness index	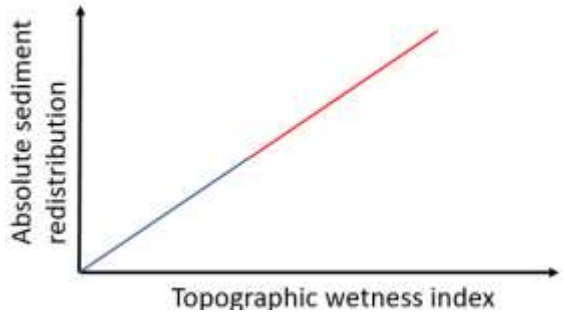

5.5. Discussion

5.5.1 The inclusion of bioturbation increases model performance

Overall, our DMMF model including bioturbation performed much better than the model without bioturbation. The DMMF model without bioturbation performed worse (RMSE of 1.18 kg ha^{-1} $year^{-1}$ and R^2 of 0.17) than the model with bioturbation (RMSE was 0.63 kg ha^{-1} $year^{-1}$ and R^2 was 0.71).

We hence argue that the higher accuracy of our model can be explained with the inclusion of bioturbation. This is confirmed by the fact that our model run without bioturbation performed similarly to previously run models without bioturbation: In earlier studies, the accuracy of the MMF model reached an RMSE in between 4.9 and 8.2 kg ha^{-1} $year^{-1}$, with an estimated R^2 of in between 0.21 and 0.57 (Jong et al., 1999; Vigiak et al., 2005; López-Vicente et al., 2008; Vieira et al., 2014; Choi et al., 2017). However, we acknowledge that previous studies were all conducted in more temperate climate zones. To be able to compare our results with previous studies, we calculated the model performance considering solely the Mediterranean and humid climate zone. Here, our model performed better than when we considered all climate zones (R^2 = 0.72, RMSE = 0.45 kg ha^{-1} $year^{-1}$), confirming the conclusion that bioturbation increased model performance. Additionally, we compared the model output with the values on sediment redistribution estimated in previous studies. Again, these were solely conducted in more humid climate regions. In the humid zone, our model predicted an erosion up to 3.5 kg m^{-2} $year^{-1}$. This estimation is in line with erosion rates due to bioturbation established by in-situ measurements in other studies (between 1.5 kg m^{-2} $year^{-1}$ and 3.7 kg m^{-2} $year^{-1}$) (Black and Montgomery, 1991; Yoo and Mudd, 2008; Yoo et al., 2005; Rutin, 1996). This also confirms the reliability of our approach.

5.5.2 The relevance of bioturbation for sediment redistribution depends on the landscape context

On the catchment scale (1 ha), our study finds that bioturbation increases erosion in all climatic zones except within the humid zone (Figure 5.5b). In contrast, bioturbation increases both, erosion and accumulation, on the plot scale (1 m^2) (Figure 5.5a). On this scale, in the arid and semi-arid zone, sediment erosion and accumulation were predicted to be about equal ((erosion and accumulation both up to 0.1 kg m^{-2} $year^{-1}$ in the arid zone, and erosion and accumulation both up to 0.2 kg m^{-2} $year^{-1}$ in the semi-arid zone (see Figure 5.5a)). Bioturbation marginally increased erosion and decreased accumulation in the semi-arid zone, but reduced by twofold the accumulation in the arid zone. In contrast, in the Mediterranean and humid zone, erosion was predicted to be almost double when compared to accumulation (predicted erosion up to 2.5 kg m^{-2} $year^{-1,}$ and accumulation up to 1.4 kg m^{-2} $year^{-1}$). Inclusion of bioturbation increased erosion up to 3 kg m^{-2} $year^{-1,}$ and accumulation up to 1.6 kg m^{-2} $year^{-1}$ in the Mediterranean zone, while it had no significant effect in humid zone. We argue that sediment redistribution due to bioturbation is heavily influenced by meso-topographic structures which determine the creation of surface runoff. Due to this, the erosion and accumulation on the plots scale is heavier impacted by bioturbation with increasing surface runoff.

According to our analysis, bioturbation increases erosion or accumulation of sediment mostly based on an interplay between topographic structures elevation, slope and TRI (Table 5.3). Over all research sites, this study found that bioturbation leads to an increase in surface erosion in areas where erosional processes dominate (upper, and/or steeper slopes), and tends to increase sediment accumulation in areas where sediment is naturally deposited, e.g. lower slopes or shallow depressions (Figure 5.8). This

finding is based on the fact that erosion in general is positively affected by slope, and negatively by surface roughness and vegetation (Rodríguez-Caballero et al., 2012; Wang et al., 2013; Kirols et al., 2015). Additionally, the redistribution of sediment is largely affected by topographic meso-/macroforms, such as rills or cliffs. These can be quantified by topographic ruggedness index (TRI) which describes the amount of elevation drop between adjusting cells of DEM (Wilson et al., 2007). At high values of this index, we would therefore expect high erosion rate, due to concentrated runoff within the connected rills or undisturbed flow of runoff from the cliffs downslope.

Our data show that one burrow provides up to 0.43 m^3 of additional loose sediment at the surface (Table 5.2), while the surface roughness increases up to 200 % (Grigusova et al., 2022). When including burrows into the model, at the slope values from 0 to 5 degrees, the presence of burrows had no impact on sediment redistribution. From 5 degrees onwards it increased sediment erosion proportionally to the slope of the hillside (an increased erosion from 0.4 g ha^{-1} $year^{-1}$ in the semi-arid zone until up to 150 kg ha^{-1} $year^{-1}$ in the Mediterranean zone, Fig. 5.A9 and A12). Similarly, at locations with sudden elevation drops 0 m until 0.2 m (lower TRI values), the presence of burrows had no impact. However, at locations with elevation drops of 0.2 until 0.5 m (higher TRI values), bioturbation increases sediment erosion by 1.5 kg ha^{-1} $year^{-1}$ (Fig. 5.A9, A12-A14). Lastly, bioturbation proportionally increased accumulation when the surface roughness values were above 0.5 (an increased accumulation from 0.2 g ha^{-1} $year^{-1}$ in semi-arid zone until 5000 kg ha^{-1} $year^{-1}$ in the Mediterranean zone, Fig. 5.A9 and A12).

We conclude that in locations with slope values over 5 degrees, or at locations with sudden drops in elevation (high TRI) and connected rills, more sediment is eroding than accumulating. Here, additional surface sediments generated by bioturbators provides more source material for erosion and thus bioturbation increases sediment erosion at these locations (Table 5.3). In contrast, at locations with a slope below 5 degrees, where processes are dominantly controlled by surface roughness, sediment accumulation caused by bioturbation increases proportionally when the surface roughness has a value above 0.5. This is likely because burrows through their above-ground structures heavily increase surface roughness (Grigusova et al., 2022), and hence the presence of bioturbating animals leads to an increase in sediment accumulation.

Additionally, we hypothesize that it is not only the additional availability of sediment on the surface and the topography of the vicinity which controls the contribution of bioturbation to sediment surface flux, but also the spatial distribution of animal burrows. We interpret that in locations with high burrow aggregation, surface flow might be redirected and centralized around the aggregates and thus increase the sediment erosion in the areas surrounding burrow aggregates (Figure 5.A15). This mechanism could explain, why bioturbation promotes sediment erosion especially in the Mediterranean zone. The relative role of burrow aggregation should be studied in detail and included in future studies.

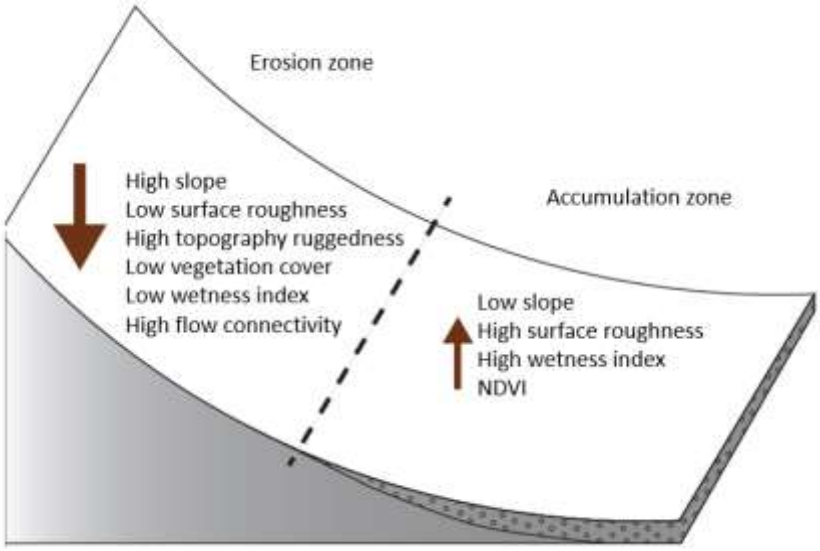

Figure 5.8. Bioturbation amplifies erosion within the erosion zone and accumulation within the accumulation zone. The zones were defined based on the values of surrounding environmental parameters. The arrow direction indicates decrease or increase of sediment amount within a pixel and thus erosion or accumulation. The arrow thickness indicates the amount of redistributed sediment. Please note that the location of the erosion zone on the upper hillside and of the accumulation zone on the lower hillside is purely conceptual. Should the respective values of environmental parameters listed for the erosion zone be found on the lower hillside, it would still be erosion zone. Vice versa for the accumulation zone. The importance of the parameters is ranked and described in section 5.5.3.

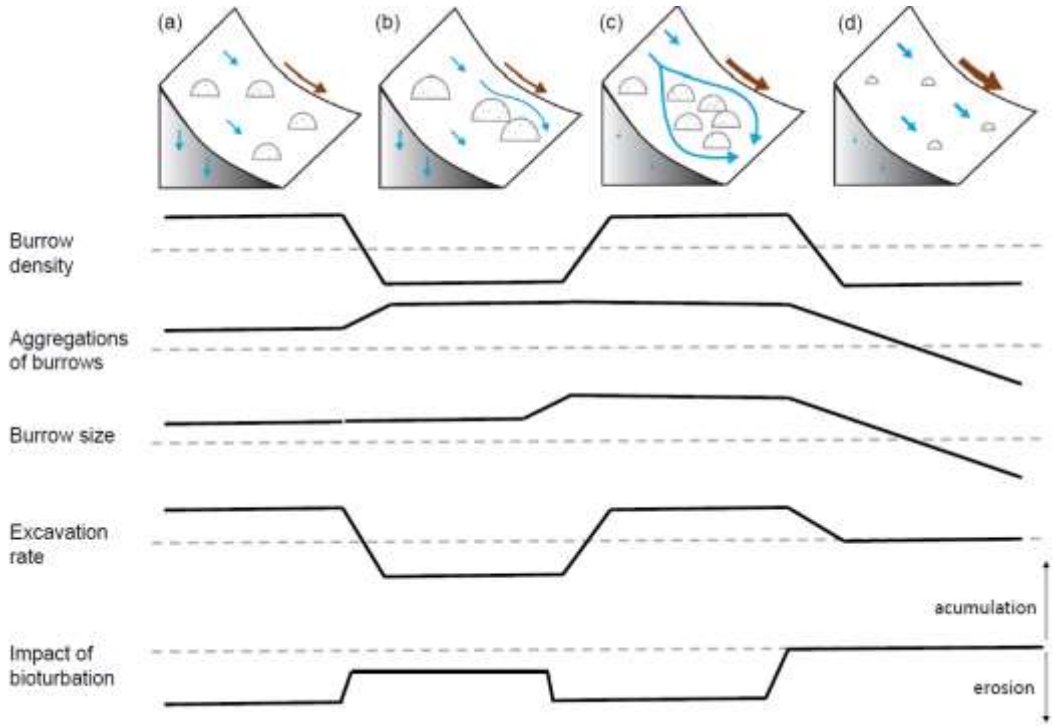

Figure 5.9. Context dependency of sediment redistribution. (a) Pan de Azúcar, (b) Santa Gracia, (c) La Campana, (d) Nahuelbuta. Brown arrows indicate the direction and magnitude of overall sediment redistribution within each climate zone. Blue arrows indicate the direction of flow (runoff vs. infiltration).

Half-moons indicate the distribution and size of burrows. The dashed line indicates the median value of each parameter for the first four parameters.

5.6. Conclusion

In summary, our results show that the presence of animal burrows leads to an increase in erosion and net sediment loss. According to our results, bioturbation enhances sediment erosion in areas where more erosion is expected and enhances sediment accumulation in areas which are more prone to accumulate sediment.

On geological time scales, as burrowing animals increase both, erosion in steeper zones, and accumulation in areas with gentler slopes and higher roughness, hillslope relief should become faster equalised and overall more flat. This tendency is the most pronounced in the Mediterranean zone with high burrow density and excavation rates, as well as high precipitation rates. Our study furthermore shows that the impact of bioturbation heavily depends on the surrounding environmental parameters.

Funding: This study was funded by the German Research Foundation, DFG [grant numbers BE1780/52-1, LA3521/1-1, FA 925/12-1, BR 1293-18-1], and is part of the DFG Priority Programme SPP 1803: EarthShape: Earth Surface Shaping by Biota, sub-project “Effects of bioturbation on rates of vertical and horizontal sediment and nutrient fluxes”.

Institutional Review Board Statement: Not applicable.

Informed Consent Statement: Not applicable.

Acknowledgments: We thank CONAF for the kind support provided during our field campaign.

Competing interests: There is no conflict of interest.

Author contribution: PG set up the model, analysed the data and wrote the manuscript draft; PG and AL performed the measurements AL, JB, NF, RB, DK, PP, LP, CdR reviewed and edited the manuscript.

Code/Data availability: Code and all raw data can be provided by the corresponding author upon request.

Special Issue statement: I would like to stress that the submission should be part of the Copernicus special Issue (Earth surface shaping by biota (ESurf/BG/ESD/ESSD/SOIL inter-journal SI) initiated by the EarthShape consortium.

References

Anderson, R. S., Rajaram, H., and Anderson, S. P.: Climate driven coevolution of weathering profiles and hillslope topography generates dramatic differences in critical zone architecture, Hydrol. Process., 33, 4–19, https://doi.org/10.1002/hyp.13307, 2019.

Beasley, D. B., Huggins, L. F., and Monke, E. J.: ANSWERS: A Model for Watershed Planning, Transactions of the ASAE, 23, 938–944, https://doi.org/10.13031/2013.34692, 1980.

Bernhard, N., Moskwa, L.-M., Schmidt, K., Oeser, R. A., Aburto, F., Bader, M. Y., Baumann, K., Blanckenburg, F. von, Boy, J., van den Brink, L., Brucker, E., Büdel, B., Canessa, R., Dippold, M. A., Ehlers, T. A., Fuentes, J. P., Godoy, R., Jung, P., Karsten, U., Köster, M., Kuzyakov, Y., Leinweber, P., Neidhardt, H., Matus, F., Mueller, C. W., Oelmann, Y., Oses, R., Osses, P., Paulino, L., Samolov, E., Schaller, M., Schmid, M., Spielvogel, S., Spohn, M., Stock, S., Stroncik, N.,

Tielbörger, K., Übernickel, K., Scholten, T., Seguel, O., Wagner, D., and Kühn, P.: Pedogenic and microbial interrelations to regional climate and local topography: New insights from a climate gradient (arid to humid) along the Coastal Cordillera of Chile, CATENA, 170, 335–355, https://doi.org/10.1016/j.catena.2018.06.018, 2018.

BEVEN, K. J. and KIRKBY, M. J.: A physically based, variable contributing area model of basin hydrology / Un modèle à base physique de zone d'appel variable de l'hydrologie du bassin versant, Hydrological Sciences Bulletin, 24, 43–69, https://doi.org/10.1080/02626667909491834, 1979.

Black, T. A. and Montgomery, D. R.: Sediment transport by burrowing mammals, Marin County, California, Earth Surf. Process. Landforms, 16, 163–172, https://doi.org/10.1002/esp.3290160207, 1991.

Boudreau, B. P.: Mathematics of tracer mixing in sediments; I, Spatially-dependent, diffusive mixing, American Journal of Science, 286, 161–198, https://doi.org/10.2475/ajs.286.3.161, 1986.

Boudreau, B. P.: The diffusion and telegraph equations in diagenetic modelling, Geochimica et Cosmochimica Acta, 53, 1857–1866, https://doi.org/10.1016/0016-7037(89)90306-2, 1989.

Braun, J., Mercier, J., Guillocheau, F., and Robin, C.: A simple model for regolith formation by chemical weathering, J. Geophys. Res. Earth Surf., 121, 2140–2171, https://doi.org/10.1002/2016JF003914, 2016.

Brosens, L., Campforts, B., Robinet, J., Vanacker, V., Opfergelt, S., Ameijeiras-Mariño, Y., Minella, J. P. G., and Govers, G.: Slope Gradient Controls Soil Thickness and Chemical Weathering in Subtropical Brazil: Understanding Rates and Timescales of Regional Soilscape Evolution Through a Combination of Field Data and Modeling, J. Geophys. Res. Earth Surf., 125, 1, https://doi.org/10.1029/2019JF005321, 2020.

Carretier, S., Goddéris, Y., Delannoy, T., and Rouby, D.: Mean bedrock-to-saprolite conversion and erosion rates during mountain growth and decline, Geomorphology, 209, 39–52, https://doi.org/10.1016/j.geomorph.2013.11.025, 2014.

Cerqueira, R.: The Distribution of Didelphis in South America (Polyprotodontia, Didelphidae), Journal of Biogeography, 12, 135, https://doi.org/10.2307/2844837, 1985.

Chen, M., Ma, L., Shao, M.'a., Wei, X., Jia, Y., Sun, S., Zhang, Q., Li, T., Yang, X., and Gan, M.: Chinese zokor (Myospalax fontanierii) excavating activities lessen runoff but facilitate soil erosion – A simulation experiment, CATENA, 202, 105248, https://doi.org/10.1016/j.catena.2021.105248, 2021.

Choi, K., Arnhold, S., Huwe, B., and Reineking, B.: Daily Based Morgan–Morgan–Finney (DMMF) Model: A Spatially Distributed Conceptual Soil Erosion Model to Simulate Complex Soil Surface Configurations, Water, 9, 278, https://doi.org/10.3390/w9040278, 2017.

Cohen, S., Willgoose, G., Svoray, T., Hancock, G., and Sela, S.: The effects of sediment transport, weathering, and aeolian mechanisms on soil evolution, J. Geophys. Res. Earth Surf., 120, 260–274, https://doi.org/10.1002/2014JF003186, 2015.

Cohen, S., Willgoose, G., and Hancock, G.: The mARM3D spatially distributed soil evolution model: Three-dimensional model framework and analysis of hillslope and landform responses, J. Geophys. Res., 115, 191, https://doi.org/10.1029/2009JF001536, 2010.

Coombes, M. A.: Biogeomorphology: diverse, integrative and useful, Earth Surf. Process. Landforms, 41, 2296–2300, https://doi.org/10.1002/esp.4055, 2016.

Corenblit, D., Corbara, B., and Steiger, J.: Biogeomorphological eco-evolutionary feedback between life and geomorphology: a theoretical framework using fossorial mammals, Die Naturwissenschaften, 108, 55, https://doi.org/10.1007/s00114-021-01760-y, 2021.

Debruyn, L. A.L. and Conacher, A. J.: The bioturbation activity of ants in agricultural and naturally vegetated habitats in semiarid environments, Soil Res., 32, 555, https://doi.org/10.1071/SR9940555, 1994.

Devia, G. K., Ganasri, B. P., and Dwarakish, G. S.: A Review on Hydrological Models, Aquatic Procedia, 4, 1001–1007, https://doi.org/10.1016/j.aqpro.2015.02.126, 2015.

Durner, W., Iden, S. C., and Unold, G. von: The integral suspension pressure method (ISP) for precise particle-size analysis by gravitational sedimentation, Water Resour. Res., 53, 33–48, https://doi.org/10.1002/2016WR019830, 2017.

Eccard, J. A. and Herde, A.: Seasonal variation in the behaviour of a short-lived rodent, BMC ecology, 13, 43, https://doi.org/10.1186/1472-6785-13-43, 2013.

Ferro, L. I. and Barquez, R. M.: Species Richness of Nonvolant Small Mammals Along Elevational Gradients in Northwestern Argentina, Biotropica, 41, 759–767, https://doi.org/10.1111/j.1744-7429.2009.00522.x, 2009.

Foster, D. W.: BIOTURB: A FORTRAN program to simulate the effects of bioturbation on the vertical distribution of sediment, Computers & Geosciences, 11, 39–54, https://doi.org/10.1016/0098-3004(85)90037-8, 1985.

François, F., Poggiale, J.-C., Durbec, J.-P., and Stora, G.: A New Approach for the Modelling of Sediment Reworking Induced by a Macrobenthic Community, Acta Biotheoretica, 45, 295–319, https://doi.org/10.1023/A:1000636109604, 1997.

Gabet, E. J., Reichman, O. J., and Seabloom, E. W.: The Effects of Bioturbation on Soil Processes and Sediment Transport, Annu. Rev. Earth Planet. Sci., 31, 249–273, https://doi.org/10.1146/annurev.earth.31.100901.141314, 2003.

Gray, H. J., Keen-Zebert, A., Furbish, D. J., Tucker, G. E., and Mahan, S. A.: Depth-dependent soil mixing persists across climate zones, Proceedings of the National Academy of Sciences of the United States of America, 117, 8750–8756, https://doi.org/10.1073/pnas.1914140117., 2020.

Grigusova, P., Larsen, A., Achilles, S., Brandl, R., del Río, C., Farwig, N., Kraus, D., Paulino, L., Pliscoff, P., Übernickel, K., and Bendix, J.: Higher sediment redistribution rates related to burrowing animals than previously assumed as revealed by time-of-flight-based monitoring, Earth Surf. Dynam., 10, 1273–1301, https://doi.org/10.5194/esurf-10-1273-2022, 2022.

Grigusova, P., Larsen, A., Achilles, S., Klug, A., Fischer, R., Kraus, D., Übernickel, K., Paulino, L., Pliscoff, P., Brandl, R., Farwig, N., and Bendix, J.: Area-Wide Prediction of Vertebrate and Invertebrate Hole Density and Depth across a Climate Gradient in Chile Based on UAV and Machine Learning, Drones, 5, 86, https://doi.org/10.3390/drones5030086, 2021.

Hakonson, T. E.: The Effects of Pocket Gopher Burrowing on Water Balance and Erosion from Landfill Covers, J. environ. qual., 28, 659–665, https://doi.org/10.2134/jeq1999.00472425002800020033x, 1999.

Hall, K., Boelhouwers, J., and Driscoll, K.: Animals as Erosion Agents in the Alpine Zone: Some Data and Observations from Canada, Lesotho, and Tibet, Arctic, Antarctic, and Alpine Research, 31, 436–446, https://doi.org/10.1080/15230430.1999.12003328, 1999.

Hancock, G. and Lowry, J.: Quantifying the influence of rainfall, vegetation and animals on soil erosion and hillslope connectivity in the monsoonal tropics of northern Australia, Earth Surf. Process. Landforms, 46, 2110–2123, https://doi.org/10.1002/esp.5147, 2021.

Hazelhoff, L., van Hoof, P., Imeson, A. C., and Kwaad, F. J. P. M.: The exposure of forest soil to erosion by earthworms, Earth Surf. Process. Landforms, 6, 235–250, https://doi.org/10.1002/esp.3290060305, 1981.

Horn, B.K.P.: Hill shading and the reflectance map, Proc. IEEE, 69, 14–47, https://doi.org/10.1109/PROC.1981.11918, 1981.

Imeson, A. C. and Kwaad, F. J. P. M.: Some Effects of Burrowing Animals on Slope Processes in the Luxembourg Ardennes, Geografiska Annaler: Series A, Physical Geography, 58, 317–328, https://doi.org/10.1080/04353676.1976.11879941, 1976.

Istanbulluoglu, E.: Vegetation-modulated landscape evolution: Effects of vegetation on landscape processes, drainage density, and topography, J. Geophys. Res., 110, 11, https://doi.org/10.1029/2004JF000249, 2005.

Jimenez, J. E., Feinsinger, P., and Jaksi, F. M.: Spatiotemporal Patterns of an Irruption and Decline of Small Mammals in Northcentral Chile, Journal of Mammalogy, 73, 356–364, https://doi.org/10.2307/1382070, 1992.

Jong, S. M. de, Paracchini, M. L., Bertolo, F., Folving, S., Megier, J., and Roo, A.P.J. de: Regional assessment of soil erosion using the distributed model SEMMED and remotely sensed data, CATENA, 37, 291–308, https://doi.org/10.1016/S0341-8162(99)00038-7, 1999.

Jumars, P. A., Nowell, A. R.M., and Self, R. F.L.: A simple model of flow—Sediment—Organism interaction, Marine Geology, 42, 155–172, https://doi.org/10.1016/0025-3227(81)90162-6, 1981.

Katzman, E. A., Zaytseva, E. A., Feoktistova, N. Y., Tovpinetz, N. N., Bogomolov, P. L., Potashnikova, E. V., and Surov, A. V.: Seasonal Changes in Burrowing of the Common Hamster (Cricetus cricetus L., 1758) (Rodentia: Cricetidae) in the City, PJE, 17, 251–258, https://doi.org/10.18500/1684-7318-2018-3-251-258, 2018.

Kinlaw, A. and Grasmueck, M.: Evidence for and geomorphologic consequences of a reptilian ecosystem engineer: The burrowing cascade initiated by the Gopher Tortoise, Geomorphology, 157-158, 108–121, https://doi.org/10.1016/j.geomorph.2011.06.030, 2012.

Kirols, H. S., Kevorkov, D., Uihlein, A., and Medraj, M.: The effect of initial surface roughness on water droplet erosion behaviour, Wear, 342-343, 198–209, https://doi.org/10.1016/j.wear.2015.08.019, 2015.

Kraus, D., Brandl, R., Achilles, S., Bendix, J., Grigusova, P., Larsen, A., Pliscoff, P., Übernickel, K., and Farwig, N.: Vegetation and vertebrate abundance as drivers of bioturbation patterns along a climate gradient, PloS one, 17, e0264408, https://doi.org/10.1371/journal.pone.0264408, 2022.

Kügler, M., Hoffmann, T. O., Beer, A. R., Übernickel, K., Ehlers, T. A., Scherler, D., and Eichel, J.: (LiDAR) 3D Point Clouds and Topographic Data from the Chilean Coastal Cordillera, 2022.

Lal, R.: Soil degradation by erosion, Land Degrad. Dev., 12, 519–539, https://doi.org/10.1002/ldr.472, 2001.

Larsen, A., Nardin, W., Lageweg, W. I., and Bätz, N.: Biogeomorphology, quo vadis? On processes, time, and space in biogeomorphology, Earth Surf. Process. Landforms, 46, 12–23, https://doi.org/10.1002/esp.5016, 2021.

Le Hir, P., Monbet, Y., and Orvain, F.: Sediment erodability in sediment transport modelling: Can we account for biota effects?, Continental Shelf Research, 27, 1116–1142, https://doi.org/10.1016/j.csr.2005.11.016, 2007.

Lehnert, L. W., Thies, B., Trachte, K., Achilles, S., Osses, P., Baumann, K., Schmidt, J., Samolov, E., Jung, P., Leinweber, P., Karsten, U., Büdel, B., and Bendix, J.: A Case Study on Fog/Low Stratus Occurrence at Las Lomitas, Atacama Desert (Chile) as a Water Source for Biological Soil Crusts, Aerosol Air Qual. Res., 18, 254-26, https://doi.org/10.4209/aaqr.2017.01.0021, 2018.

Li, G., Li, X., Li, J., Chen, W., Zhu, H., Zhao, J., and Hu, X.: Influences of Plateau Zokor Burrowing on Soil Erosion and Nutrient Loss in Alpine Meadows in the Yellow River Source Zone of West China, Water, 11, 2258, https://doi.org/10.3390/w11112258, 2019a.

Li, T. C., Shao, M. A., Jia, Y. H., Jia, X. X., Huang, L. M., and Gan, M.: Small-scale observation on the effects of burrowing activities of ants on soil hydraulic processes, Eur J Soil Sci, 70, 236–244, https://doi.org/10.1111/ejss.12748, 2019b.

Li, T., Shao, M.'a., Jia, Y., Jia, X., and Huang, L.: Small-scale observation on the effects of the burrowing activities of mole crickets on soil erosion and hydrologic processes, Agriculture, Ecosystems & Environment, 261, 136–143, https://doi.org/10.1016/j.agee.2018.04.010, 2018.

Li, Z. and Zhang, J.: Calculation of Field Manning's Roughness Coefficient, Agricultural Water Management, 49, 153–161, https://doi.org/10.1016/S0378-3774(00)00139-6, 2001.

Lilhare, R., Garg, V., and Nikam, B. R.: Application of GIS-Coupled Modified MMF Model to Estimate Sediment Yield on a Watershed Scale, J. Hydrol. Eng., 20, 745, https://doi.org/10.1061/(ASCE)HE.1943-5584.0001063, 2015.

López-Vicente, M., Navas, A., and Machín, J.: Modelling soil detachment rates in rainfed agrosystems in the south-central Pyrenees, Agricultural Water Management, 95, 1079–1089, https://doi.org/10.1016/j.agwat.2008.04.004, 2008.

Malizia, A. I.: Population dynamics of the fossorial rodent Ctenomys talarum (Rodentia: Octodontidae), Journal of Zoology, 244, 545–551, https://doi.org/10.1111/j.1469-7998.1998.tb00059.x, 1998.

Merritt, W. S., Letcher, R. A., and Jakeman, A. J.: A review of erosion and sediment transport models, Environmental Modelling & Software, 18, 761–799, https://doi.org/10.1016/S1364-8152(03)00078-1, 2003.

Meserve, P. L.: Trophic Relationships among Small Mammals in a Chilean Semiarid Thorn Scrub Community, Journal of Mammalogy, 62, 304–314, https://doi.org/10.2307/1380707, 1981.

Meyer, H., Reudenbach, C., Hengl, T., Katurji, M., and Nauss, T.: Improving performance of spatio-temporal machine learning models using forward feature selection and target-oriented validation, Environmental Modelling & Software, 101, 1–9, https://doi.org/10.1016/j.envsoft.2017.12.001, 2018.

Meysman, F. J. R., Boudreau, B. P., and Middelburg, J. J.: Relations between local, nonlocal, discrete and continuous models of bioturbation, J Mar Res, 61, 391–410, https://doi.org/10.1357/002224003322201241, 2003.

Milstead, W. B., Meserve, P. L., Campanella, A., Previtali, M. A., Kelt, D. A., and Gutiérrez, J. R.: Spatial Ecology of Small Mammals in North-central Chile: Role of Precipitation and Refuges, Journal of Mammalogy, 88, 1532–1538, https://doi.org/10.1644/16-MAMM-A-407R.1, 2007.

Monteverde, M. J. and Piudo, L.: Activity Patterns of the Culpeo Fox (Lycalopex Culpaeus Magellanica) in a Non-Hunting Area of Northwestern Patagonia, Argentina, Mammal Study, 36, 119–125, https://doi.org/10.3106/041.036.0301, 2011.

Morgan, R. P. C. and Duzant, J. H.: Modified MMF (Morgan–Morgan–Finney) model for evaluating effects of crops and vegetation cover on soil erosion, Earth Surf. Process. Landforms, 33, 90–106, https://doi.org/10.1002/esp.1530, 2008.

Morgan, R. P. C., Quinton, J. N., Smith, R. E., Govers, G., Poesen, J. W. A., Auerswald, K., Chisci, G., Torri, D., and Styczen, M. E.: The European Soil Erosion Model (EUROSEM): a dynamic approach for predicting sediment transport from fields and small catchments, Earth Surf. Process. Landforms, 23, 527–544, https://doi.org/10.1002/(SICI)1096-9837(199806)23:6<527:AID-ESP868>3.0.CO;2-5, 1998.

Morgan, R.P.C.: A simple approach to soil loss prediction: a revised Morgan–Morgan–Finney model, CATENA, 44, 305–322, https://doi.org/10.1016/S0341-8162(00)00171-5, 2001.

Morgan, R.P.C., Morgan, D.D.V., and Finney, H. J.: A predictive model for the assessment of soil erosion risk, Journal of Agricultural Engineering Research, 30, 245–253, https://doi.org/10.1016/S0021-8634(84)80025-6, 1984.

Nearing, M. A., Foster, G. R., Lane, L. J., and Finkner, S. C.: A Process-Based Soil Erosion Model for USDA-Water Erosion Prediction Project Technology, Transactions of the ASAE, 32, 1587–1593, https://doi.org/10.13031/2013.31195, 1989.

Nkem, J. N., Lobry de Bruyn, L. A., Grant, C. D., and Hulugalle, N. R.: The impact of ant bioturbation and foraging activities on surrounding soil properties, Pedobiologia, 44, 609–621, https://doi.org/10.1078/S0031-4056(04)70075-X, 2000.

Oeser, R. A., Stroncik, N., Moskwa, L.-M., Bernhard, N., Schaller, M., Canessa, R., van den Brink, L., Köster, M., Brucker, E., Stock, S., Fuentes, J. P., Godoy, R., Matus, F. J., Oses Pedraza, R., Osses McIntyre, P., Paulino, L., Seguel, O., Bader, M. Y., Boy, J., Dippold, M. A., Ehlers, T. A., Kühn, P., Kuzyakov, Y., Leinweber, P., Scholten, T., Spielvogel, S., Spohn, M., Übernickel, K., Tielbörger, K., Wagner, D., and Blanckenburg, F. von: Chemistry and microbiology of the Critical Zone along a steep climate and vegetation gradient in the Chilean Coastal Cordillera, CATENA, 170, 183–203, https://doi.org/10.1016/j.catena.2018.06.002, 2018.

Pelletier, J. D., Barron-Gafford, G. A., Breshears, D. D., Brooks, P. D., Chorover, J., Durcik, M., Harman, C. J., Huxman, T. E., Lohse, K. A., Lybrand, R., Meixner, T., McIntosh, J. C., Papuga, S. A., Rasmussen, C., Schaap, M., Swetnam, T. L., and Troch, P. A.: Coevolution of nonlinear trends in vegetation, soils, and topography with elevation and slope aspect: A case study in the sky islands of southern Arizona, J. Geophys. Res. Earth Surf., 118, 741–758, https://doi.org/10.1002/jgrf.20046, 2013.

Penman, H.: Natural evaporation from open water, hare soil and grass, Proceedings of the Royal Society of London. Series A, Mathematical and physical sciences, 193, 120–145, https://doi.org/10.1098/rspa.1948.0037, 1948.

Pollacco, J. A. P.: A generally applicable pedotransfer function that estimates field capacity and permanent wilting point from soil texture and bulk density, Can. J. Soil. Sci., 88, 761–774, https://doi.org/10.4141/CJSS07120, 2008.

Qin, Y., Yi, S., Ding, Y., Qin, Y., Zhang, W., Sun, Y., Hou, X., Yu, H., Meng, B., Zhang, H., Chen, J., and Wang, Z.: Effects of plateau pikas' foraging and burrowing activities on vegetation biomass and soil organic carbon of alpine grasslands, Plant Soil, 458, 201–216, https://doi.org/10.1007/s11104-020-04489-1, 2021.

Reichman, O. J. and Seabloom, E. W.: The role of pocket gophers as subterranean ecosystem engineers, Trends in Ecology & Evolution, 17, 44–49, https://doi.org/10.1016/S0169-5347(01)02329-1, 2002.

Renard, K., Foster, G., Weesies, G., and Porter, J.: RUSLE: The Revised Universal Soil Loss Equation, Journal of Soil Water Conservation, 30–33, 1991.

Ridd, P. V.: Flow Through Animal Burrows in Mangrove Creeks, Estuarine, Coastal and Shelf Science, 43, 617–625, https://doi.org/10.1006/ecss.1996.0091, 1996.

Rodríguez-Caballero, E., Cantón, Y., Chamizo, S., Afana, A., and Solé-Benet, A.: Effects of biological soil crusts on surface roughness and implications for runoff and erosion, Geomorphology, 145-146, 81–89, https://doi.org/10.1016/j.geomorph.2011.12.042, 2012.

ROO, A. P. J. de, WESSELING, C. G., and RITSEMA, C. J.: LISEM: A SINGLE-EVENT PHYSICALLY BASED HYDROLOGICAL AND SOIL EROSION MODEL FOR DRAINAGE BASINS. I: THEORY, INPUT AND OUTPUT, Hydrol. Process., 10, 1107–1117, https://doi.org/10.1002/(SICI)1099-1085(199608)10:8<1107:AID-HYP415>3.0.CO;2-4, 1996.

Rutin, J.: The burrowing activity of scorpions (Scorpio maurus palmatus) and their potential contribution to the erosion of Hamra soils in Karkur, central Israel, Geomorphology, 15, 159–168, https://doi.org/10.1016/0169-555X(95)00120-T, 1996.

Schiffers, K., Teal, L. R., Travis, J. M. J., and Solan, M.: An open source simulation model for soil and sediment bioturbation, PloS one, 6, e28028, https://doi.org/10.1371/journal.pone.0028028, 2011.

Shannon, C. E.: A Mathematical Theory of Communication, Bell System Technical Journal, 27, 379–423, https://doi.org/10.1002/j.1538-7305.1948.tb01338.x, 1948.

Shull, D. H.: Transition-matrix model of bioturbation and radionuclide diagenesis, Limnol. Oceanogr., 46, 905–916, https://doi.org/10.4319/lo.2001.46.4.0905, 2001.

Simonetti, J. A.: Microhabitat Use by Small Mammals in Central Chile, Oikos, 56, 309, https://doi.org/10.2307/3565615, 1989.

Soetaert, K., Herman, P. M. J., Middelburg, J. J., Heip, C., deStigter, H. S., van Weering, T. C. E., Epping, E., and Helder, W.: Modeling ^{210}Pb-derived mixing activity in ocean margin sediments: Diffusive versus nonlocal mixing, J Mar Res, 54, 1207–1227, https://doi.org/10.1357/0022240963213808, 1996.

Taylor, A. R., Lenoir, L., Vegerfors, B., and Persson, T.: Ant and Earthworm Bioturbation in Cold-Temperate Ecosystems, Ecosystems, 22, 981–994, https://doi.org/10.1007/s10021-018-0317-2, 2019.

Temme, A. J.A.M. and Vanwalleghem, T.: LORICA – A new model for linking landscape and soil profile evolution: Development and sensitivity analysis, Computers & Geosciences, 90, 131–143, https://doi.org/10.1016/j.cageo.2015.08.004, 2016.

Tews, J., Brose, U., Grimm, V., Tielbörger, K., Wichmann, M. C., Schwager, M., and Jeltsch, F.: Animal species diversity driven by habitat heterogeneity/diversity: the importance of keystone structures, Journal of Biogeography, 31, 79–92, https://doi.org/10.1046/j.0305-0270.2003.00994.x, 2004.

Tomasella, J., Hodnett, M. G., and Rossato, L.: Pedotransfer Functions for the Estimation of Soil Water Retention in Brazilian Soils, Soil Sci. Soc. Am. J., 64, 327–338, https://doi.org/10.2136/sssaj2000.641327x, 2000.

Trauth, M. H.: TURBO: a dynamic-probabilistic simulation to study the effects of bioturbation on paleoceanographic time series, Computers & Geosciences, 24, 433–441, https://doi.org/10.1016/S0098-3004(98)00019-3, 1998.

Tucker, G. E. and Hancock, G. R.: Modelling landscape evolution, Earth Surf. Process. Landforms, 35, 28–50, https://doi.org/10.1002/esp.1952, 2010.

Übernickel, K., Pizarro-Araya, J., Bhagavathula, S., Paulino, L., and Ehlers, T. A.: Reviews and syntheses: Composition and characteristics of burrowing animals along a climate and ecological gradient, Chile, Biogeosciences, 18, 5573–5594, https://doi.org/10.5194/bg-18-5573-2021, 2021a.

Übernickel, K., Ehlers, T. A., Paulino, L., and Fuentes Espoz, J.-P.: Time series of meteorological stations on an elevational gradient in National Park La Campana, Chile, 2021b.

Vanwalleghem, T., Stockmann, U., Minasny, B., and McBratney, A. B.: A quantitative model for integrating landscape evolution and soil formation, J. Geophys. Res. Earth Surf., 118, 331–347, https://doi.org/10.1029/2011JF002296, 2013.

Vieira, D.C.S., Prats, S. A., Nunes, J. P., Shakesby, R. A., Coelho, C.O.A., and Keizer, J. J.: Modelling runoff and erosion, and their mitigation, in burned Portuguese forest using the revised Morgan–Morgan–Finney model, Forest Ecology and Management, 314, 150–165, https://doi.org/10.1016/j.foreco.2013.12.006, 2014.

Vigiak, O., Okoba, B. O., Sterk, G., and Groenenberg, S.: Modelling catchment-scale erosion patterns in the East African Highlands, Earth Surf. Process. Landforms, 30, 183–196, https://doi.org/10.1002/esp.1174, 2005.

Voiculescu, M., Ianăş, A.-N., and Germain, D.: Exploring the impact of snow vole (Chionomys nivalis) burrowing activity in the Făgăraș Mountains, Southern Carpathians (Romania): Geomorphic characteristics and sediment budget, CATENA, 181, 104070, https://doi.org/10.1016/j.catena.2019.05.016, 2019.

Wang, B., Zheng, F., Römkens, M. J.M., and Darboux, F.: Soil erodibility for water erosion: A perspective and Chinese experiences, Geomorphology, 187, 1–10, https://doi.org/10.1016/j.geomorph.2013.01.018, 2013.

Wei, X., Li, S., Yang, P., and Cheng, H.: Soil erosion and vegetation succession in alpine Kobresia steppe meadow caused by plateau pika—A case study of Nagqu County, Tibet, Chin. Geograph.Sc., 17, 75–81, https://doi.org/10.1007/s11769-007-0075-0, 2007.

Welivitiya, W. D. D. P., Willgoose, G. R., and Hancock, G. R.: A coupled soilscape–landform evolution model: model formulation and initial results, Earth Surf. Dynam., 7, 591–607, https://doi.org/10.5194/esurf-7-591-2019, 2019.

Wheatcroft, R. A., Jumars, P. A., Smith, C. R., and Nowell, A. R. M.: A mechanistic view of the particulate biodiffusion coefficient: Step lengths, rest periods and transport directions, J Mar Res, 48, 177–207, https://doi.org/10.1357/002224090784984560, 1990.

Whitesides, C. J. and Butler, D. R.: Bioturbation by gophers and marmots and its effects on conifer germination, Earth Surf. Process. Landforms, 41, 2269–2281, https://doi.org/10.1002/esp.4046, 2016.

Wilkinson, M. T., Richards, P. J., and Humphreys, G. S.: Breaking ground: Pedological, geological, and ecological implications of soil bioturbation, Earth-Science Reviews, 97, 257–272, https://doi.org/10.1016/j.earscirev.2009.09.005, 2009.

Williams, J. R. (Ed.): Sediment-yield prediction with Universal Equation using runoff energy factor. In Present and prospective technology for predicting sediment yield and sources: Proceedings of the Sediment-Yield Workshop, ARS-S-40, United States Department of Agriculture (USDA), New Orleans, USA, 1975.

Wilson, M. F. J., O'Connell, B., Brown, C., Guinan, J. C., and Grehan, A. J.: Multiscale Terrain Analysis of Multibeam Bathymetry Data for Habitat Mapping on the Continental Slope, Marine Geodesy, 30, 3–35, https://doi.org/10.1080/01490410701295962, 2007.

Wischmeier, W. and Smith, D. D.: Predicting rainfall erosion losses - A guide to conservation planning, Agriculture Handbook, 1–58, 1978.

Wood, S. N.: Generalized Additive Models, Chapman and Hall/CRC, 2006.

Wösten, J.H.M. (Ed.): Soil Quality for Crop Production and Ecosystem Health, Developments in Soil Science, Elsevier, 1997.

Wu, C., Wu, H., Liu, D., Han, G., Zhao, P., and Kang, Y.: Crab bioturbation significantly alters sediment microbial composition and function in an intertidal marsh, Estuarine, Coastal and Shelf Science, 249, 107116, https://doi.org/10.1016/j.ecss.2020.107116, 2021.

Yair, A.: Short and long term effects of bioturbation on soil erosion, water resources and soil development in an arid environment, Geomorphology, 13, 87–99, https://doi.org/10.1016/0169-555X(95)00025-Z, 1995.

Yoo, K. and Mudd, S. M.: Toward process-based modeling of geochemical soil formation across diverse landforms: A new mathematical framework, Geoderma, 146, 248–260, https://doi.org/10.1016/j.geoderma.2008.05.029, 2008.

Yoo, K., Amundson, R., Heimsath, A. M., and Dietrich, W. E.: Process-based model linking pocket gopher (Thomomys bottae) activity to sediment transport and soil thickness, J. Geophys. Res., 33, 917, https://doi.org/10.1130/G21831.1, 2005.

Yu, C., Zhang, J., Pang, X. P., Wang, Q., Zhou, Y. P., and Guo, Z. G.: Soil disturbance and disturbance intensity: Response of soil nutrient concentrations of alpine meadow to plateau pika bioturbation in

the Qinghai-Tibetan Plateau, China, Geoderma, 307, 98–106, https://doi.org/10.1016/j.geoderma.2017.07.041, 2017.

Zevenbergen, L. W. and Thorne, C. R.: Quantitative analysis of land surface topography, Earth Surf. Process. Landforms, 12, 47–56, https://doi.org/10.1002/esp.3290120107, 1987.

Zhang, Q., Li, J., Hu, G., and Zhang, Z.: Bioturbation potential of a macrofaunal community in Bohai Bay, northern China, Marine pollution bulletin, 140, 281–286, https://doi.org/10.1016/j.marpolbul.2019.01.063, 2019.

Zhang, S., Fang, X., Zhang, J., Yin, F., Zhang, H., Wu, L., and Kitazawa, D.: The Effect of Bioturbation Activity of the Ark Clam Scapharca subcrenata on the Fluxes of Nutrient Exchange at the Sediment-Water Interface, J. Ocean Univ. China, 19, 232–240, https://doi.org/10.1007/s11802-020-4112-2, 2020.

Supplementary material

Table 5.A1: R^2 and RMSE of random forest models trained for the prediction of soil properties needed for model parametrization. RMSE is root mean square error.

Variable	R^2	RMSE
Soil water content	0.80	0.05
Bulk density	0.60	0.22
Porosity	0.63	0.09
Silt	0.64	0.04
Middle silt	0.64	0.04
Sand	0.68	0.09
Middle sand	0.64	0.05
Organic components	0.77	0.05
Organic carbon	0.70	0.03

Table 5.A2. Model sensitivity analysis. For the analysis, the minimum, maximum and mean value of each parameter was calculated. The model was run for a catchment of 1km^2 with homogenous mean parameters. Then, the minimum and maximum values of each parameter were tested. Each parameter was stepwise changed to its minimum or maximum value while the remaining parameters stayed homogenous. The significance of the parameter was estimated by a t-test conducted between the erosion estimated by the model with homogenous mean parameters and the erosion estimated by the model with varying minimum and maximum parameter values. Only significant parameters are shown.

Abbreviation	Parameter	mean value	min value	max value	mean erosion	min erosion	max erosion
R	precipitation	19.9	0.2	65.6	0.07	0	4.1
P_c	clay content	10.61	3.87	34.64	0.07	0.07	0.07

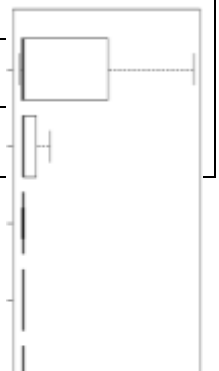

P_z	silt content	38.49	13.32	59.59	0.07	0.04	0.11	
P_s	sand content	47.04	24.13	79.17	0.07	0.07	0.07	
theta_init	water content	3.87	2.38	12.68	0.07	0.09	0.06	
n_s	roughness	0.97	0	236.75	0.07	0.34	0.01	
GC	vegetation	79.54	50.38	92.48	0.07	0.01	0.004	
DEM	Slope of DEM	18.21	0	89.78	0.07	0	inf.	Erosion in kg m^{-1}

Table 5.A3. Summary of GAM models. We analyzed the impact of parameters within a 1-meter and 10-meter distance from burrows. The Stars indicate p-values of the selected parameters. p*** < 0.001, p** < 0.01, p* < 0.05, p. < 0.1. One GAM model was run per parameter. Only results for models with an explained variance above 5 % are shown.

Parameters	Within 1 meter from burrows				Within 10 meters from burrows			
	PdA	SG	LC	NA	PdA	SG	LC	NA
Explained Variance	3.8 %	37 %	46 %	42 %	2.0 %	13 %	52 %	73 %
Burrow density	.				.			
Elevation			***	***	*		*	***
Slope		***					*	**
Aspect	.	**		*	*			.
Roughness		***					**	*
TPI								
TRI		**		**				
Plan curvature		.						.
Profile curv.		**	.					
NDVI			**			**		.
Sinks			*	***	*		*	
Wetness				**				
Flow direction								
Flow path								
Catchment		*			*			

Catchment slope		***		.				

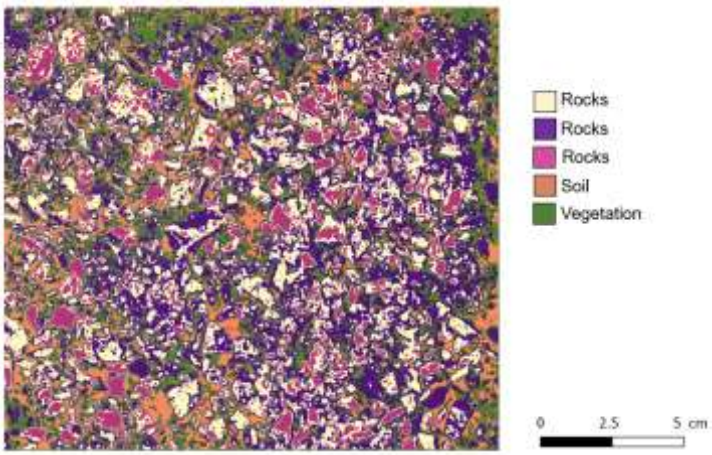

Figure 5.A1. Example of the unsupervised k-means classification of the surface photo from La Campana. The collection of in-situ data is explained in section 3.1., the estimation of soil properties in section 3.2. The image was classified into 5 classes using unsupervised k-means classification; the land cover was then assigned manually. In some cases, like in this case for rocks, multiple k-means classes stand for the same land cover. These were then unified to the class “rocks”.

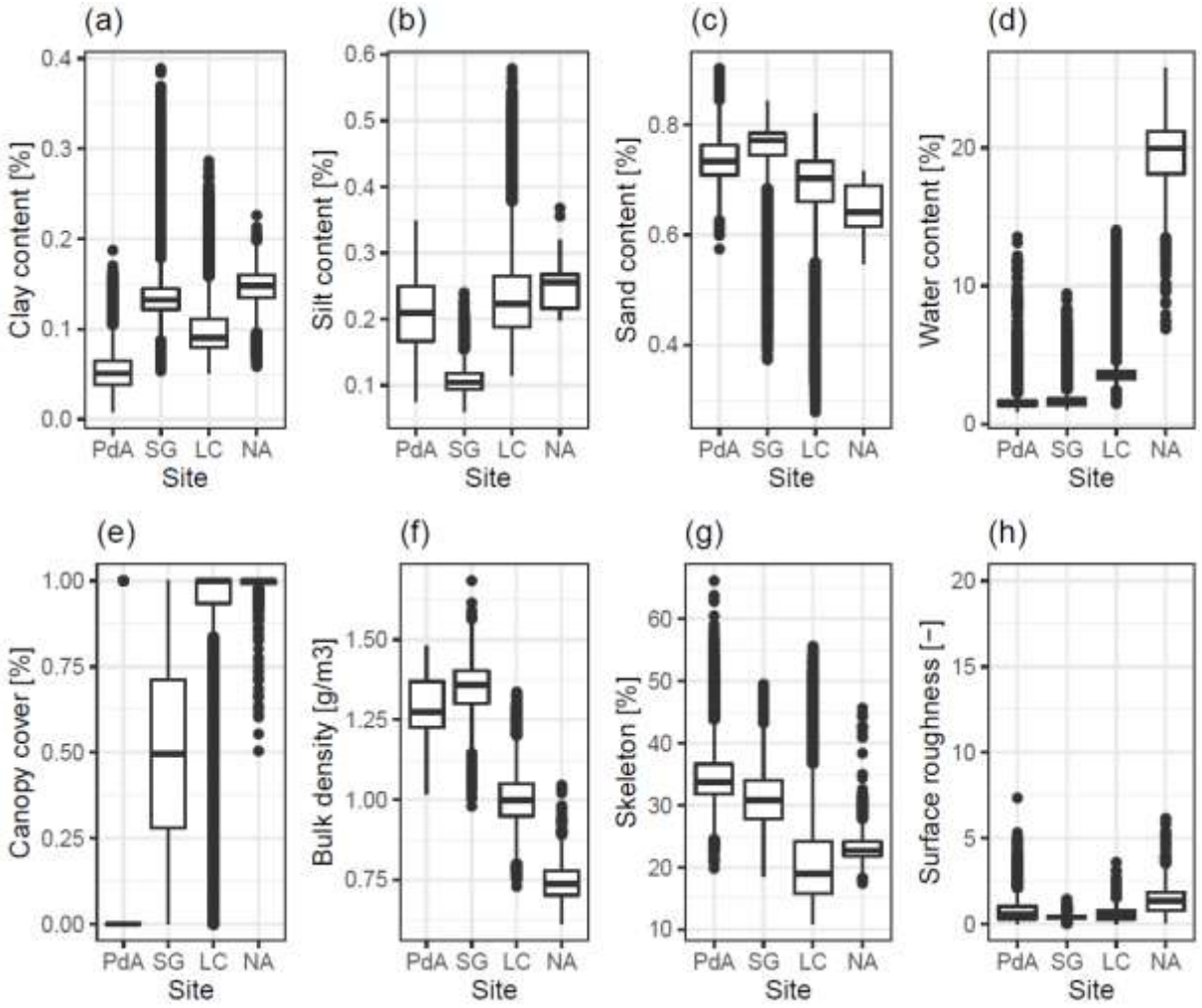

Figure 5.A2. Input parameter values per site. The barplots show all pixel values within the researched catchments for each site. The seemingly black lines outside of whiskers are as well outliers.

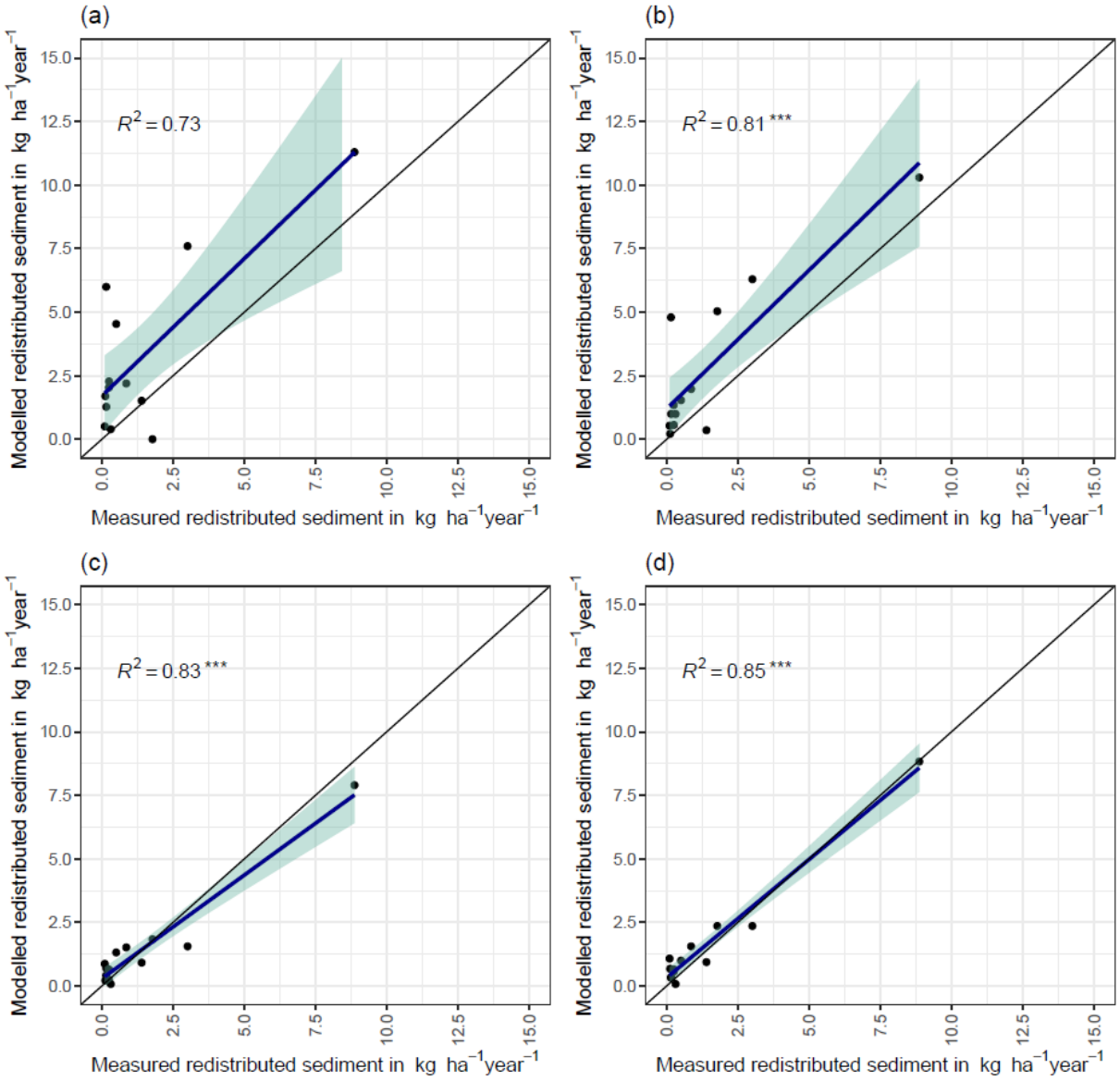

Figure 5.A3. Measured and modelled redistributed sediment for different scenarios. (a) Model without bioturbation. (b) Model with entrances. (c) Model with mounds. (d) model with burrows.

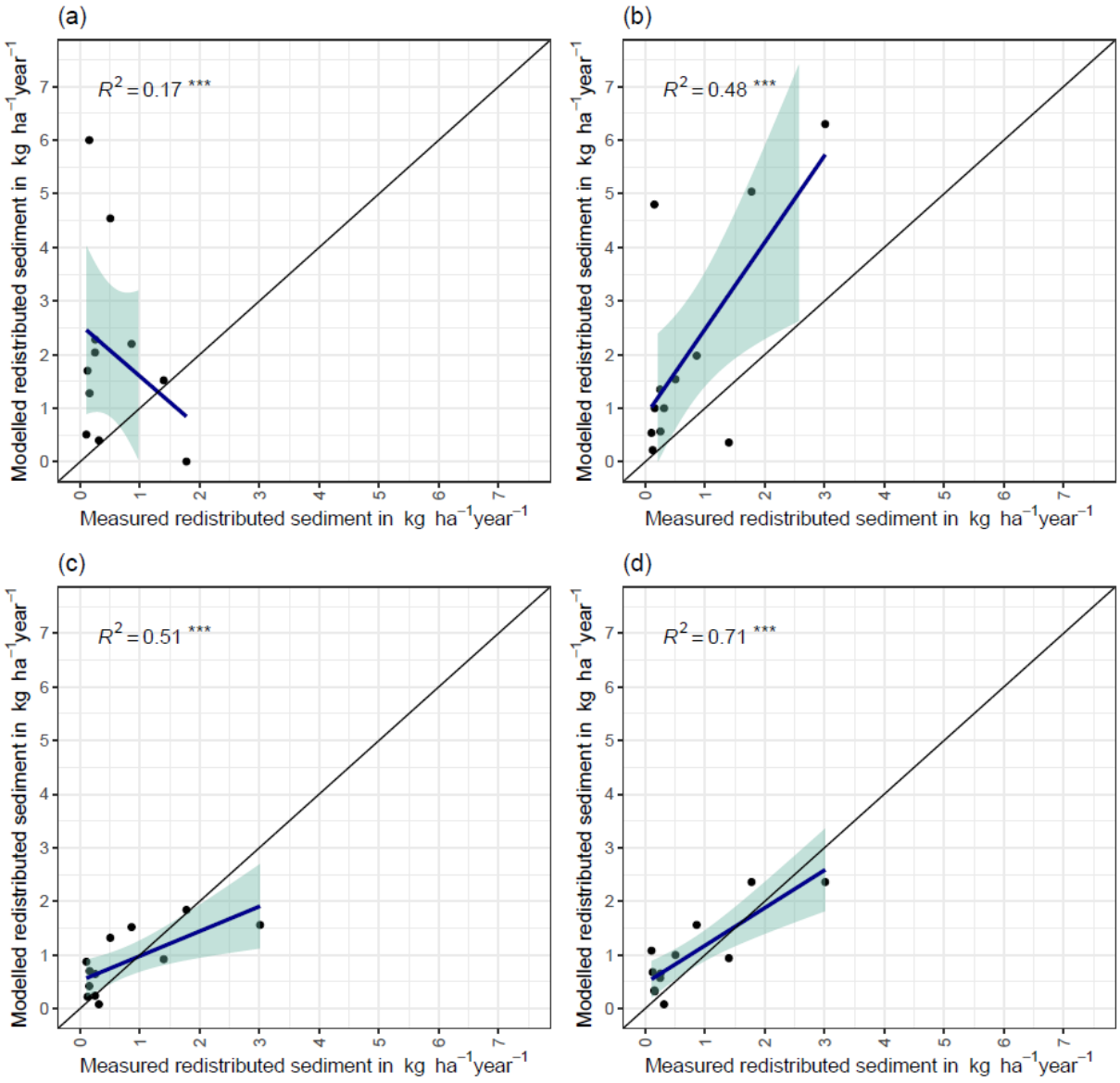

Figure 5.A4. Measured and modelled redistributed sediment without an outlier. (a) Model without bioturbation. (b) Model with entrances. (c) Model with mounds. (d) model with burrows.

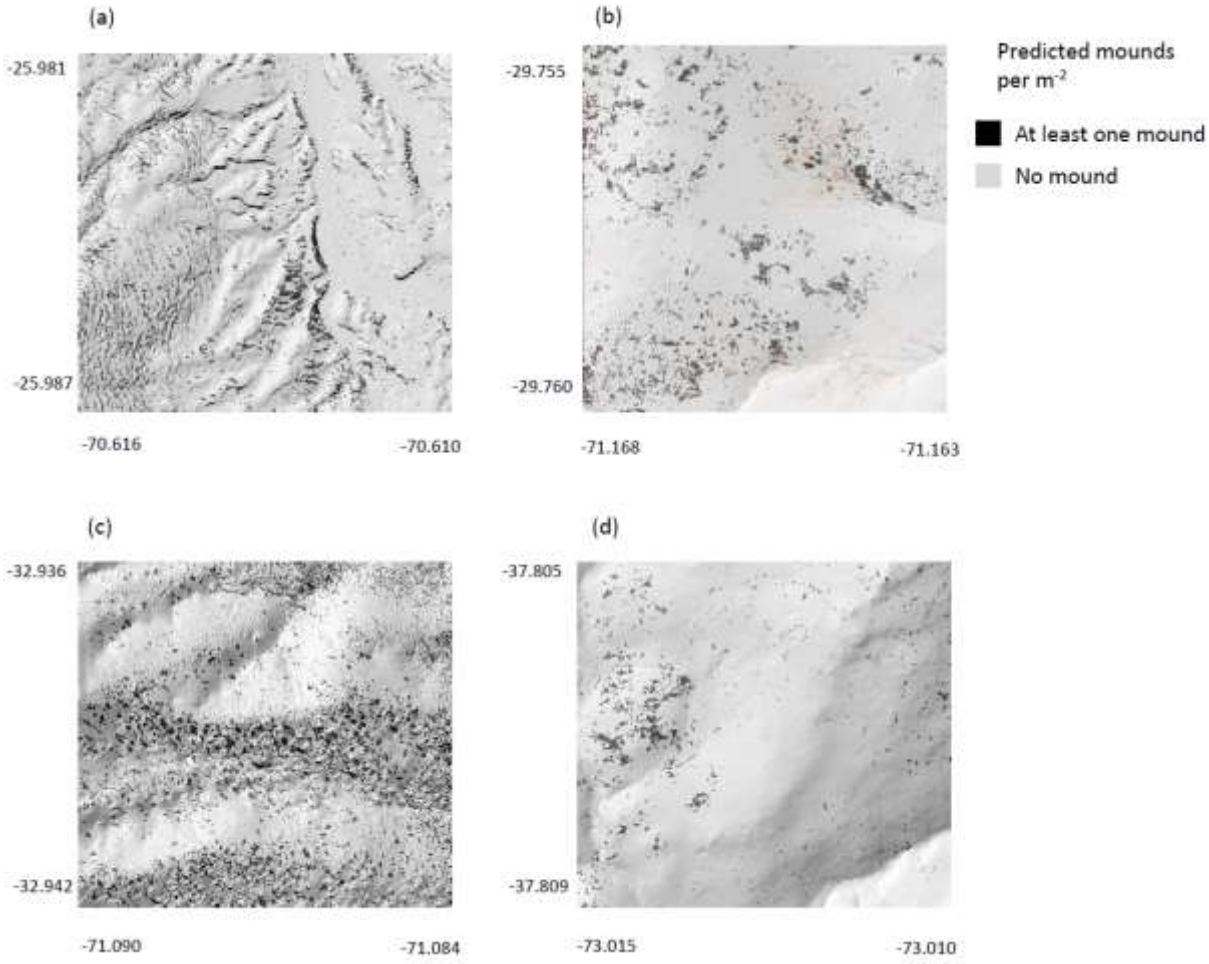

Figure 5.A5. Predicted mounds in all climate zones. (a) Pan de Azúcar, (b) Santa Gracia, (c) La Campana, (d) Nahuelbuta.

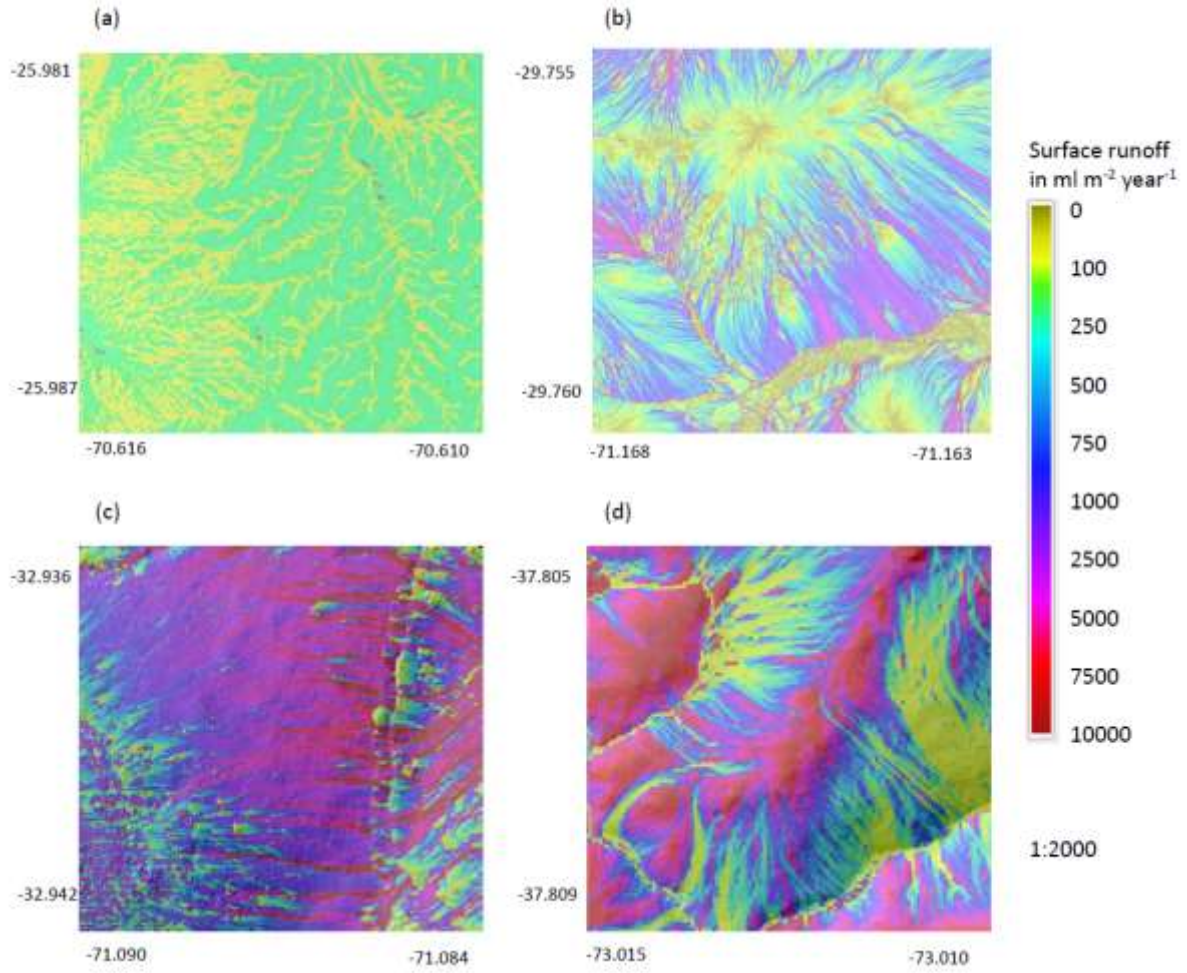

Figure 5.A6. Catchment-wide predicted surface runoff. Colors indicate surface runoff. (a) Pan de Azúcar, (b) Santa Gracia, (c) La Campana, (d) Nahuelbuta.

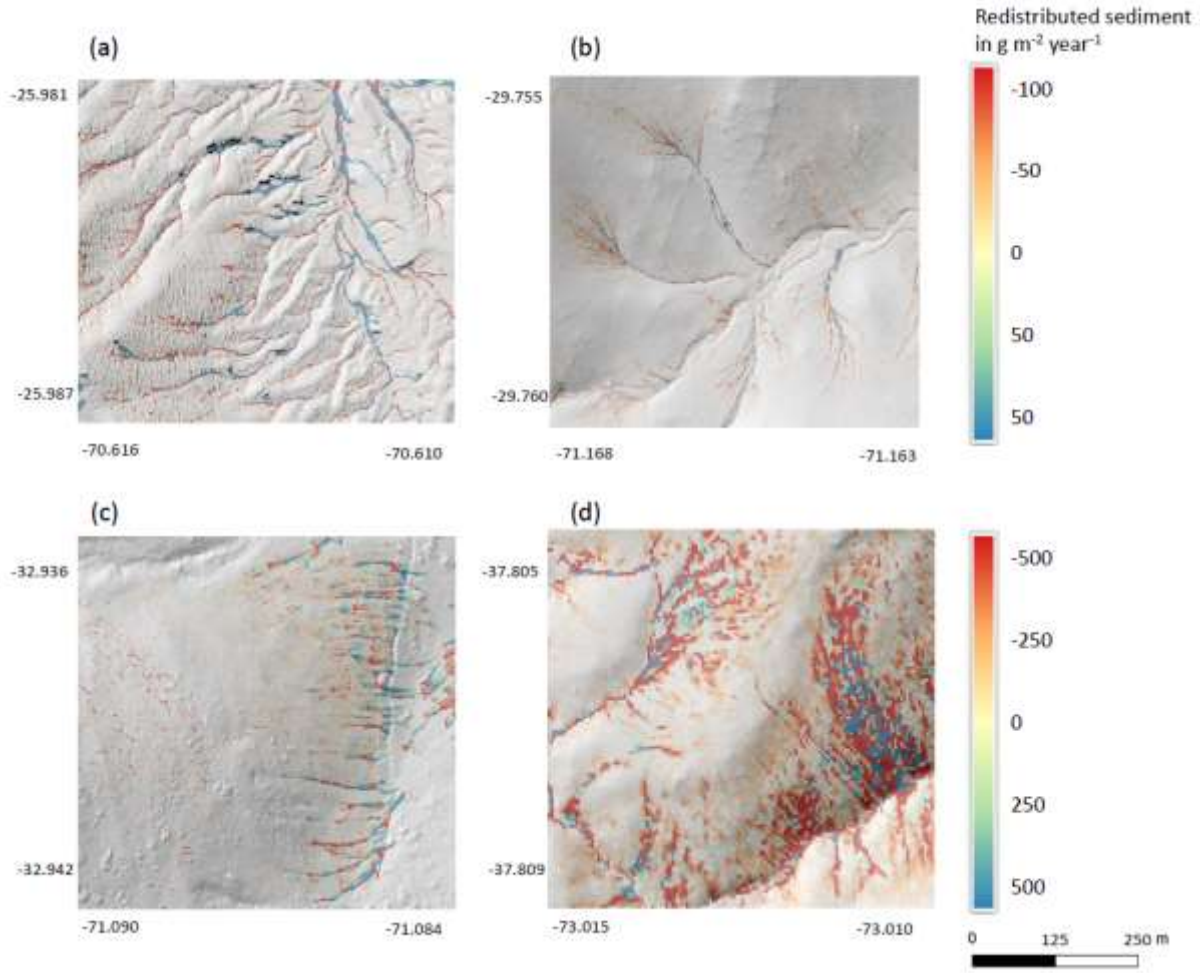

Figure 5.A7. Catchment-wide predicted sediment redistribution. Colours indicate sediment redistribution. Positive values indicate sediment accumulation; negative values indicate sediment erosion. Grey shadows indicate the hill shading. (a) Pan de Azúcar, (b) Santa Gracia, (c) La Campana, (d) Nahuelbuta.

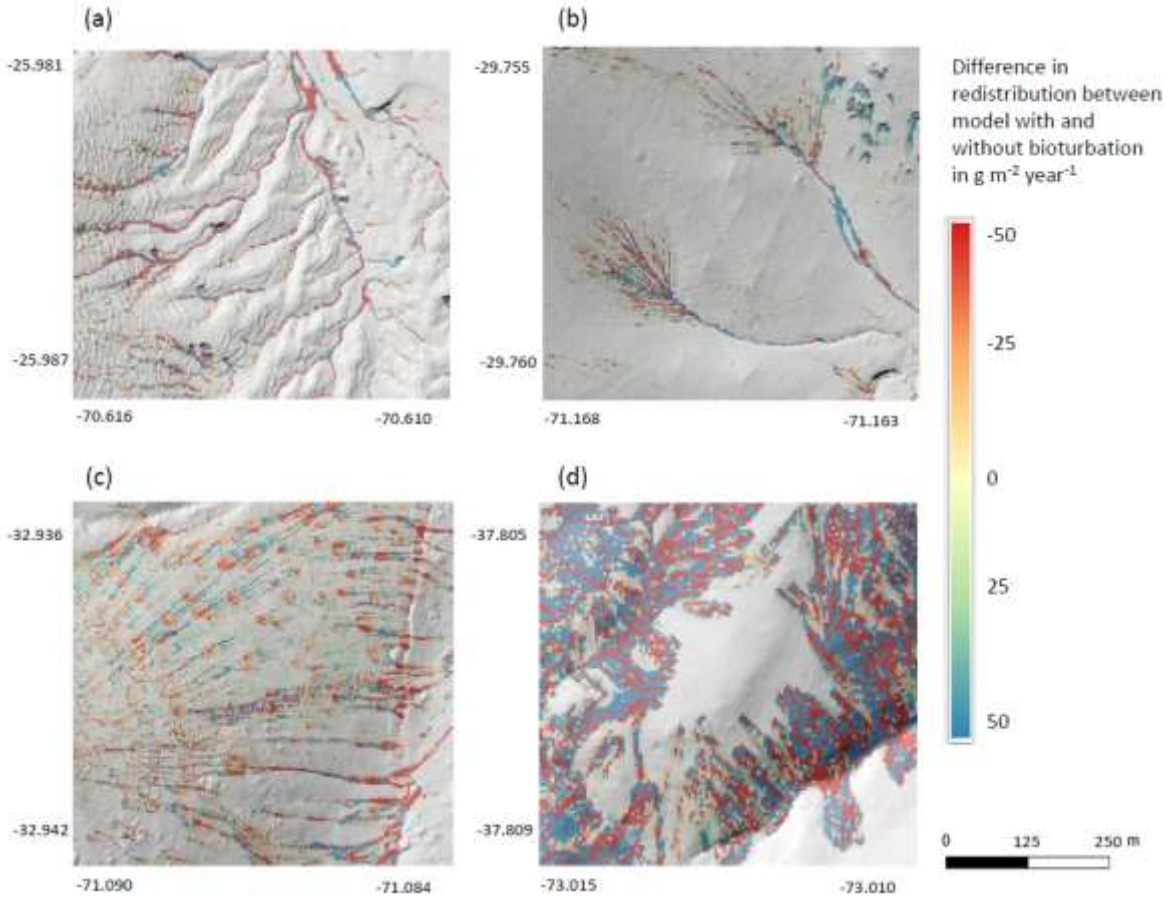

Figure 5.A8. Catchment-wide impact of bioturbation on sediment redistribution. Colour indicates the impact. Positive values indicate bioturbation enhanced sediment accumulation, negative values indicate bioturbation enhanced sediment erosion. Grey shadows indicate the hill shading. (a) Pan de Azúcar, (b) Santa Gracia, (c) La Campana, (d) Nahuelbuta.

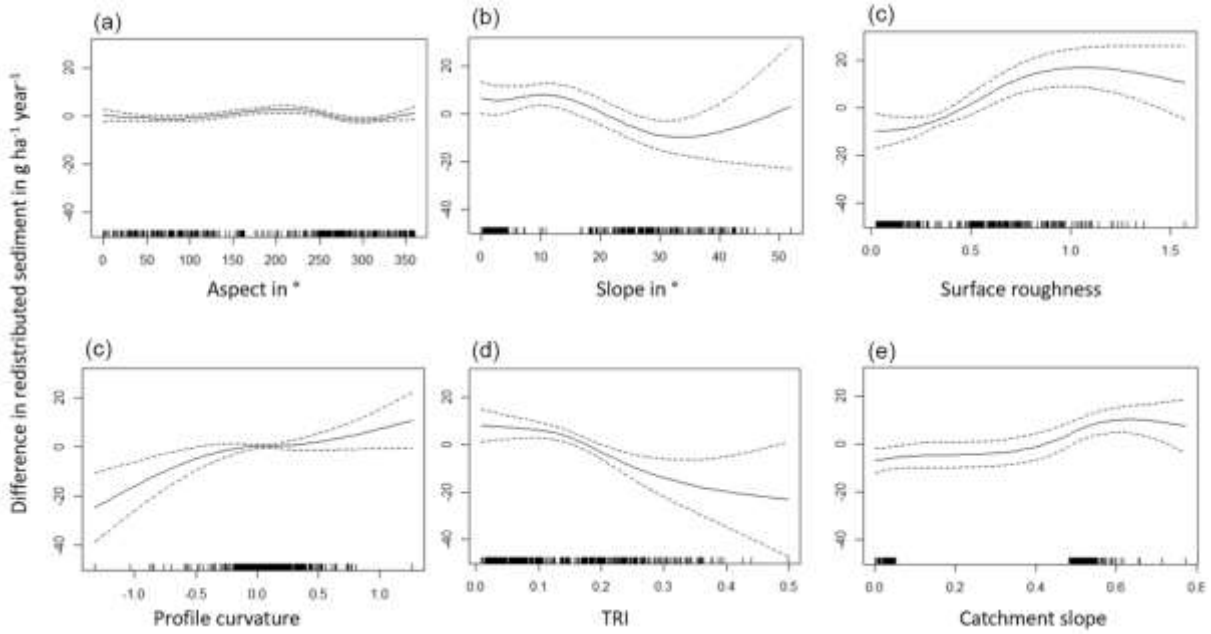

Figure 5.A9. Environmental parameters influencing impact of bioturbation on sediment redistribution in Santa Gracia within 1-meter distance from burrows. Positive values indicate bioturbation enhances sediment accumulation at the respective parameter values, negative values indicate bioturbation enhances sediment erosion at the respective parameter values.

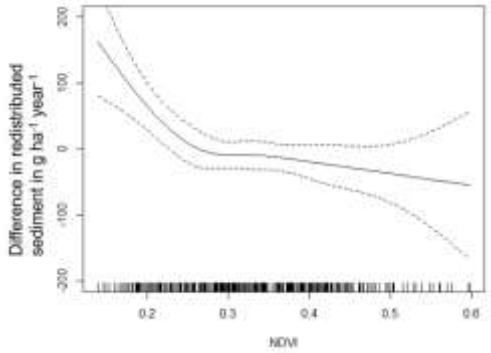

Figure 5.A10. Environmental parameters influencing impact of bioturbation on sediment redistribution in Santa Gracia within 10-meter distance from burrows. Positive values indicate bioturbation enhances sediment accumulation at the respective parameter values, negative values indicate bioturbation enhances sediment erosion at the respective parameter values.

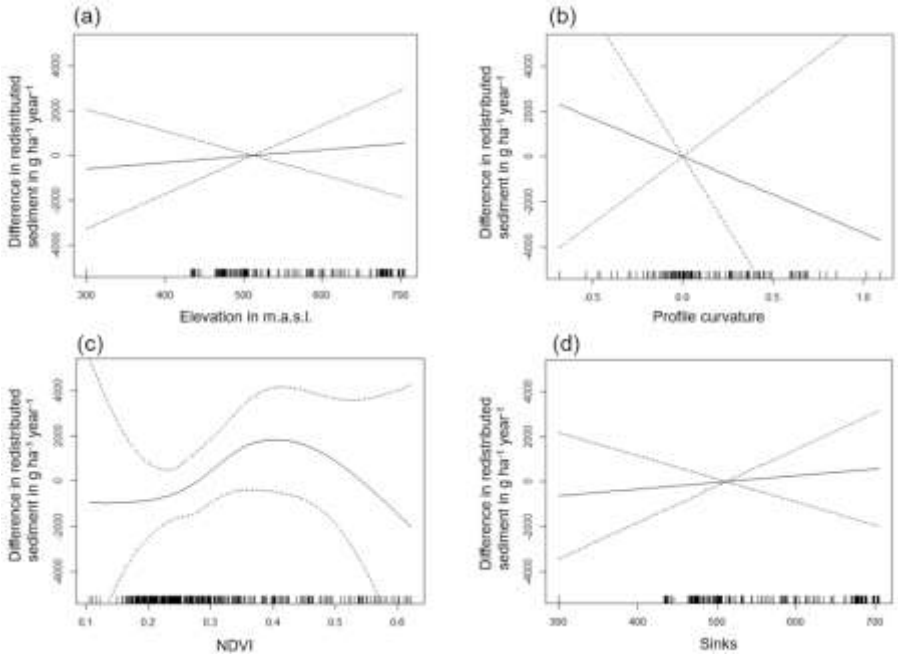

Figure 5.A11. Environmental parameters influencing impact of bioturbation on sediment redistribution in La Campana within 1-meter distance from burrows. Positive values indicate bioturbation enhances sediment accumulation at the respective parameter values, negative values indicate bioturbation enhances sediment erosion at the respective parameter values.

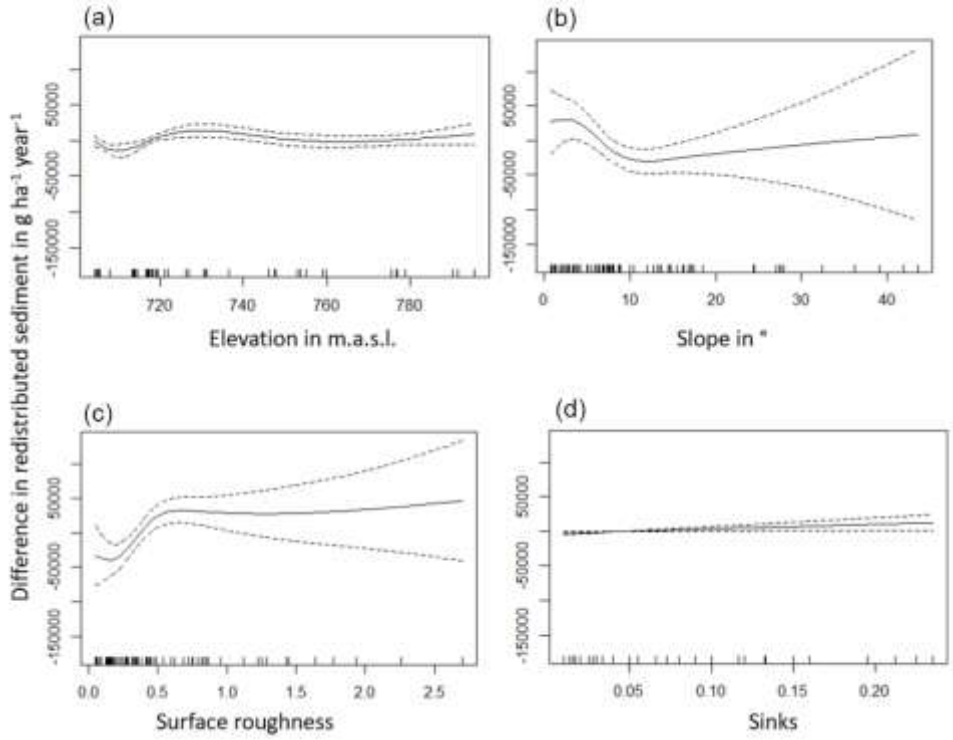

Figure 5.A12. Environmental parameters influencing impact of bioturbation on sediment redistribution in La Campana within 10-meter distance from burrows. Positive values indicate bioturbation enhances sediment accumulation at the respective parameter values, negative values indicate bioturbation enhances sediment erosion at the respective parameter values.

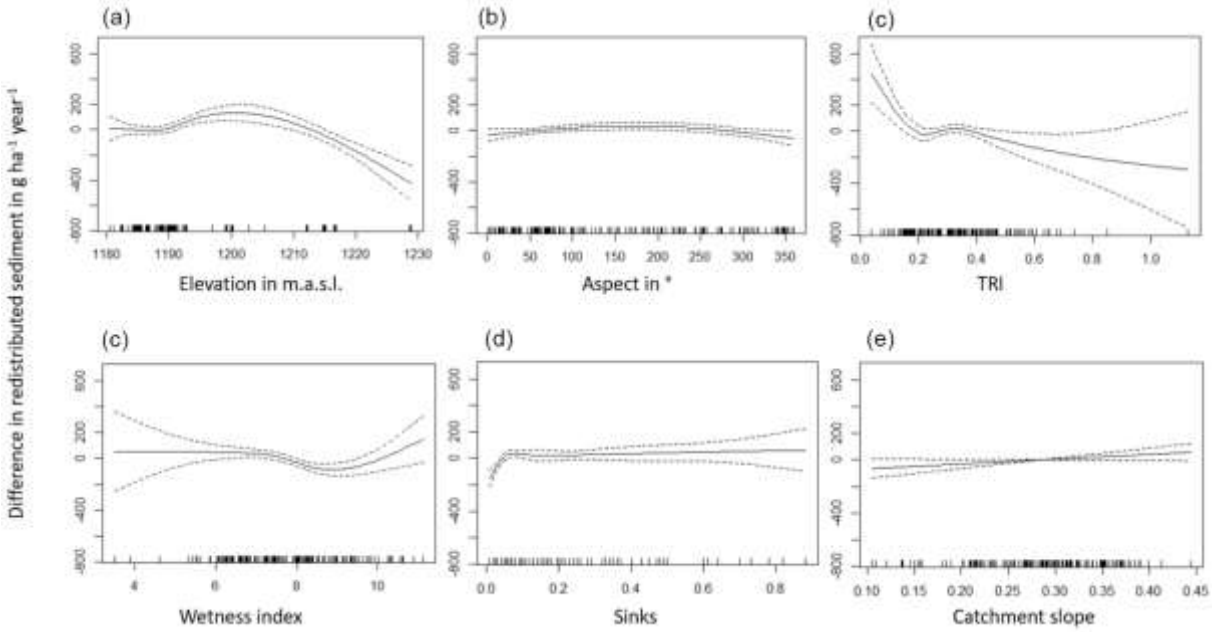

Figure 5.A13. Environmental parameters influencing impact of bioturbation on sediment redistribution in Nahuelbuta 1-meter distance from burrows. Positive values indicate bioturbation enhances sediment accumulation at the respective parameter values, negative values indicate bioturbation enhances sediment erosion at the respective parameter values.

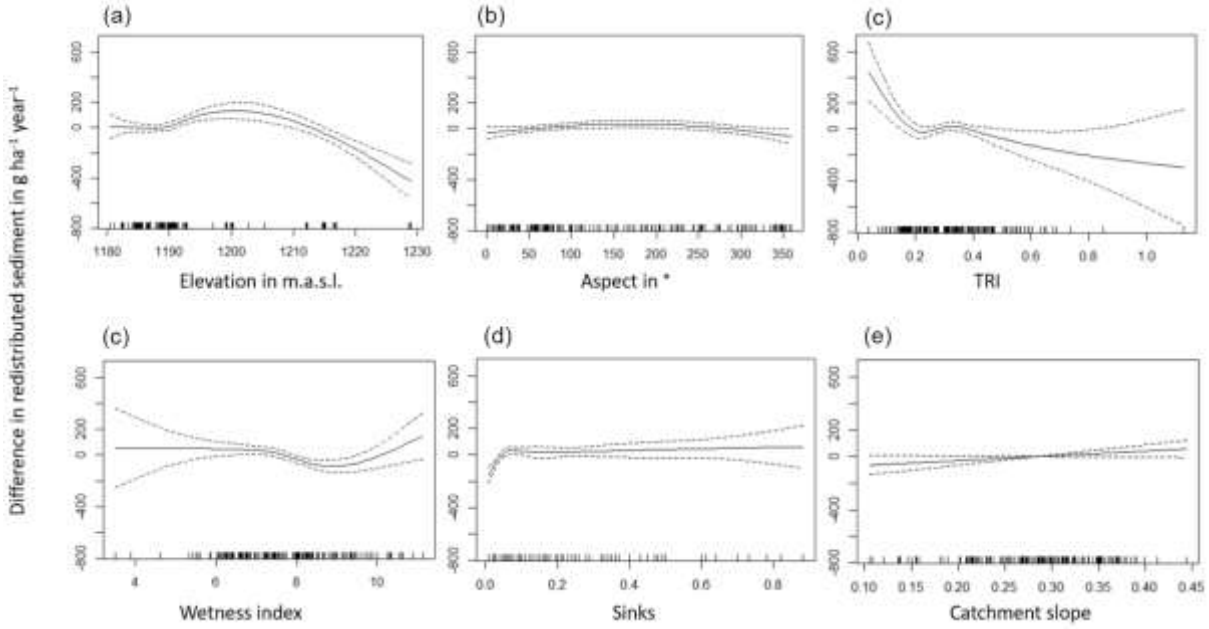

Figure 5.A14. Environmental parameters influencing impact of bioturbation on sediment redistribution in Nahuelbuta 10-meter distance from burrows. Positive values indicate bioturbation enhances sediment accumulation at the respective parameter values, negative values indicate bioturbation enhances sediment erosion at the respective parameter values.

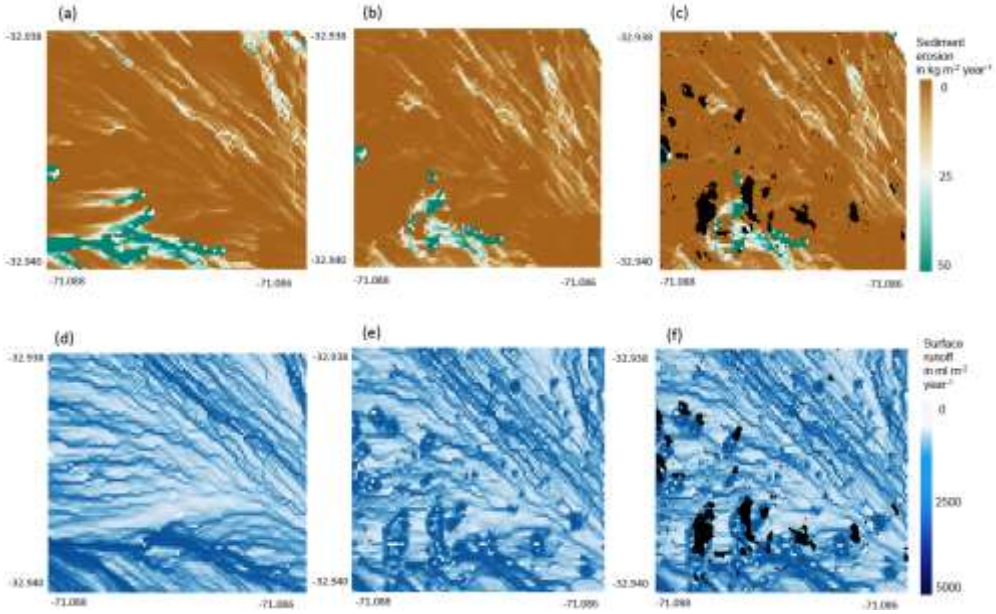

Figure 5.A15. Burrow aggregation concentrates the runoff and increases erosion. Example for the north-facing hillside in Mediterranean La Campana for the time period of one year. (a) Sediment erosion as estimated by model without bioturbation. (b) Sediment erosion as estimated by model with bioturbation. (c) Sediment erosion as estimated by model with bioturbation with predicted burrow locations. (d) Surface runoff as estimated by model without bioturbation. (e) Surface runoff as estimated by model with bioturbation. (f) Surface runoff as estimated by model including bioturbation and predicted burrow locations. Black colour indicates, at least one burrow was located within this pixel. Four neighbouring pixels which contain a burrow form a burrow aggregation.

6. Conclusion

In my thesis I analysed the interplay between burrow distribution (WP1, section 3), bioturbator-driven redistribution (WP2, section 4), surrounding environment and impact of bioturbation on catchment-wide rainfall-driven sediment redistribution (WP3, section 5).

6.1 Hypothesis

To study these interplays, I set up 4 hypotheses:

My results confirmed the H1, distribution of burrows created by bioturbating animals depends on vegetation patterns (WP1, section 3 and 5). The density of burrows created by bioturbating animals was predicted the best by in-situ measured vegetation cover as well as by the diameter and height of shrubs. In the arid and semi-arid climate zone, cacti height and coverage were important predictors while in the humid zone, rather tree trunk diameter and coverage were selected by the model. However, as well the biodiversity of the plants was important in all climate zones. When predicting the density of burrows using UAV images, vegetation heterogeneity indices were important. The density of vertebrate burrows increased with the shrub, herb and cacti cover in all climate zones and decreased with the tree canopy cover in the humid climate zone. The density of invertebrate burrows was higher in rockier areas with less vegetation in all sites (section 3). Lastly, the vegetation index describing high leaf area index was an important predictor. The burrow distribution was catchment-wide best predicted by WorldView-2 NIR band and NDVI as well as single vegetation land cover classes. The topography features calculated from LiDAR data were not selected as important predictors, except for aspect (section 5).

My thesis partially confirms the hypothesis H2, saying that bioturbator-driven sediment redistribution depends on the rainfall-driven redistribution (WP2, section 4). An increased amount of sediment excavation by the animal was observed immediately after rainfall events in the Mediterranean climate zone: Here, the animals were observed to reconstruct their burrows after the rainfall while simultaneously excavate more additional sediment to the surface. In the arid climate zone, the sediment excavation was mostly not proceeded by a rainfall event. Additionally, to the dependence on rainfall-triggered sediment redistribution, bioturbator-driven sediment redistribution as well depended on the season. The multi-daily monitoring of burrows identified a time period from Mai until August, during which the animals more actively excavate the sediment to the surface. However, even from September until April, rainfall event was still followed by the animal excavating more sediment to the surface.

The results confirmed H3 saying that surrounding environment determined the magnitude of the burrow' impact on the catchment-wide rainfall-driven sediment redistribution (WP3, section 5). The results showed, that most determining environmental parameters were elevation, surface roughness and inclination as well as vegetation cover derived from NDVI. Bioturbation increased sediment erosion in areas where erosional processes dominate (high elevation, high inclination, low surface roughness, low vegetation cover); and similarly increased sediment accumulation in areas where sediment is naturally deposited (high surface roughness, high vegetation cover, low inclination)

My results partially confirmed the hypothesis H4 saying, that bioturbation increases sediment erosion. Bioturbation increased sediment erosion in all but humid climate zone. The multi-daily monitoring of burrows revealed an increase in erosion of over 300% when compared to burrow embedding areas

(section 4). According to the output of the soil erosion model, bioturbation increased erosion the most in the Mediterranean zone, followed by arid and semi-arid zone. The impacts of bioturbation were not significant in the humid zone (section 5).

6.2 Suitability of the applied methods

In the first working package, I used UAV images and WorldView-2 data to predict the catchment-wide density and distribution of burrows created by bioturbating animals. The most suitable model was random forest, applied with predictors estimated from WorldView-2 data.

My study showed that Time-of-Flight cameras are a suitable technique to monitor surface changes at a very high spatial and temporal resolution. Our approach with multi-daily monitoring of 4 frames per day was shown to be suitable to distinguish between bioturbator-driven and rainfall-driven sediment redistribution. However, due to backscattering of sunlight, the quality of frames taken at night was higher.

In the third working package, I integrated bioturbation into a soil erosion model by adjusting the input parameters at predicted burrow locations. This approach allowed to integrate bioturbation into the model without predefining its impacts on the redistribution during the model parametrisation. The inclusion of bioturbation increased the accuracy of the modelled sediment redistribution. Already the inclusion of solely burrow entrances or mounds significantly improved the model. The best results were obtained when the burrow structures; including the burrow topography, soil properties and impacts on surrounding vegetation; were integrated into the model parametrisation. The results were similar for all climate zones and thus did not depend on the position of the sediment fence used for validation.

6.3 New contributions

My thesis closes several research gaps and provides new insights regarding the interplay between bioturbation, sediment redistribution and environment:

Within WP1, I showed that the density of bioturbator's burrows does not only depend on vegetation and rock cover as previously assumed, but also on vegetation height, diversity and heterogeneity. Additionally, I found out that the vegetation patterns determining burrow distribution differ along the climate gradient.

Within WP2, I unveiled the dynamics between bioturbator-driven and rainfall-driven sediment redistribution. My results showed that the animals excavate new sediment to the surface after each rainfall event - a dynamic previously not known, which up until now consecutively lead to an underestimation of the impacts of bioturbation on sediment redistribution by previous authors.

Within WP3, I estimated, analysed and compared the catchment-wide impacts of bioturbation on sediment redistribution along the climate gradient. I found out that bioturbation increases sediment erosion as previously assumed. However, the magnitude of their impact varies along the climate gradient and is not significant in the humid zone. In contrast to previous studies, I was capable to analyse the impacts of bioturbation within a spatial context – The output of my model showed that bioturbation does not uniformly increase erosion throughout the catchment. Lastly, I was able to identify the environmental parameters which cause this variation throughout the catchment.

Additionally, my thesis showed possibilities of several previously not tested methods:

Within WP1, I predicted the density and distribution of burrows into the area in catchments largely covered by canopy. This approach was previously not tested, as the mapping of bioturbators burrows was limited to catchments with no or low vegetation cover. Within WP2, I, for the first time, used Time-of-Flight technology, which I integrated into a camera system, to monitor surface changes at a very high spatial and temporal resolution. Within WP3, I tested in the field the suitability of sediment fences constructed of geotextile for the validation of my model. Additionally, I, for the first time, integrated vertebrate burrow structures into a soil erosion model as well as the seasonality and variability of their burrowing behaviour. Lastly, no previous authors estimated the impacts of bioturbation on sediment redistribution at such a high spatial (0.5 m) and temporal (daily) resolution for such a long time period (6 years).

6.4 Perspectives and future investigations

The here used methods and results can be further improved and integrated into studies researching long-term impacts of bioturbation on sediment redistribution.

Approaches combining remote sensing and machine learning were previously shown to be a suitable technique for mapping of vegetation parameters (Sprot et al. 2021, Holden et al. 2021, Puliti et al. 2018). I propose a future study might concentrate to combine UAV, airborne and satellite remote sensing images, which might make it possible to upscale burrow distribution into the whole catchments at a higher accuracy. After being the first to test Time-of-Flight based cameras for surface monitoring, further investigations need to be done for multi-annual time period and within areas not only embedding burrows but without any visible sign of burrowing activity within a distance. However, an approach needs to be developed to deal with the light backscattering during daytime.

To estimate long-term impacts, bioturbation needs to be integrated into landscape evolution models. First attempts to include bioturbation into these models were done previously (Temme and Vanwalleghem, 2016; Yoo and Mudd, 2008; Pelletier et al., 2013). However, a uniform distribution and uniform spatial and temporal impact of bioturbation was precoded in these models. My results showed that the impacts of bioturbation on sediment redistribution are not temporally and spatially uniform and distribution of bioturbation is not uniformly positively associated with vegetation. To realistically upscale long-term impacts of bioturbation, and estimate how bioturbation affect habitats, influence weathering processes and shape the landforms, the spatial and temporal variations estimated within this thesis need to be considered.

References

Pelletier, J. D., Barron-Gafford, G. A., Breshears, D. D., Brooks, P. D., Chorover, J., Durcik, M., Harman, C. J., Huxman, T. E., Lohse, K. A., Lybrand, R., Meixner, T., McIntosh, J. C., Papuga, S. A., Rasmussen, C., Schaap, M., Swetnam, T. L., and Troch, P. A.: Coevolution of nonlinear trends in vegetation, soils, and topography with elevation and slope aspect: A case study in the sky islands of southern Arizona, J. Geophys. Res. Earth Surf., 118, 741–758, https://doi.org/10.1002/jgrf.20046, 2013.

Temme, A. J.A.M. and Vanwalleghem, T.: LORICA – A new model for linking landscape and soil profile evolution: Development and sensitivity analysis, Computers & Geosciences, 90, 131–143, https://doi.org/10.1016/j.cageo.2015.08.004, 2016.

Vanwalleghem, T., Stockmann, U., Minasny, B., and McBratney, A. B.: A quantitative model for integrating landscape evolution and soil formation, J. Geophys. Res. Earth Surf., 118, 331–347, https://doi.org/10.1029/2011JF002296, 2013.

Yoo, K. and Mudd, S. M.: Toward process-based modeling of geochemical soil formation across diverse landforms: A new mathematical framework, Geoderma, 146, 248–260, https://doi.org/10.1016/j.geoderma.2008.05.029, 2008.

Zusammenfassung

Die Grabaktivität terrestrischer Bioturbatoren beeinflusst die Mikrotopographie, Rauheit der Oberfläche die physikalischen Eigenschaften des Bodens. Durch die Umarbeitung von Sedimenten erhöhen Bioturbatoren die Durchlässigkeit und Porosität des Bodens, was zu Auswirkungen auf die Infiltrations- und Erosionsraten führt. Der Bau von unterirdischen Gängen verteilt und konzentriert Nährstoffe und wirkt sich besonders positiv auf die Kohlenstoffspeicherung im Boden aus.Frühere Studien haben mehrere Forschungslücken offen gelassen. Die Studien konzentrierten sich nur auf die Lebensraumpräferenzen der einzelnen Arten und berücksichtigten nicht die unterschiedliche Menge an ausgegrabenem Sediment und die Baudichte einzelner Arten. Es bleibt daher unklar, welche Umweltparameter innerhalb des Einzugsgebiets hauptsächlich mit der hohen Dichte und Verteilung aller vorhandenen Baute von Bioturbatoren zusammenhängen. Darüber hinaus ging die vorherigen Autoren nicht auf die tägliche Aushubdynamik des Sediments durch das Tier ein, ob und wie sie mit der durch einzugsgebietsweiten Niederschlag getriebenen Sedimentumverteilung zusammenhängt und wie viel Sediment die Bioturbatoren das ganze Jahr über an die Oberfläche austragen.

Meine Dissertation war Teil des EarthShape-Konsortiums mit der übergeordneten Forschungsfrage, wie die Mikroorganismen, Tiere und Pflanzen die Form und Entwicklung der Erdoberfläche beeinflussen. Die Studie wurde an vier Studienstandorten entlang der chilenischen Küstenkordilleren durchgeführt: aridem Pan de Azúcar, semi-aridem Santa Gracia, mediterranem La Campana und humidem Nahuelbuta. Der Arbeitsablauf bestand aus 3 Arbeitspaketen mit dem Endziel, die einzugsgebietsweiten Auswirkungen der Bioturbation zu bestimmen.

Innerhalb des ersten Arbeitspakets habe ich getestet, ob die Dichte der Höhlen und die Verteilung der Bauten durch Vegetationsmuster vorhergesagt werden können, die aus UAV- und WorldView-2-Daten berechnet wurden. Dann habe ich das beste Modell für eine einzugsgebietsweite Vorhersage verwendet. Innerhalb des zweiten Arbeitspakets habe ich getestet, ob die bioturbatorgetriebene Sedimentumverteilung von der niederschlagsgetriebenen Sedimentumverteilung abhängt. Zu diesem Zweck habe ich mehrere Time-of-Flight-basierte Kameras aufgestellt, die die Sedimentumverteilung auf der Grabenoberfläche und um den Graben herum überwachen. Im dritten Arbeitspaket habe ich die Bioturbation in ein Bodenerosionsmodell integriert. Dann habe ich den Einfluss der Bioturbatoren auf die Sedimentverteilung und die Umweltparameter bestimmt, die über das Ausmaß dieses Einflusses entscheiden.

Meine Ergebnisse zeigten, dass die Verteilung der von bioturbierenden Tieren geschaffenen Bauten hängt von Vegetationsmustern ab. Die Dichte der von bioturbierenden Tieren geschaffenen Höhlen wurde am besten durch die in-situ gemessene Vegetationsbedeckung sowie den Durchmesser und die Höhe der Sträucher vorhergesagt. In der ariden und semiariden Zone waren Kakteenhöhe und Bedeckung wichtige Prädiktoren, während in der feuchten Zone eher Baumstammdurchmesser und Bedeckung durch das Modell ausgewählt wurden. Aber auch die Artenvielfalt der Pflanzen war in allen Klimazonen wichtig. Bei der Vorhersage der Dichte von Höhlen unter Verwendung von UAV-Bildern waren ebenfalls Indizes der Vegetationsheterogenität wichtig. Die Dichte der Bauten nahm mit der Strauch-, Kräuter- und Kakteenbedeckung in allen Klimazonen zu und mit der Baumkronenbedeckung in der feuchten Klimazone ab. Die Dichte der Wirbellosenbauten war in felsigeren Gebieten mit weniger

Vegetation an allen Standorten höher. Schließlich war der Vegetationsindex, der einen hohen Blattflächenindex beschreibt, ein wichtiger Prädiktor. Die Bautenverteilung wurde im gesamten Einzugsgebiet am besten durch das WorldView-2 NIR-Band und NDVI sowie einzelne Vegetationslandbedeckungsklassen vorhergesagt. Die aus LiDAR-Daten berechneten Topografiemerkmale wurden nicht als wichtige Prädiktoren ausgewählt, mit Ausnahme des Aspekts.

Zweitens, die Ergebnisse zeigten, dass die durch Bioturbatoren ausgelöste Sedimentumverteilung von der durch Niederschlag ausgelösten Umverteilung abhängt. Unmittelbar nach Niederschlagsereignissen in der mediterranen Klimazone wurde ein erhöhter Sedimentaustrag durch die Tiere beobachtet: Hier wurde beobachtet, dass die Tiere nach den Regenfällen ihre Bauten rekonstruierten und gleichzeitig mehr zusätzliches Sediment an die Oberfläche gruben. Hingegen, in der ariden Klimazone ging dem Sedimentaustrag meist kein Niederschlagsereignis voraus.

Die Ergebnisse bestätigten, dass die Umgebung das Ausmaß der Auswirkungen des Grabens auf die durch Niederschläge ausgelöste Sedimentumverteilung im gesamten Einzugsgebiet bestimmt. Die Ergebnisse zeigten, dass die wichtigsten Umweltparameter Höhenlage, Oberflächenrauheit und -neigung sowie Vegetationsbedeckung, abgeleitet von NDVI, waren. Bioturbation erhöhte Sedimenterosion in Gebieten, in denen Erosionsprozesse dominieren (Überhang, starke Neigung, geringe Oberflächenrauhigkeit, geringe Vegetationsbedeckung); und ähnlich erhöhte Sedimentansammlung in Gebieten mit natürlicher Sedimentablagerung (hohe Oberflächenrauhigkeit, hohe Vegetationsbedeckung, geringe Neigung)

Das Modeloutput hat gezeigt, dass Bioturbation die Sedimenterosion verstärkt. Bioturbation verstärkte die Sedimenterosion in allen außer der humiden Klimazone. Die Überwachung der Bauten zeigte eine Zunahme der Erosion von über 300 % im Vergleich zu den Einbettungsbereichen der Bauten. Nach den Ergebnissen des Bodenerosionsmodells erhöhte die Bioturbation die Erosion am stärksten in der mediterranen Zone, gefolgt von der ariden und semiariden Zone. Die Auswirkungen der Bioturbation waren in der humiden Zone nicht signifikant.

Um langfristige Auswirkungen abzuschätzen, muss die Bioturbation in Landschaftsentwicklungsmodelle integriert werden. Allerdings wurde in diesen Modellen von einer gleichmäßigen Verteilung und räumlichen und zeitlichen Auswirkung der Bioturbation ausgegangen. Meine Ergebnisse zeigten, dass die Auswirkungen der Bioturbation auf die Sedimentumverteilung zeitlich und räumlich nicht einheitlich sind und die Verteilung der Bioturbation nicht einheitlich positiv mit der Vegetation assoziiert ist. Um die langfristige Auswirkungen der Bioturbation realistisch vorherzusagen, müssen die in dieser Arbeit geschätzten räumlichen und zeitlichen Variationen berücksichtigt werden.

Erklärung

Hiermit versichere ich, dass ich meine vorliegende Dissertation

(Titel einfügen)

selbstständig, ohne unerlaubte Hilfe Dritter angefertigt und andere als die in der Dissertation angegebenen Hilfsmittel nicht benutzt habe.

Alle Stellen, die wörtlich oder sinngemäß aus veröffentlichten oder unveröffentlichten Schriften entnommen sind, habe ich als solche kenntlich gemacht. Dritte waren an der inhaltlich-materiellen Erstellung der Dissertation nicht beteiligt; insbesondere habe ich hierfür nicht die Hilfe eines Promotionsberaters in Anspruch genommen.

Kein Teil meiner Dissertation wurde und wird in keinem anderen Promotions- oder Habilitationsverfahren verwendet und hat noch keinen sonstigen Prüfungszwecken gedient.

Mit dem Einsatz von Software zur Erkennung von Plagiaten bin ich einverstanden.

Declaration

I hereby affirm that I have prepared my present dissertation

(insert title)

Independently, without the unauthorized assistance of third parties and have not used any aids other than those specified in the dissertation.

I have marked as such all passages that are taken literally or in spirit from published or unpublished writings. Third parties were not involved in the content-material preparation of my dissertation; in particular, I did not use the support of a doctoral advisor for this purpose.

No part of my dissertation has been and will not be used in any other doctoral or postdoctoral procedures and has not yet served any other examination purposes.

I agree to the use of software for plagiarism detection.

Vorname Nachname
First name Family name _____

Datum, Unterschrift
Date, Signature _____

Curriculum Vitae

Paulina Grigusova
Rudolf-Breitscheid-Straße 15
35037 Marburg / Stadtwald
0176 822 845 27
grigusova.p@gmail.com

PRACTICAL EXPERIENCE

2019/05 – now **Philipps University Marburg**
Scientific Assistant within EarthShape project
• Processing and analysis of remote sensing data, with main focus on UAV, WorldView-2, Sentinel-2 data, point clouds, change detection
• Application of machine learning algorithms
• Field work in Chile (UAV flights and Time-Of-Flight cameras maintenance)
• Modelling of sediment redistribution
Supervision: Prof. Dr. Jörg Bendix

2017/09 – 2017/10 **German Research Centre for Geosciences, Potsdam**
Section 1.4. - Remote Sensing
Research Internship
• Processing and Analysis of RapidEye Data, with main focus on vegetation and agriculture data, with ArcMap, Erdas and R
• Atmospheric correction of optical satellite data with ATCOR
• Preprocessing, Testing and Optimizing of Algorithms in R
• Statistical Analysis of satellite and in-situ data with R
Supervision: Claudia Vallentin

2016/05 – 2016/09 **Project GlobE – Wetlands in East Africa**
Hydrology Research Group, University of Bonn
Student assistant
• Modelling of water fluxes and soil moisture dynamics with Hydrus-1D
• Simulating feedbacks between pedosphere, hydrosphere and biosphere
• Analysis of climate, soil water and soil-physical data
• Derivation of soil properties using pedotransfer functions
• Teaching experience
Supervision: Dr. Constanze Leemhuis, Geofrey Gabiri

EDUCATION

2019/05 – 2023/04	**Philipps University Marburg** **PhD in Geography** *Specialization:* Environmental modelling, Remote sensing *PhD thesis:* „Interplay between bioturbation, environment and sediment redistribution: New insights provided by combining remote sensing, machine learning and semi-empirical modelling" *Supervisor:* Prof. Dr. Jörg Bendix, Dr.A. Annegret Larsen (WUR Wageningen)
2016/10 - 2019/03	**Philipps University Marburg** **Master of Science in Physical Geography** *Specialization:* Environmental Informatics *Master thesis:* „Predicting multi-taxa plant and animal species diversity at Mount Kilimanjaro using Sentinel-2 data" *Supervisor:* Prof. Dr. Thomas Nauss
2012/10 – 2016/04	**Rheinish Friedrich Wilhelm University Bonn** **Bachelor of Science in Geography** *Specialization:* Environmental Modelling and Hydrology *Bachelor thesis:* „Modelling water-fluxes and soil moisture dynamics in a wetland in Uganda " *Supervisor:* Prof. Dr. Bernd Diekkrüger

EXTRACURRICULUM ACTIVITIES

2020/12 - now	Society for tropical ecology	Scientific board member
2020/05 - now	University of Marburg	Representative for international students
2020/12 – 2022/06	Hessen mentoring	Mentee within ProAcademia program
2018/04 - 2018/12	Portal Mauerstraße, Marburg	Support for refugee families
2014/09 - 2016/09	UNICEF	Student working group Bonn
2013/10 – 2016/09	Connexxion e.V. Bonn	Support for international students
2013/08 – 2013/10	Cape Town / South Africa	Support in social and ecological projects

Language skills	Slovak	native speaker
	German	near native/fluent (C2)
	English	excellent command (C1)
GIS – Skills	ArcGIS, QGIS	
Programming skills	R	expert
	Python	advanced
	IDL	beginner
Hobbies	Rock climbing, paragliding, camping, yoga	

LIST OF PUBLICATIONS

Grigusova, P.; Larsen, A.; Achilles, S.; Klug, A.; Fischer, R.; Kraus, D.; Übernickel, K.; Paulino, L.; Pliscoff, P.; Brandl, R.; Farwig, N.; Bendix, J. Area-Wide Prediction of Vertebrate and Invertebrate Hole Density and Depth across a Climate Gradient in Chile Based on UAV and Machine Learning. Drones 2021, 5, 86. https://doi.org/10.3390/drones5030086

Grigusova, P., Larsen, A., Achilles, S., Brandl, R., del Río, C., Farwig, N., Kraus, D., Paulino, L., Pliscoff, P., Übernickel, K., and Bendix, J.: Higher sediment redistribution rates related to burrowing animals than previously assumed as revealed by time-of-flight-based monitoring, Earth Surf. Dynam., 10, 1273–1301, https://doi.org/10.5194/esurf-10-1273-2022 , 2022.

Grigusova, P., Larsen, A., Brandl, R., del Río, C., Farwig, N., Kraus, D., Paulino, L., Pliscoff, P., and Bendix, J.: Mammalian bioturbation amplifies rates of both, hillslope sediment erosion and accumulation, in coastal Chile, Biogeosciences [preprint], https://doi.org/10.5194/egusphere-2023-84 , 2023.

Grigusova, P., Larsen, A., Brandl, R., Farwig, N., and Bendix, J.: Spatial and temporal vegetation patterns along Chilean climate gradient estimated by WorldView-2 and Landsat time-series (in preparation)

Stallman, K., Bendix, J., Larsen, A., Brandl, R., Farwig, N., and Grigusova, P.: Spatial and temporal vegetation patterns along Chilean climate gradient estimated by WorldView-2 and Landsat time-series (in preparation)

Kraus D, Brandl R, Achilles S, Bendix J, Grigusova P, Larsen A., Pliscoff P., Übernickel K, Farwig N, 2022. Vegetation and vertebrate abundance as drivers of bioturbation patterns along a climate gradient. PLOS ONE 17, e0264408. doi:10.1371/JOURNAL.PONE.0264408

Kraus D, Brandl R, Bendix J, Grigusova P., Köhler S, Larsen A, Pliscoff P, Farwig N.: Bioturbation enhances C and N contents of near-surface soils in the desert while it promotes adverse effects in climate regions providing more food and shelter resources. (in review)

Kraus D, Brandl R, Bendix J, Grigusova P., Larsen A, Farwig N.: Meta-analysis: The positive link between geo- and biodiversity and the importance of scales. (in preparation)

WORKSHOPS AND OUTREACH

2022/03 UAV: Innovation and Praxis. German Association for Geodesy, Geoinformation and Land Management. Workshop.

2022/12 Presentation of the thesis results. Soil Geography and Landscape Group at Wageningen University & Research

CONFERENCE CONTRIBUTIONS

2020/05 European Geoscience Assembly EGU, online
Area-wide detection and spatial modeling of signs of bioturbation activity along a climate and elevation gradient in Chile using UAVand their dependence on vegetation and soil characteristics (presentation)

2021/04 European Geoscience Assembly EGU, online
Identification of the preferred areas for animal burrowing activitywith regard to the land cover, topography and soil properties usingvery high resolution WorldView-2 and LiDAR data (presentation)

2021/08 50th Annual Meeting of the Ecological Society, online
Quantification of microtopography and sediment deposition caused by animal burrowing activity using continuous surface monitoring (presentation)

2021/12 British Ecology Society: Ecology across borders, online
Prediction of burrow density and depth based on in-situ and UAV obtained vegetation patterns and machine learning (poster)

2021/04 European Geoscience Assembly EGU in Vienna, Austria
Impacts of burrowing animals on surface processes (presentation)

2022/06 Annual conference of Society for Tropical ecology in Montpellier, France
The potential of in-situ and remote sensing datasets on the analysis of impacts of bioturbation on vegetation in Chile (joined presentation with Diana Kraus)

2022/08 Soil Science Congress in Glasgow, Scotland
Effect of animal bioturbation on chemical and physical soil properties and sediment redistribution across climate gradients

2022/10 AK Klima in Würzburg
Climate determines the impact of bioturbation on landscape (poster)

2022/11 Mid-European Geomorphology Meeting in Kaprun / Salzburg, Austria
Influence of bioturbation on sediment redistribution along climate gradient in Chile (presentation)

2023/04 European Geoscience Assembly EGU in Vienna, Austria
Influence of bioturbation on sediment redistribution along climate gradient in Chile estimated by combining semi-empirical modelling, remote sensing and machine learning (presentation)